ENERGY PILES IN COOLING DOMINATED CLIMATES

A Dissertation

by

GHASSAN ANIS AKROUCH

Submitted to the Office of Graduate and Professional Studies of
Texas A&M University
in partial fulfillment of the requirements for the degree of

DOCTOR OF PHILOSOPHY

Chair of Committee,	Jean-Louis Briaud
Co-Chair of Committee,	Marcelo Sanchez
Committee Members,	Charles Aubeny
	Christopher C. Mathewson
Head of Department,	Robin Autenrieth

May 2014

Major Subject: Civil Engineering

ABSTRACT

Air pollution is one of the main environmental problems mankind faces in the 21st century caused by to the extensive use of fossil fuels. One of the opportunities to overcome this problem is to develop new technologies and methods to profit from the energy stored in the ground. A promising high-efficiency technology for the thermal control of buildings is the shallow geothermal energy. This technology is growing rapidly because it consumes less conventional energy for operation, which in turn results in fewer CO_2 emissions. This technology harnesses constant and moderate ground temperature for thermal control of a building using foundation piles. Outside air temperature changes with the season, while ground temperature remains moderate and constant. In summer, ground temperature is lower than air temperature, and so the ground may be used as a heat sink. The opposite is true in winter; the ground becomes a heat source. This technology is used efficiently in cold, heating dominated climates. Could this be true in hot, cooling dominated climates?

To achieve the ultimate goal and answer the above question, this study considered the different elements of a full SGES, namely: soil, climate, energy pile, and ground source heat pump. First, The need for a new, easy, and quick in-situ method to thermally characterize soils lead to the development of the Thermal Cone Test. Second, the soil-climate interaction and its effect on the thermodynamic efficiency of energy piles was an important factor to consider, where the decrease in soil saturation leads to a decrease in the heat exchange rate of energy piles. Third, the thermal use of foundation

pile changes the pile and surrounding soil temperature where both materials are temperature dependent. This change in temperature leads to a change in the mechanical behavior of energy piles. Fourth, a full-scale test on installed and instrumented energy piles group was needed to understand the thermodynamics of a full system and to provide experimental data for a full economic study. Finally, this study was capped by an economic analysis to evaluate the cost, benefits, payback period, and feasibility of SGES in cooling dominated climates.

The study presented in this dissertation found that integrating energy piles in heating and cooling systems in hot, cooling dominated climates could be economical and environmentally friendly solution, but attention should be paid to the thermodynamic efficiency of the system when unsaturated soil layer is encountered, and to the long term mechanical behavior of foundation piles in high plasticity clay where additional settlement could take place resulting from the increased creep rate caused by soil heating.

DEDICATION

I dedicate my dissertation to my father Anis, whose words of encouragement and support were my main source of energy and patience; to my wonderful mother Randa, who's my main source of love and warm-heartedness (and cooking lessons); to my brother Ibrahim, who's my main source of believing in a bright and great future; to my sister Madona, who's my main source of strength; and finally, to my youngest brother Imad, whose words and jokes wash away all the stress.

ACKNOWLEDGEMENTS

I would like to express my cordial gratitude to my committee chair and academic advisor, Dr. Jean-Louis Briaud. I was very lucky to work under Dr. Briaud's supervision for the last four years. His "fighter" spirit, humorous attitude, positive energy, strong technical skills, and dedication to help his students made my Ph.D. a journey as smooth as possible. I would like to extend my gratitude to my committee co-chair, Dr. Marcelo Sanchez, who was always there to assist me in my work, answer my questions, and guide me in the right direction. I would like also to thank Dr. Charles Aubeny and Dr. Christopher Mathewson for serving on my advisory committee and giving me helpful advice during my preliminary defense. Additional thanks go to Dr. Mathewson for teaching me how to use the 1956 calculator, a.k.a. slide ruler. I would like to recognize and thank Dr. Chloé Arson, who was a member in my advisory committee in the early stages of my research work before she joined Georgia Tech University.

I also deeply appreciate the financial support from the Buchanan Chair at Texas A&M University during my Master's and Ph.D. degree. I would like to thank Skanska General Contractors, Berkel and Company Contractors, TD Industries, and Britt Rice Electrics for funding and installing the full-scale test at the Liberal Arts Building.

I owe a lot to Dr. Marc Ballouz and to Ms. Hala Ballouz. Their advice, support, and love always made me feel among family here in the US. Special thanks go to Marcelle Bechara, who helped me to take the life-changing decision in the moments of

confusion. Great thanks go to Lacey Bodnar for being a great support during my studies since we met at Texas A&M University. She always proofread my work, reports, and papers. Great thanks also go to Oswaldo Bravo de Los Rios, Conpu Yao, Muhammad Ehsanul Bari, Layal Maddah, Basheer Kassas, and Mohsen Madhavi for being great friends and for making my time in College Station unforgettable.

Deep thanks and sincere gratitude go to Daniela Hanjoul for being a wonderful supportive friend from overseas.

Last but not least, Thank you my parents, Anis and Randa Akrouch who taught me to always carry my book in one hand, my pen in the second hand, and fight in the frontlines of challenges. Thank you my Brothers Ibrahim and Imad Akrouch, Thank you my sister, Madona Akrouch. Without your support, I would not have made it.

NOMENCLATURE

ACI	American Concrete Institute
AFR	Air Flow Rate
ASHP	Air Source Heat Pumps
ASTM	American Society for Testing and Materials
BH	Borehole
CH	High Plasticity Clay
CPT	Cone Penetration Test
CO_2	Carbon Dioxide
COP	Coefficient Of Performance
DMD	Electric Demand for the heat pump
EAT	Entering Air Temperature
EER	Energy Efficiency Ratio
EWT	Entering Water Temperature
GHE	Ground Heat Exchanger
GPM	Gallons Per Minute
GSHP	Ground Source Heat Pump
HC	Heating Capacity of the heat pump
HCF	Heat Carrying Fluid
HDPE	High Density Polyethylene
HE	Heat Extraction rate

HVAC	Heating, Ventilation, and Air Conditioning
HyGCHP	Hybrid Ground Coupled Heat Pump
HW	Hot Water generation
IWT	Inlet Water Temperature
LAT	Leaving Air Temperature
LCC	Life Cycle Cost
LWT	Leaving Water Temperature
OWT	Outlet Water Temperature
PEX	Cross-linked Polyethylene
PVC	Poly Vinyl Chloride
PWP	Pore Water Pressure
RH	Relative Humidity
SC	Sensible Cooling capacity
SSL	Shallow Soil Layer
SGES	Shallow Geothermal Energy System
SWCC	Soil Water Characteristic Curve
TC	Total Cooling capacity
TCT	Thermal Cone Test
THM	Thermo-Hydro-Mechanical
TID	Thermally Independent Depth
WF	Water Flow Rate
A	Cross section area

c_h	Horizontal consolidation coefficient
c_p	Specific heat capacity
C	Volumetric heat capacity
C_u	Coefficient of uniformity
C_c	Coefficient of curvature
D	Diameter
f_u	Ultimate pile friction
E	Elasticity modulus
J	Joule
L	Length
Q	Heat exchange rate
q_u	Ultimate pile tip resistance
R	Thermal resistance
r	radius
k	Hydraulic conductivity
n	Creep exponent
S	Pile displacement
S_l	Liquid degree of saturation
t	time
T	Temperature
U	Temperature dissipation ratio
u	Water pressure

W	Watt
z	depth
λ	Thermal conductivity
ϕ	Porosity
Δ	Difference
θ	Volumetric water content
ν	Creep exponent factor ratio
κ	Texture dependent parameter
χ	Shaper parameter 1
η	Shape parameter 2
α	Thermal diffusivity
β	Thermal expansion coefficient
ρ	Density
γ	Unit weight
ε	Strain
σ	Stress
ψ	Matric suction
ζ	Thermal efficiency ratio
μ	Viscosity
ω	Water content

TABLE OF CONTENTS

Page

LIST OF FIGURES

Page

LIST OF TABLES

Page

1 INTRODUCTION

1.1 NEED

One of the biggest challenges of the 21st century will be to mitigate environmental damage and the trend of climate change initiated as the world industrialized over the last approximately 150 years. To power this rapid modernization, mankind relied almost exclusively on non-renewable sources known as fossil fuels: oil, coal, and natural gas. These energy sources result in negative environmental impacts from their extraction, refinement, transport, and burning. Perhaps most notably, burning oil and coal releases greenhouse gases such as carbon dioxide (CO_2), Methane (CH_4), and Nitrous Oxide (N_2O). Emitting these and other pollutants into the air degrades the environment and may cause or exacerbate health problems.

In contrast, renewable energy sources such as geothermal, solar, wind, and wave energy do not produce harmful by-products. These "clean" energies exist now in abundance, and perhaps most importantly, will exist in perpetuity. Unfortunately, the utilization of these energy sources currently accounts for only a small percent of U.S. energy consumption. As Figure 1-1 shows, biomass, geothermal, solar, and wind (excluding hydro-electric) accounted for only 0.12% of total electricity generation in 1950 and 4.06% in 2010, with an increase of a mere 3.94% over 60 years. To prevent and reverse the deleterious effects of air pollution, research should focus on developing and improving methods and techniques to profit from the renewable energy sources. The energy is out there; we just need the tools to harness it.

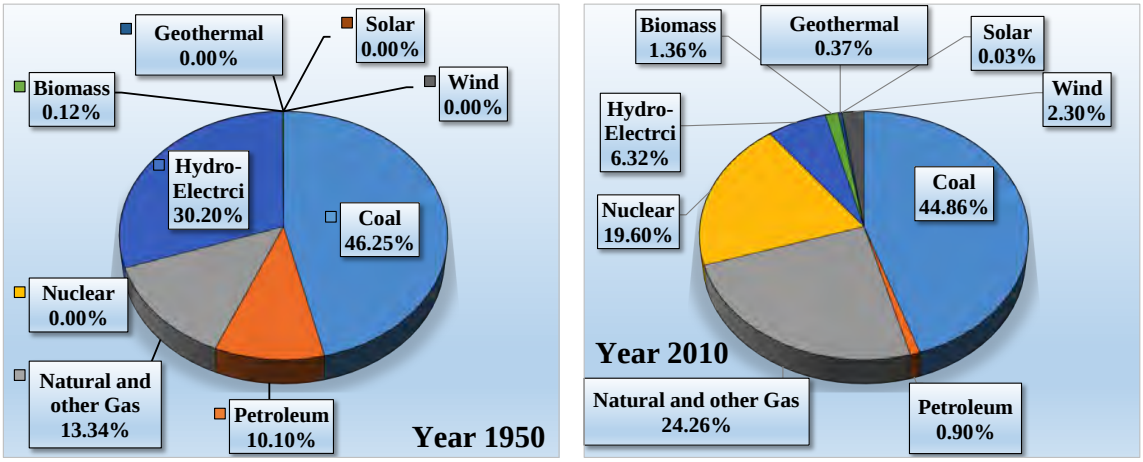

Figure 1-1 USA electricity production by sector *(Source: U.S Energy Information Administration, www.eia.gov)*

A surprising place where gains can be made in reducing consumption of non-renewable energy and air pollution is in buildings. According to the U.S Green Building Council, in the United States buildings account for 36% of total energy use, 65% of electricity consumption, and 30% of greenhouse gas emission. Heating and cooling consists of 29% of energy consumption in a typical house (Figure 1-2). A promising high-efficiency renewable energy technology suitable for use in buildings is the shallow geothermal energy system (SGES). The use of SGES is growing rapidly because it consumes less conventional energy for operation, which in turn results in fewer CO_2 emissions. This technology harnesses constant and moderate ground temperature for thermal control of a building. The traditional use of this technology requires drilling boreholes known as Ground Heat Exchangers (GHE) to circulate a Heat Carrying Fluid (HCF) through fitted High Density Polyethylene (HDPE) pipes. The drilling and

installation increases the initial cost of the system, which makes it difficult to convince the clients to adopt these heating and cooling systems. When piles are used as a foundation system of a structure, the integration of HDPE pipes into the foundation piles makes the system more cost effective, because the piles are already required to support the building.

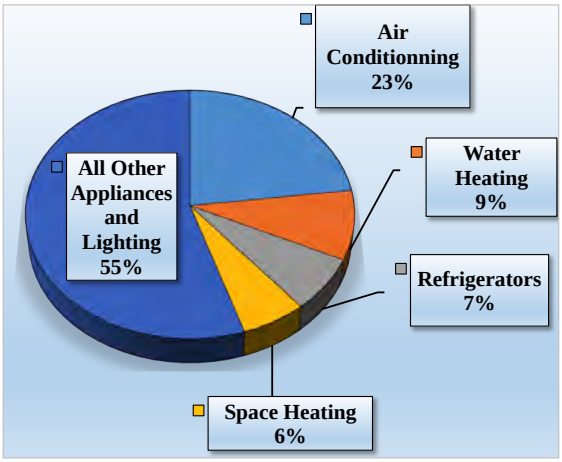

Figure 1-2 Homes electricity consumption by sector *(Source: U.S. Energy Information Administration, Annual Outlook 2012, Early Release, Table 4. www.eia.gov)*

The use of energy piles as GHE for SGES was proved to be energy efficient and environmentally friendly in cold, heating dominated climates. The question that this research will answer is: Is the use of energy piles for SGES in hot, cooling dominated climates energy efficient and environmentally friendly as well?

1.2 SGES THEORY AND OVERVIEW

To understand how a SGES works, it is important to first understand how a conventional heating and cooling system, such as an Air Source Heat Pump (ASHP) works. The main concept of a SGES is to transfer heat with a more constant and moderate medium. In geothermal energy application, this medium is the ground beneath our feet. Below a certain depth, referred to as the Thermally Independent Depth (TID), soil temperature is moderate, constant, and equal to the annual mean air temperature. In winter, ground temperature is warmer than air temperature, and so the ground may be used as a source of heat to warm the building. The opposite is true in summer; the ground becomes a heat sink. This difference in temperature makes geothermal energy systems more efficient than conventional HVAC systems, and results in reduced energy bills and CO_2 gas emissions. In heating mode, geothermal energy systems extract the heat from the ground and supply it to the structure resulting in a pile and soil temperature decrease. In cooling mode, the system removes the heat from the building and injects it in the soil resulting in a pile and soil temperature increase.

Figure 1-3 shows a conventional heating and cooling system in cooling mode, with an example of the temperature that may be expected at each of the components (T_{Ref} corresponds to the refrigerant temperature). The system is composed of two main components: the heating and cooling unit and the duct system. The heating and cooling unit is composed of 4 main parts: evaporator (located inside the building), compressor, condenser (located outside the building), and expansion valve. The room warm air is circulated through the evaporator of the heat pump and returned as a cool air. The heat

removed from the air is gained by the heat pump refrigerant at the evaporator level that circulates at low pressure and low temperature. The refrigerant circulates through a compressor that compresses and turns it to high-pressure, high temperature fluid. At the condenser level, the heat gained by the refrigerant is exchanged with the outside air by forced convection mechanism. Note that when cooling is needed, the outside air is already at high temperature, which is a key difference between conventional and geothermal heating and cooling system. The refrigerant then passes through the expansion valve that returns it to low pressure and temperature fluid and the cycle starts again.

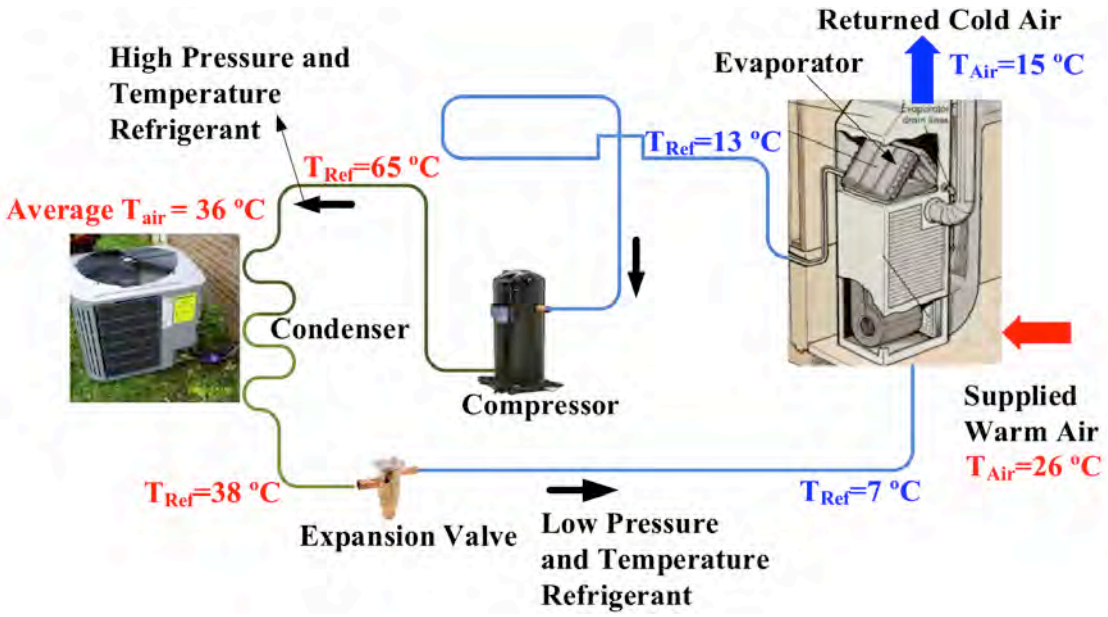

Figure 1-3 Conventional heating and cooling system in cooling mode

Figure 1-4 illustrates a full SGES in cooling mode with a representative example temperature at each of the components. The main difference between conventional HVAC and SGES is at the condenser level (in cooling mode). In SGES, the heat gained by the refrigerant is exchanged with the loop that is circulating the HCF, which is usually a water and antifreeze mixture. The different components of the SGES are detailed in Table 1-1.

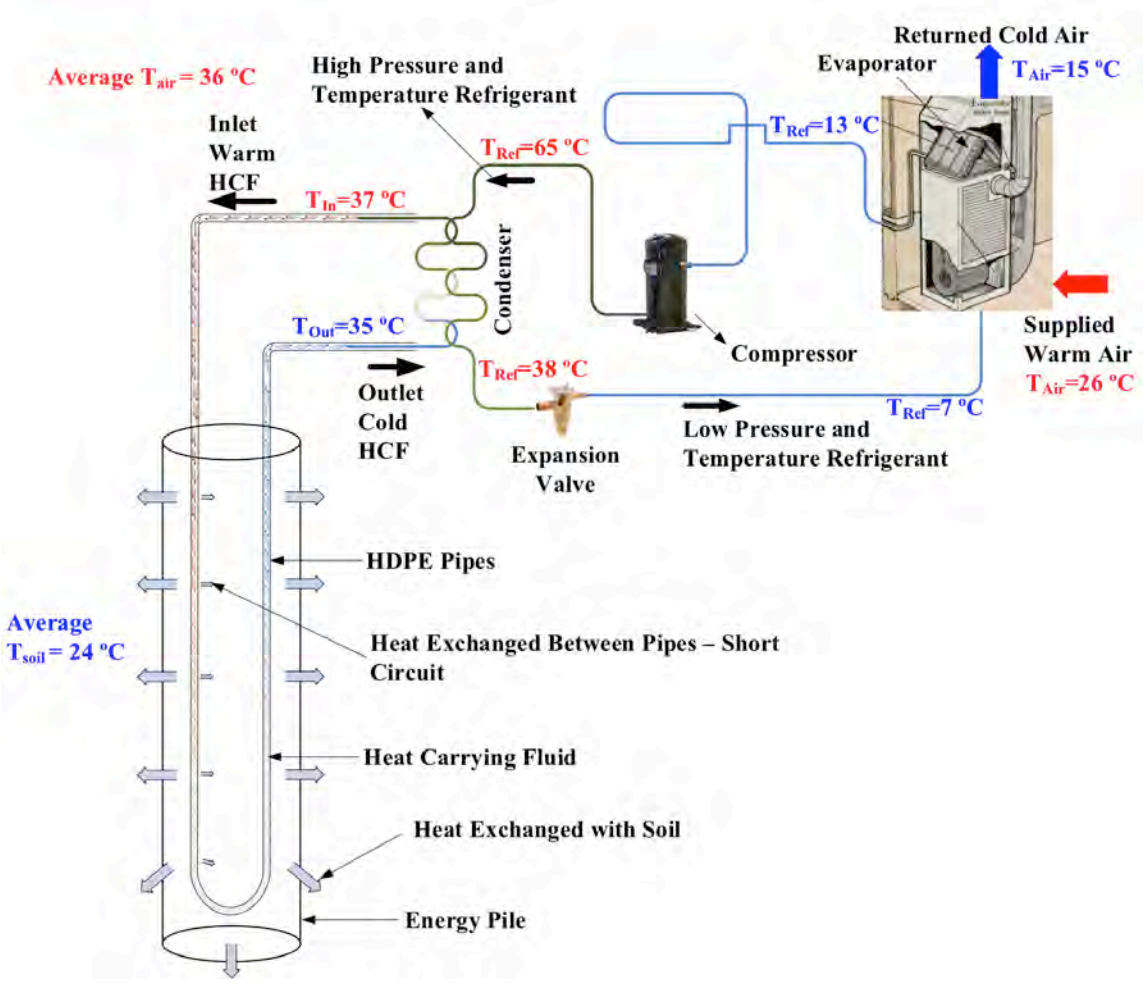

Figure 1-4 Shallow geothermal energy system using energy piles in cooling mode

Table 1-1 Shallow geothermal energy system components (*After Alaska Center for Energy and Power Cold Climate Housing Research Center)*

Main Component	Sub Component	Description
Ground Heat Exchanger	Pipes	• HDPE pipes • Circulates the HCF
	Heat Carrying Fluid	• Usually water with anti-freeze and anti-corrosion mixture. • Moves the heat exchanged with the ground to the heat pump or vice versa
	Pump	• Circulates the HCF in the pipes
	Manifold	• Plumbing connections • Combine individual tubing loops
Heat Pump Unit	Condenser	• The heat exchanger • Exchanges heat between ground exchanger HCF and heat pump refrigerant liquid in cooling mode • Called the evaporator in heating mode
	Compressor	• Compresses the heat pump refrigerant after drawing it from the evaporator. • Increases the refrigerant temperature by increasing the pressure and decreasing the volume.
	Evaporator	• The heat exchanger • Exchanges heat between heat pump refrigerant liquid and the air in the room in cooling mode • Called the condenser in heating mode
	Expansion Valve	• Reduces the pressure and temperature of the refrigerant liquid

So how does a SGES work? Assuming a building peak cooling load Q, the heat pump works by sucking the warm air from the building and blowing it on the heat pump evaporator, which circulates a cold refrigerant. Because of the temperature gradient between the incoming air and evaporator refrigerant, heat transfers from the air to the

evaporator by a forced convection mechanism, resulting in a colder air output from the heat pump. The refrigerant absorbs the heat and circulates through a compressor that compresses it and turns it into a hot and high-pressure fluid that circulates in the heat pump condenser. In SGES, the condenser exchanges heat with the ground heat exchanger loop that circulates the HCF. Because the ground is at a moderate and constant temperature, the thermal gradient between the condenser and the ground heat exchanger fluid is higher than the gradient between the condenser and the outside air. This difference results in a more efficient heat exchange rate in shallow geothermal systems. In heating mode, the cycle is reversed. The condenser is located inside the building, and the heat exchange between the refrigerant and the ground loops occurs at the evaporator level. The HCF circulates at low temperature in the HDPE pipes to extract heat from the ground. Figures 1-5 and 1-6 illustrate the difference between conventional and geothermal systems in cooling and heating modes respectively.

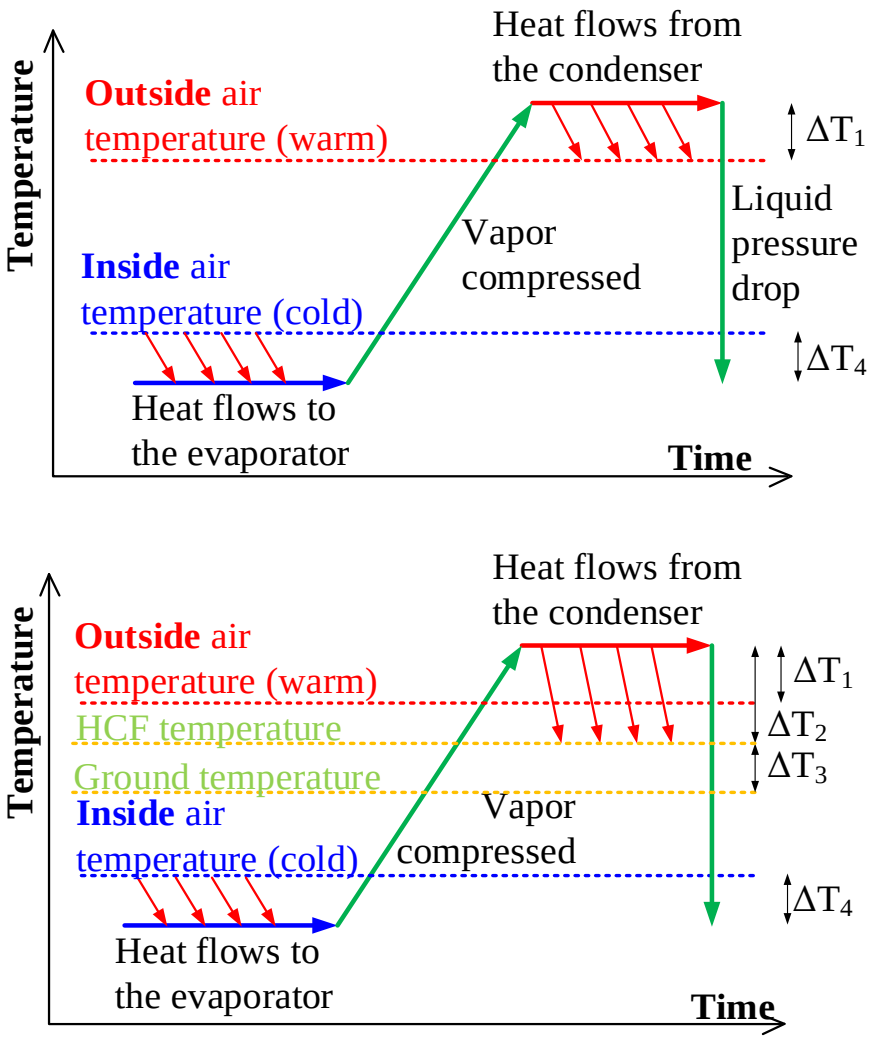

ΔT_1=Temperature difference between liquid in condenser and air

ΔT_2=Temperature difference between liquid in condenser and HCF

ΔT_3=Temperature difference between HCF and ground

ΔT_4=Temperature difference between liquid in evaporator and air

Figure 1-5 Heat transfer in cooling mode: (a) conventional and (b) geothermal systems

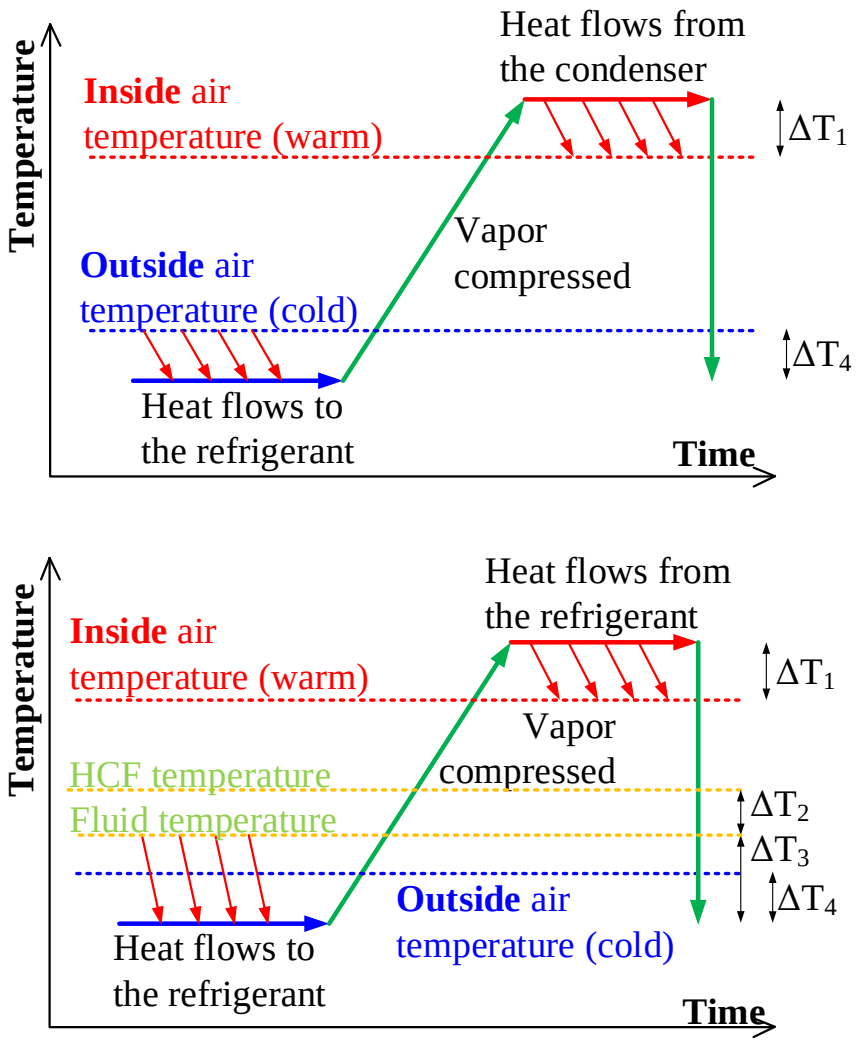

ΔT_1=Temperature difference between liquid in condenser and air

ΔT_2=Temperature difference between HCF and ground

ΔT_3=Temperature difference between liquid in evaporator and HCF

ΔT_4=Temperature difference between liquid in evaporator and air

Figure 1-6 Heat transfer in heating mode: (a) conventional and (b) geothermal systems

The mechanism for heat transfer from the HCF to the soil is illustrated in Figure 1-7, in cooling mode as an example. The heat, Q, transfers from the HCF to the HDPE pipe by convection (q_{conv1}). At the pile wall (point A), the temperature is equal to the fluid temperature. The heat then transfers through the HDPE pipe (from point A to point B) by conduction (q_{cond1}). The heat continues towards the soil by conduction in the pile element from point B to point C (q_{cond2}). At the interface between the pile and the soil (point C), the heat transfer occurs mainly by conduction, (q_{cond3}) or by convection if ground water flow exists (q_{conv2}).

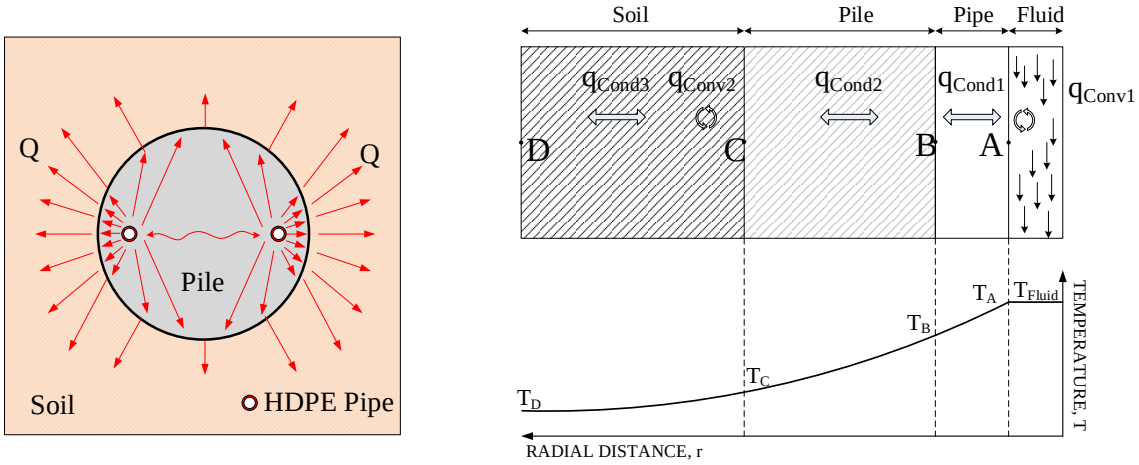

Figure 1-7 Heat transfer from HCF to the soil (Not to scale)

1.3 OTHER HVAC SYSTEMS FOR COMMERCIAL BUILDINGS

Another type of heating and cooling system that is commonly used in large commercial buildings is shown in Figure 1-8. The major parts of this system are the air handling

ducts, the hot water boiler, the chiller, and the cooling tower. The air handling part contains a filter, heating coil, cooling coil, and a humidifier. The filter is used to clean the building air, the heating coil is used to heat the building air when the system is on heating mode, the cooling coil is used to cool the building air when the system is on cooling mode, and the humidifier is used to humidify or dehumidify the building air. In the system presented in Figure 1-8, water is used as a circulation fluid in the heating and cooling coils. In heating mode, the building air absorbs the heat from circulated water at the heat coil level where the hot water is generated using water boilers that runs on fuel or electricity. In cooling mode, the circulating water absorbs heat from the building air and carries it to a chiller that uses the vapor-compression concept (described in Section 1.2) to remove the heat from the water. The energy removed by the chillers is carried by water in another circuit to a cooling tower that exchanges heat with the outside air and bring the water to a cooler level.

In conventional commercial buildings and institutes where the system described above is used, the water boiler, chiller, and cooling tower are used for one building only. The heating and cooling system at Texas A&M University is a particular case where centralized boilers, chiller, and cooling tower are used at four different central plants across the university campus. The central plants collect water from all the connected buildings through underground distribution system and process it for heating and cooling using the boilers and chillers respectively. After the water is heated or cooled, it is pumped again to the connected buildings. In such system for stand-alone buildings,

energy piles could be used to impact water temperature before it is pumped into the cooling tower, which results in higher efficiency.

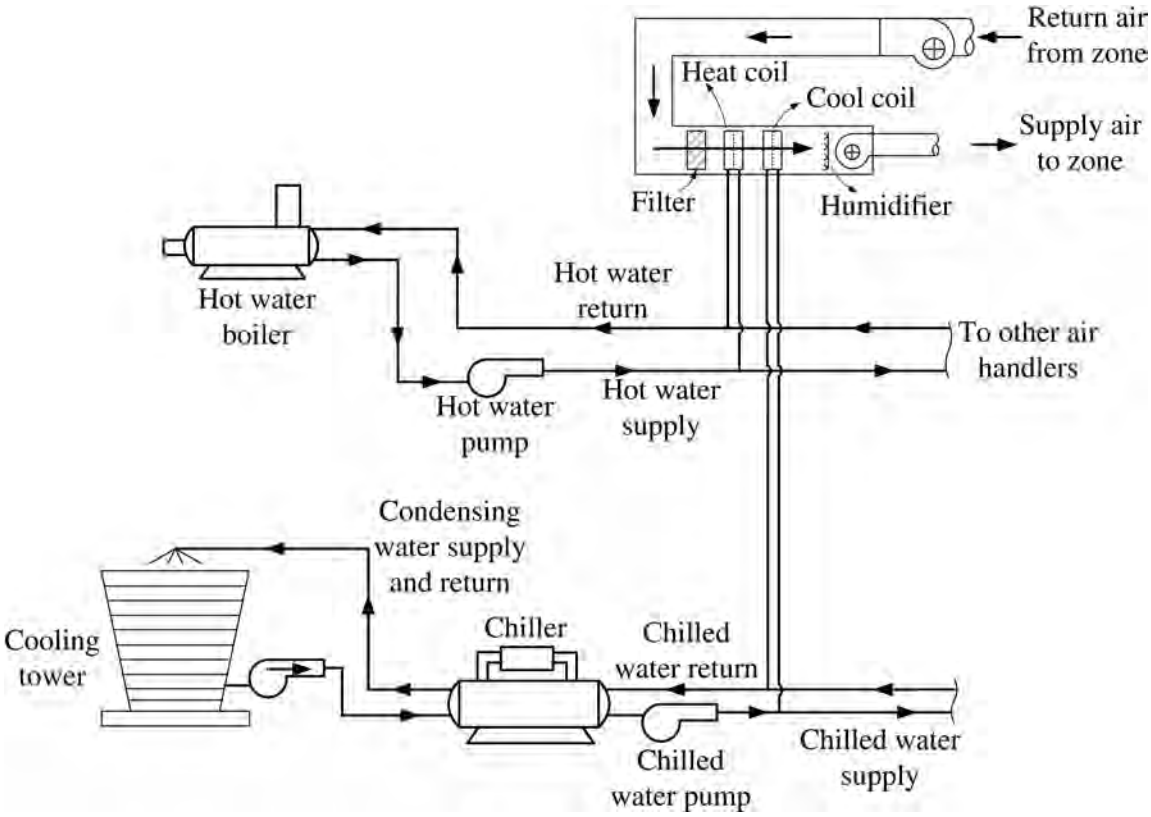

Figure 1-8 Other heating and cooling systems for large commercial buildings

1.4 OBJECTIVES

The ultimate goal of this research is to determine how efficient energy piles are for heating and cooling systems in cooling dominated climates, as compared to their efficiency in heating dominated climate zones. To achieve this objective, different tests should be performed to study each element of the SGES and the interactions between

them, where the main elements are: 1) soil, 2) energy pile, 3) geothermal heat pump, and 4) the climate (Figure 1-9).

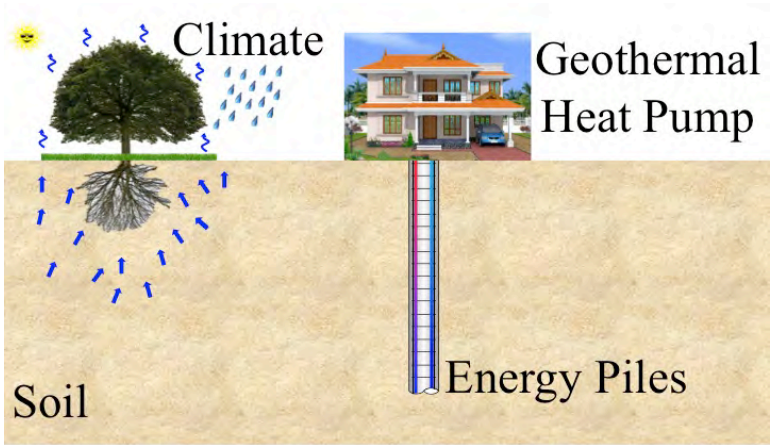

Figure 1-9 Elements of a shallow geothermal energy system

The components of the system interact via several processes. Climate affects the system because of its variability throughout the year, which influences the soil moisture profile and as a result directly impacts soil thermal properties. A change in thermal properties has a corresponding significant impact on the heat exchange rate of energy piles. The geothermal heat pump influences the system by transferring thermal energy from the heat pump to the pile and soil. Raising the pile and soil temperature causes a coupled Thermo-Hydro-Mechanical (THM) phenomenon on the soil. The interaction between the different elements is summarized in Figure 1-10. The inner circle shows the general topic related to how the system functions and the adjacent box identifies the specific property, which was investigated.

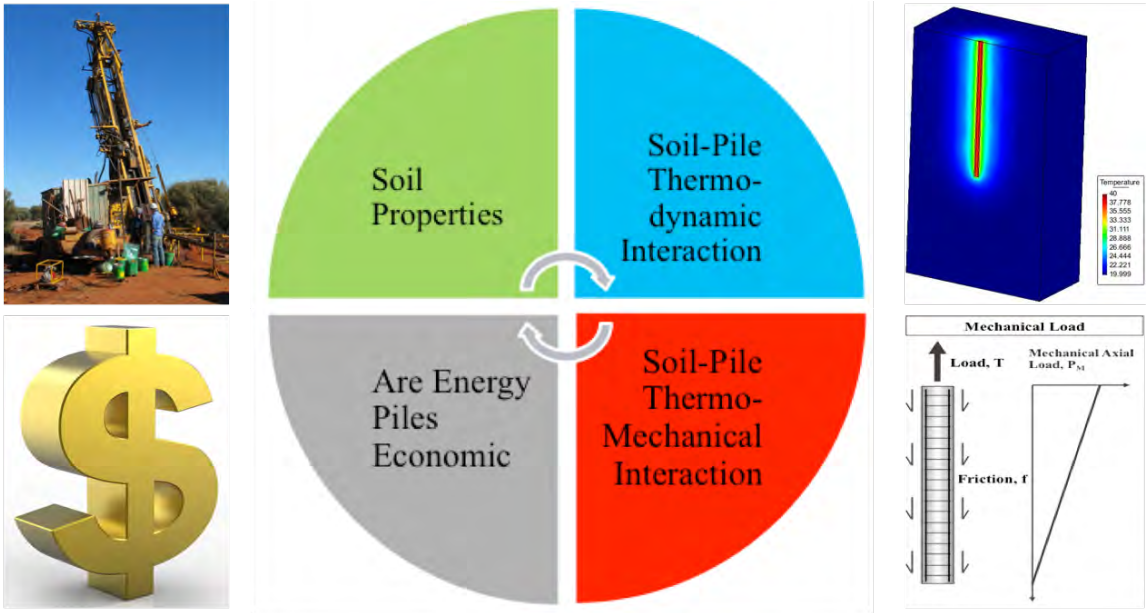

Figure 1-10 Project elements and interactions

The objectives of this research were:

1. Develop a new, easy, and quick in-situ test to measure soil thermal properties in the field: the Thermal Cone Test (TCT).
2. Evaluate the thermodynamic efficiency of energy piles in unsaturated soils.
3. Evaluate the short- and long-term thermo-mechanical behavior of energy piles in high plasticity clays.
4. Perform a full-scale test on a group of energy piles in a cooling dominated climate.
5. Study the economic feasibility of using energy piles for heating and cooling purposes in cooling dominated climates.

1.4.1 Objective 1: Develop a new, easy, and quick in-situ test to measure soil thermal properties in the field: the Thermal Cone Test (TCT)

Heat exchange and transfer in soil depends on soil thermal properties. Most of the heat transfer between the energy pile and the soil is governed by conduction. High soil effective thermal conductivity (λ_e) enables rapid energy balance between the piles and the thermal reservoir consisting of the soil out of the pile influence zone. The performance of energy piles is thus highly dependent on the ground thermal properties. Heating tests usually performed in the laboratory change the soil porosity and water content. Moreover, sampling can change the ground microstructure. In-situ tests minimize soil disturbance from sampling and make it possible to test a large volume of soil. In this dissertation, a new test was developed to evaluate soil thermal properties in-situ under natural conditions. The proposed test consisted of instrumenting the Cone Penetration Test (CPT) cone with a heater and thermocouple. The heater was used to apply a thermal load on the soil to increase its temperature, and the thermocouple was used to record the increase in soil temperature after turning off the heater. Similarly to how the pore pressure dissipation curve is used to evaluate the hydraulic conductivity of the soil, the measured temperature decay curve from the test was used to back calculate the soil thermal properties.

1.4.2 Objective 2: Evaluate the thermodynamic efficiency of energy piles in unsaturated soils

Soil thermal properties are dependent on soil type, dry density, and water content. The heat exchange between energy piles and soil is mainly dependent on soil thermal

properties; thus, it depends mainly on soil conditions. In the traditional design of borehole heat exchangers, the soil is assumed to be homogenous and saturated. This simplification is good in the case of long borehole heat exchangers. However, energy piles are relatively short; therefore, a significant part of the pile is in contact with the soil where the degree of saturation (S_l) changes over the year. This change of degree of saturation induces changes in soil thermal properties, which in turn affects the thermal performance of energy piles. This research presents a new analytical solution that was developed to evaluate the thermodynamic efficiency of energy piles in unsaturated soils. Thermodynamic efficiency is defined as the ratio of heat exchanged when the soil is in an unsaturated condition to the heat exchanged when the soil is in saturated conditions. The new analytical solution was verified against a numerical model, which was itself validated by laboratory experiments on energy pile sections in soil ranging from dry to saturated. The laboratory test was numerically modeled using the finite element code CODE_BRIGHT. The results from the numerical simulation were verified against the measured data from the lab test. The numerical model was extended to account for the pile depth. The thermodynamic efficiency of energy piles was evaluated from the numerical model and compared to the analytical solution and the measured data.

1.4.3 Evaluate the short- and long-term thermo-mechanical behavior of energy piles in high plasticity clays

When designing foundation piles, both short-term and long-term behaviors are of great importance. In service limit state, short-term behavior represents load redistribution in the pile and immediate settlement, while long-term behavior represents time dependent

mechanisms such as consolidation and creep. In addition, the impact of temperature change on ultimate capacity of energy piles is of great importance. The use of foundation piles as ground heat exchangers induces temperature changes in the pile and the soil, where both materials are temperature dependent. In cooling dominated climates, the soil and pile will experience an increase in temperature most of the year because of the SGES. This change in temperature induces a volume change in the pile, which influences the pile-soil friction. This mechanism causes a redistribution of the load in the pile. The change in soil temperature induces complex coupled Thermo-Hydro-Mechanical phenomena.

The evaluation of the thermo-mechanical behavior of energy piles was undertaken from a full-scale test on instrumented energy piles. The piles were installed at the Riverside campus of Texas A&M University. The piles were instrumented with temperature sensors, strain gages, and dial gages to track the temperature change in the pile and the deformation along the pile axis and pile top. The piles were subjected to a mechanical and then a thermo-mechanical load. During the two steps the pile head displacement, the strain development in the pile, temperature in the pile, and soil temperature were measured. The measured load redistribution in the pile was evaluated and compared to the theoretical load distribution; this represents the short-term behavior. From the pile head load-displacement, the soil viscous exponent (n) was evaluated under mechanical load only, and thermo-mechanical load. The viscous exponent was used to extrapolate the load-settlement behavior of energy piles with and without geothermal use

of foundation piles, representing the long-term behavior. The impact of temperature change on ultimate capacity of energy piles in cooling and heating mode was evaluated.

1.4.4 Perform a full-scale test on a group of energy piles in a cooling dominated climate

Most of the research and existing energy pile construction has been done in regards to heating dominated climates, primarily in Europe. The assessment of energy pile performance in a cooling dominated climate (Texas in this case) was performed in this research through a full-scale test on three energy piles installed and instrumented as part of the new Liberal Arts Building foundation. The energy piles were connected to a geothermal heat pump. From this test, the change in pile-soil temperature caused by heat exchange was evaluated in order to predict the long-term performance and feasibility of energy pile systems in cooling dominated climates.

1.4.5 Study the economic feasibility of using energy piles for heating and cooling purposes in cooling dominated climates

In order for the use of geothermal energy systems to become widespread, developers and building owners must have confidence that they will see a return on their investment. An economic study was thus conducted to evaluate the initial cost and the payback period of SGES. The economic study investigated the initial and operational cost of a SGES in comparison to a conventional HVAC system. The Liberal Arts Building at Texas A&M University provided the case study for this section.

1.5 SIGNIFICANCE OF RESEARCH

This research will enable engineers to design SGES in cooling dominated climates while taking into account the different elements of the system and the interaction between them. The engineer will be able to evaluate the effect of soil saturation on thermodynamic efficiency of energy piles using a quick and easy method. Engineers will also understand the short- and long-term thermo-mechanical behavior of energy piles and take into account load redistribution in the pile and its time dependent behavior. Engineers, practitioners, and clients will understand the economic benefits of using SGES in cooling dominated climates.

1.6 RESEARCH APPROACH

This dissertation addresses different topics related to the use of energy piles in cooling dominated climates, as described in section 1.3. The work presented in this research is balanced between theoretical and practical, numerical and experimental. In each of the objectives previously identified, the following approach was used:

- First, a conceptual background was developed.
- Secondly, experimental work was performed in the lab or in-situ.
- Thirdly, a numerical modeling approach was used to simulate the experimental work (where needed), an analytical solution was proposed, and a comparison between experimental-numerical and analytical methods was performed.
- Finally, conclusions were made and recommendations were proposed.

1.7 ORGANIZATION OF DISSERTATION

This dissertation is organized into seven sections.

Section 1 provides the introduction and identifies the problem statement, the significance of the research, and the objectives of the research. Section 2 is the literature review, covering the fundamentals of heat transfer, soil thermal properties, soil thermo-mechanical behavior, and the current state of energy pile technology.

The third section describes the proposed thermal cone (TCT) test. In this section, 11 in-situ tests at different locations were performed. The in-situ test was numerically modeled to simulate a wide range of soil thermal properties. Based on the numerical simulation, a relationship between a measured parameter and soil thermal properties was developed. The relationship was validated against the measured data from the in-situ test.

The fourth section investigates the thermodynamic efficiency of energy piles in unsaturated soils. The work in this section is divided into three parts. Part 1 presents a simple analytical solution of the problem. The analytical solution is then compared to the experimental and numerical results. Part 2 presents a laboratory test to investigate the heat transfer in soils ranging from dry to fully saturated. Part 3 provides a numerical model to simulate the laboratory test and to simulate a full pile.

The fifth section investigates the short- and long-term thermo-mechanical behavior of energy piles. Short-term behavior includes the thermally induced stresses and strains in the piles. Long-term behavior refers to the time-dependent deformation of energy piles under a thermo-mechanical load. In addition, this section evaluates the impact of temperature change on the ultimate capacity of energy piles. This section presents full-scale tests on instrumented energy piles at the Riverside campus of Texas

A&M University. Energy piles were subjected to mechanical and thermo-mechanical loads. During the tests, strains and temperature along the pile, pile head load-displacement, and climatic conditions were monitored. From the measured data, the load redistribution in the pile, the time-dependent parameters, and the ultimate capacity of energy piles were evaluated. Based on the measured data, the long-term behavior of energy piles was evaluated with and without geothermal use.

The sixth section presents a full-scale test on three instrumented energy piles at the new Liberal Arts Building at Texas A&M University. The energy piles are part of the foundation of the new building. The piles are connected to a geothermal heat pump that was used to heat and cool the crawl space of the building. The temperature along the pile and in the soil at different locations was measured to better understand the heat transfer mechanism in and around the energy piles because of the operation of geothermal heat pumps in cooling dominated climates.

The seventh section is an economic study of a SGES in cooling dominated climates. The initial and operational cost of SGES and conventional HVAC system were calculated and compared.

2 LITERATURE REVIEW

2.1 GENERAL REVIEW

Between 1855 and 1857, Peter von Rittinger was the first to develop and build a heat pump (David B. L., 2008). The first ground source heat pump (GSHP) was developed and built by Robert C. Webber in 1940. The utilization of GSHP results in many benefits, including reduced energy consumption (up to 72% compared to electrical resistance heating and standard air conditioning, less maintenance, comfort for building inhabitants, and an environmentally friendly approach to heating and cooling. There are two categories of GHE used for GSHP, which each have advantages and disadvantages: the open loop and closed loop (Figure 2-1). In an open loop system, the water is pumped from a well, circulated into the heat exchanger of the GSHP, and then injected in the ground using a different injection well. A key point in the open loop system is that the extraction and injection wells must be placed far enough apart to ensure thermal recharge of the source. Closed loop systems circulate a constant mass of water in a closed circuit. The water mass transports the heat from and to the GSHP. Different types of closed loop configurations exist: vertical loop field, horizontal loop field, and pond loop field. Vertical closed loop field (Figure 2-1b) consists of vertically drilled boreholes fitted with HDPE pipes and filled with grout. The borehole diameter ranges from 75 mm to 150 mm and the length ranges from 50 to 150 m. HDPE pipes are joined at the bottom of the borehole in a U shape. The boreholes are filled with grout to close any gaps that may have been created during the installation process, to stabilize the

borehole, and to enhance the heat transfer rate between the HCF and the soil (Sagia et al., 2012). Vertical loop fields are used when the area of land is limited. As an example, a single house that needs 3 tons of heating capacity requires around three boreholes with a length of 80 to 110 m.

The pipes in a horizontal closed loop field (Figure 2-1c) are laid horizontally in a trench in a slinky or straight way depending on the amount of land available. The efficiency of the system is mainly dependent on the depth of the trench. The main advantage of a horizontal loop field is the low price of excavation compared to the price of drilling. As an example, a single house that needs 3 tons of heating capacity requires around three loops 120 to 180 m long, placed at a depth of 1 to 2m. The least common configuration is the pond loop field (Figure 2-1d) because it depends on a pond or a body of water close to the building. The pond loop consists of a slinky configuration of HDPE pipes placed at the bottom of a pond or water source.

(a) Open vertical loop field

(b) Closed vertical loop field

(c) Closed horizontal loop field

(d) Closed pond loop field

Figure 2-1 Different heat exchangers loop field

The practice of fitting HDPE pipes into foundation structural elements gained success in the late 1980's. The practice started in 1984 with energy piles, which are the focus of this dissertation, and in 1996 with diaphragm walls (Brandl, 1998, 2006; Xia C. et al., 2012) (Figure 2-2). The unique concept of an energy pile is to use the building foundation for heat exchange and structural support at the same time. The aim of this integration is to reduce the initial drilling cost of the heat exchanger. However, this

integration introduces new thermodynamic, engineering, and economic challenges. Energy piles have already been tested (Laloui et al., 2003; 2006, 2011; Kenllwolf et al., 2011; Aymata et al., 2012) and constructed (Brandl, 2003, 2006; Ooka et al. 2007; Gao et al., 2008; Preene and Powrie, 2009; Adam and Markiewicz, 2009) for the purpose of building thermal control.

Figure 2-2 HDPE integrated in diaphragm walls (left) and foundation piles (right)

From a thermodynamics point of view, the sustainability of the geothermal system is improved if the heat extracted from the ground to warm the building in the winter is re-injected into the ground by cooling the building during the summer. By alternating heating and recharge modes, part of the heat extracted during the winter is stored during the summer. In cooling dominated climates, the heat extraction/injection is unbalanced, where heat injection in the soil is dominant over the year. This unbalance results in an increase in soil temperature over the operational years, which should be

taken into account during the design stage. From a thermodynamic perspective, the main inputs for designing a SGES are soil thermal properties. Easily and accurately evaluating these properties leads to an economical design. Energy piles are relatively short; therefore, a significant part might be embedded in unsaturated soil conditions. As a result, energy pile thermal performance will be affected by climate and soil moisture, because soil thermal properties are highly dependent on soil saturation conditions.

From the geotechnical and structural point of view, the design of pile foundations includes the consideration of its behavior under vertical loading and overturning loading. In both cases, the ultimate limit state and the serviceability limit state must be satisfied. Piles generate their capacity from the combination of side friction and point resistance. Therefore, it is very important to determine how geothermal piles will differ from regular piles when it comes to side friction and point resistance, both in terms of strength (large strain) and deformation (small strain). It is expected that a temperature increase will induce an expansion of all the phases present in the soil (solid skeleton and pore fluids). In the same way it is expected that winter heat extraction will decrease the temperature of the ground, thus resulting in soil contraction. The change in soil temperature will impact the creep process and affect the time-dependent behavior of energy piles.

From an economic point of view, it was determined from a case study in Ghent, Belgium, that energy consumption can decrease by 31% per year when using a GSHP system compared to a traditional heating system (Desmedt et al, 2010). The GSHP system became more cost effective than a traditional HVAC system after only 8.5 years

of use. However, Belgium is considered a heating dominated climate. Therefore, this finding should be verified in a cooling dominated climate.

2.2 SOIL TEMPERATURE AND HEAT TRANSFER IN SOIL

Soil temperature is an important factor in many soil processes, such as evaporation and soil aeration, chemical reactions within the soil, and seed germination, seedling growth, root development, and microbial activity. The application of GSHP added to this list an important process, which is the heat exchange between GHE and the soil. The processes described above mainly occur within the Shallow Soil Layer (SSL), which is a layer of varying depth where soil temperature varies around the year in response to heat exchange processes that take place at the soil surface. Below this layer, the soil temperature becomes constant and moderate. The SSL extends to a depth of 2 to 5 m. depending mainly on soil thermal properties. The heat exchanged at the soil surface propagates in the soil by different heat transfer phenomena: conduction, convection, and radiation. Conduction heat transfer occurs at the molecular level when an increase in temperature excites and causes rapid vibrations of molecules that result in collision and excitation of neighbor molecules. Radiation heat transfer is energy transfer in form of electromagnetic waves. According to Stefan-Boltzmann law, only bodies with temperatures higher than -273.15 °C radiate energy. Convection heat transfer is the transfer of energy between a moving fluid over a solid body at different temperature. Radiation heat transfer is negligible in soils, and its effect in sands is less than 1% of the overall heat transfer (Rees et al., 2000). Convection heat transfer is significant when groundwater flow conditions exist; but conduction is the most relevant process

associated with heat transfer in soils and it is controlled by the well-known Fourier's Law (Eq. 2.1) (Fourier, 1822).

$$q_{cond} = -\lambda_e \frac{dT}{dx} \tag{2.1}$$

Combining Fourier's Law and the energy conservation equations results in the transient partial differential equation of conduction heat transfer in soil (Eq. 2.2). Note that in Eq. 2.2, soil is assumed to be homogenous and isotropic.

$$\frac{d^2T}{dx^2} + \frac{d^2T}{dy^2} + \frac{d^2T}{dz^2} = \frac{C}{\lambda_e}\frac{d^2T}{dt^2} \tag{2.2}$$

In Eq. 2.1 and 2.2, C (Joule/m^3.K) is the volumetric heat capacity and T is temperature. Analytical solutions of Eq. 2.2 for different conditions, geometries, and boundary conditions have been developed (Carslaw and Jaeger, 1945).

Assuming that the seasonal variation of soil-air interface temperature oscillates sinusoidally (Eq. 2.3) over the year, with a mean value T_{mean} equal to the annual mean air temperature, an amplitude A_0 equal to $(T_{max} - T_{min})/2$, where T_{max} and T_{min} are the maximum and minimum air temperature respectively, an angular frequency ω (s^{-1}), and an oscillation period P (s), soil is homogeneous and isotropic, the soil temperature at a depth z (m) and time t (s) is shown in Eq. 2.4 (Kasuda and Archenbach, 1965).

$$T(0,t) = T_{mean} + A_0 \sin(\omega t) \tag{2.3}$$

$$T(z,t) = T_{mean} + A_0 e^{\frac{-z}{\sqrt{P\alpha/\pi}}} \sin\left[\omega t - \frac{-z}{\sqrt{P\alpha/\pi}}\right] \tag{2.4}$$

Soil is a porous multiphase material constituted of three main phases: solids (soil grains), liquid (water), and gas (air). When soil is fully saturated, all pores are filled with water; when soil is fully dry, all pores are filled with air; when soil is partially saturated, pores are filled with a mixture of water and air. When soil is dry, the conduction heat transfer takes place between soil particles that are in direct contact. The relationship between soil effective thermal conductivity and water content (ω) can be explained by solid particle and water interaction (Figure 2-3). At a very low water content (the exact value of which depends on soil texture and soil-specific surface area referred here as "θ_1"), the water film thickness is very thin and not enough to improve the contact between soil particles. Therefore, the soil thermal conductivity remains constant up to θ_1. After this water content threshold is exceeded, water bridges between solid particles start developing and increasing, which results in a rapid increase in thermal conductivity. Eventually, the increase in water content depends on the displacement of air by water. When this happens, the rate of increase in effective thermal conductivity slows (Sepaskhah and Borsma, 1979; Taranwski and Gori, 2002).

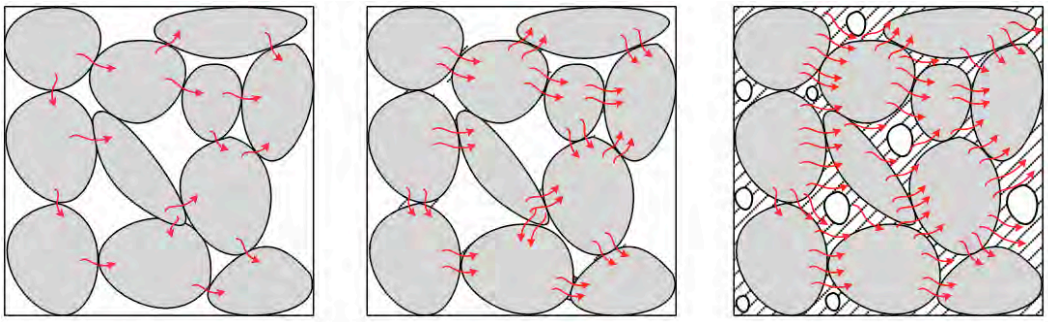

Figure 2-3 Heat flow in dry soil (a), partially saturated soil (b), and saturated soil (c)

2.3 SOIL THERMAL PROPERTIES

Soil thermal properties mainly depend on mineral content, porosity, degree of saturation, and temperature. The influence of each of those parameters is described below.

- **Minerals:** The thermal conductivity of quartz is higher than other minerals that constitute the soil. Cohesive soils have less mineral content; therefore, coarse-grained soils tend to have higher thermal conductivity than fine-grained soils.
- **Porosity:** The thermal conductivity of minerals is higher than that of air and water. Therefore, an increase in porosity increases the volumetric fraction of air and water, which results in a decrease of soil thermal conductivity.
- **Degree of saturation:** An increase in degree of saturation increases the volumetric fraction of water and decreases that of air. The thermal conductivity of air (λ_{air} =0.025 W/m.C) is much lower than that of water (λ_{water} =0.6 W/m.C);

therefore, an increase of degree of saturation increases soil effective thermal conductivity (Figure 2-4a).

- **Temperature:** Thermal conductivity of ice (λ_{ice} = 2.22 W/m.C at 0°C) is approximately four times higher than water thermal conductivity (λ_{water} = 0.6 W/m.C); therefore, when soil temperature drops below freezing, a part of the water will become ice and therefore increase the thermal conductivity (Figure 2-4b).

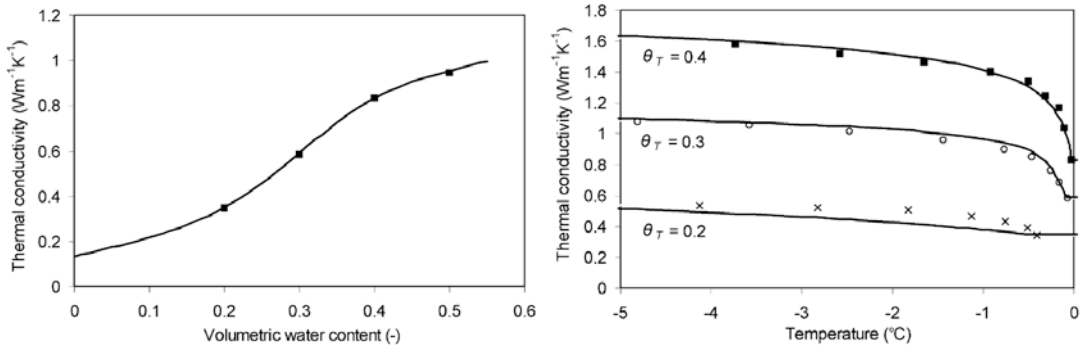

(a) **(b)**

Figure 2-4 (a) Thermal conductivity vs. volumetric water content and (b) temperature for different volumetric ice contents (right) *(From Hansson et al., 2004)*

Different models have been developed in the literature to predict the effective thermal conductivity of partially saturated soils, and they vary in complexity and applicability (Kersten, 1949; Gemant, 1952; Van Rooyen and Winterkon, 1957; De Vries, 1963; Johansen, 1975; Campbell, 1985; Côté and Konard, 2005; Lu and Horton, 2007). One of the first models developed was by Kersten (1949), and was based on a

large number of laboratory measurements. This is an empirical model that relates the effective thermal conductivity of soil to water content and requires only the bulk density ρ_b (kN/m^3) as an input parameter.

Johansen (1975) was the first to introduce the normalized thermal conductivity concept (λ_n). The Johansen model was developed based on the data provided by Kersten (1949). Johansen provided a relationship between the normalized thermal conductivity and soil degree of saturation for fine grained and coarse-grained soils. Côté and Konard (2005) adopted the same concept as Johansen and expanded it to include more types of soils in frozen and unfrozen conditions. Lu and Horton (2007) also adopted the same concept and proposed another model based on a large database of soil testing, which they claim provides a better prediction of soil thermal conductivity than other models, especially at low moisture content.

2.3.1 Johansen (1975)

Based on the data published by Kersten (1949) on soil effective thermal conductivity of coarse and fine-grained materials, Johansen (1975) was the first to introduce the concept of normalized thermal conductivity. This concept is characterized by a single curve that relates the normalized thermal conductivity to the soil degree of saturation (Eq. 2.5). In this concept, the soil effective thermal conductivity can be predicted by knowing saturated and dry thermal conductivities (λ_{sat} and λ_{dry} respectively), and the function of soil degree of saturation f (S_l). When $\lambda = \lambda_{dry}$, f (S_l) = 0 represents the lower limit condition. The upper limit condition occurs when $\lambda = \lambda_{sat}$, and f(S_l) = 1.

$$\lambda_n = \frac{\lambda_e - \lambda_{dry}}{\lambda_{sat} - \lambda_{dry}} = f\left(S_l\right) \tag{2.5}$$

The empirical equation of f (S_l) proposed by Johansen is given in Eq. 2.6 for unfrozen medium and fine sand and Eq. 2.7 for unfrozen fine-grained soils.

$$\lambda_n = 0.7\log\left(S_l\right) + 1 \quad \left(S_l > 0.05\right) \tag{2.6}$$

$$\lambda_n = \log\left(S_l\right) + 1 \quad \left(S_l > 0.1\right) \tag{2.7}$$

The saturated thermal conductivity λ_{sat} can be calculated using a geometric mean equation as given in Eq. 2.8:

$$\lambda_{sat} = \lambda_s^{1-\phi}\lambda_w^{\phi} \tag{2.8}$$

where λ_s is the solids thermal conductivity (Table 2-1), λ_w is the water thermal conductivity, and ϕ is the porosity as a decimal. The solids thermal conductivity can be calculated using a geometric mean equation and the quartz content of the total solids, m (unitless) (Eq. 2.9).

$$\lambda_s = \lambda_q^{m}\lambda_0^{1-m} \tag{2.9}$$

with λ_q representing the quartz thermal conductivity and λ_0 the thermal conductivity of other minerals. Variable λ_0 was assumed to be 2 W/m.K. for soils with m > 0.2 and 3 W/m.K. for soils with m ≤ 0.2 W/m.K,

The soil dry thermal conductivity can be calculated as a function of the bulk density of soil using the semi-empirical equation proposed by Johansen (1975) (Eq. 2.10).

$$\lambda_{dry} = \frac{0.135\rho_b + 64.7}{2700 - 0.947\rho_b} \tag{2.10}$$

Table 2-1 Average value for thermal conductivity of solid particles computed from various sources *(After Côté and Konard, 2005)*

Material	ρ_s (g/cm^3)	λ_s (W/m.K)
Rock		
Anorthosite	2.73	1.8
Basalt	2.90	1.7
Diabase	2.98	2.3
Dolostone	2.90	3.8
Gabbro	2.92	2.2
Gneiss	2.75	2.6
Granite	2.75	2.5
Limestone	2.70	2.5
Marble	2.80	3.2
Quartzite	2.65	5.0
Sandstone	2.80	3.0
Schist	2.65	1.5
Shale	2.65	2.0
Syenite	2.80	2.0
Trap rock	2.90	2.0
Soil and Organic Matter		
Coal	1.35	0.26
Peat	1.50	0.25
Silt and clay	2.75	2.90

2.3.2 Côté and Konard (2005)

Based on a large database that includes different soil types in frozen and unfrozen conditions, Côté and Konard (2005) proposed an empirical equation of the function λ_n. Beside the degree of saturation, this empirical function includes the soil texture dependent parameter κ (Eq. 2.11)

$$\lambda_n = \frac{\kappa S_l}{1+(\kappa-1)S_l} \tag{2.11}$$

Some values of the parameter κ provided in their paper are given in Table 2-2.

Table 2-2 κ factor in Eq. 2.11 *(From Côté and Konard, 2005)*

Soil Type	**κ**	
	Unfrozen	*Frozen*
Gravels and coarse sands	4.60	1.70
Medium and fine sands	3.55	0.95
Silty and clayey soils	1.90	0.85
Organic fibrous soils (peat)	0.60	0.25

The saturated thermal conductivity of the unfrozen soil can be calculated using the geometric mean equation provided in their paper:

$$\lambda_{sat} = \lambda_s^{1-\phi} \times 0.6^{\phi} \tag{2.12}$$

In addition, and based on their large database, they provided an empirical equation for the prediction of the dry thermal conductivity, as given in Eq. 2-13.

$$\lambda_{dry} = \chi 10^{-\eta\phi} \tag{2.13}$$

where χ and η are unitless particle shape parameters, as given in Table 2-3.

Table 2-3 χ and η factors in Eq. 2.13 *(From Côté and Konard, 2005)*

Material	**χ**	**η**
Crushed rocks and gravels	1.70	1.80
Natural mineral soils	0.75	1.20
Organic fibrous soils (peat)	0.30	0.87

2.3.3 Lu and Horton (2007)

Based on a database of 12 different soils, Lu and Horton (2007) proposed an empirical equation for λ_n (Eq. 2.14). Lu and Horton used an exponential function of λ_n and claimed that their model was better at predicting soil thermal conductivity than the Johansen (1975) and Côté and Konard (2005) models.

$$\lambda_n = \exp\left\{\alpha\left[1 - S_l^{(\alpha-1.33}\right]\right\} \tag{2.14}$$

In Eq. 2.14, α is a unitless soil texture dependent factor and 1.33 is a shape factor. The factor α was obtained by fitting used data to Eq. 2.14 and it was found that it is equal to 0.96 for coarse textured soil and 0.27 for fine textured soils. In addition, Lu and Horton (2007) provided an empirical linear equation to predict soil dry thermal conductivity (Eq. 2.15) as a function of porosity.

$$\lambda_{dry} = -a\phi + b \tag{2.15}$$

where "a" and "b" are fitting parameters and found to be 0.56 and 0.51 respectively (for $0.2 < \phi < 0.6$).

Other relevant soil thermal properties to energy pile design which were not defined in the discussion of the papers above include volumetric heat capacity C ($J/m^3.K$), specific heat capacity c_p (J/kg.K), and thermal diffusivity α (m^2/sec). The volumetric heat capacity is the amount of heat required to raise a unit volume by 1°C. The specific heat capacity is the amount of heat required to raise a unit weight of a material by 1°C. This property is similar to the elasticity modulus in mechanical problems. The soil volumetric heat capacity can be calculated using Eq. 2.16

$$C_{soil} = \sum_{i=1}^{4} \rho_i \times \theta_i \times c_{p,i} \quad \text{i = solids, organic matter, water, air} \tag{2.16}$$

where θ is the volumetric fraction of each phase. Thermal diffusivity is the ratio of thermal conductivity to the volumetric heat capacity. This property describes how fast heat propagates in the soil.

2.4 EFFECT OF CLIMATIC FACTORS ON SOIL THERMAL PROPERTIES

Different climatic zones exist across the world, differing in four main factors: 1) air temperature, 2) rainfall, 3) evapotranspiration, and 4) relative humidity (RH). Each of these four factors affects thermal properties, moisture content (degree of saturation profile), and the water table in the SSL. For traditional long boreholes used as heat exchangers, the soil can be assumed to be homogenous during the design process because climate-induced variations occur at a shallow depth relative to the total length of the borehole. This assumption is not valid for energy piles. The mechanical and thermodynamic performance of energy piles is significantly affected by soil variability because a greater proportion of these piles are in direct contact with the SSL.

Rainfall distributions, and the resulting elevation and fluctuation of the ground water table, is another parameter that impacts soil properties and conditions. Well-distributed rainfall and snow, characteristic of cold climates, keeps the SSL saturated over the year. Conversely, rainfalls in hot climates are infrequent and sporadic which significantly impact the saturation profile.

Furthermore, evapotranspiration, which is the sum of evaporation and transpiration, impacts the soil moisture profile. Because of the high temperatures in hot

climates, water evaporates and trees and grass pull water from the ground, which results in soil drying. This influences the moisture content profile in the SSL. Changes in RH also affect soil moisture. Soil suction is related to RH through the psychometric law, and the water content (or degree of saturation) depends on suction via the soil water retention curve (Fredlund and Xing, 1994; Lu and Nikos, 2004).

In conclusion, climatic factors impact soil conditions in the SSL, especially the soil saturation profile (Figure 2-5). Because of the direct relationship between soil thermal properties and degree of saturation, these factors should be taken into account when designing energy piles, especially in hot climates.

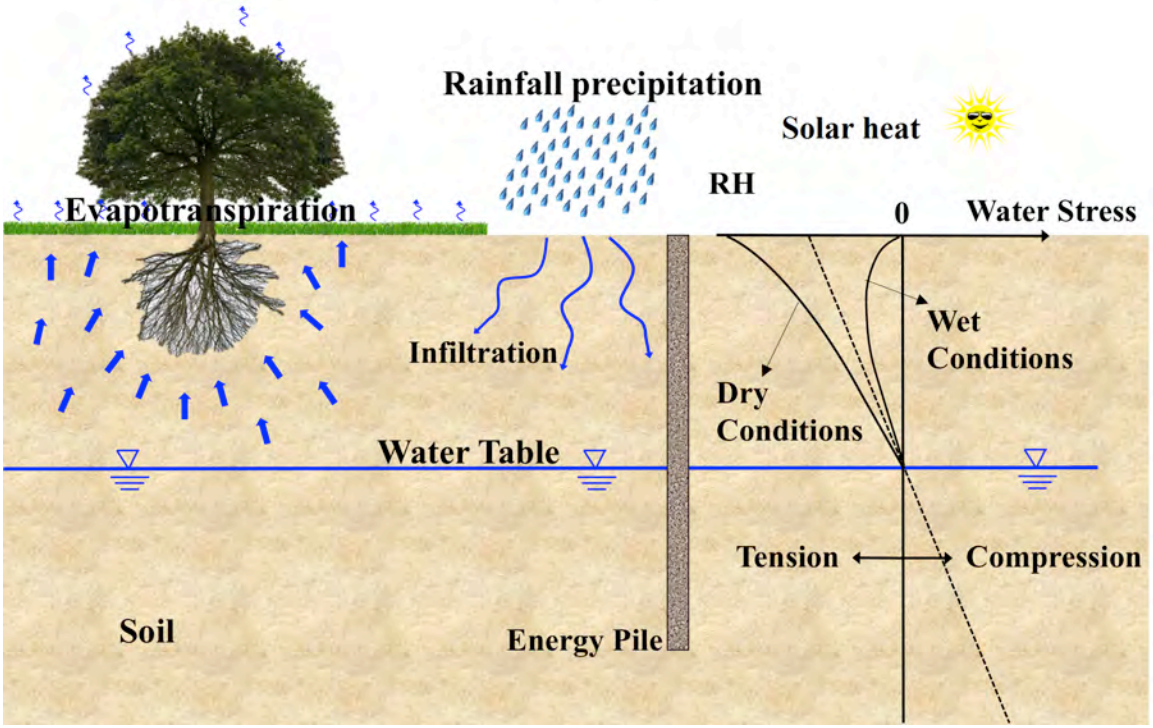

Figure 2-5 Climatic factors

2.5 THERMO-MECHANICAL BEHAVIOR OF SOILS AND ENERGY PILES

The properties and behavior of soil and concrete are temperature dependent (Farouki O.T, 1986, Cekerevac and Laloui, 2004; McCormac and Brown, 2009); therefore, the operation of SGES will impact the behavior of the foundation piles. Knowledge on the thermo-mechanical behavior of energy piles is progressively growing thanks to the increasing number of thermo-mechanical full-scale load tests that have been performed and reported in literature. All the reported tests (Brandl, 1998, 2006; Laloui et al., 2003; Laloui et al., 2006; Bourne-Webb et al., 2009; McCartney and Rosenberg, 2011; Amataya et al., 2012; Kalanhidou et al., 2012; Olgun et al., 2012; McCartney and Murphy, 2012; Stewart and McCartney, 2013) concluded that the use of energy piles as GHE for SGES induce a change in stress and strain and load redistributions in the pile. From the information gathered in those tests it was possible to relate the change in the mechanical response of the tested piles to the increased temperature level, soil strength, and boundary conditions. The thermo-mechanical behavior of energy piles was described by Bourne-Webb et al. (2009) and Amataya et al. (2012) using a simple approach based on a review of thermo-mechanical load tests on energy piles. When analyzing an energy pile, the load distribution and strain profile are both of great importance. Under mechanical load only, the stresses in the pile are directly related to strains. When the vertical pile is subjected to a thermal load, it experiences additional thermal strains. These additional strains are referred to as $\varepsilon_{T\text{-}Obs}$, which is the measured strain resulting from the thermal load around a neutral point. The neutral point is defined as the point where there is no change in strain because of the thermal load on the

pile. When the pile is heated, it experiences expansion and it moves upward above and downward below the neutral point. The opposite is true when the pile is cooled; it experiences contraction and it moves downward above the neutral point and upward below the neutral point. Another part of the vertical strain is restrained because of the soil resistance ($\varepsilon_{T\text{-}Rest}$). The sum of $\varepsilon_{T\text{-}Obs}$ and $\varepsilon_{T\text{-}Rest}$ is the free strain ($\varepsilon_{T\text{-}Free}$), which is the strain that the pile would experience if it were not inhibited by the soil and the structure. The thermal stresses (σ_T) caused by the restrained strains and the thermally induced load, P_T, can be calculated using Eq. 2.17. Note that the negative sign means that the developed thermal load is in the opposite direction of the measured strain.

$$P_T = -EA\varepsilon_{T-restrained} = -EA\left(\varepsilon_{Free} - \varepsilon_{T-observed}\right) = -EA\left(\beta\Delta T - \varepsilon_{T-observed}\right) = \sigma_T A \quad (2.17)$$

β is the coefficient of thermal expansion ($^oC^{-1}$), E is the Young's modulus of the pile material (MPa), and A is the cross sectional area of the pile (m^2). In energy piles, the total load in the pile is the sum of the mechanical and thermal load. More details with different examples about this approach are presented in Bourne-Webb et al. (2009) and Amataya et al. (2012).

Amataya et al. (2012) summarized the results of three full thermo-mechanical tests performed on energy piles at different locations. The first test was performed on two energy piles (a heat sink pile and a main test pile) at Lambeth College, London, UK (Bourne-Webb et al., 2009). The heat sink pile was tested without any mechanical load while the main test pile was tested under a load of 1200 kN maintained for 46 days. The piles were subject to both heating and cooling cycles. The second test was performed on a pile that is a part of new building foundation (Laloui et al., 2003, 2006). The energy

pile was tested at different mechanical load levels ranging from 0 (T1) to 1300 kN (T7) corresponding to different building construction stages. The pile was subjected only to heating cycles. The third test was part of an operational GSHP system of 143 piles installed in Bad Schallerbach, Austria (Brandl, 1998, 2006). During operation, the energy piles experienced both heating and cooling cycles. More details on soil conditions, testing program, and testing conditions can be found in the original publications of each test. Amataya et al. (2012) summarized the results of the three tested piles. The thermally induced axial stress and soil-pile friction for the test without any mechanical loads (London heat sink pile and Lausanne T1) are presented in Figure 2-6. It was shown that energy piles exhibited a linear elastic behavior under thermal load. The rate of increase in axial stress was observed as 192 kPa/°C for the London pile and 104 kPa/°C for the Lausanne pile. The rate of increase in pile-soil friction was observed to be 2.1–2.5 kPa/°C for the London pile and between 0.5 and 1.5 kPa/°C for the Lausanne pile.

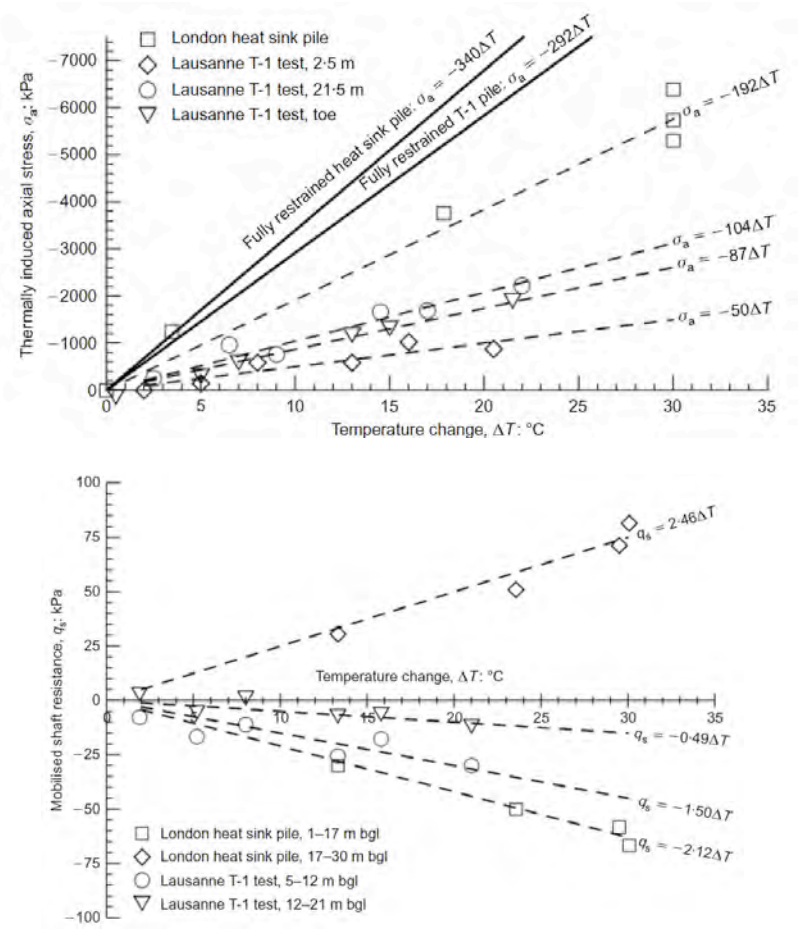

Figure 2-6 Thermally induced axial stress and soil-pile friction without mechanical load *(From Amataya et al., 2012)*

Figure 2-7 shows the thermally induced axial stress and pile-soil friction when piles were subjected to thermal and mechanical loads. The results show that under thermo-mechanical loads, the thermally induced stress was larger than the results under thermal load only and were observed to be 329 kPa/°C for the London pile and 153 kPa/°C for the Lausanne pile. In addition, the thermally induced pile-soil friction

increased under thermo-mechanical load and ranged from 1.5 to 5.9 kPa/°C for the London pile and 0.5 to 5 kPa/°C for the Lausanne pile.

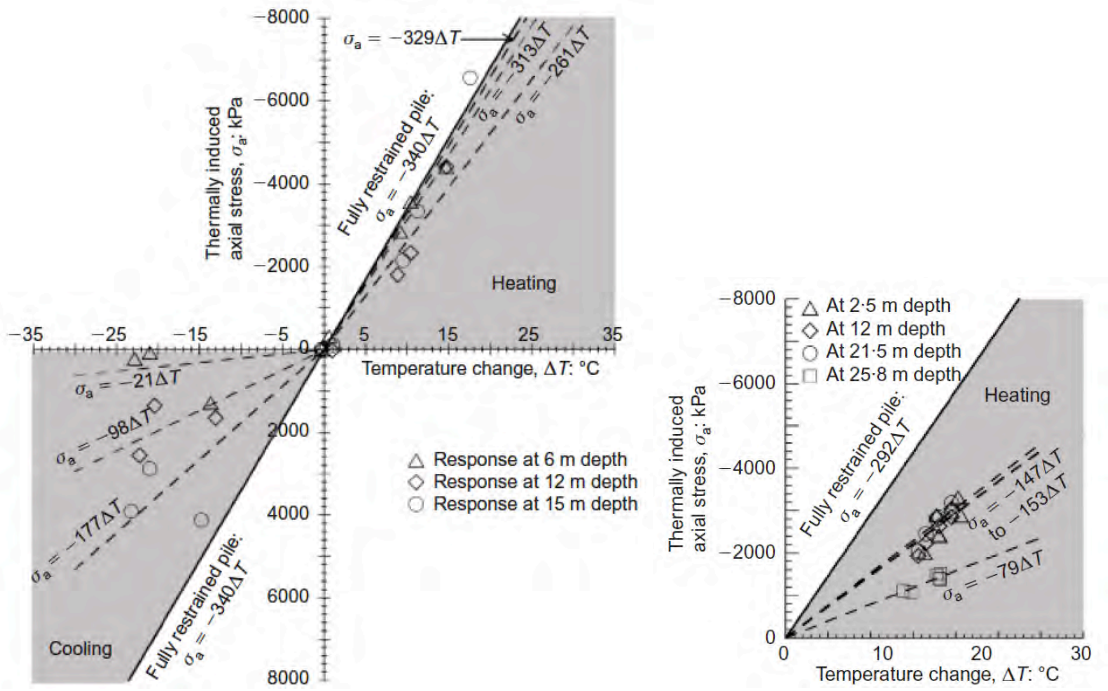

Figure 2-7 Thermally induced axial stress and soil-pile friction under thermo-mechanical load *(From Amataya et al., 2012)*

McCartney and Rosenberg (2011) performed a series of centrifuge tests on scaled energy piles subjected to thermo-mechanical loads. The tested piles were only subjected to heating cycles. From the load-settlement curves of the tested piles (Figure 2-8), McCartney and Rosenberg concluded that when heating the pile from 15 to 60 °C (ΔT = 45 °C), the pile experiences an increase in side shear of 40%. However, in practice, the

increase in pile temperature ΔT that a pile would experience would be around 15 °C, and so the above value would be less.

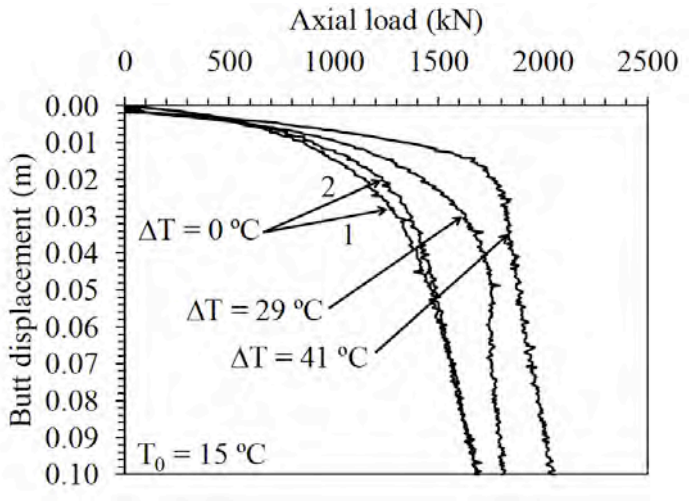

Figure 2-8 Load-settlement curve for scale-model energy pile *(From McCartney and Rosenberg, 2011)*

Understanding the long-term behavior of energy piles and in particular their displacements is very important to limit their impact on the structural integrity of the building. This may be accomplished by limiting the additional deformation to within tolerable limits. During their lifetime piles exhibit creep related to the time dependent movements under a constant mechanical load applied by the superstructure. The creep rate is dependent on soil type, soil texture, applied stress level, and temperature. This last factor is more significant in clayey soils (Mitchell and Campanella, 1964; Mitchell and Campanella, 1986; Burghignoli et al., 2000; Briaud et al., 2013). As an example, Figure

2-9 presents the experimental results of a triaxial creep test performed by Mitchell et al. (1968) on undisturbed San Francisco Bay mud samples in undrained conditions. The strain rate and strain increased after raising the soil sample temperature by 16.7 °C, which is close to the typical temperature increase in geothermal applications. The strain rate of the samples increased by a factor of approximately 10, after the start of the temperature changes. In addition, Figure 2-9b shows that the strain rate decreased with an increase in strain, but more slowly for higher temperatures.

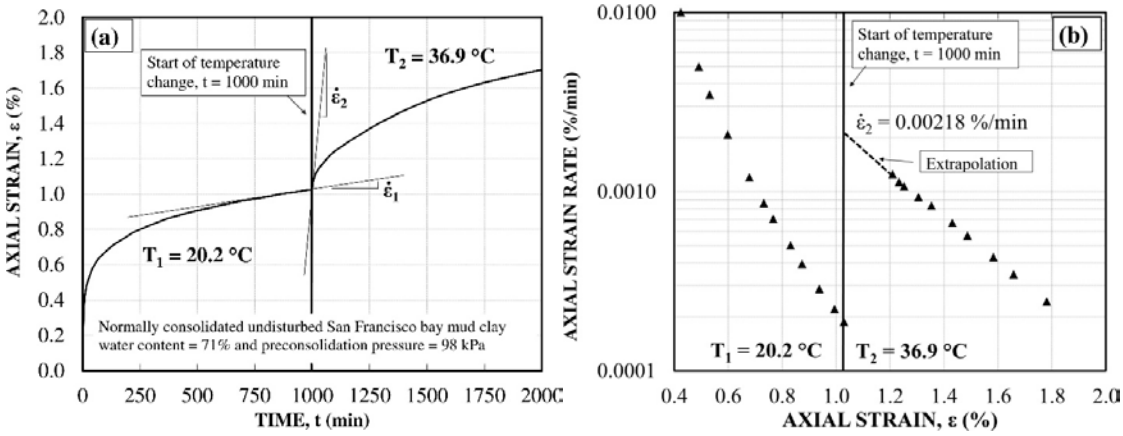

Figure 2-9 Axial strain vs. time (a) and strain rate vs. axial strain (b) of an undisturbed San Francisco Bat mud sample subjected to temperature change
(Modified from Mitchell et al., 1968)

There are some additional experimental studies looking at the effect of temperature on the time-dependent response of clays; they are mainly focused on the behavior of the Boom clay, a material studied in the context of the design of nuclear waste disposal (e.g. De Bruyn and Thimus, 1996; Cui et al., 2009; Romero, 1999).

Romero (1999) found that the effect of temperature on normally consolidated samples of Boom clay is quite noticeable, while the impact of temperature on creep rate for over-consolidated samples is practically negligible.

Based on extensive in-situ creep tests on grouted anchors at the National Geotechnical Experimental Site (Texas A&M University), Briaud (1998) proposed the following model (Eq. 2.18) to evaluate the time dependent displacement of anchors and piles:

$$\frac{S_t}{S_1} = \left(\frac{t}{t_1} \right)^n \tag{2.18}$$

In Eq. 2.18, n is the viscous exponent and t (min), t_1, S_t (m), and S_1 (m) are the time, reference time, the displacement at time t, and the displacement at time t_1 respectively. The viscous exponent can be evaluated from field creep test or from the pressuremeter test (Briaud, 2013). The value of n is obtained from the slope of the plot of log S_t/S_{t1} vs. log t/t_1 from field creep test or as the slope of the plot of log E_t/E_{t1} vs. log t/t_1 from pressuremeter test (Briaud, 2013). E_t and E_{t1} are the secant modulus measured during a pressure holding step from a pressuremeter test corresponding to t and t_1 respectively.

2.6 FEASIBILITY OF SHALLOW GEOTHERMAL ENERGY SYSTEMS

Shallow geothermal energy systems are known to be more efficient than convectional HVAC in terms of power consumption and associated CO_2 gas emissions. The use of energy piles, as GHE for SGES, is relatively new and uncommon worldwide; therefore, very few publications exist that deal with the feasibility of such systems. This

technology is very active in European countries (i.e. Austria, Germany, and the UK) while it is still under development in the USA because of the lack on information and full-scale tests. The aim of the economic feasibility study in this dissertation is to evaluate the financial benefit of adopting SGES in future buildings in cooling dominated climates. To achieve this goal, a Life Cycle Cost (LCC) analysis was performed. LCC analysis is a method to determine the most effective system among a range of different alternatives that can be technically implemented. LCC accounts for all costs related to the installation, operation, and maintenance of a SGES over a defined period of time. LCC accounts for inflation rates, energy price increases, and future maintenance and rehabilitation. In a LCC, the factors that should be considered are:

- **Loads and efficiencies:** this item is related to the magnitude of the heating and cooling loads that are related to building sizes. In addition, it is related to the efficiency and performance of used heat pumps
- **Initial and installation subsurface materials cost:** this item looks at the initial cost of the materials constituting the embedded part of the SGES system including HDPE pipes and grout or concrete. This item also looks at the installation cost of the GHE including drilling, pipes, and grout.
- **Initial and installation equipment cost:** this item looks at the equipment costs and installation cost of heat pumps and conventional HVAC systems.
- **Initial and installation controls cost:** this item looks at the initial and installation cost of the control systems for both SGES and conventional HVAC.

- **Replacement equipment cost:** this item looks at the equipment expected life, the future equipment cost, and future labor cost of both systems.
- **Energy consumption cost:** this factor looks at operational cost (fuel oil, natural gas, propane, wind, solar, etc.) for both systems and inflation rates.
- **Maintenance cost:** this factor looks at the maintenance cost and inflation over time of the heating and cooling system.
- **Water consumption cost:** this item looks at the cost of water consumption of SGES compared to conventional HVAC. This factor is important to consider when comparing the SGES to systems that consume a lot of water during operation, such as a cooling tower system.
- **CO_2 emission cost:** this item looks at the cost of individual and global CO_2 gas emission. At the individual level, some countries and states started new policies of taxing CO_2 emissions to push industries and people toward using more green and energy efficient systems. At the global level, CO_2 gas emission contributes to the climate change problem, which exacerbates disasters around the world, including droughts and floods.

2.7 NUMERICAL MODELING

In this dissertation, the numerical modeling tool that was used to model the different laboratory and in-situ tests was CODE_BRIGHT (Olivella et al., 1996). This program is able to compute coupled thermo-hydro-mechanical (THM) non-isothermal problems in unsaturated/saturated soils (e.g. Alonso et al., 1999; Gens et al. 2008; Sanchez et al., 2012). The theoretical framework of this tool is presented in brief in this section to

avoid repetition in the different sections of the dissertation. A detailed theoretical framework can be found in Olivella et al. (1996). All the problems numerically solved in this dissertation only include the thermal and hydraulic problem. Problems involving liquid pressure, air pressure, and temperature changes in soils, are addressed in CODE_BRIGHT by solving the equation associated with balance of the water mass (Eq. 2.19), balance of the air mass (Eq. 2.20), and balance of the internal energy, respectively (Eq. 2.21). The dependent variables are calculated from the unknowns using the constitutive equations. For example, water flux will be calculated using Darcy's law and heat flux will be calculated using Fourier's law. In the following equation, "w" and "a" superscripts refer to water and air species respectively; "l" and "g" subscripts refer to liquid and gas respectively.

$$\frac{\partial}{\partial t}\overbrace{\left(\theta_l^w S_l \phi + \theta_g^w S_g \phi\right)}^{\text{Mass of water in liquid and gas phase}} + \nabla \overbrace{\left(j_l^w + j_g^w\right)}^{\text{Total flux of water}} = \overbrace{f^w}^{\text{External supply of water}} \tag{2.19}$$

$$\frac{\partial}{\partial t}\overbrace{\left(\theta_l^a S_l \phi + \theta_g^a S_g \phi\right)}^{\text{Mass of air in liquid and gas phase}} + \nabla \overbrace{\left(j_l^a + j_g^a\right)}^{\text{Total flux of air}} = \overbrace{f^a}^{\text{External supply of air}} \tag{2.20}$$

$$\frac{\partial}{\partial t}\overbrace{\left(E_s \rho_s \left(1-\phi\right) + E_l \rho_l S_l \phi + E_g \rho_g S_g \phi\right)}^{\text{Internal energy in solid, liquid, and gas phase}} + \nabla \overbrace{\left(i_c + j_{Es} + j_{El} + j_{Eg}\right)}^{\text{Total flux of energy}} = \overbrace{f^Q}^{\text{External supply of heat}} \tag{2.21}$$

where:

θ_l^w = mass of water per unit volume of liquid

θ_l^a = mass of water per unit volume of gas respectively

j_l^w = total mass flux of water in the liquid phase

j_g^w = total mass flux of water in the gas phase

E_s, E_l, E_g = internal energy of the solid, liquid, and gas phase, respectively

i_c = conductive heat flow

ϕ = porosity

ρ_s, ρ_l, ρ_g = soild, liquid, and gas density, respectively

j_{Es}, j_{El}, j_{Eg} = net flow of energy in mineral, of energy in liquid, and of energy in gas, respectively

f^w,f^a ,f^w = the internal / external supply of water, air, and energy respectively.

The balance equations (Eq. 2.19, 2.20, and 2.21) have to be solved in conjunction with the constitutive equations of Darcy' law for liquid flow (Eq. 2.22), and Fourier' law for heat flow (Eq. 2.23).

$$q_l = -K_l\left(\nabla P_l - \rho_l g\right) \tag{2.22}$$

$$i_c = -\lambda \nabla T \tag{2.23}$$

In these equations, q_l is the liquid flow, P_l (MPa) is the liquid pressure, g (m/sec^2) is the gravity, K_l is the hydraulic permeability (m/sec), and i_c (W/m^2) is the conduction heat flow. K_l can be expressed as a function of the intrinsic permeability, k, and the relative permeability function, $k_{r,l}$, that defines the variation of k with liquid saturation condition (Eq. 2.24). In CODE_BRIGHT, λ (w/m.K) is expressed as a function of the dry and saturated thermal conductivities and the liquid degree of saturation S_l using the square root model (Eq. 2.25)

$$K_l = k\frac{k_{r,l}}{\mu_l} \text{ with } k_{r,l} = S_e^{\phi} \text{ where } S_e = \frac{S_l - S_{lr}}{S_{ls} - S_{lr}} \tag{2.24}$$

$$\lambda = \lambda_{sat}\sqrt{S_l} + \lambda_{dry}\left(1 - \sqrt{S_l}\right) \tag{2.25}$$

S_e, S_{lr}, and S_{ls} are the effective, minimum or residual, and maximum degree of liquid saturation respectively, and μ_l (kg/sec.m) is water viscosity. The degree of saturation can be related to the suction Ψ (MPa) (Eq. 2.26) using the water retention curve. As an example, van Genuchten (1980) model of the retention curve is presented in Eq. 2.27.

$$\psi = P_g - P_l \tag{2.26}$$

$$S_e = \left[1 + \left(\frac{\psi}{P_0} \right)^{\frac{1}{1-\lambda_0}} \right]^{-\lambda_0} \tag{2.27}$$

P_g, (MPa) P_0 (MPa), and λ_0 (unitless) are gas pressure, air entry value, and van Genuchten model fitting parameter respectively.

3 THERMAL CONE TEST

The Cone Penetration Test (CPT) is an in-situ test to determine soil stratigraphy and strength. In addition, the CPT cone may be instrumented with a sensor to measure pore water pressure in the soil, in order to locate the water table and determine the soil hydraulic conductivity k [cm/s] and horizontal consolidation coefficient c_h (m^2/s). The soil hydraulic properties are determined using the Pore Water Pressure dissipation test (PWP). This section of the dissertation presents an in-situ test to determine soil thermal properties using the CPT. The test, called the Thermal Cone Test (TCT), consists of instrumenting the CPT cone with a thermocouple and the CPT rod with a heater. The initial testing plan was to use the heater element to apply a thermal load on the soil, and then use the thermocouple to measure the resulting soil temperature decay after turning off the heater. However, it was found in this study that during the pushing process, the CPT cone temperature increases because of the friction between the soil and the cone and this increase in temperature can be relayed on in back calculating soil thermal properties. The measured curve of soil temperature decay with time is then used to back calculate the soil thermal properties, using a methodology similar to the one used for calculating the soil hydraulic properties from the pore water pressure dissipation test. The use of the CPT method requires calibration of the TCT, the methodology for which is presented in this section of the dissertation using extensive numerical simulation supported by 11 in-situ TCT tests and laboratory measurements.

3.1 INTRODUCTION

With the growth of engineering applications, such as energy geo-structures, where heat propagation in the soil is an important parameter, the ability to accurately and easily quantify soil thermal properties is of great importance. These properties are used to study the soil behavior under thermal or coupled Thermo-Hydro-Mechanical loading. Soil thermal properties are currently evaluated by laboratory and in-situ tests, which may be classified as steady state or transient methods. Some steady state methods include: the Guarded Hot Plate test (ASTM C177), the Cylindrical Configuration test (Kersten, M.S., 1949), the In-Situ Sphere test (Mochlinski, K. 1964), and the Heat Meter test (Scott, R.F., 1969). Examples of transient methods are: the Probe Method (Van der Held and Van Drunen, 1949), the Periodic Temperature Waves (Forbes, J.D. 1849), and the Thermal Shock Method (Shannon and Wells, 1947).

The TCT test uses existing equipment, including the CPT cone and rod. The main advantage of the TCT test is the ability to evaluate soil stratigraphy, mechanical properties, and hydraulic properties using the CPT cone during the test. In addition, the TCT test is an easy and quick test and it is performed under natural soil conditions at any depth that can be reached by the CPT rod. The proposed test is classified as a transient in-situ test because the temperature is variable with time.

An in-situ test based on a thermal probe instrumented with thermocouples was proposed by Lutenegger and Lally (2001). In the thermal probe test, the probe is pushed in the soil to the desired depth and after 24 hours, a constant heat load Q (W/m) is applied by the probe. From the recorded temperature increase, the thermal conductivity

of the soil is back calculated using the infinite line heat source theory. This paper carries the methodology further and makes use of existing geotechnical testing tools. The approach proposed in this paper (based on the TCT) provides two major advantages over the thermal probe test. First, the duration of the thermal probe test is 24 hours plus additional heating time, while the duration of TCT test is less than 1 hour. Secondly, only soil thermal conductivity is obtained from the thermal probe test, but when using the methodology proposed for the TCT, thermal conductivity and thermal diffusivity can be obtained as well. It is worth mentioning that these thermal properties are obtained in addition to the other properties derived from the CPT (i.e. from the same exploration) including soil stratigraphy, mechanical properties, and hydraulic properties.

This section of the dissertation details the proposed set-up for the TCT and associated methodology to calculate the thermal properties of the soil at different depths. Extensive numerical simulations validated by experimental in-situ tests were used to calibrate the TCT. The calibration curves were validated by in-situ TCT and laboratory tests. A novelty of the proposed approach is that it enables in-situ and quick characterization of the thermal conductivity of the soil.

3.2 CONCEPTUAL BACKGROUND OF THE THERMAL CONE TEST

The CPT cone is instrumented with a thermocouple and the rod is instrumented with a heater (Figure 3-1) to enhance the CPT device. The initial plan was to apply a thermal pulse with a heater (at the desired position) and to track the temperature decay in the soil with the thermocouple. However, during the test, it was noticed that friction between soil and CPT cone generates sufficient heat to increase the cone temperature. This

increase in cone temperature decays after stopping the cone at the desired depth. The thermal properties of the soil are then back calculated from the cone temperature versus time decay curve produced from the thermocouple readings. However, this section of the dissertation presents both the results of temperature decay caused by the friction between soil and cone and cause by the thermal load applied by the heater element.

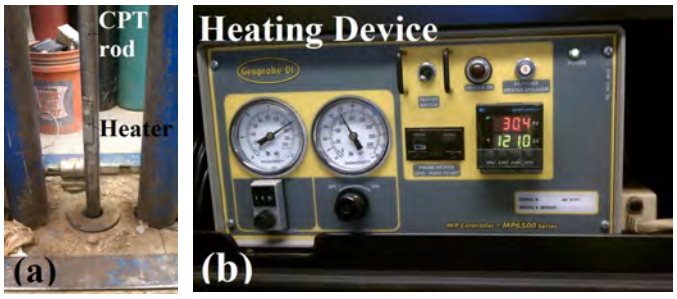

Figure 3-1 Heater element installed on CPT rod (a) and heating device (b)

The idea for the proposed in-situ test was inspired by the pore water pressure (PWP) dissipation test (Janbu and Senneset, 1974; Wissa, et al., 1975; Torstensson, B.A., 1975) and the equivalency between soil thermal flow problems and soil hydraulic flow problems (Table 3-1). The PWP dissipation test results are used to back calculate the soil hydraulic conductivity k (cm/s) using an empirical equation (Eq. 3.1) (Mayne, P., 2007) and soil horizontal consolidation coefficient c_h (m^2/s(Eq. 3.2) (Teh and Houlsby, 1991). These formulas are based on the time t_{50} to 50% dissipation of the initial excess pore water pressure ΔU_i recorded from the test, and the time factor corresponding to 50% dissipation, T_{50}.

Table 3-1 Equivalency between thermal flow and hydraulic flow problems *(Briaud, 2013)*

Parameter	Flow of Water	Flow of Heat
Quantity	Volume V (m^3)	Heat Q (J)
Potential	Head h (m)	Temperature T (K)
Gradient	Hydraulic gradient i_h (unitless)	Temperature gradient i_t (K/m)
Flux	Flow rate Q (m^3/s)	Heat transfer rate H (J/s)
Flux density	Velocity v (m/s)	Heat flow q (J/s.m^2)
Conductivity	Hydraulic conductivity k_h (m/s)	Thermal conductivity k_t (J/s.K.m)
Law	Darcy	Fourier
Storage	Compressibility	Specific heat c_p (J/kg.K)

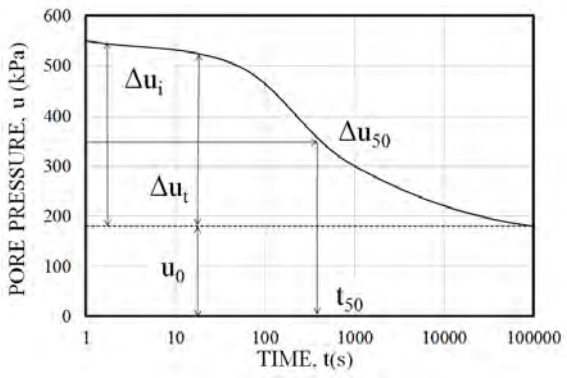

Figure 3-2 Results of Pore Water Pressure (PWP) dissipation test

$$k\left(cm/\sec\right)\approx\frac{1}{\left(251\times t_{50}\right)^{1.25}} \tag{3.1}$$

$$c_h\left(m^2/\sec\right)\approx\frac{T_{50}\times a^2\times\sqrt{I_R}}{t_{50}} \tag{3.2}$$

where, "a" is the cone diameter (m), I_R is the rigidity index of the soil (IR= G/s_u), G (kPa) is the elastic shear modulus, and s_u (kPa) is the undrained shear strength. Because

of the similarity between the dissipation of pore pressure and heat dissipation, this section of the dissertation proposes two formulas to back calculate the effective thermal conductivity (Eq. 3.3) and thermal diffusivity (Eq. 3.4) from the temperature dissipation curve obtained from the TCT similar in form to Eq. 3.1 and Eq. 3.2, respectively, as follows:

$$\lambda(W/mK) \approx \frac{1}{\left(A \times t_{50}\right)^{B}} \tag{3.3}$$

$$\alpha\left(m^2/s\right) = \frac{T_{50} \times a^2 \times \chi}{t_{50}} \tag{3.4}$$

where A, B, χ, and T_{50} are unitless parameters determined from the calibration of the TCT test. Note that in Eq. 3.3 and Eq. 3.4, t_{50} (sec) is the recorded time from the TCT and T_{50} is the time factor normalized against the soil thermal diffusivity and cone diameter, required to dissipate half of the initial increase in temperature, ΔT_i.

3.3 METHODOLOGY

The temperature decay technique to evaluate material properties was used in different commercial tools, for example, the Fredlund Thermal Conductivity Sensor that was developed by GCTS to evaluate the matric suction from temperature measurement. The majority of the instruments require calibration to relate the measured parameter to the output parameter. The main measurement from the TCT test is the cone temperature decay vs. time; therefore, a calibration curve needs to be developed to relate soil thermal properties to the measured parameter, which is t_{50} in the TCT application. The following methodology was used to develop the calibration curve: first, 11 in situ TCT tests were performed at different sites and soil samples were extracted from each site for

laboratory testing. Secondly, a numerical model was developed to simulate the TCT test and it was validated by one of the 11 in-situ tests. Thirdly, the numerical model was used extensively to simulate a wide range of soil thermal properties, and from each simulation, t_{50} was evaluated. Fourthly, the calibration parameters A, B, χ, and T_{50} (Eq. 3.3 and 3.4) were evaluated from the numerical model results. Finally, the proposed equations (Eq. 4 and Eq. 5) were validated by comparing calculated to measured thermal properties from the laboratory and in situ tests.

3.4 IN-SITU TEST LOCATION AND SOIL STRATIGRAPHY

Eleven thermal cone tests were performed at three different sites: 1) Liberal Arts Building at Texas A&M University campus in College Station, 2) Fugro backyard site in Houstin, Texas, and 3) National Experiment Geotechnical Sites at Riverside (National Sand Site), Texas A&M University in College Station. At the liberal arts building, the thermal cone study was part of a larger project on energy piles at Texas A&M University, where three 18 m long piles from the foundation of the new Liberal Arts building were instrumented with thermal loops. Figures 3-3, 3-4, and 3-5 shows the location of each of the sites listed here respectively. At the Liberal Arts Building site, the TCT was performed at two different locations referred as CPT1 and CPT2 while the soil samples were extracted from a location between CPT1 and CPT2 and close to energy piles location.

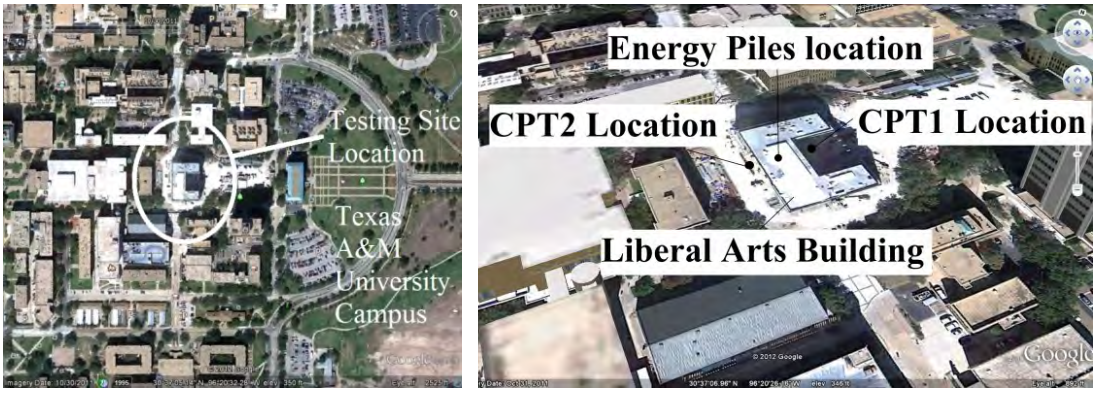

Figure 3-3 Liberal Arts Building testing site

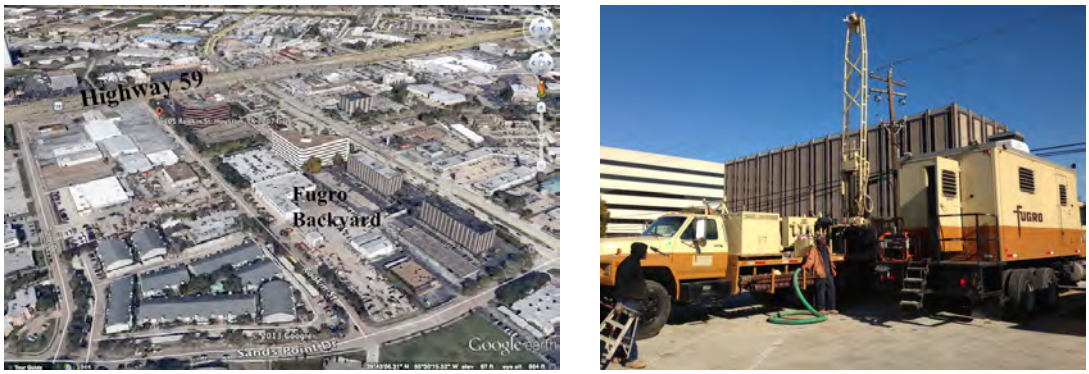

Figure 3-4 Fugro backyard testing site

Figure 3-5 National Sand Site testing site

The testing program used to evaluate the TCT method included two main components, 1) laboratory testing on soil samples to determine the soil thermal properties of the site; and 2) in-situ testing using the CPT cone. Tests occurred at five different locations. The sampling depths, and a listing of the tests performed at each location, are summarized in Table 3-2.

Table 3-2. Testing program for soil thermal properties

Test Site	Depth (m)	Extracted sample ID	Laboratory Test	TCT Test	
				CPT1	***CPT2***
Liberal Arts Building	4	S7-9-10-8-11-A	x	x	x
	7	S17-19-10-8-11-A	x		
	10	S27-29-13-8-11-A	x	x	x
	13	S37-39-11-8-11-A	x		x
	16	S47-49-13-8-11A	x		
Fugro Backyard	6.6	FB-S1-6-6	x	x	
	8.6	FB-S2-8-6	x	x	
	9.6	FB-S3-9-6	x	x	
National Sand Site	4	NS-S1-4-0	x	x	
	6.1	NS-S2-6-1	x	x	
	9.1	NS-S3-9-1	x	x	

The soil stratigraphy at the Liberal Arts Building site was evaluated based on: i) the soil investigation report for the new Liberal Arts building prepared by STL Engineers; ii) the CPT results obtained during the TCT in-situ tests; and iii) drilling logs during sample extractions. The soil was composed mainly of high plasticity clays that extended to the bottom of the drilling and CPT logs. More specifically, the soil

investigation concluded that the top 1.2 meters consisted of fill low plasticity clay (CL). The second layer, which extends to a depth of 14 meters, was a high plasticity greenish gray to light brown, stiff to hard, clay layer (CH). This layer became hard at a depth of 11.5 meters from the ground surface. The third layer consisted of olive gray, stiff to hard, high plasticity clay (CH) and extended to the end of the borehole. The results of the soil investigation, including water content ω(%), and undrained shear strength s_u (kPa), are presented in Figure 3-6. In this figure the log is limited to a depth of 15 m.

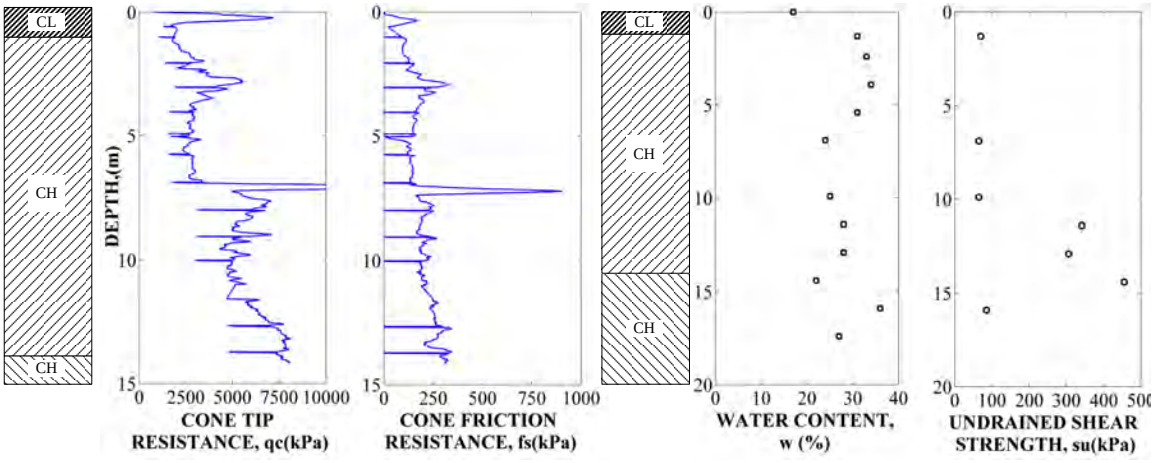

Figure 3-6 Engineering soil properties profile – Liberal Arts Building site

The soil stratigraphy at Fugro site was evaluated from the CPT tests performed during the TCT (Figure 3-5). The soil consists of a relatively deep layer of high plasticity clay (CH) with an average CPT tip resistance of 2,900 kPa and an average friction resistance of 129 kPa. The clay layer overlays a dense silty sand layer that

extend at least to the end of the borehole. The average CPT tip resistance of 35,000 kPa and an average friction resistance of 1,260 kPa.

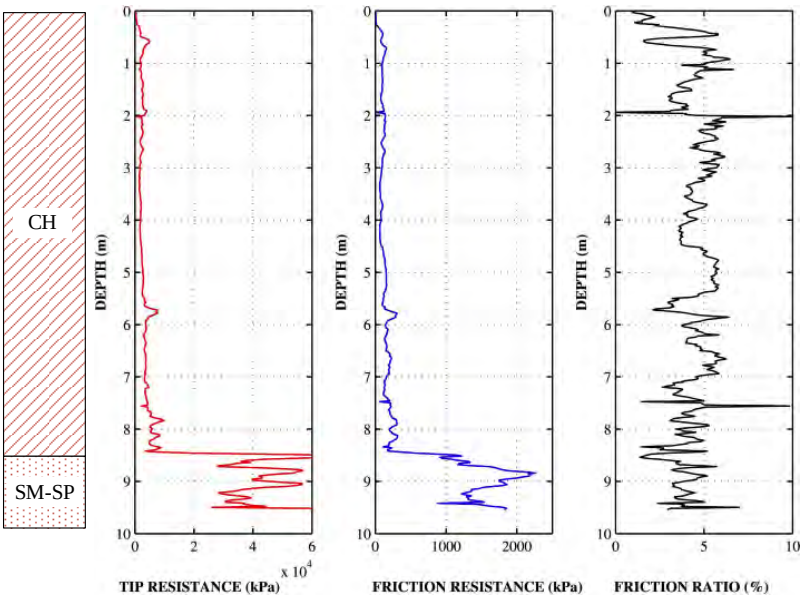

Figure 3-7 CPT test profile – Fugro site

The soil stratigraphy and properties at the National Geotechnical Sand Site was reported in previous studies (Hueckel and Pellingrini, 1992; Bruner et al., 1994; Briaud, 1993; Marcontell and Briaud, 1994; Simon and Briaud, 1996; Tao and Briaud, 1995). The stratigraphy at this site consists of a 3 m. layer of silty sand, overlaying a 3 m. layer of clean sand. The third layer extends to a depth of 13 m and it consists of a clayey sand layer. Below this layer, a hard shale layer exists. The soil stratigraphy, properties summary, and CPT data at this site are presented in Figure 3-6.

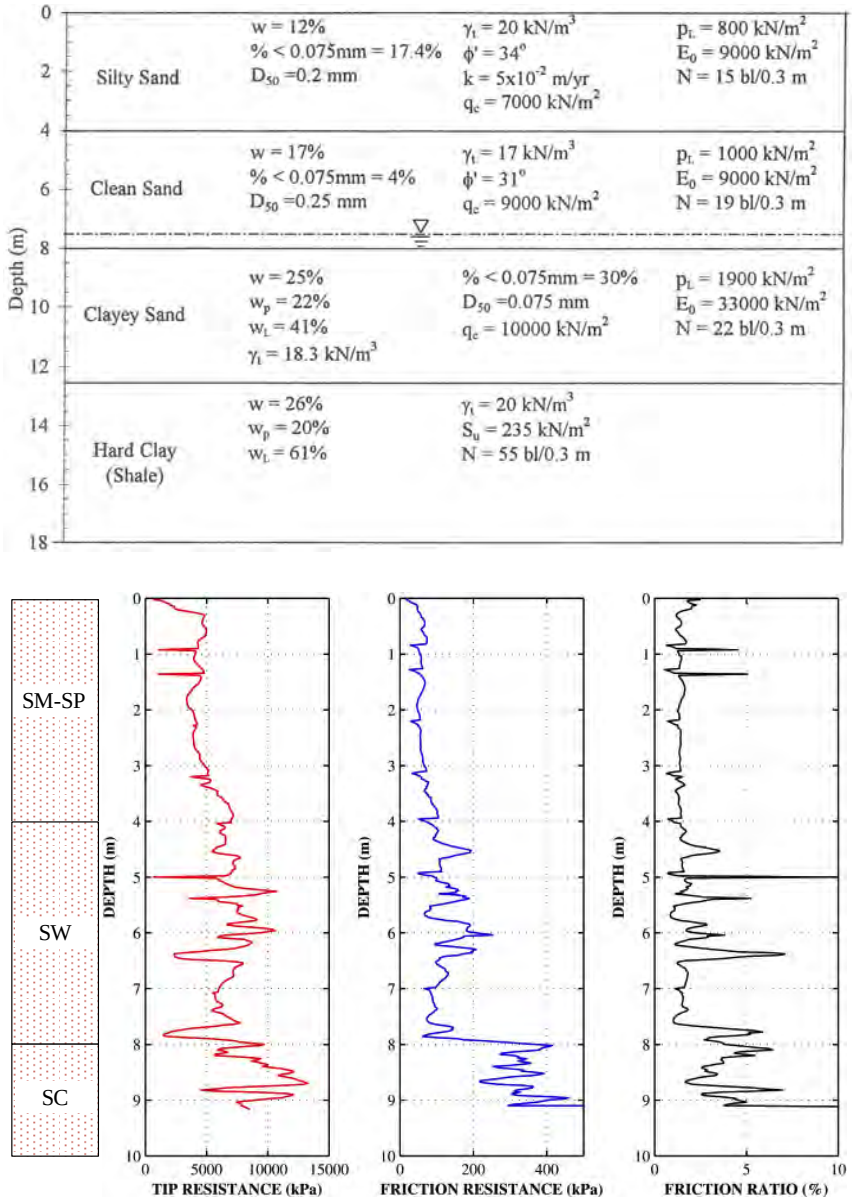

Figure 3-8 Engineering soil properties profile and CPT test – National Sand Site

3.5 IN-SITU THERMAL CONE TEST

The initial plan of the TCT test consisted of pushing the CPT cone into the soil until the heater element was at the depth D_z where the thermal properties needed to be evaluated

(Figure 3-9). The TCT test consisted of two phases. During Phase I of the test, the cone was positioned at the depth under study, and the heater was turned on to apply a temperature fluctuating around 121 °C by 5°C. During the tests performed in this study, the heater was kept on for 30 minutes and a thermocouple located below the heater recorded the increase in cone temperature resulting from soil/cone friction (ΔT_i) and its subsequent decay (Figure 3-10).

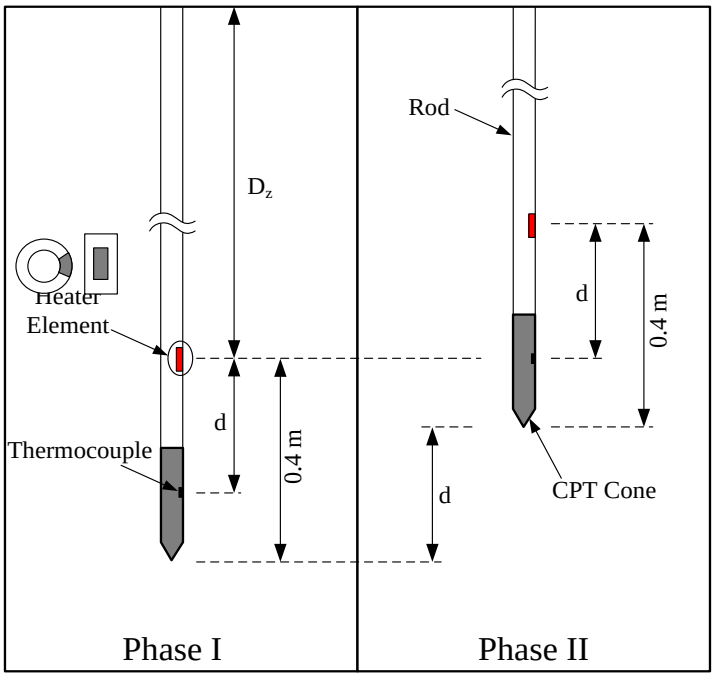

Figure 3-9 Phase I and phase II of TCT test

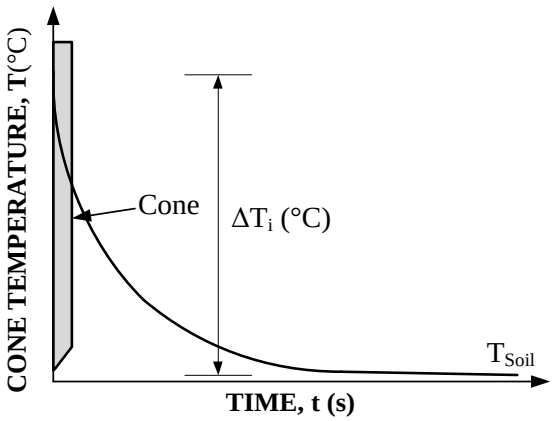

Figure 3-10 Cone temperature decay during phase I

After performing the tests at Liberal Arts Building site, it was found that temperature decay resulting for the pulse imposed by the heater cannot be captured properly due to the delay in the pushing up process of the cone after finishing the heating phase. In addition, it was found that soil-cone friction generates enough heat to heat up the CPT cone that can be relayed on in back calculating soil thermal properties.

In the second phase of the test, the heater was turned off and the cone was pulled up so the thermocouple was leveled at the initial heater location (Figure 3-9) and the temperature variation was then recorded.

3.6 LABORATORY TESTS

Soil samples were extracted from each of the testing locations (Figure 3-11). The samples were extracted at depths corresponding to the depth were the TCT was performed (Table 3-2).

Figure 3-11 Drilling and sampling

The experimental laboratory set-up is shown in Figure 3-12; the samples were tested using the thermal shock method (Shannon and Wells, 1947). This method consists of measuring the temperature increase at the center of a cylindrical sample after applying constant temperature boundary conditions, and then using the temperature variation to back calculate soil thermal properties utilizing the analytical solution for this problem (Carslaw, H.S, 1945). To accomplish this, the cylindrical soil samples were put in the oven at a constant temperature and a thermocouple was inserted into the center of the cylindrical sample (L=2D, where L (m) and D (m) are the sample length and diameter respectively) to measure the temperature variation.

Figure 3-12 Thermal shock testing method of soil samples

3.7 EXPERIMENTAL RESULTS

3.7.1 In-situ thermal cone results

The measured temperature variations at the thermocouple level during the TCT test at the Liberal Arts Building, Fugro backyard, and National Sand sites are presented in Figure 3-13, 3-14, and 3-15 respectively.

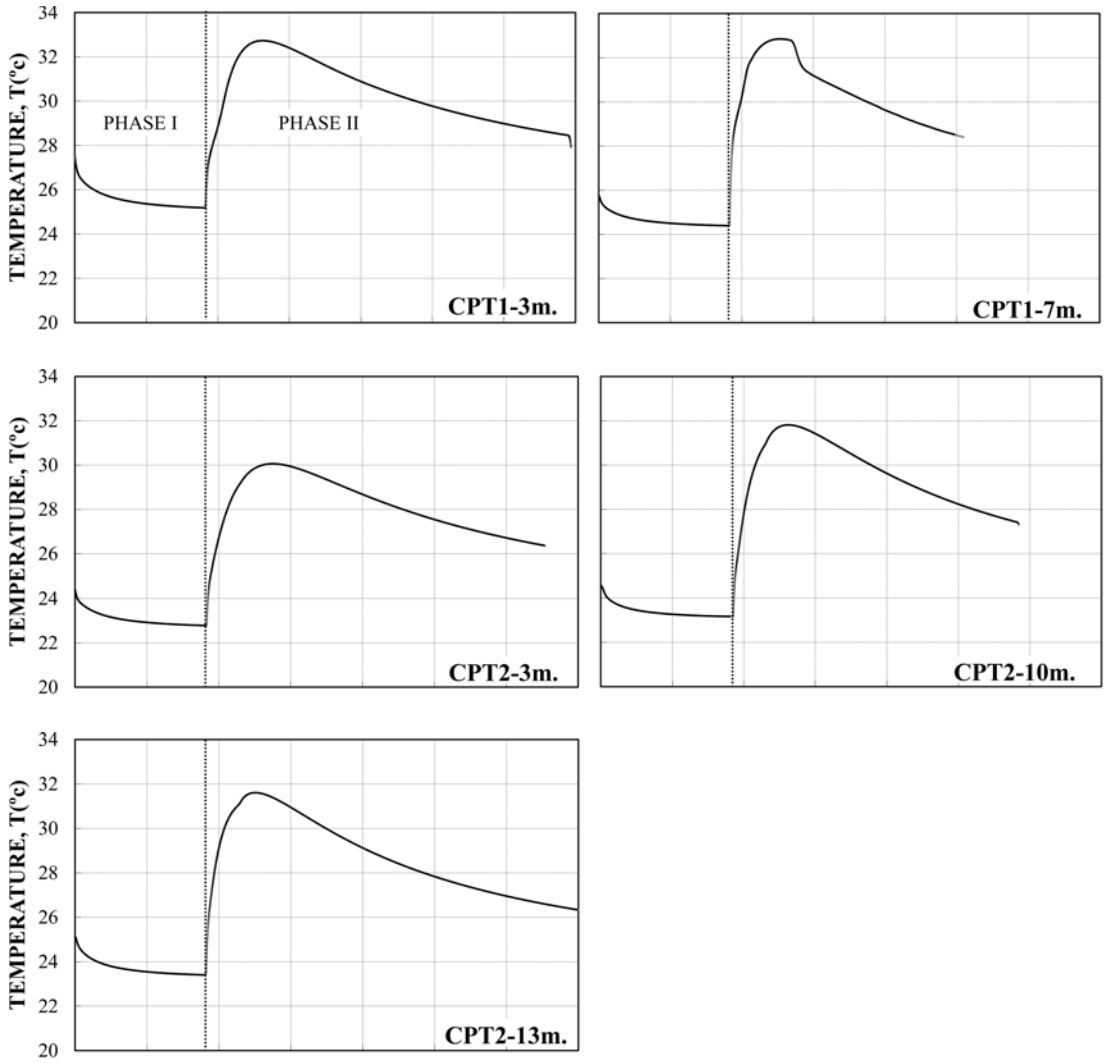

Figure 3-13 In-situ TCT results at Liberal Arts Building site

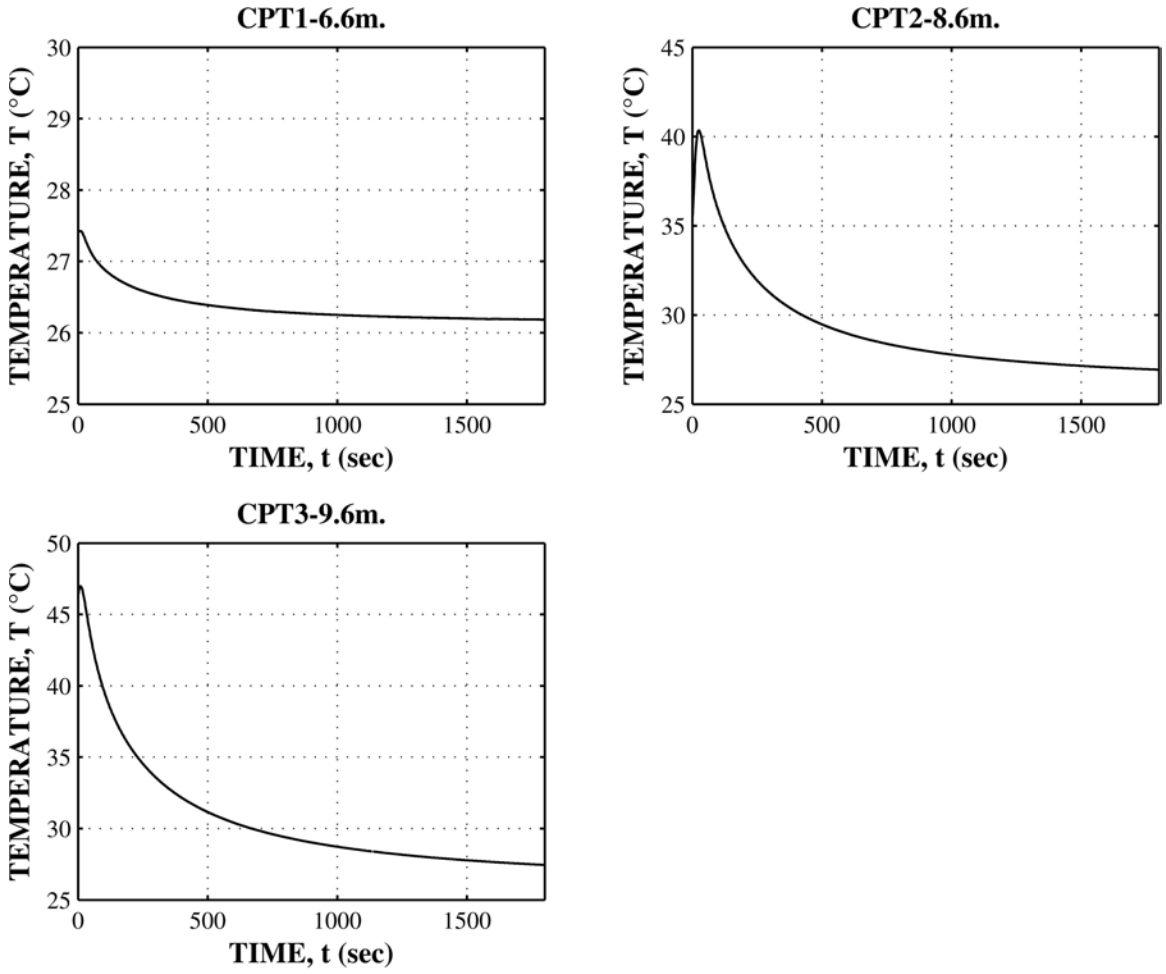

Figure 3-14 In-situ TCT results at Fugro backyard Site (Phase I only)

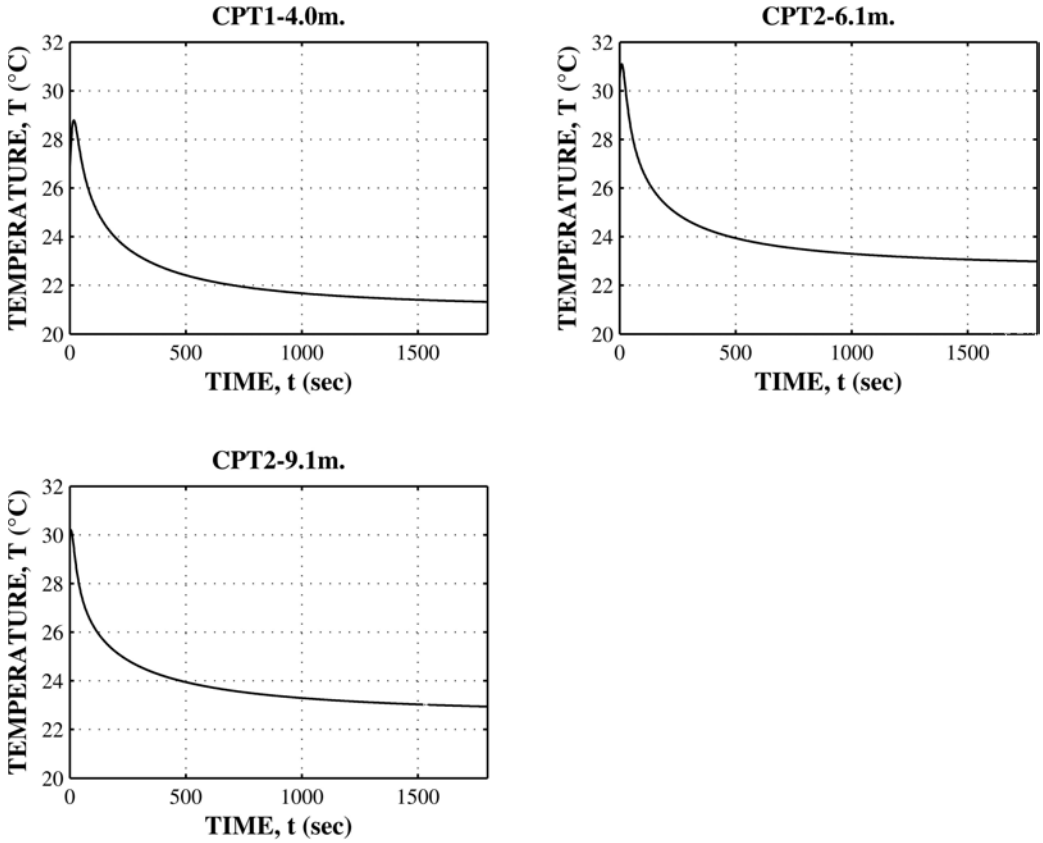

Figure 3-15 In-situ TCT results at National Sand site (Phase I only)

At the beginning of phase II, the cone had already cooled down. When it was moved up to the heated location, its temperature increased because of the heat transfer from the soil, until which point it reached thermal equilibrium with the soil. After that, the soil and cone temperature decayed together. The measured results during phase I showed only a decrease of cone temperature, which indicates that the operation of heater during phase I didn't impact the temperature decay at the thermocouple level. It was noticed from the measured temperature that the true soil temperature decay after stopping the heater (phase II) cannot be captured well by the adapted heating procedure,

and therefore, phase II cannot be used to evaluate soil thermal properties. The cone temperature increase in Phase I because of the friction between the soil and the cone during CPT penetration; therefore, the temperature decay for Phase I can be used to back calculate the thermal properties and there is no need for a heater. In addition, using the results from Phase I will significantly reduce the TCT test duration.

3.7.2 In-situ test data reduction

It was noticed from the TCT experimental results that the data obtained from the in-situ test did not capture the exact initial (T_i) and final (T_F) temperatures. At the beginning of the test, the data exhibited a flat or a bumpy portion (Figure 3-13, 3-14, and 3-15), which should be ignored during the data reduction. In addition, and because of the short duration of the test, the final temperature (which is equal to the undisturbed soil temperature) was not captured because theoretically, it takes infinity time for the temperature to come back to its initial undisturbed value. For those reasons, a data-fitting technique with a parabolic model (Eq. 3.5) was used to evaluate T_0 and T_F from the experimental data. The unknown parameters of Eq. 3.5 (a and b) can be evaluated from fitting the measured data into a linear function as given in Eq. 3.6. T_0 is unknown; therefore, trial and error method is used to best fit the measured data. The final temperature T_F is the asymptotic value of the function given in Eq. 3.5 and it is equal to 1/b.

$$T_0 - T(t) = \frac{t}{a + bt} \tag{3.5}$$

$$F(T,t) = \frac{t}{T_0 - T(t)} = a + bt \tag{3.6}$$

When T_0 and T_f were determined, t_{50} was evaluated and it is the time corresponding to dissipate half of the initial increase in temperature. As an example, the data reduction of the TCT test performed at Fugro site at a depth of 8.6 m is presented in Figure 3-16. From the data analysis it was found that parameters "a" and "b" of Eq. 3.5 were found to be 5.3288 and 0.0495 respectively. T_0 and T_F were found to be 45 °C and 25.79 °C respectively.

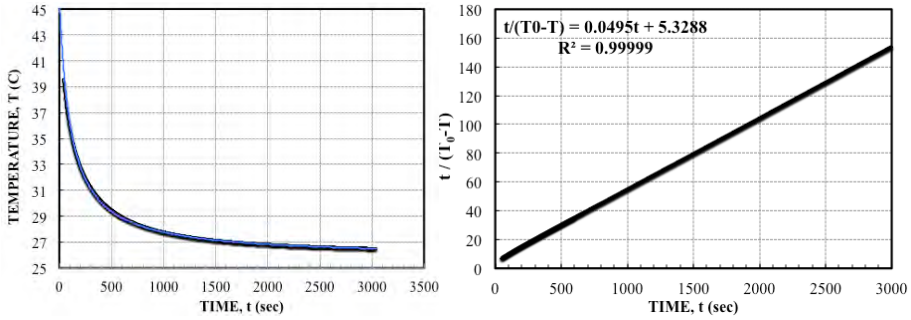

Figure 3-16 Data reduction example (Fugro Site - 8.6 m.)

3.7.3 Laboratory test results

The soil samples collected from the testing site were tested in the laboratory for thermal properties using the thermal shock method (Shannon and Wells, 1947) described earlier in Section 3.6 (Table 3-3). The laboratory tests were performed by applying a sample boundary temperature of 35°C. Table 3-4 summarizes the measured parameters from the in-situ tests as well as engineering and thermal properties from the laboratory tests.

Table 3-3 Soil thermal properties from laboratory tests

Testing Site	Sample ID	Sample Depth (m)	λ (W/m.K.)	α (m^2/s)	C (MJ/m^3K)
Liberal Arts Building	S7-9-10-8-11-A	4.0	0.61	2.7×10^{-7}	2.26
	S17-19-10-8-11-A	7.0	0.58	1.89×10^{-7}	3.06
	S27-29-13-8-11-A	10.0	0.45	1.45×10^{-7}	3.10
	S37-39-11-8-11-A	13.0	0.61	2.24×10^{-7}	2.73
	S47-49-13-8-11-A	16.0	0.4	1.27×10^{-7}	3.13
Fugro Backyard	FB-S1-6-6	6.6	1.05	4.16×10^{-7}	2.52
	FB-S2-8-6	8.6	1.25	4.88×10^{-7}	2.56
	FB-S3-9-6	9.6	1.35	4.85×10^{-7}	2.78
National Sand Site	NS-S1-4-0	4	1.55	7.15×10^{-7}	2.21
	NS-S2-6-1	6.1	1.41	6.13×10^{-7}	2.30
	NS-S3-9-1	9.1	1.67	6.18×10^{-7}	2.70

Table 3-4 In-situ TCT results needed in Eq. 3.3 and Eq. 3.4

Site			In-situ Test	From Laboratory Test				
	Test ID	Depth (m)	t_{50} (sec)	λ	C	γ_d	n	S
Liberal Arts Building	CPT1-3	4.0	254	0.61	2.26	13.0	0.49	98
	CPT1-7	10.0	275	0.45	3.10	13.1	0.49	99
	CPT2-3	4.0	270	0.61	2.26	13.0	0.49	98
	CPT2-10	10.0	180	0.45	3.10	13.1	0.49	99
	CPT2-13	13.0	219	0.61	2.73	14.9	0.42	92
Fugro Backyard	CPT1-4	6.6	85	1.05	2.52	17.80	0.32	87
	CPT1-6.1	8.6	73	1.25	2.56	16.27	0.38	82
	CPT1-9.1	9.6	78	1.35	2.78	16.25	0.38	97
National Sand Site	CPT1-6.6	4	109	1.55	2.21	17.3	0.35	62
	CPT1-8.6	6.1	99	1.41	2.30	15.5	0.41	65
	CPT1-9.6	9.1	110	1.67	2.70	17.7	0.33	100

3.8 NUMERICAL ANALYSIS

To develop a calibration curve for the TCT test that relates the thermal properties to the measured parameter, t_{50}, a series of numerical simulations were performed. The numerical model results were verified against the measured data from the in-situ TCT tests. The aim of this activity is to achieve a better understanding of the TCT and to validate the numerical models proposed for the in-situ test. The numerical model was then used to simulate a wide range of thermal properties that covers the range of values found for soils. Phase I and Phase II of the TCT test were modeled using 2D and 3D numerical models, respectively. The finite element program CODE_BRIGHT (Olivella et al., 1996) was used for the simulations. In this problem, temperature is the main variable; therefore, only the thermal problem was solved. Problems involving temperature changes in soils are addressed in CODE_BRIGHT by solving the equation associated with balance of the internal energy.

The analysis was carried out assuming that the samples were almost fully saturated (Table 3-4). A 2D axisymmetric model (centered around the vertical axis of the cone device) was adopted for simulating the decay of the temperature observed during Phase I (i.e. the decay related to the thermal variation generated by the penetration of the cone). This assumption was possible because the cone temperature increased in an axisymmetric manner during the cone pushing process. The second phase of the test needed to be modeled as a 3D problem, because the heat source was located in a narrow area on the side of the device, and therefore the 2D axisymmetric idealization

was too crude for this case. The model geometry and dimensions of the two test phases are presented below in Figure 3-17.

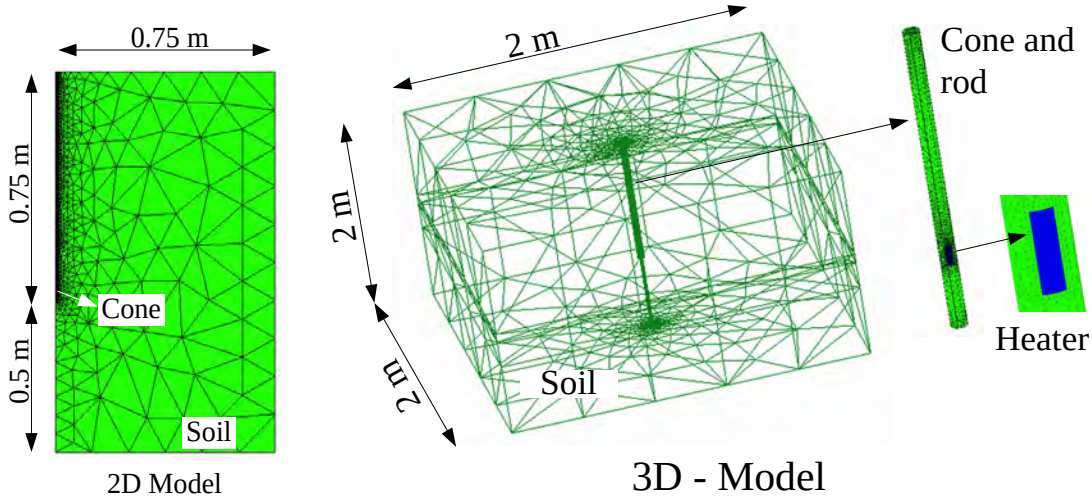

Figure 3-17 2D (a) and 3D (a) modeling of phase I and phase II respectively

For the two phases of the test, the initial conditions were set to the measured values during the in situ test. For Phase II, the movement of the cone was simulated by imposing the initial soil temperature to the cone and the heater at the beginning of phase II. The results of the 2D and 3D models for the two phases of the five tests from the Liberal Arts Building site were plotted against the measured data and are presented in Figures 3-18 and 3-19, respectively.

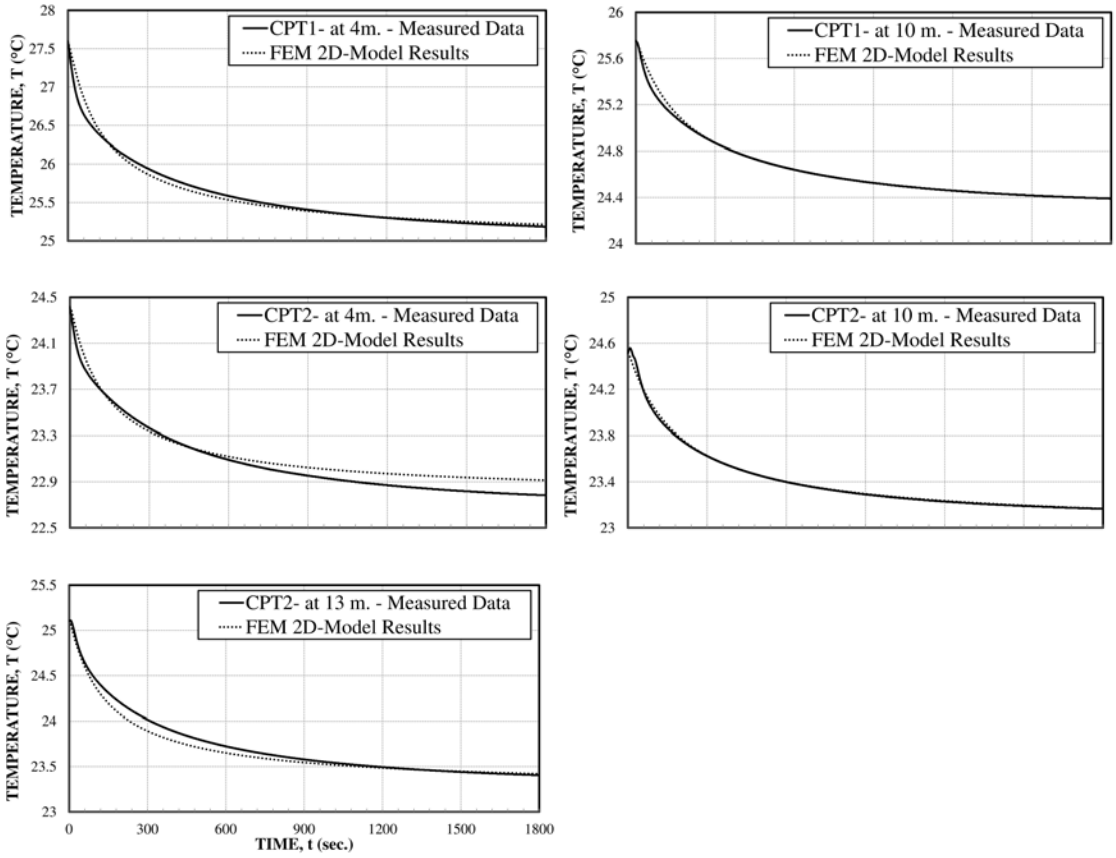

Figure 3-18 Measured and calculated results for phase I – Liberal Arts Building site

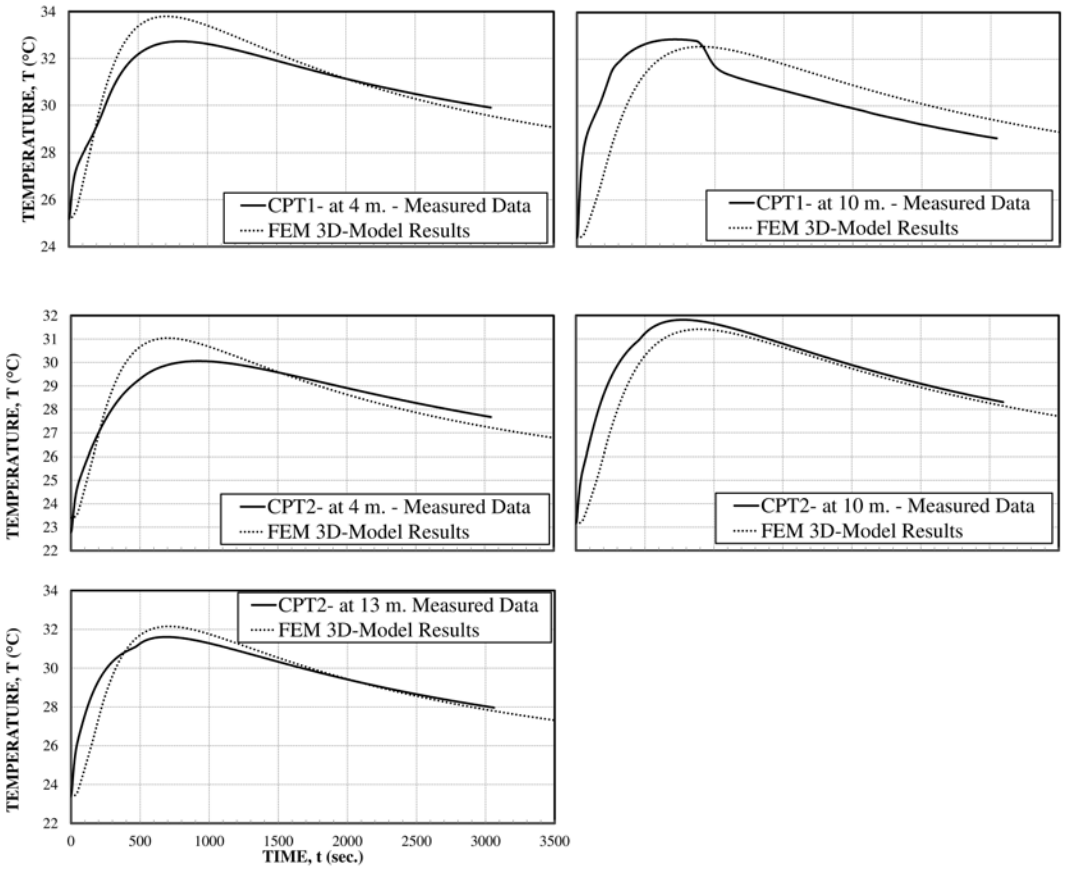

Figure 3-19 Measured and calculated results for phase II – Liberal Arts Building site

The results presented in Figures 3-18 and 3-19 for Phases I and II respectively of the TCT indicate that the numerical model results compare well with the measured data.

The 3D numerical model was used to investigate the temperature field generated around the cone during the two phases of the test. Figure 3-19 shows the temperature evolution at different horizontal (a) and vertical (b) locations designated by alphabetic letters. The results show that during the performed test, and for the soil conditions at the testing location, the heating process did not impact the cone temperature decay.

Furthermore, the results in Figure 3-20 support the observations during the in-situ test that there was no thermal interference between the heater and the thermocouple location.

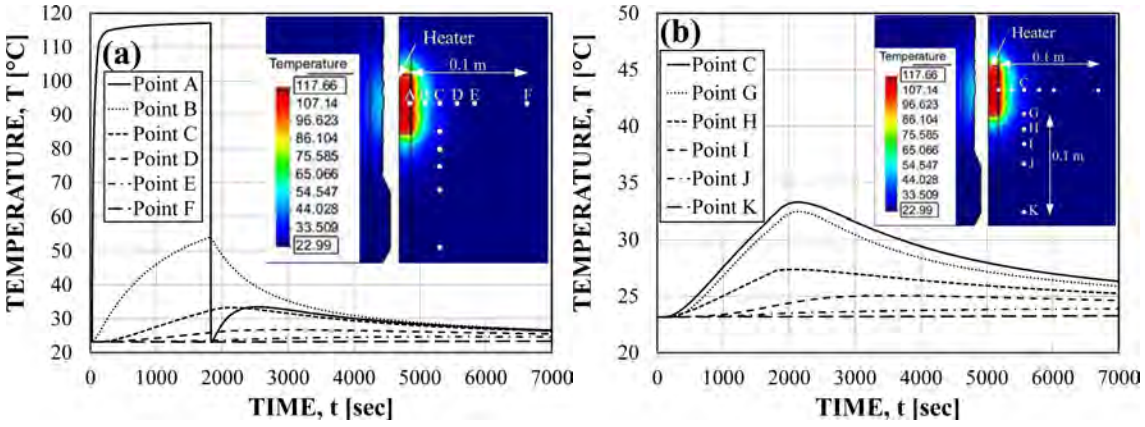

Figure 3-20 Soil temperature around the thermal cone – Liberal Arts Building site

3.9 CALIBRATION CURVE

In order to develop the calibration curve and to find the parameters A, B, T_{50}, and χ presented in equations Eq. 3.3 and Eq. 3.4, a unique set of parameters where used in all the 2D numerical simulations (Table 3-5). The density, porosity, and liquid degree of saturation were constant for all numerical simulations. For each set of numerical model parameters presented in Table 3-5, the thermal diffusivity α (Eq. 3.7), t_{50} and T_{50} were evaluated. The results from the numerical model were used to plot the thermal conductivity against t_{50} and the temperature dissipation ratio U (Eq. 3.8) against the time factor T (Eq. 3.8).

$$\alpha\left(m^2/\sec\right)=\frac{\lambda\left(W/m.K\right)}{C\left(W.\sec/m^3.K\right)} \tag{3.7}$$

$$U=1-\frac{T_{\max}-T\left(t\right)}{T_{\max}-T_{\min}} \tag{3.8}$$

$$T=\frac{\alpha t}{a^2} \tag{3.9}$$

where T_{max}, T_{min}, T(t) are the maximum temperature, minimum temperature, and temperature at time t, respectively.

It was noticed by analyzing the results, that for low thermal conductivity, the variation of t_{50} was higher than the variation of t_{50} for high thermal conductivity. In addition, the volumetric heat capacity had a small impact on t_{50} for different thermal conductivity values.

Table 3-5 t_{50} (sec) from 2D model

λ (W/m.K)	**C (MJ/m^3K)**				
	1	2	3	4	5
0.3	300	281	289	305	325
0.6	155	144	146	151	170
0.9	103	96	99	105	111
1.2	97	72	75	79	85
1.5	61	60	61	61	62
1.8	54	47	47	48	54
2.1	48	43	41	43	45
2.4	41	34	36	37	39
2.7	37	31	32	35	36

Figure 3-21 is the plot of thermal conductivity λ versus t_{50}. On this figure, the average calibrated curve from the numerical analysis data (Table 3-5) is plotted. The measured data from the performed in-situ tests showed an offset by a factor of 1.4 from the numerical analysis calibrated curve; therefore, the adjusted curve that takes into account this offset is used to predict soil thermal conductivity from in-situ measurement.

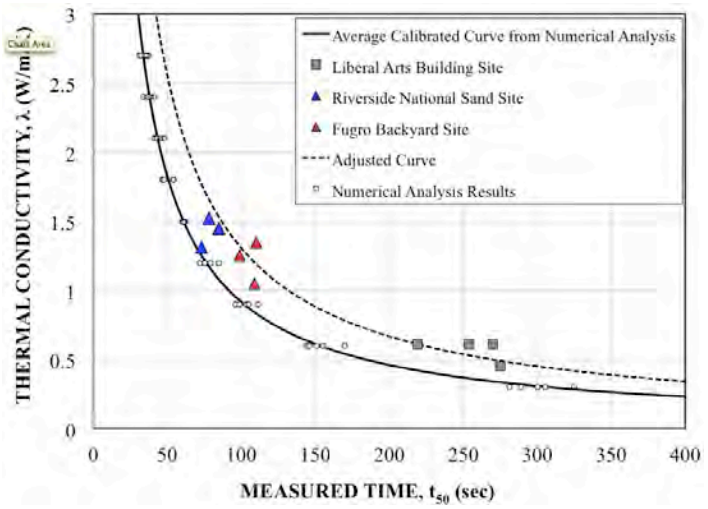

Figure 3-21 Thermal conductivity variation vs. t_{50}

The thermal conductivity can be predicted from Phase I of the TCT test using Eq. 3.10:

$$\lambda(W/m.K.) == \frac{110}{\left(t_{50}(\text{sec})\right)^{0.968}} \tag{3.10}$$

To determine T_{50} required the calculation of α and using the numerical analysis results (Table 3-5), the normalized temperature dissipation U (Eq. 3.8) was plotted

against the time factor T (Eq. 3.9). It was found that these curves are dependent on the volumetric heat capacity only (Figure 3-22), which implies that the time factor T_{50} depends on the volumetric heat capacity value. The factor χ in Eq. 3.6 can now be integrated in $T_{50,}$ where T_{50} becomes a variable dependent on the volumetric heat capacity value.

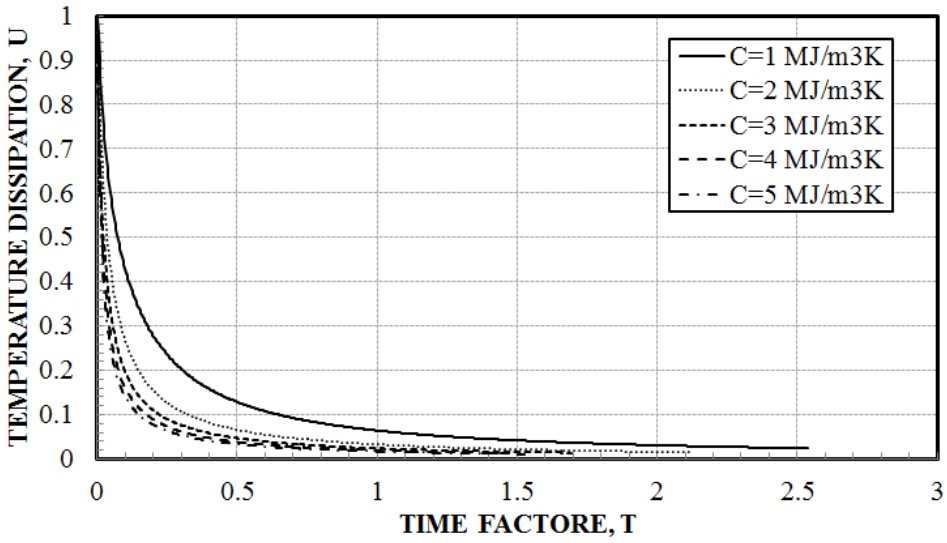

Figure 3-22 Temperature dissipation U vs. time factor T

Based on the numerical model results and measured data, the following equation (Eq. 3.11) is proposed to obtain the time factor T_{50} as a function of C (MJ/m^3K):

$$T_{50} = \frac{0.0728}{C^{1.032}} \tag{3.11}$$

The soil thermal diffusivity can now be calculated using Eq. 3.12.

$$\alpha\left(m^2/\sec\right)=\frac{\left(\frac{0.0728}{C^{1.032}}\right)\times a^2}{t_{50}\left(\sec\right)} \tag{3.12}$$

Here "a" is the diameter of the CPT cone; in this study it's equal to 0.0357 m.

3.10 STEP BY STEP PROCEDURE TO PERFORM THE THERMAL CONE TEST

The step-by-step procedure to perform the TCT test and calculate soil thermal properties is the follows:

- **Step 1:** Propose the test location and depth where mechanical and thermal (and maybe hydraulic) properties need to be evaluated.
- **Step 2:** Move the CPT truck equipped with the thermal cone to the testing location.
- **Step 3:** Push the thermal cone to the desired depth where the thermal properties need to be evaluated.
- **Step 4:** Record the cone friction and tip resistance during the pushing process.
- **Step 5:** Stop the cone at the desired depth.
- **Step 6:** Record the cone temperature decay vs. time for at least 30 minutes.
- **Step 7:** Evaluate t_{50} from the measured temperature decay.
- **Step 8:** Calculate thermal conductivity using Eq. 3.9.
- **Step 9:** Evaluate the volumetric heat capacity of the soil at the desired depth using the water content and dry unit weight (Eq. 2.16).
- **Step 10:** Calculate the thermal diffusivity using Eq. 3.11.

- **Step 11:** Repeat step 3 to step 10 for the next target depth.

3.11 CONCLUSIONS

This section of the dissertation presents an in situ method called the Thermal Cone Test or TCT to evaluate soil thermal properties using the CPT cone. The proposed TCT does not require a special heater but rather relies on the friction naturally generated by the penetration of the cone point in the soil. The TCT was evaluated through laboratory tests, through 11 in-situ TCT tests, and through numerical simulations. The proposed method enables the evaluation of soil effective thermal conductivity from in-situ measurement, while the evaluation of thermal diffusivity requires the evaluation of volumetric heat capacity from dry density and water content (Eq. 10). The only parameter that needs to be measured from the TCT in the field is t_{50}. The proposed method was verified against data from 11 in-situ scale TCT tests. Future work may include an extensive experimental program to provide enough information to include other soil parameters to the proposed equations in this paper.

4 ENERGY PILES IN UNSATURATED SOILS

4.1 INTRODUCTION

Traditionally, separate boreholes called Borehole Heat Exchangers or BHEs have been used with HDPE pipes to circulate the HCF. These boreholes are relatively deep (50 – 150 m) with a diameter ranging from 75 to 150 mm. Each borehole is fitted with a single or double U-tube HDPE pipe for circulating the HCF and the remaining annulus is filled with grout to stabilizes the borehole and enhance the heat transfer rate between the HCF and the soil (Sagia et al., 2012). It is more economical to integrate the HDPE pipes in the piles of the foundation (when such piles are used) because it decreases the initial installation cost of the system. Many analytical models have been published to analyze the transient heat transfer of GHEs. The common assumptions of these models are that 1) the soil is defined as an infinite isotropic homogenous medium with initial uniform temperature, 2) the heat transfer is limited to a 1D problem in the radial direction, 3) the vertical heat transfer along the GHE axis is neglected, and 4) the only heat transfer mechanism is conduction and it is controlled by Fourier's law (Fourier, 1822). The simplest equation is Kelvin's model, which is also known as the infinite line source model because the GHE is treated as an infinite line source of constant heat (Ingersoll et al., 1948, 1954). The finite line source model treats the GHE as a finite line source of heat and accounts for the length of the GHE (Zeng et al., 2002). The cylindrical source model (Carslaw and Jaeger, 1946) assumes that the GHE is a constant cylindrical heat

source. These models are the basis of the GHE sizing equation proposed by Kavanaugh and Rafferty (1997).

Energy piles are relatively short; therefore, a part of these piles is embedded in the SSL; in this layer, the soil saturation and associated thermal properties vary through the year because of the seasonal moisture change. Besides porosity, mineral content, grain size distribution, and particle shape, soil thermal properties are highly dependent on the soil degree of saturation, S_l. Table 4-1 recalls the models that use the normalized thermal conductivity concept proposed by Johansen (1975).

Table 4-1 Different λ_n functions

Author	Coarse grained Soil	Fine Grained Soil
Johansen (1975)	$\lambda_n = 0.7\log\left(S_l\right)+1.0$	$\lambda_n = \log\left(S_l\right)+1.0$
Côté and Konard (2005)	$\lambda_n = \frac{3.55\times S_l}{1+2.55\times S_l}$	$\lambda_n = \frac{1.9\times S_l}{1+0.9\times S_l}$
Lu and Horton (2007)	$\lambda_n = \exp\left\{0.96\left[1-S_l^{-0.37}\right]\right\}$	$\lambda_n = \exp\left\{0.27\left[1-S_l^{-1.06}\right]\right\}$
Square Root Model	$\lambda_n = \sqrt{S_l}$	

The design of BHEs neglects the SSL and its change in properties during the year because BHE are relatively long and the impact of the SSL on the overall BHE thermal performance is not significant (Eskilson, 1987). On the other hand, energy piles are relatively short and a significant part of the piles is located within the SSL; therefore, the

change in soil saturation conditions may significantly impact heat exchange rate of energy piles (Figure 4-1).

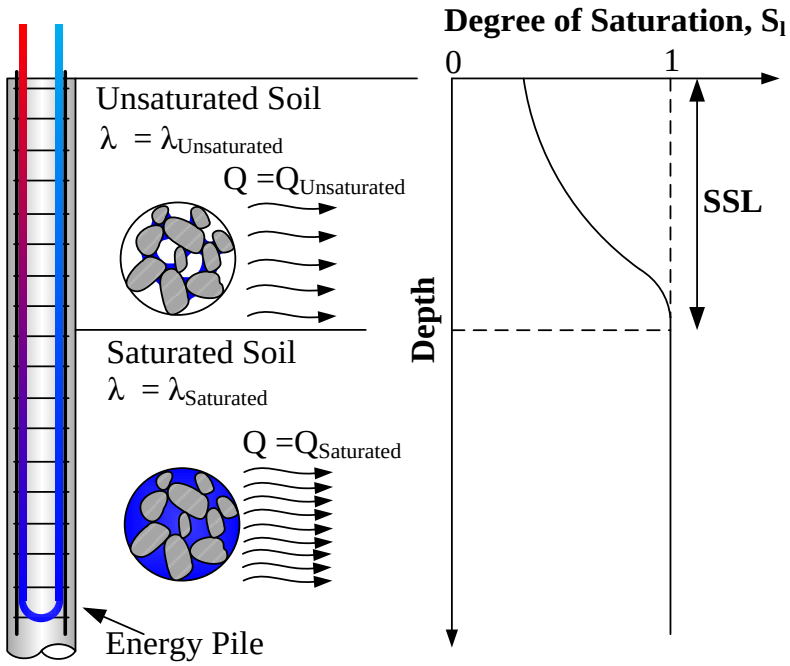

Figure 4-1 Energy pile in unsaturated and saturated Soil

Thomas and Rees (2009) analyzed the heat transfer from a slab in 1D and 2D geometries and evaluated the effect of water table fluctuation on the heat exchange rate from the slab. The authors concluded that the heat exchange rate decreases by 35% in 1D problem and 20% in 2D problem when the water table is located at 10 m below slab level compared to a water table located at the slab level (fully saturated conditions). Choi et al. (2011) analyzed an energy pile in saturated and unsaturated soil conditions by

changing the water table level from ground level to the bottom of the pile. The analysis showed that the fluctuation of water table results in a decrease of the heat exchange rate of energy piles by 40% compared to heat exchange rate in fully saturated conditions when the water table is located at ground level. This section of the dissertation extends the investigation on the influence of unsaturated soil conditions on the thermal performance of energy piles through an analytical solution called the thermal efficiency function. The solution of this function is based on the cylindrical heat source theory. To validate the solution, a series of laboratory tests were performed on energy pile sections in soil ranging from dry to saturated conditions. The laboratory tests were modeled numerically and the model was validated against the measured data. The model was extended to account for the pile profile and the thermal efficiency function was evaluated and compared to the analytical solution. The results showed good consistency between analytical, numerical, and experimental results.

4.2 CLOSED FORM SOLUTION OF ζ FUNCTION

The thermal efficiency of energy piles ζ in unsaturated soil is defined in Eq. 4.1

$$\zeta = \frac{\text{Amount of Heat Exchanged when Soil is Unsaturated}}{\text{Amount of Heat Exchanged when Soil is Fully Saturated}} = \frac{Q_{unsat}}{Q_{sat}} \qquad (4.1)$$

When the soil is fully saturated, the heat exchange rate is maximum and ζ = 1 (Figure 4-2a). When the soil saturation profile is variable (Figure 4-b), the heat exchange rate in the soil becomes variable (Figure 4-2c) because of the dependence of soil thermal properties on the degree of saturation (Table 4-1). The existing analytical solutions in literature (i.e. cylindrical heat source theory) do not account for the variable

soil saturation profile. As a result, to evaluate the heat exchange profile in partially saturated soils, advanced computational methods are currently required. This paper proposes a simple analytical method to deal with this problem. The proposed method uses the cylindrical heat source theory and the soil saturated thermal conductivity to calculate the heat exchange profile (Figure 4-2a). The result is multiplied by the thermal efficiency function (Figure 4-2d), which is related to the soil saturation conditions, pile geometry, and pile thermal properties. The final output of this method is the heat exchange rate of energy piles in variable soil saturation profile conditions (Figure 4-2c).

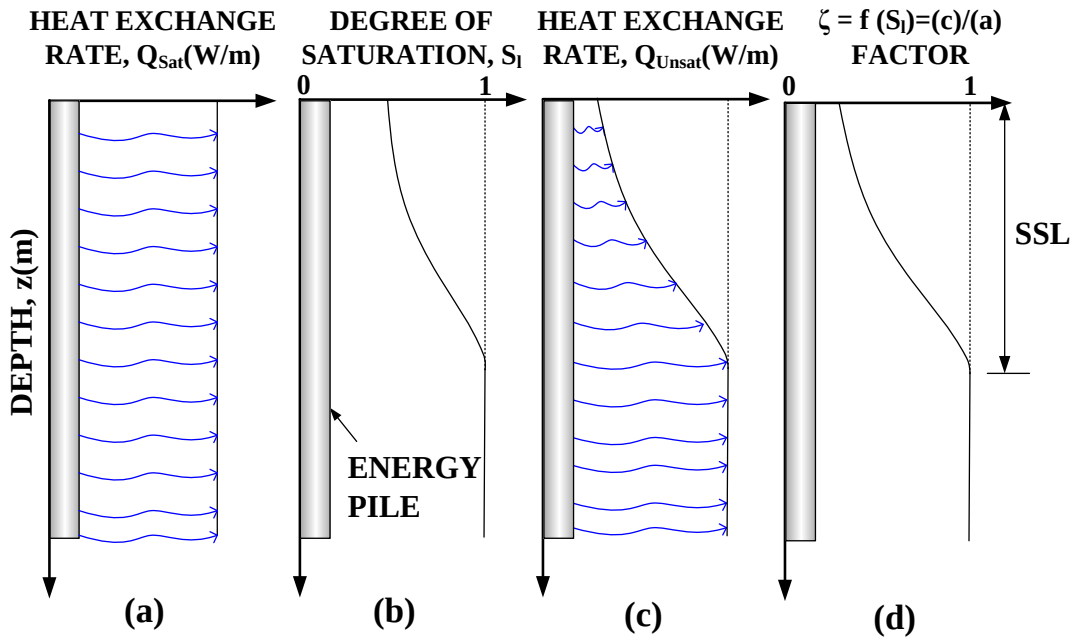

Figure 4-2 Heat exchange profile in saturated and unsaturated soils

The proposed equation is based on the following assumptions:

- Soil and pile thermal properties are isotropic and independent of temperature.
- Energy piles behave as a cylindrical source of heat (Bourne-Webb et al., 2009) with an average uniform temperature at the pile wall.
- Moisture evaporation and underground water movements are not significant.
- The soil and pile are at an initial temperature equal to T_0 (ºC).

Based on the cylindrical heat source theory, the increase in temperature ΔT (ºC) at a radial distance r (m) from the center of the cylinder of radius r_0 (m) at time t (sec) is given by Eq. 4.2 (Ingersoll, 1948):

$$\Delta T(r,t) = T(r,t) - T_0 = \frac{Q(W/m)}{\lambda_{soil}(W/m.K)} G(T_N = \frac{\alpha t}{r_0^2}, p = \frac{r}{r_0}) \tag{4.2}$$

with

$$G(\frac{\alpha t}{r_0^2}, \frac{r}{r_0}) = \frac{1}{\pi^2}\int_0^{\infty} \frac{e^{-\beta^2 z} - 1}{J_1^2(\beta) + Y_1^2(\beta)} \left[J_0(p\beta) Y_1(\beta) - J_1(\beta) Y_0(p\beta) \right] \frac{d\beta}{\beta^2} \tag{4.3}$$

J_0 and J_1 are the first kind Bessel function of orders zero and one, Y_0 and Y_1 are the second kind Bessel function of orders zero and one, and α (m^2/s) is the soil thermal diffusivity. For r = r_0, T (r_0,t) is the pile wall temperature denoted by T_w (ºC). The heat exchange rate Q in Eq. 4.2 is the amount of heat released from an energy pile during its operation, and is related to the difference between the HCF (T_F (ºC)) and the energy pile wall temperature through the thermal resistance of energy piles, R_{pile} ($K.m^2/W$) (Eq. 4.4).

$$T_F - T_W = R_{Pile} \times \frac{Q}{2\pi r_0} \tag{4.4}$$

Using Eq. 4.2 and Eq. 4.4 to solve for Q provides the following equation:

$$Q(W/m) = \frac{T_F - T_0}{\left(\frac{G\left(T_N,1\right)}{\lambda_{soil}} + \frac{R_{Pile}}{2\pi r_0}\right)} \tag{4.5}$$

In the unsaturated-saturated soil profile problem, the variable is the soil thermal conductivity that changes with the degree of saturation. When the soil is saturated, $\lambda = \lambda_{sat}$ and $Q = Q_{sat}$:

$$Q_{Sat}(W/m) = \frac{T_F - T_0}{\left(\frac{G\left(T_N,1\right)}{\lambda_{Sat.}} + \frac{R_{Pile}}{2\pi r_0}\right)} \tag{4.6}$$

When the soil is unsaturated, $\lambda = \lambda_{unsat}$ and $Q = Q_{unsat}$:

$$Q_{Unsat}(W/m) = \frac{T_F - T_0}{\left(\frac{G\left(T_N,1\right)}{\lambda_{Unsat.}(z)} + \frac{R_{Pile}}{2\pi r_0}\right)} \tag{4.7}$$

The function ζ is equal to the ratio between Eq. 4.7 and Eq. 4.6 and is expressed as:

$$\zeta = \frac{Q_{Unsat}(W/m)}{Q_{Sat}(W/m)} = \frac{\left(\frac{G\left(z,1\right)}{\lambda_{Sat.}} + \frac{R_{Pile}}{2\pi r_0}\right)}{\left(\frac{G\left(T_N,1\right)}{\lambda_{Unsat.}(z)} + \frac{R_{Pile}}{2\pi r_0}\right)} \tag{4.8}$$

Eq. 4.8 can be re-written using Eq. 2.5 and replacing λ_{unsat} with its corresponding equation:

$$\zeta = \frac{Q_{Unsat}(W/m)}{Q_{Sat}(W/m)} = \frac{\left(\frac{G\left(T_N,1\right)}{\lambda_{Sat.}} + \frac{R_{Pile}}{2\pi r_0}\right)}{\left(\frac{G\left(T_N,1\right)}{\left(\lambda_{sat} - \lambda_{dry}\right)\times\lambda_n + \lambda_{dry}} + \frac{R_{Pile}}{2\pi r_0}\right)} \tag{4.9}$$

The function λ_n can be replaced by any of the equations presented in Table 4-1.

To better understand the ζ function, two examples are presented in Figure 4-3 to evaluate the shape of the ζ function for coarse and fine-grained soils. For the two examples, it was assumed that $G(T_N,1) = 0.25$, $\lambda_{dry} = 0.9$ W/m.K, $\lambda_{sat} = 2.65$ W/m.K, $R_{pile} = 0.1$ K.m^2/W, $r_0 = 0.15$ m and the equations of λ_n from Table 4-1 are used.

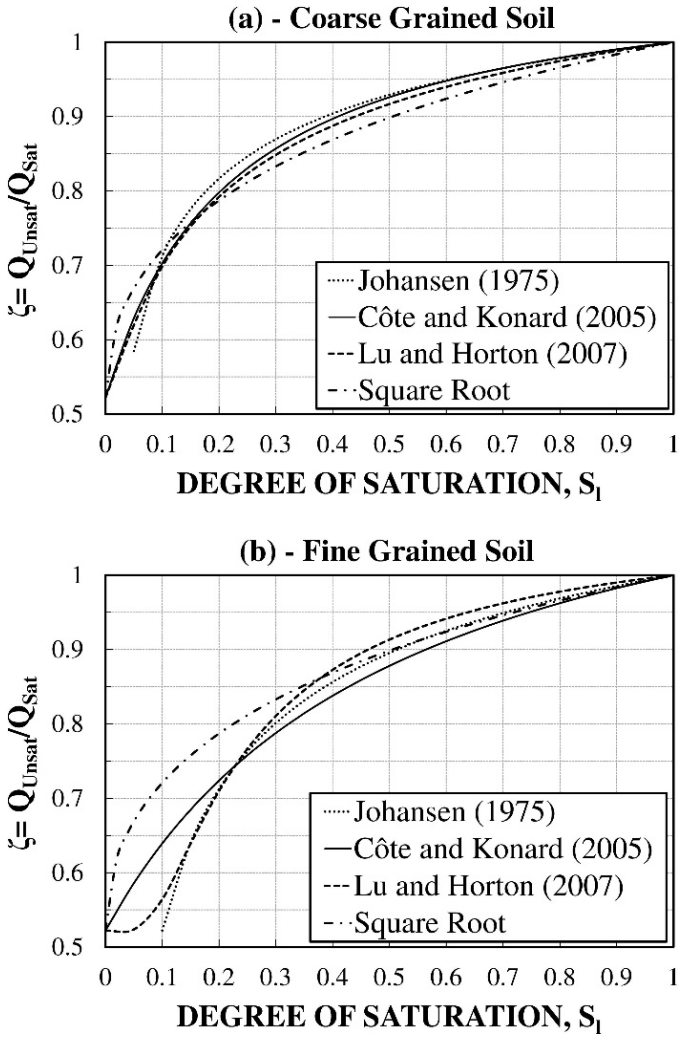

Figure 4-3 ζ Function example for coarse and fine-grained soil

The shape of the ζ function presented in Figure 4-3 can be explained by the dependence of the soil thermal conductivity on the degree of saturation. At a very low water content (the exact value of which depends on soil texture and soil-specific surface area, referred here as "θ_1"), the water film thickness is very thin and not enough to improve the contact between soil particles. Therefore, the soil thermal conductivity and the resulting heat exchange ratio remains constant up to water content θ_1. After this water content threshold is exceeded, water bridges between solid particles start to develop. This leads to a rapid increase in thermal conductivity, heat exchange ratio, and thermal efficiency factor. Eventually, the increase in water content depends on the displacement of air by water. At higher degrees of saturation, the rate of increase in thermal conductivity, heat exchange ratio, and thermal efficiency factor slows down (Sepaskhah and Boersma, 1979; Tarnawski and Gori, 2002).

Figure 4-4 presents a sensitivity analysis of the ζ function to the parameters involved in the analytical solution (Eq. 4.7) to better understand the impact of each parameter. The dry and saturated thermal conductivity were set to 1 and 2 W/m.K, respectively. The radius of the energy piles was set to 0.15 m. Four different values of λ_n were used (0 (fully dry), 0.3, 0.6, and 0.9). Two values of $R_{Exchanger}$ were used, 0.05 to represent to BHE and 0.25 to approximate the Energy pile. The results show that the ζ function decreases with time represented by the G function, which implies that the thermal efficiency of energy piles over a long period of time also decreases. This may be alleviated by using energy piles for part of the year only. In addition, the results show that the change rate of ζ slows with increasing time, which implies that ζ tends to a

steady state after a certain length of operation. Figure 4-4 shows that the ζ function increases with the increase of GHE thermal resistance. This implies that for the same λ_{GHE}, ζ increases with an increase in the size of the GHE. Conversely, for the same GHE size, the ζ function increases with a decrease in thermal conductivity of the GHE. Figure 4-4 shows that for a low degree of saturation, the range of ζ values for high and low thermal resistance is larger than for a high degree of saturation.

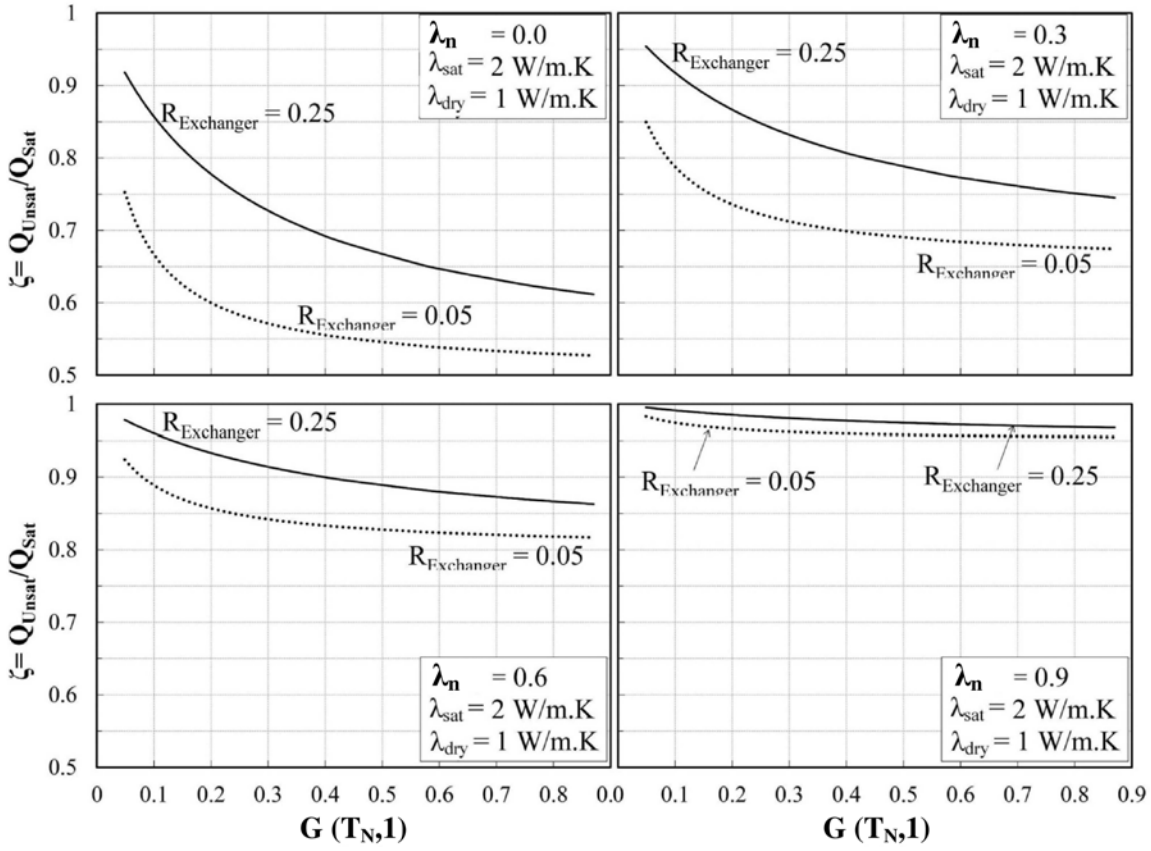

Figure 4-4 Sensitivity analysis of ζ function

The degree of saturation is depth dependent and related to the matric suction ψ = (Pg-Pl) (MPa) through the Soil Water Characteristic Curve (SWCC) (van Genuchten, 1980; Fredlund and Xing, 1994). The function λ_n in Eq. 4.9 can be replaced by any of the equations presented in Table 4-1. Using the square root model for λ_n and van Genuchten's law for the SWCC (Eq. 4.10), the equation of ζ is given by Eq. 4.11.

$$S_l = \left(S_{ls} - S_{rl}\right)\left[1 + \left(\frac{P_g - P_l}{P_0 \frac{\sigma_T}{\sigma_0}}\right)^{\frac{1}{1-\lambda_0}}\right]^{-\lambda_0} + S_{rl} \tag{4.10}$$

$$\zeta = \frac{Q_{Unsat}(W/m)}{Q_{Sat}(W/m)} = \frac{\left(\frac{G(z,1)}{\lambda_{Sat.}} + \frac{R_{Pile}}{2\pi r_0}\right)}{\left(\frac{G(z,1)}{\left(\lambda_{sat} - \lambda_{dry}\right)\times\sqrt{\left(S_{ls} - S_{rl}\right)\left[1 + \left(\frac{P_g - P_l}{P_0 \frac{\sigma_T}{\sigma_0}}\right)^{\frac{1}{1-\lambda_0}}\right]^{-\lambda_0} + S_{rl} + \lambda_{dry}}} + \frac{R_{Pile}}{2\pi r_0}\right)} \tag{4.11}$$

S_{rl} and S_{ls} are the residual and maximum degree of saturation, P_0 (MPa) is the air entry at the reference temperature T_r (ºC) (usually room temperature), P_g and P_l are the gas and liquid pressure (MPa), and σ_0 and σ_T (Eq. 4.12) are the surface tension at the temperature at which P_0 was measured and at any temperature, respectively (N/m).

$$\sigma_T = 0.03059 \exp\left(\frac{252.93}{273.15 + T}\right) \tag{4.12}$$

4.3 LABORATORY TEST SETUP AND RESULTS

The impact of soil saturation conditions on energy pile thermal performance was evaluated trough 12 laboratory experiments that were conducted at Texas A&M University on energy pile sections in sand ranging from dry to saturated conditions. During each test, the soil thermal response and properties were measured.

4.3.1 Laboratory samples test

The thermal conductivity of the sand material was changed for every test by changing the sample water content / degree of saturation, and was measured for each test using the Shannon and Wells (1947) method described in Section 3.6 of this dissertation. The measured engineering and thermal properties of the sand material used in the laboratory pile test are presented in Table 4-2. This table shows the effective soil thermal conductivity, degree of saturation S_l, porosity n, void ratio e, gravimetric water content ω, total unit weight γ_T, and dry unit weight γ_d. Figure 4-5 shows the variation of measured thermal conductivity versus the measured water content for the 12 tests.

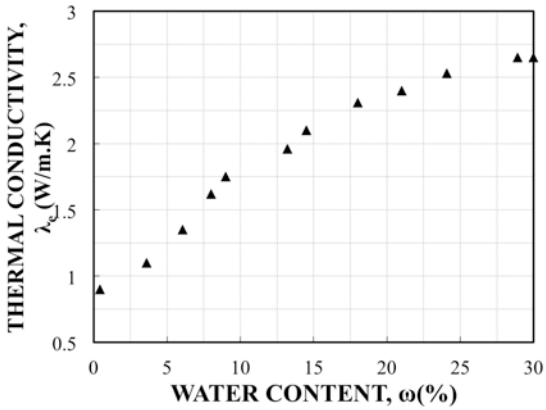

Figure 4-5 Experimental effective thermal conductivity vs. water content

Table 4-2 Measured engineering and thermal properties of the experimental sand

Section	Test ID	λ_e (W/m.K)	S_l	n	ω (%)	γ_T (kN/m^3)	γ_d (kN/m^3)
Geometry I	Test 1	0.9	0.015	0.45	0.50	14.74	14.68
	Test 2	1.35	0.188	0.47	6.06	15.02	14.16
	Test 3	1.75	0.311	0.44	9.00	16.22	14.88
	Test 4	2.1	0.480	0.45	14.50	16.72	14.60
	Test 5	2.4	0.715	0.44	21.01	17.88	14.78
	Test 6	2.65	1.000	0.45	30.02	19.02	14.62
Geometry II	Test 7	1.10	0.111	0.47	3.61	14.66	14.15
	Test 8	1.62	0.245	0.47	8.00	15.22	14.09
	Test 9	1.96	0.421	0.46	13.20	16.25	14.36
	Test 10	2.31	0.59	0.45	18.00	17.20	14.58
	Test 11	2.53	0.84	0.44	24.02	18.31	14.76
	Test 12	2.65	1.00	0.44	28.90	19.20	14.88

From Table 4-2, it is evident that the porosity and dry unit weight were almost constant for the 12 tests, with average values of 0.45, and 14.5 kN.m^3 respectively.

The measured thermal conductivity was normalized (Eq. 2.5) and compared to the existing models in the literature that predict the thermal conductivity as a function of soil degree of saturation (Figure 4.6a). The models presented in Figure 4-6(a) are: Johansen (1975), Côté and Konard (2005), and Lu and Horton (2007) for coarse-grained soil. The three models show a larger offset from the measured data for a degree of saturation below 0.7. The Lu and Horton (2007) and Côté and Konard (2005) model parameters were modified to fit the measured data (Figure 4.6b) and it was found that $\alpha = 0.80$ and $\kappa = 2.45$ are more accurate parameters for the sand used in this test.

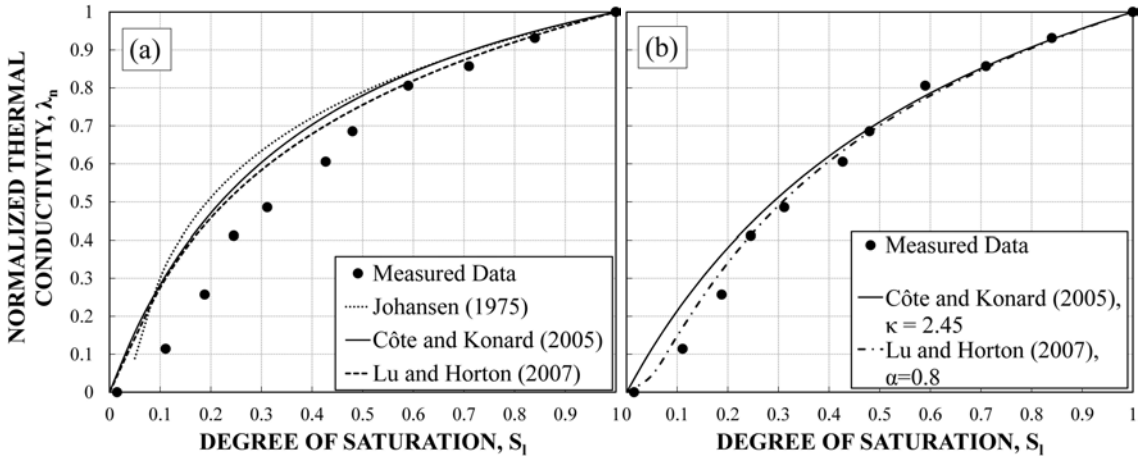

Figure 4-6 Measured and calculated normalized thermal conductivity λ_n vs. S_l

4.3.2 Laboratory pile test

The 12 laboratory tests were performed on two different energy pile circular sections, Geometry I and Geometry II, with section diameters of 300 and 400 mm respectively. Six tests (Test 1 to Test 6) were performed using Geometry I and another six tests (Test

7 to Test 12) were performed using Geometry II. In each test, different soil engineering and thermal properties were used (Table 4-2). The laboratory tests consisted of putting a concrete cylinder section poured in the lab and fitted with two PVC pipes inside a square wood box (1.2 m L x 1.2 m W x 0.25 m H) filled with sand (Figure 4-7). Points B-G on the figure below represent the locations of six thermocouples.

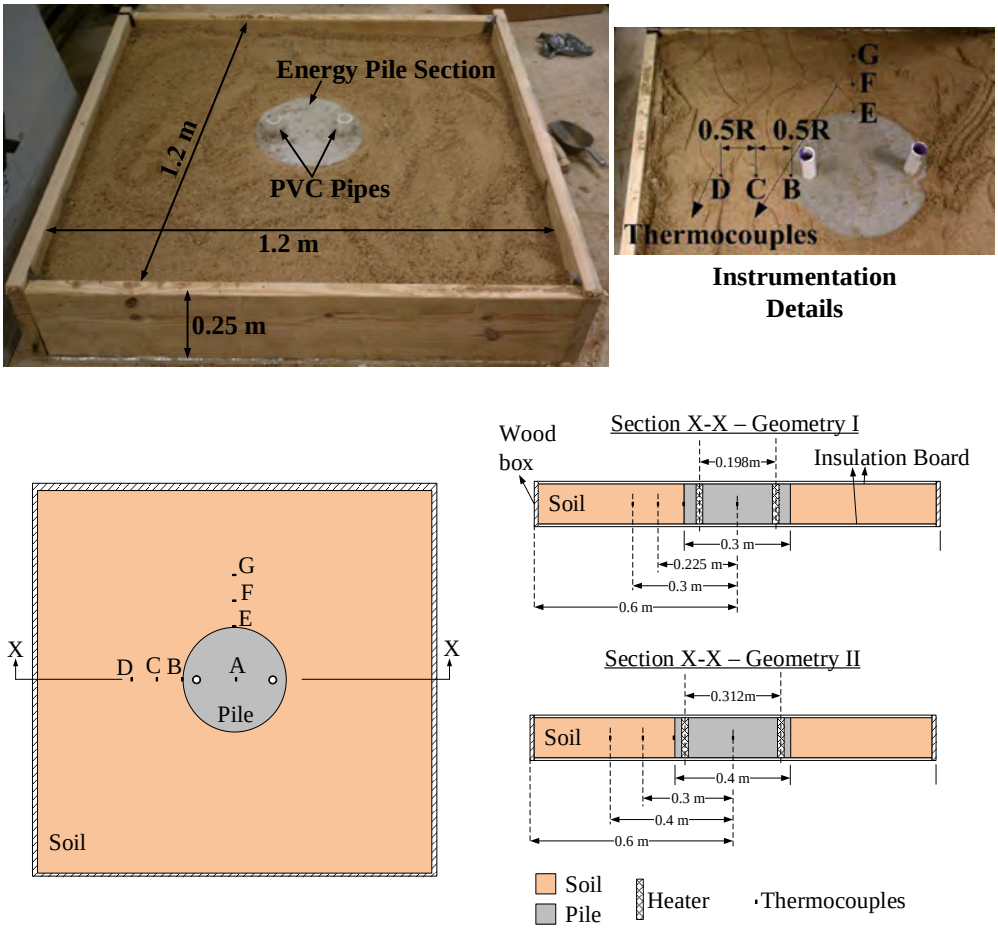

Figure 4-7 Laboratory test setup

This setup simulates a planar section of an energy pile at a specific depth. To prevent heat from transferring in the vertical direction, and to reduce the test to a 2D problem, the wood box was enclosed from the top and the bottom with foam insulation boards. Two different concrete mixtures were used for the concrete pile sections to create different thermal conductivities in Geometry I and Geometry II (1.3 and 1.4 W/m.K respectively). The PVC pipes used in the tests were 42 mm outer diameter and 38 mm inner diameter for Geometry I, and 28 mm outer diameter and 25 mm inner diameter for Geometry II. The thermal conductivity of the PVC making up the pipes was 0.15 W/m.K. The PVC pipes were closed at the bottom and filled with water. Two aquarium heaters with a temperature regulator were used to control the water temperature inside the PVC pipes. The temperature of the water inside the pipes was kept at a constant value of 37 °C during the tests for Geometry I and 30 °C during the tests for Geometry II. In all the tests, the sand was maintained at the same porosity and void ratio. The sand used in these lab tests was poorly graded sand with coefficients of uniformity (C_u) and curvature (C_c) of 1.4 and 1.11, respectively.

The sand box (Figure 4-7) was instrumented with type T thermocouples from OMEGA to measure the temperatures at the pile section wall and at fixed radial distances in the sand. For each test, the thermocouples were placed at radial distances r = r_0, r = 1.5r_0, and r = 2r_0 from the center of the pile. A data logger type HI 98804 from HANNA Instruments was used to monitor and log the data.

4.3.3 Laboratory pile test results

The main measurements from the laboratory pile tests were the pile-soil interface temperature and the soil temperature. As shown in the laboratory pile test setup in Figure 4-7, the temperature measurements were taken at different locations denoted by alphabetic letters: B, C, D, E, F, and G. The water temperature in the two pipes was equal; therefore, it was reasonable to assume symmetry in the temperature distribution around the pile section wall and in the soil. Temperature measurements were recorded for 48 hours. Figure 4-8 shows an example of the temperature increase at different locations during Test 1 for Geometry I.

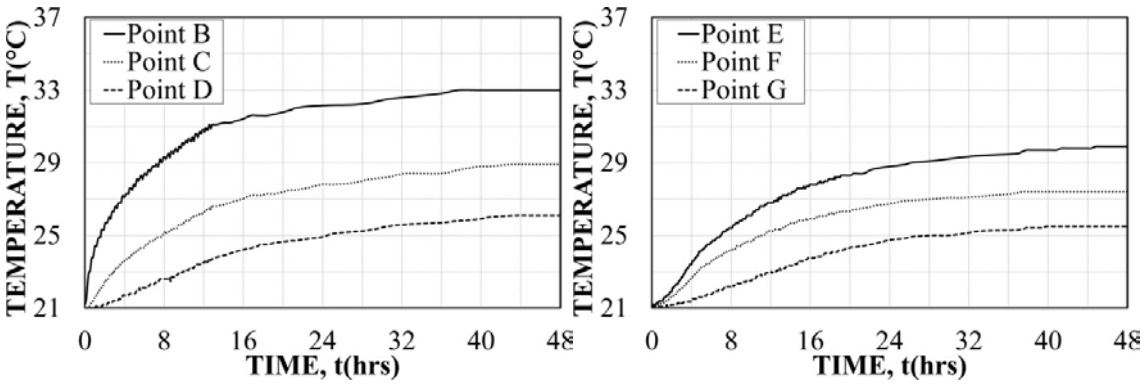

Figure 4-8 Plot of temperature variation during Test 1

Figure 4-9 shows the temperatures measured after reaching steady state at each of the points mentioned above for the 12 tests. These plots show that the temperature at the energy pile wall was not uniform and the temperature difference between the two extremes decreases with an increase in soil saturation. At points C and F ($r = 1.5r_0$), and

D and G ($r = 2\ r_0$), the temperature increase in the soil comes close to cylindrical form. The temperature difference between points C-F and D-G decreases with the increasing soil saturation.

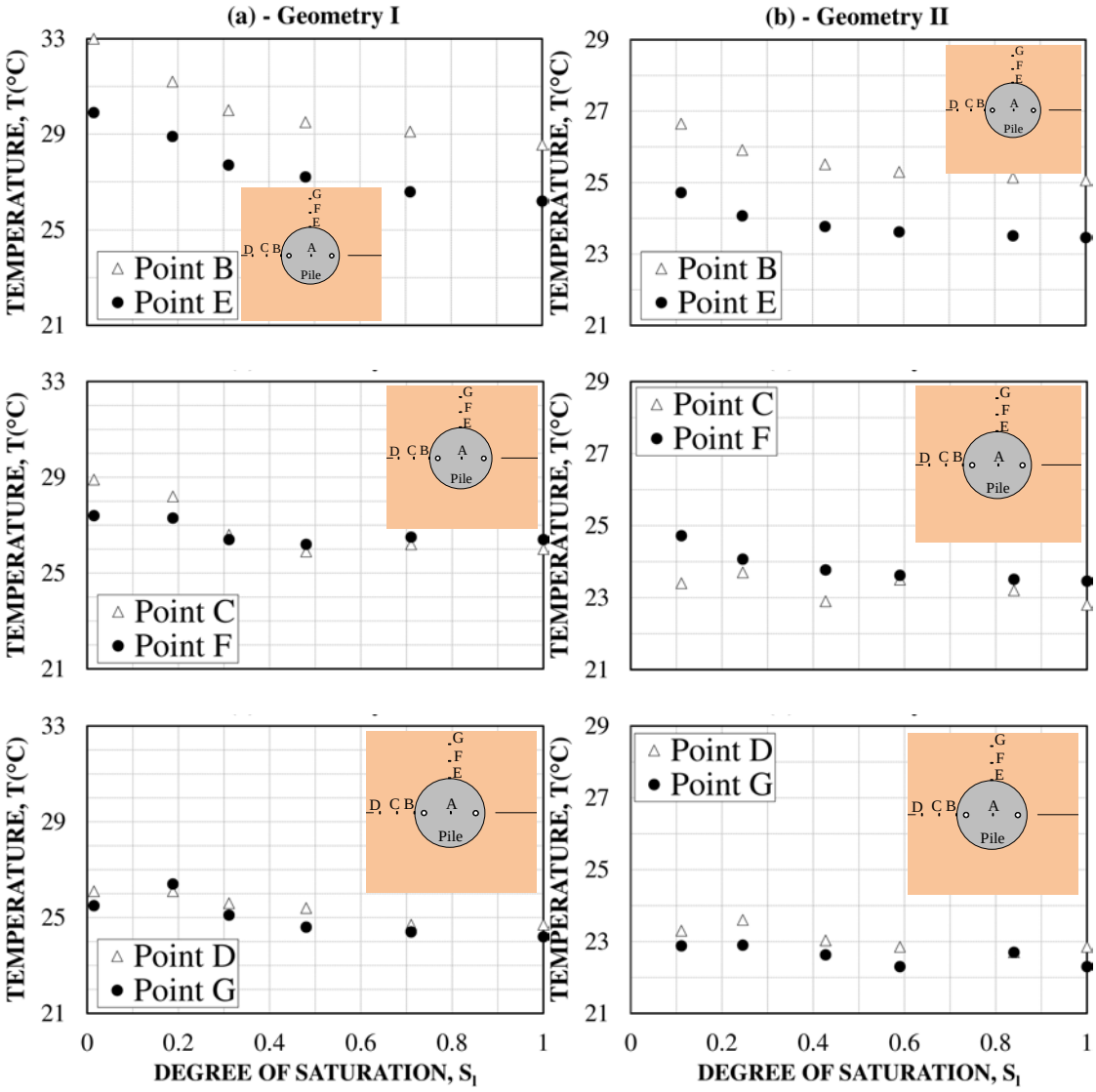

Figure 4-9 Measured pile wall and soil temperature vs. degree of saturation

In unsaturated conditions, the pile-soil interface temperature increases which causes a decrease in the temperature gradient between the HCF and the pile wall, and results in a decrease in the heat exchange rate of the energy pile and the SGES performance.

4.4 NUMERICAL MODELING

The results of the laboratory pile tests and laboratory sample tests provide important data to validate a numerical modeling approach, which can later be extended and applied to other geometries. The numerical model results were verified against the measured data from the laboratory pile test. The numerical model was used to evaluate the heat flux, q, (W/m^2) at the pile wall for different degrees of soil saturation. From the results of the heat flux, the thermal efficiency was evaluated and compared to the analytical solution (Eq. 4.9) for different expressions of λ_n (Table 4-1). This gave the variation of ζ vs. S_l at a specific depth of the pile. The numerical model was then extended to account for the soil saturation profile. Different saturation conditions and soil types were used in the pile profile model and from this model the saturation profile was evaluated with its associated heat flux profile. From the heat flux profile, the ζ was evaluated by dividing Q_{Unsat} to Q_{Sat} and compared to the analytical solution presented in this paper. This gave the ζ curve along the pile for a certain soil saturation profile. From this result, the average thermal efficiency ratio was evaluated by integrating the ζ profile over the depth of the pile.

4.4.1 Laboratory pile test model results

Figure 4-10 shows the geometry, mesh, initial conditions, and boundary conditions of the laboratory pile test numerical model. The initial conditions were the starting temperature of the sand, concrete, and PVC pipes, which were at room temperature (21 °C). The boundary conditions corresponded to room temperature at the edges of the model (21 °C) and water temperature at the inner wall of the pipes (37 °C for Geometry I and 30 °C for Geometry II). The material properties used in the numerical model are presented in Table 4-2 for each test.

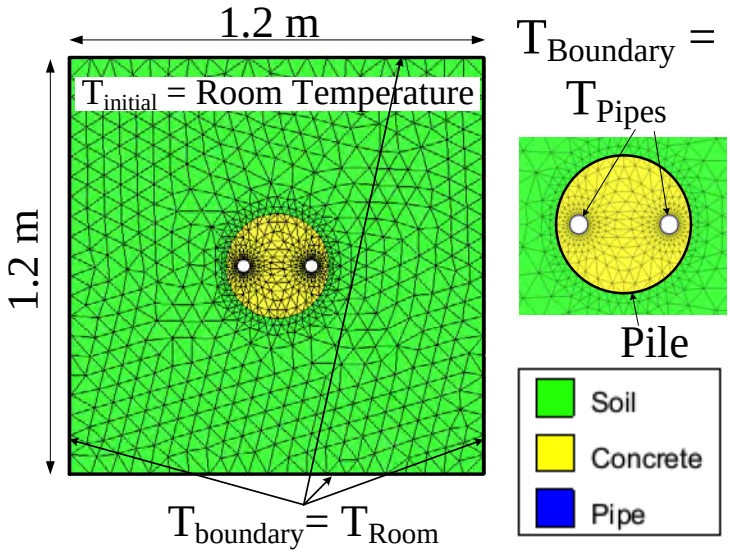

Figure 4-10 Numerical model and initial boundary conditions

To verify the numerical model, the measured temperature increase at points B to G from Test 1 were compared to the results from the numerical simulation for the same

test (Figure 4-11). The calculated and measured temperature showed good consistency, which validated the use of the numerical model to calculate the temperature distribution and conduction heat flux in the soil.

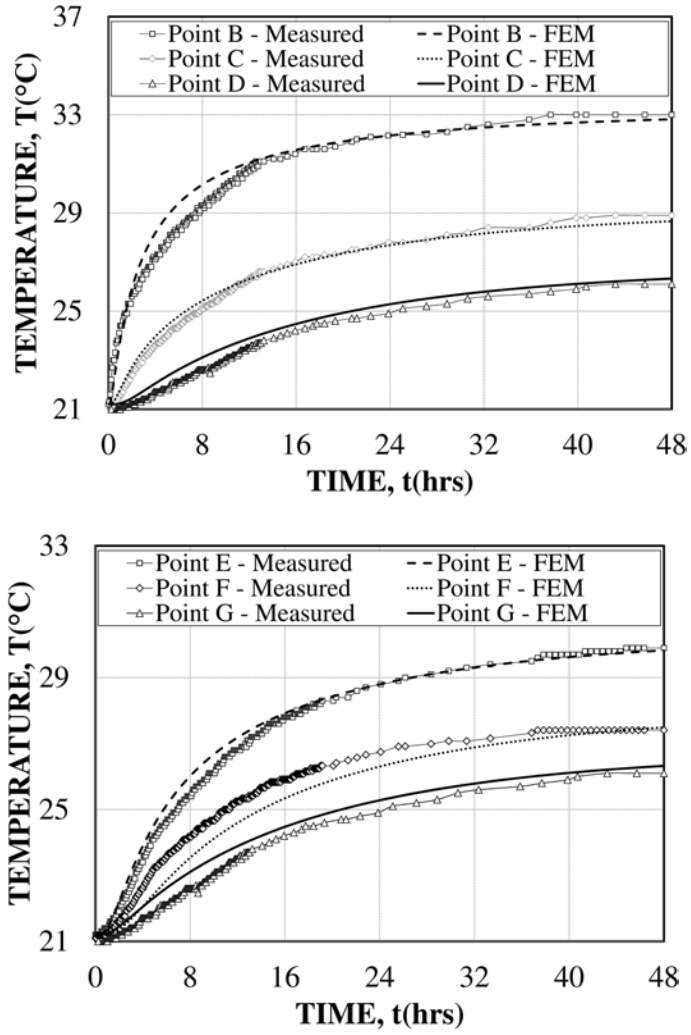

Figure 4-11 Measured and calculated temperature increase from Test 1

From the numerical simulation results, the temperature contours at time t = 48 hours are plotted in Figure 4-12 for laboratory tests 1, 6, 7, and 12. Tests 1 and 6 are from Geometry I for fully dry and fully saturated conditions, respectively. Test 7 and 12 are from Geometry II for partially saturated (S_l = 0.11) and fully saturated conditions, respectively.

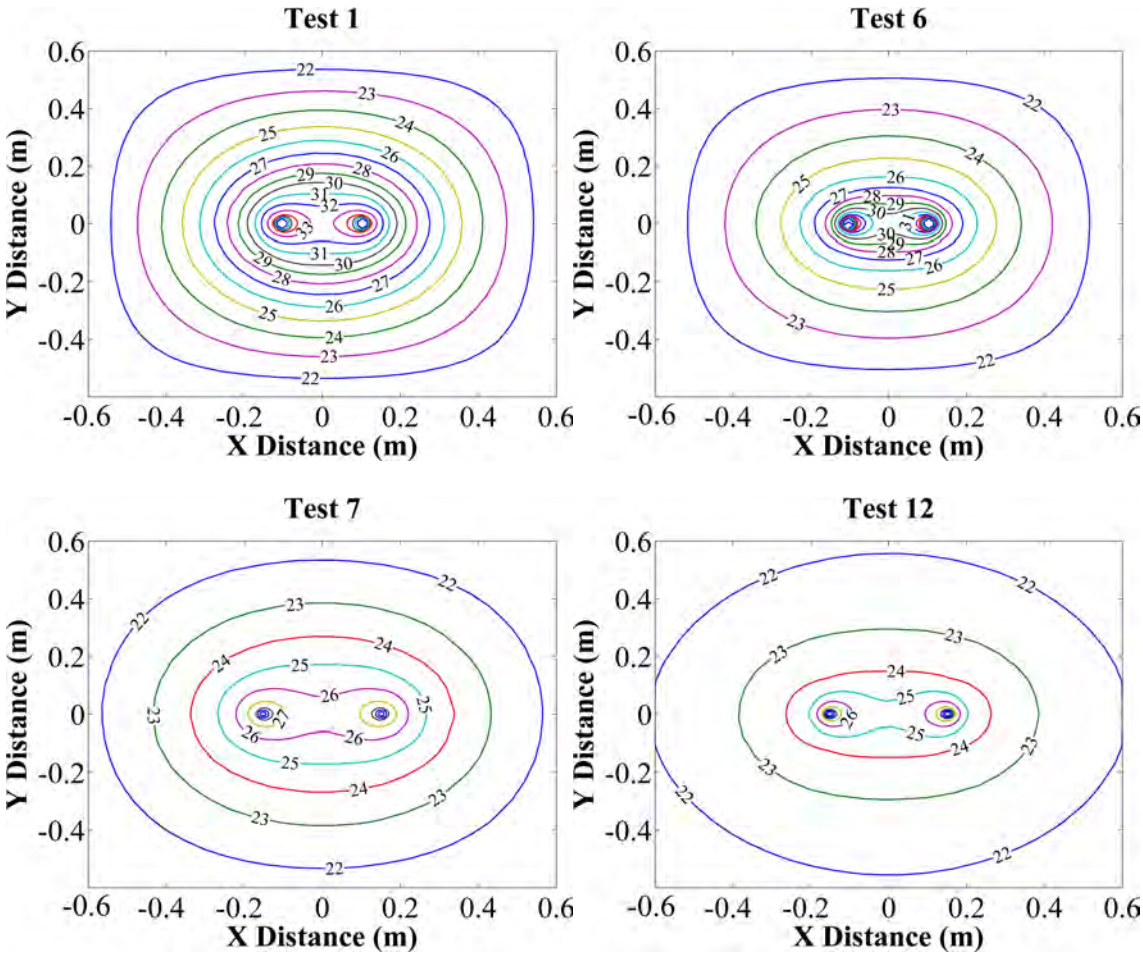

Figure 4-12 Temperature (°C) contours for Tests 1, 6, 7, and 12

Figure 4-13 presents the calculated and measured temperatures at the pile wall and shows that the temperature at the pile wall was not uniform; the temperature was maximum at the point closest to the pipes and minimum at the point furthest from the pipes.

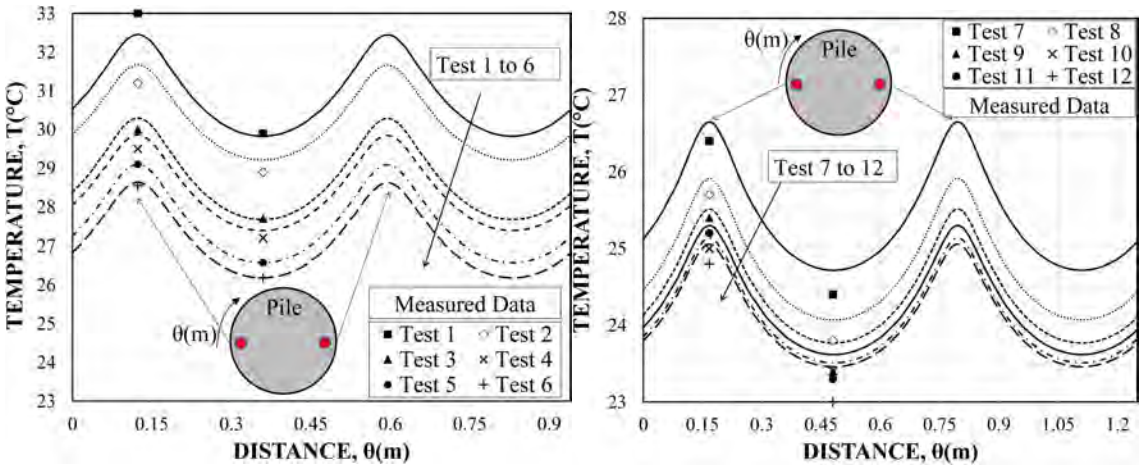

Figure 4-13 Temperature distribution around pile wall

Figure 4-14 presents the computed heat flux at the pile-soil interface. The heat flux increased with the increase in soil degree of saturation and it was maximum at the closest point to the pipes and minimum at the furthest point.

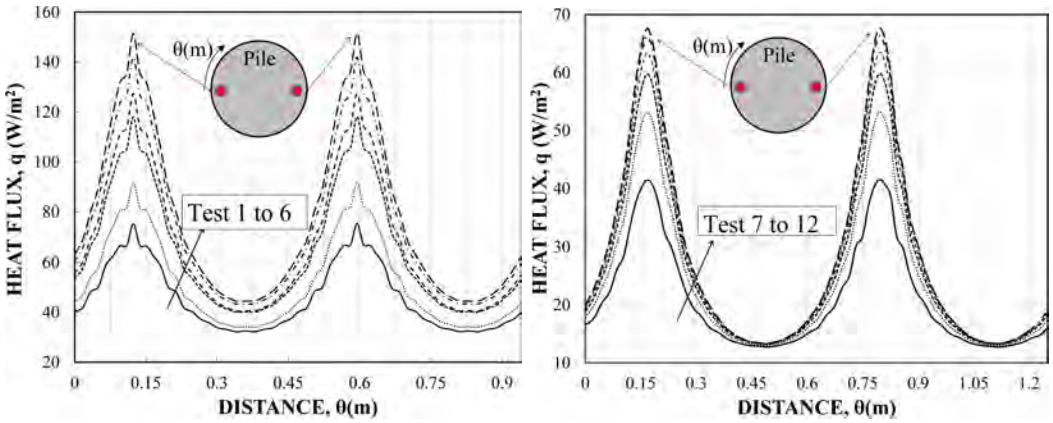

Figure 4-14 Heat flux distribution around pile wall (Left: Geometry I, Right: Geometry II)

The thermal efficiency factor (Eq. 4.1) was evaluated from the results of Figure 4-14. The total amount of heat released from the pile was evaluated by integrating the heat flux curve over the perimeter of the pile section. The results of ζ were plotted against calculated values from the analytical solution (Eq. 4.9) for the different degrees of saturation (Figure 4-15).

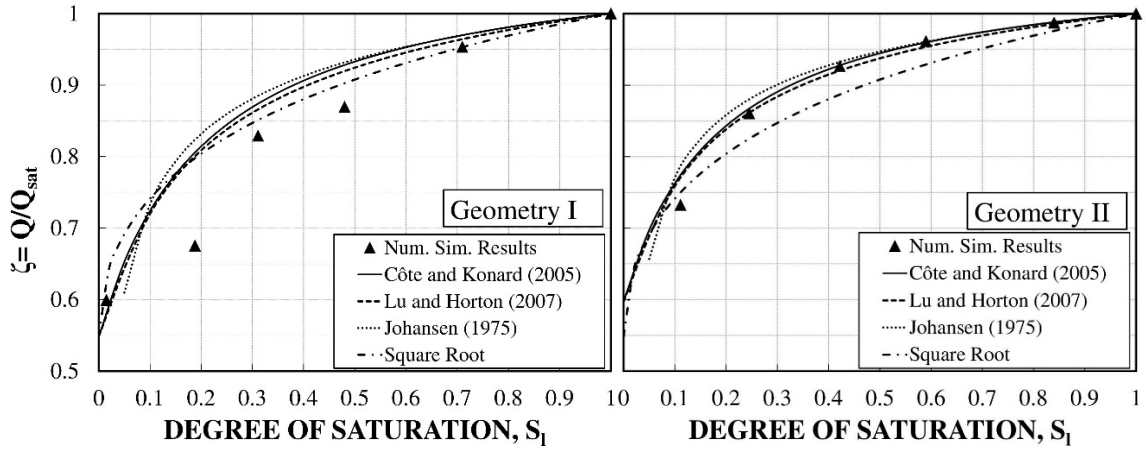

Figure 4-15 Measured and calculated ζ for Geometry I and II

Figure 4-15 shows that the analytical solutions using the different equation for λ_n gave a good prediction of the thermal efficiency factor compared to the FEM method results.

4.4.2 Pile profile numerical model

The slice section of the pile used in Geometry I of the laboratory test was extended to the entire length of pile to account for the pile profile. The same finite element software, CODE_BRIGHT, was used and a pile length L = 18 m was evaluated. In the numerical model, a water table was located at a depth z_w (m) from the ground level. Three different soil types characterized by van Genuchten model parameters were used in the numerical simulation. For each soil type, five cases were analyzed, resulting in a total of 15 simulations, where the variable was the water table elevation. The five cases for each soil type corresponded to five values of z_w/L and were 0 (case 1), 0.25, 0.5, 0.75, and 1.0 (case 5). The change in water table elevations resulted in a change in soil saturation profiles. Case 1 corresponds to a fully saturated soil condition where the water table is at the ground surface while Case 5 corresponds to the water table being at the bottom of the pile. For each case, the soil saturation and heat flux profile were derived from the numerical model, and then the ζ profile was evaluated and compared to the values calculated from the analytical solution. The geometry of the numerical model, and an example of initial and boundary conditions for $z_w/L = 0.5$, is shown in Figure 4-16.

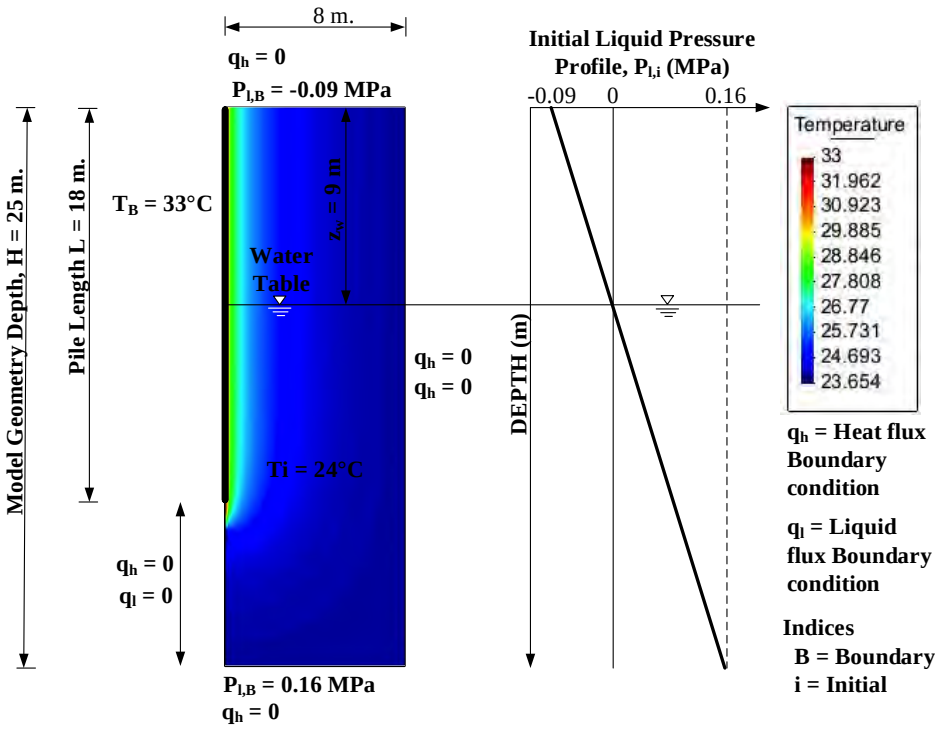

Figure 4-16 Geometry, initial, and boundary conditions of the numerical model

The properties of the three soil types used in the numerical simulations in terms of van Genuchten model parameters are presented in Table 4-3. The data from Clayton (1996), Brooks and Corey (1964), and Vanapelli et al. (1964) were used in the simulations. The assumed dry and saturated thermal conductivity in the numerical simulations for all soil types were 0.9 and 2.65 W/m.K, respectively. The thermal conductivity values were assumed for the validation purpose of the analytical solution presented in this paper.

Table 4-3 van Genuchten model parameters for sand, silt, and sandy clay

Soil Type	P_0 (kPa)	λ_0	S_{rl}	ϕ
Sand (Clayton, 1996)	3.4	0.75	0.122	0.38
Silt (Brooks and Corey, 1964)	90	0.78	0.303	0.46
Sandy Clay (Vanapelli et al., 1999)	120	0.2	0.050	0.34

The simulation corresponded to a time of 100 days. The derived thermal efficiency ratio was then compared to the results of the analytical solution (Eq. 4.11). In the analytical solution, the square root model for the normalized thermal conductivity and van Genuchten model for the SWCC were used. These two models were the same used in the numerical simulations. The results from the numerical solution (Num. Sol.) and the analytical solution (Ana. Sol.) and their corresponding degrees of saturation profile are plotted in Figure 4-17 for the different cases considered.

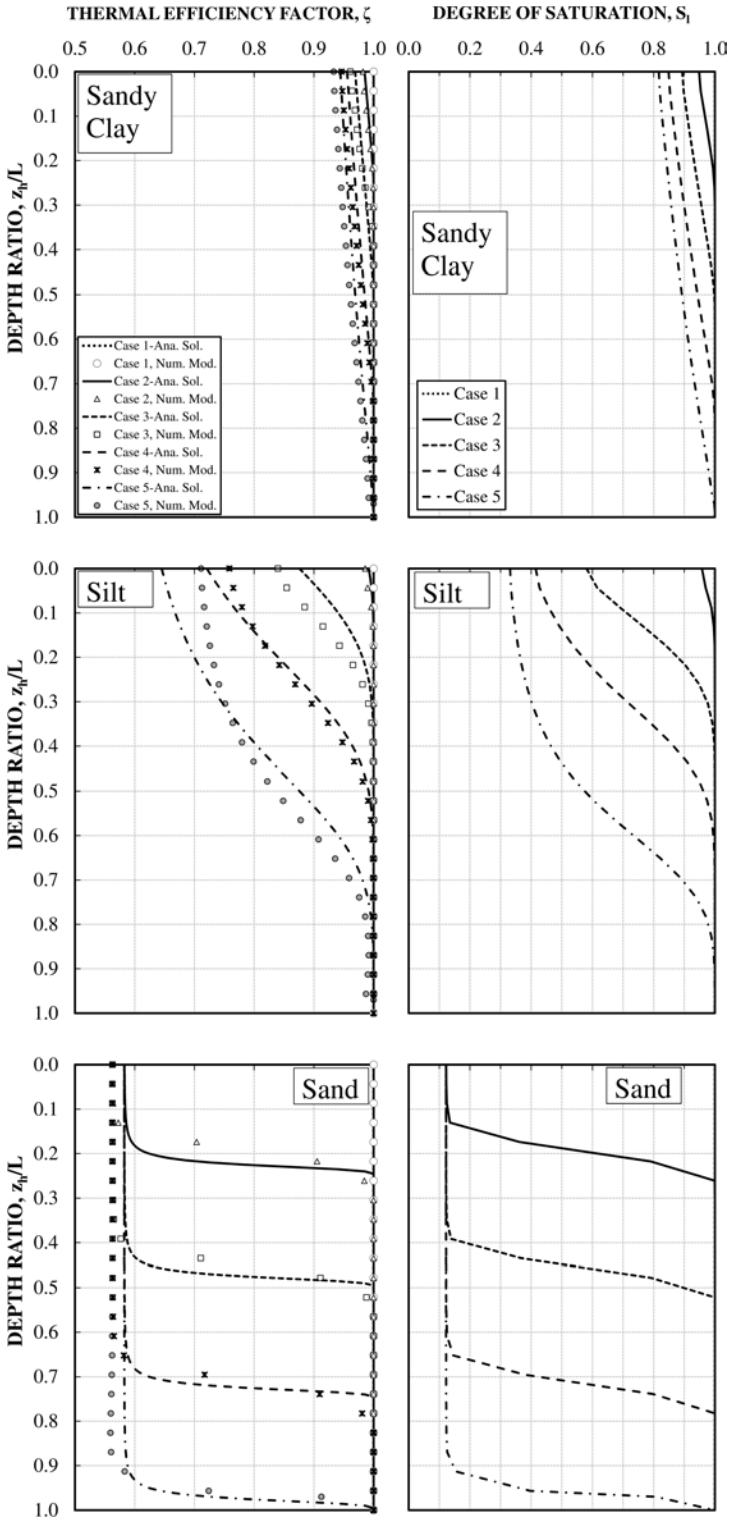

Figure 4-17 Thermal efficiency ratio and soil saturation profile for the different cases

The overall average thermal efficiency factor was evaluated for each of the 15 cases from the analytical solution and the numerical model by integrating the value of ζ over the relative depth z_w/L. The results (Figure 4-18) show that the analytical solution gave a good prediction of ζ compared to the finite element method solution.

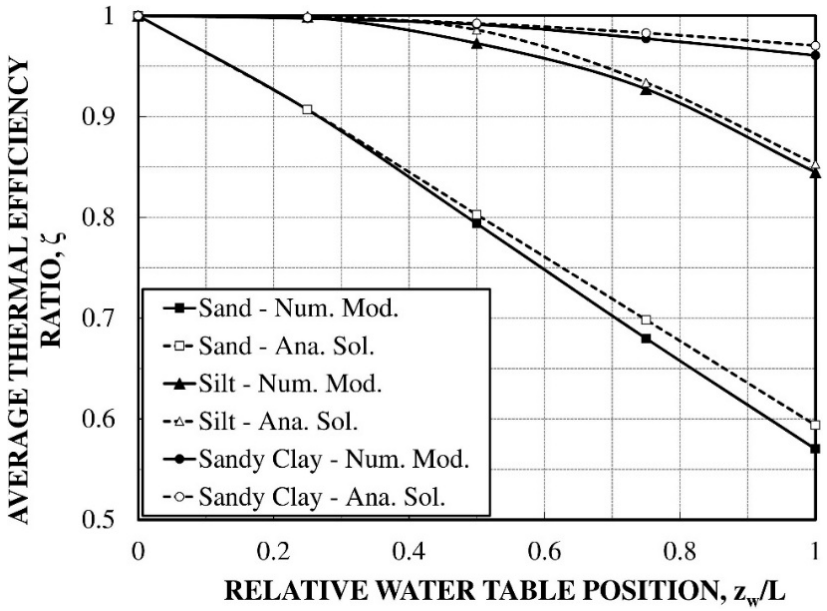

Figure 4-18 Average thermal efficiency ratio

4.5 CONCLUSIONS

This section of the dissertation presented a simple method to evaluate the heat exchange rate of energy piles in unsaturated soil conditions. The solution is based on the cylindrical heat source theory and gives the ζ function relating the ratio of the heat exchanged between an energy pile and the surrounding soil in unsaturated and saturated conditions. The ζ function depends on soil thermal properties, the degree of saturation,

and the thermal resistance of the energy pile. The ζ function was first developed to work at a specific depth, and was verified by laboratory tests and numerical simulation results on pile sections simulating an energy pile slice at a certain depth. The measured data showed a good consistency with the analytical solution and also showed, for the given conditions during the test that the performance of energy piles could drop by 40% in sand and at very low saturation conditions. The analytical solution for ζ was then developed to account for the profile of the energy pile by introducing the matrix suction parameter in the degree of saturation equation, which includes the depth variable. The analytical solution for the ζ curve was compared to the results of the 2D numerical simulations of the energy pile in axisymmetric problem and for various soil saturation profiles. The analytical solution showed relatively good consistency with the results from the numerical simulation. The difference between the two solutions may come from neglecting the propagation of heat in the vertical direction in the analytical solution. However, for preliminary sizing and design, and to avoid complicated numerical modeling of energy piles in partially saturated soils, the analytical solution can be useful.

5 THERMO-MECHANICAL BEHAVIOR OF ENERGY PILES IN HIGH PLASTICITY CLAY

5.1 INTRODUCTION

Energy pile use introduces new engineering challenges because the changes of temperature in the foundation pile and ground induce additional deformations and forces in the foundation element and coupled thermo-hydro-mechanical phenomena in the soil. Several published full-scale tests investigated this aspect of energy piles and showed thermally induced deformation and forces in the foundation element. In parallel, significant progress has been made in the understanding of thermal properties of soils and on the effect of cyclic thermal load on ground and foundation behavior. However, the effect of temperature on the creep rate of energy-piles has received practically no attention in the past. This section of the dissertation evaluates the thermo-mechanical behavior of energy piles at service and ultimate limit states based on experimental results of in-situ tension thermo-mechanical tests on energy piles of different length performed in a very stiff high plasticity clay. Service limit state represents load distribution in the pile and time-dependent deformation under service conditions. Ultimate state represents the ultimate capacity of energy piles. During the in-situ tests, the piles were subjected to thermal loading by circulating hot water in fitted pipes, simulating a thermal load in a cooling-dominated climate, at different levels of mechanical loading. The axial strain and temperature in the pile, and the load-displacement of the pile were monitored during the tension test at different locations along the center of the pile and at the pile head

respectively. The data showed that as the temperature increased the observed creep rate of the energy pile in this high plasticity clay also increased, which will lead to additional time-dependent displacement of the foundation over the life time of the structure. It was also found that the use of geothermal piles caused practically insignificant thermally induced deformation and loads in the pile itself. In addition, the results showed that the use of foundation piles as ground heat exchangers impacted the load-settlement response of energy piles without impacting its ultimate capacity.

5.2 TEST LOCATION AND MATERIAL ENGINEERING PROPERTIES

The in-situ test was performed at the National Geotechnical Experimentation Site (NGES) at Texas A&M University, Riverside campus, which is located 12 km west of the main University campus (Figure 5-1). Two main sites are located at the NGES: clay and sand sites. The soil properties of the two sites were reported in previous studies (Hueckel and Pellingrini, 1992; Bruner et al., 1994; Briaud, 1993; Marcontell and Briaud, 1994; Simon and Briaud, 1996; Tao and Briaud, 1995). The experiment reported in this section of the dissertation was conducted on a pile installed at the clay site.

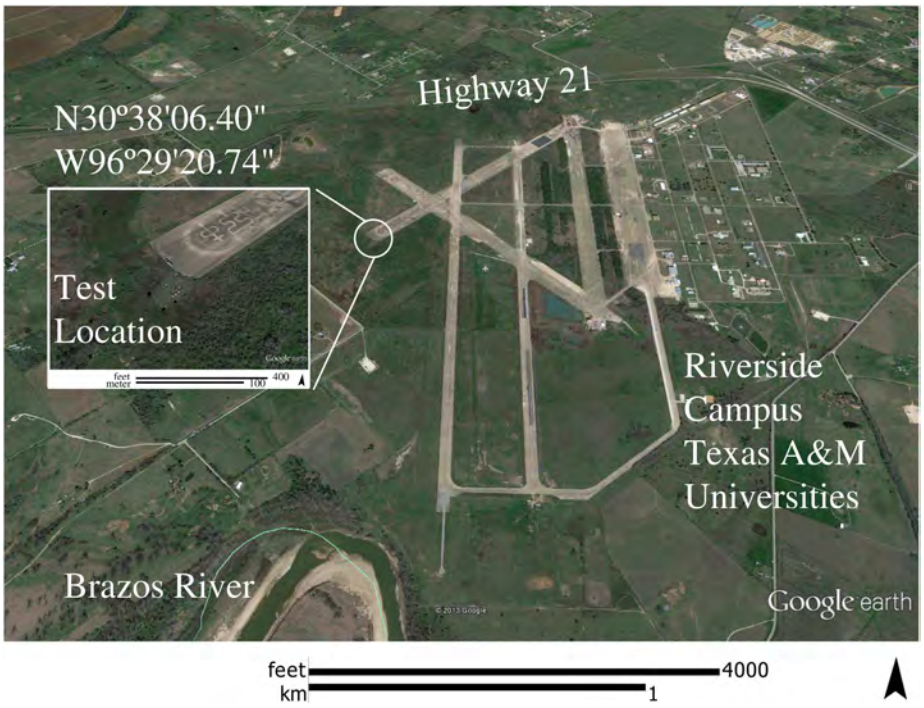

Figure 5-1 NGES clay site location from Google earth

The clay site covers an area of approximately 5500 m^2. Briaud (1997) summarized many of the laboratory and in situ tests performed at the site since 1980, and concluded that the stratigraphy of this site is composed of four layers. The top layer is red and gray very stiff high plasticity clay of a uniform thickness (about 5.5 m). The second layer is a sand layer with variable thickness averaging 1 m. Below this layer is dark gray clay-shale with inter-bedded fine-grained sand layers with an average thickness of 6.5 m. The fourth layer is a very hard dark clay (shale) layer that extends to a depth of 50 m. The soil stratigraphy, laboratory tests results, in-situ tests results, and average soil properties of each layer are summarized in Figure 5-2.

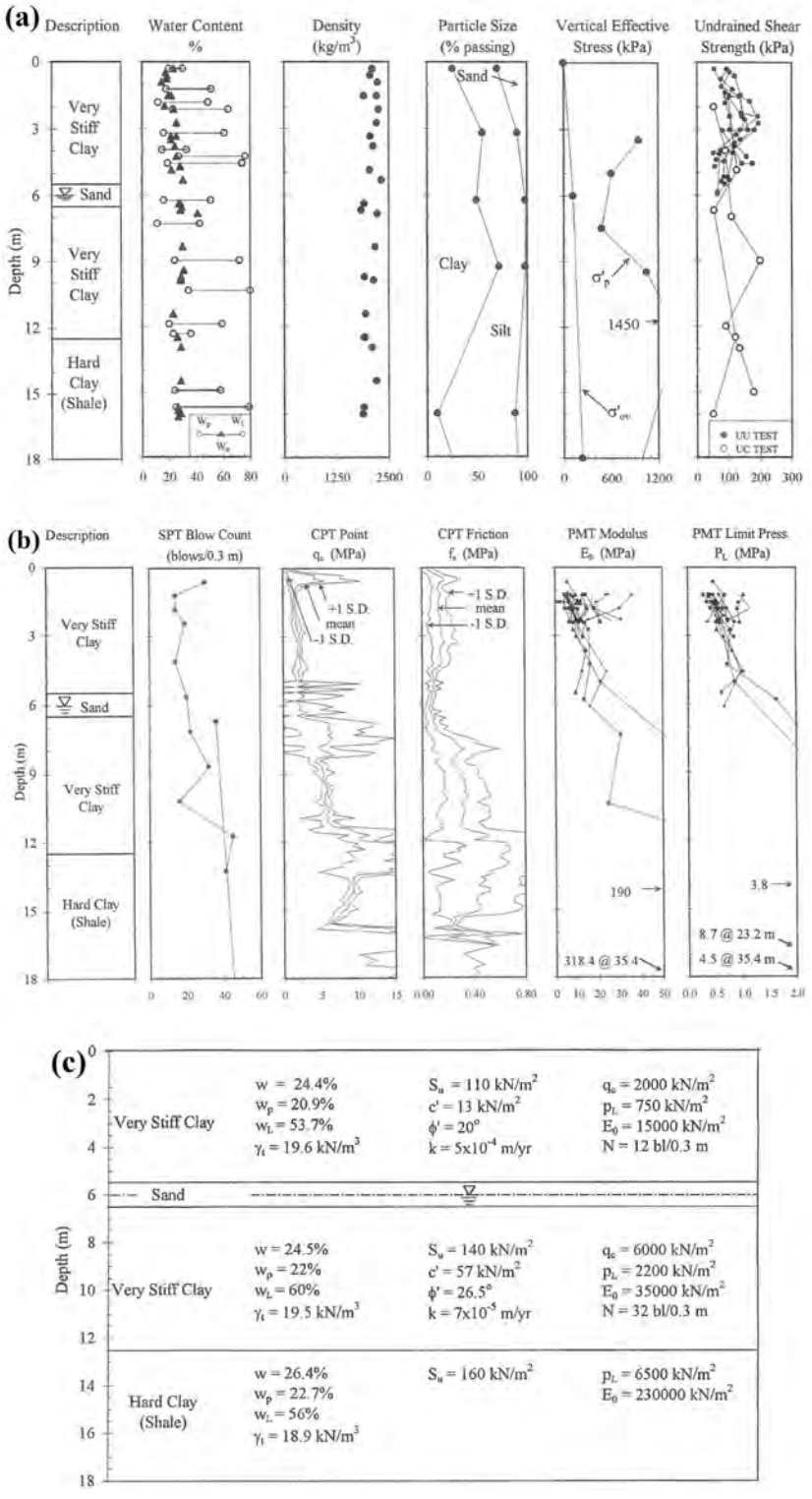

Figure 5-2 Summary of soil properties and stratigraphy from laboratory tests (a), field, tests (b), and soil profile (c) at NGES-TAMU clay site (*From Briaud, 1993*)

The compressive strength of the grout used for the tested pile was measured in the laboratory by unconfined compression on 0.05 m. diameter samples. The measured compressive strength at 28 days ranged from 22.5 to 27.6 MPa with an average of 25.7 MPa. The unit weight of the grout was 18.4 kN/m^3 and the elasticity modulus was estimated from the compressive strength to be 17,400 MPa. The PEX pipes used to circulate the water in the piles conformed to ASTM F876/F877 standards as per the manufacturer.

5.3 SOIL AND GROUT THERMAL PROPERTIES

There is no data reported in the literature on the thermal properties of the soil layers where the piles were installed. To determine these properties, three soil samples were extracted from the site during the drilling process at a depth of 1 m., 2.1 m., and 5.1 m. and labeled N2-2-4, N2-8-10, and N2-16-18, respectively. The Shannon and Wells (1947) method, described in Section 3.6 of this dissertation, was used to evaluate the soil and grout thermal properties.

The measured engineering and thermal properties of the tested samples are summarized in Table 5-1, including the thermal conductivity λ (W/m.C), volumetric heat capacity C (MJ/m^3.C), thermal diffusivity α (m^2/s), total unit weight γ_T (kN/m^3), dry unit weight γ_d (kN/m^3), gravimetric water content w (%), porosity n, and degree of saturation S (%).

Table 5-1 Measured engineering and thermal properties of tested soil samples

Sample ID	Depth (m)	λ	C	α x 10^{-7}	γ_T	w	γ_d	n	S
N2-2-4	1.0	0.61	2.6	2.32	20.9	16.6	17.9	0.3	98
N2-8-10	2.1	0.82	2.8	2.86	19.3	25.9	15.3	0.41	98
N2-16-18	5.1	0.85	2.8	2.95	19.1	27.1	15.0	0.42	98
Grout	-	0.87	3.3	2.62	18.4	-	-	-	-

5.4 TEST LAYOUT AND SETUP DETAILS

The tension test layout and details are shown in Figure 5-3. The tested piles were labeled N7, N8, N9, N10, and N11. Piles N7 and N8 were part of a group of eight piles installed at the NGES clay site labeled N1 to N8 to study the creep behavior of piles. N7 and N8 were energy piles; the remaining six piles were used to study the creep of piles under mechanical loading only and are not discussed in this dissertation. The piles N7 and N8 were drilled on July the 17th, 2013, and were grouted up to the ground level on the same day. The instrumented steel rebar and pipes were inserted in the drilled holes immediately after finishing the drilling process and before grouting. All the piles were 0.18 m in diameter and 5.5 m long. Each of the piles was reinforced with a 25 mm diameter steel bar placed at the center of the drilled hole; the steel was of grade 75 with a yielding stress f_y equal to 517 MPa and an elasticity modulus E_{Steel} equal to 204,000 MPa. The two energy piles were each fitted with 19 mm inner diameter and 23 mm outer diameter PEX pipes U shape loops. The pipe legs of the U were 0.1 m apart center to center and were bent at a distance of 0.4 m from the bottom of the pile. A concrete slab (9x6x0.3 m^3) was used as a platform to drill the piles and to perform the load test. The slab was reinforced with #6 bars in a mesh of 0.3 m x 0.3 m. When the slab was

poured, eight circular openings of 0.3 m diameter and two circular opening of 0.15 m diameter were kept in the slab at the location of the eight nails and the two boreholes, respectively. This ensured an easy drilling and pile installation process.

Piles N9, N10, and N11 were used to evaluate the ultimate capacity of energy piles in heating and cooling mode in high plasticity clays. Those piles were drilled and grouted on August the 29th, 2013. The instrumented steel rebar and pipes were inserted in the drilled holes immediately after finishing the drilling process and before grouting. All the piles were 0.18 m in diameter and drilled to the same depth. Piles N9 and N10 were grouted to have a bonded length of 2.1 m, while pile N11 was grouted to have a bonded length of 2.7 m. Each of the piles was reinforced with a 25 mm diameter steel bar placed at the center of the drilled hole with same properties as the bars used for N7 and N8. The piles were each fitted with 19 mm inner diameter and 23 mm outer diameter PEX pipes U shape loops. The pipe legs of the U were 0.1 m apart center to center and were bent at a distance of 0.1 m from the bottom of the pile. A schematic of the pile locations and representative cross sections of piles N7/N8 and N9/N10/N11 is provided in Figure 5.3, below.

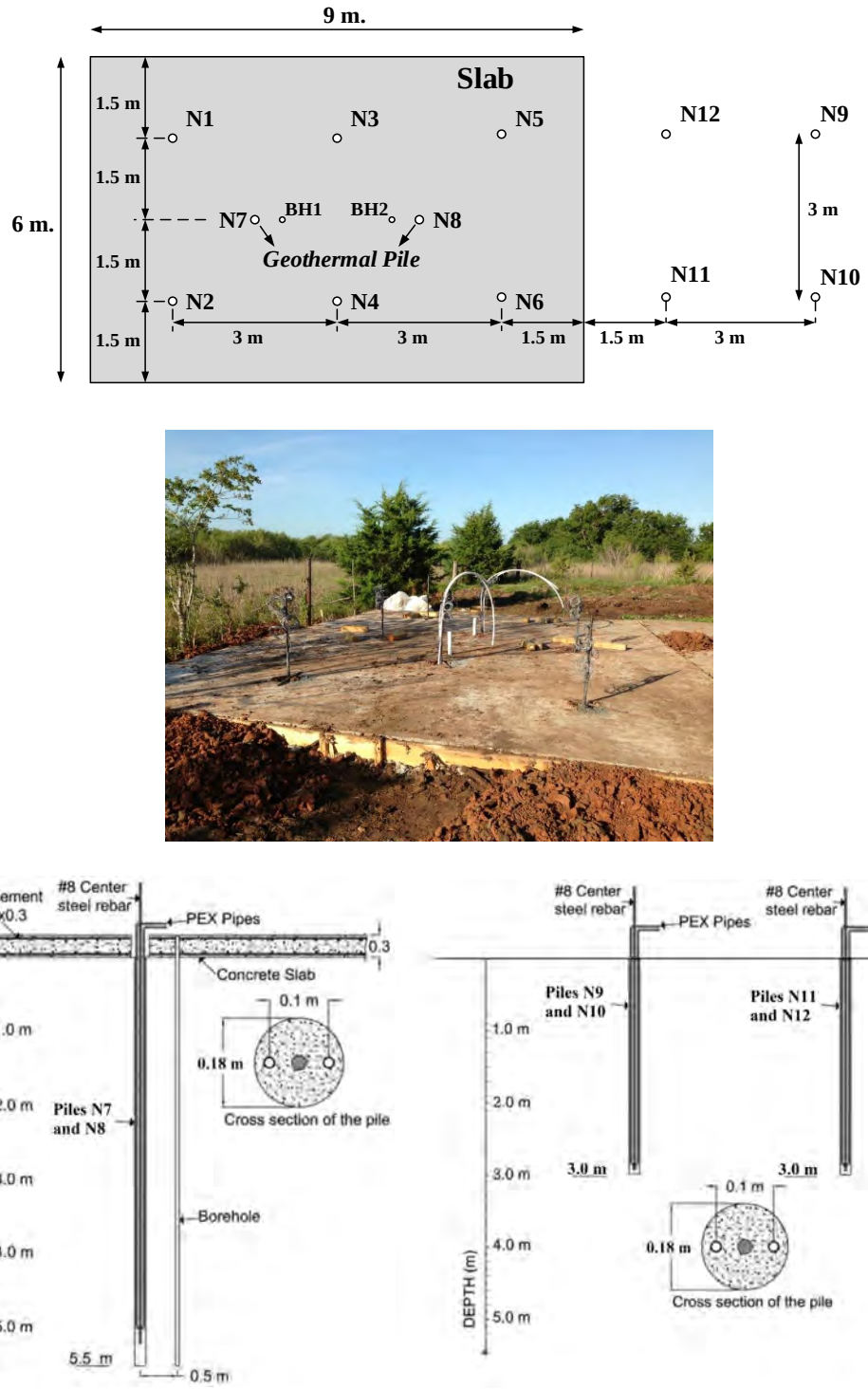

Figure 5-3 Piles layout with slab dimensions; picture of mat; cross section of piles N7and N8; cross section for piles N9, N10, and N11

To avoid a power disconnection, a 3 kW Honda portable power generator was used as the power source for the instruments and tools at the site. A central hole hydraulic jack of 500 kN capacity was used to apply the load on the nail. The circulated water in the pipes was stored in a small tank. The water was circulated from the tank to the energy pile using a 1/2 HP portable cast iron water pump.

5.5 INSTRUMENTATION

The energy piles were instrumented to monitor the main tests variables: displacement, strains, temperature, and relative humidity. Table 5-2 summarizes the instrumentation used for piles N7, N8, and table 5-3 summarizes the instrumentation used for piles N9, N10, and N11.

Table 5-2 Instrumentation summary in piles N7 and N8

	Instrument	Measurement	Number Used
Mechanical Measurement	Strain gauge model UFCA-5-11 installed along the pile at depth z = 1, 1.2, 1.4, 2.4, 3.4, and 4.4 m	Strain in the pile	6
	Dial gauge	Pile head displacement	2
	Pressure gauge	Pressure applied on the loading frame	2
	Load cell model 3000 from Geokon	Load applied on the pile	1
Thermal Measurements	Thermocouple type T from Omega, installed along the pile and borehole at depth z = 1, 1.2, 1.4, 2.4, 3.4, and 4.4 m	Temperature along the pile and the borehole adjacent to the pile	12
	Thermocouple type T from Omega	Water Temperature	1
	Air temperature and relative humidity sensor from Extech	Weather conditions during the test	1

Table 5-3 Instrumentation summary in piles N9, N10, and N11

	Instrument	Measurement	Number Used
Mechanical Measurement	Dial gauge	Pile head displacement	2
	Pressure gauge	Pressure applied on the loading frame	2
	Load cell model 3000 from Geokon	Load applied on the pile	1
Thermal Measurements	Only in piles N9 and N11: Thermocouple type T from Omega, installed along the pile at depth z = 0.5, 1.5, and 2.5 m.	Temperature along the pile and the borehole adjacent to the pile	3 per pile
	Thermocouple type T from Omega	Temperature in the water tank	1
	Air temperature and relative humidity sensor from Extech	Weather conditions during the test	1

For piles N7 and N8, the central steel bar was instrumented with six strain gages at different levels to track the strains that developed in the pile under thermo-mechanical loading. The strain gauges used for the test were model UFCA-5-11 from Tokyo Sokki Kenkyuji Co. Ltd. Full bridge strain gauges with temperature and bending compensation were used. At the same level as the strain gauges, six thermocouples type T from OMEGA were installed in both the pile and adjacent borehole, BH1 and BH2 located at 0.5 m center to center from the energy piles. The thermocouples in the pile tracked the temperature changes at the center of the energy pile in order to relate the changes in strain with the changes in temperature. The thermocouples in the adjacent borehole tracked the temperature in the soil because of the thermal use of the pile. For

piles N9 to N11, the central steel bar was instrumented with only three thermocouples at different depths (Table 5-3) to track the temperature change along the pile.

A load cell model 3000 from GEOKON was used to measure the applied load at the pile. In addition, and for a double check, the load on the pile was measured from the pressure gauges installed on the hydraulic jack. Dial gauges were placed at the top of the energy pile to measure the vertical pile displacement. The instruments were connected to read out boxes and data loggers in order to electronically store the measured data and the other part was read manually. The air temperature and relative humidity during the test was recorded using a temperature and relative humidity USB data logger from Extech.

5.6 IN-SITU TEST PLAN

The aim of the in-situ test program was to understand the behavior of energy piles at both service and ultimate state conditions under mechanical and thermo-mechanical loads. Piles N7 and N8 were tested under service load while piles N9 to N11 were tested to failure.

The testing program on piles N7 and N8 was divided into two rounds, Round 1 and Round 2. In Round 1, five tension load tests were performed on energy pile N7, referred to as Test 1, Test 2, Test 3, Test 4, and Test 5 with a tension force T of 40, 100, 150, 200, and 256 kN respectively applied at the top of the pile. In Round 2, two tension load tests were performed on pile N7 referred to as Test 4 and Test 5 with a tension force T of 200 and 256 kN respectively. In addition, three tension load tests were performed

on pile N8 referred to as Test 3, Test 4, and Test 5 with a tension force T of 150, 200, and 256 kN, respectively (Table 5-4).

Table 5-4 Testing plan

Pile – Round	Test ID	Tension Load
Pile N7 – Round 1	Test 1	40
	Test 2	100
	Test 3	150
	Test 4	200
	Test 5	256
Pile N7 – Round 2	Test 4	200
	Test 5	250
Pile N8 – Round 1	Test 3	150
	Test 4	200
	Test 5	250

In each test, the pile was mechanically loaded for 1 hour (60 min). After 1 hour of applying the load, the water pump was turned on to circulate the water into the pile. The water was heated by the high temperature weather and the work done by the water pump, resulting in an increase in circulating water temperature of 10 to 15 ºC in Round 1, and using a water heater in Round 2 resulting in pile temperature increase of 12 to 15 ºC. The water pump was run for 4 hours after finishing the mechanical loading step. The total time of the test was 5 hours (300 min). During this time, the pile and soil temperature, axial strain in the pile, air temperature and relative humidity, and circulating water temperature was monitored using the instrumentation described in the

previous section. The full-scale test (Pile N7-Round 1) sequence is visualized in Figure 5-4 with the time on the horizontal axis and the applied tension load on the vertical axis. The same sequence was used for pile N7-Round 1 and N8-Round 2 tests. The shaded area under each test represents the time frame when thermal load was applied.

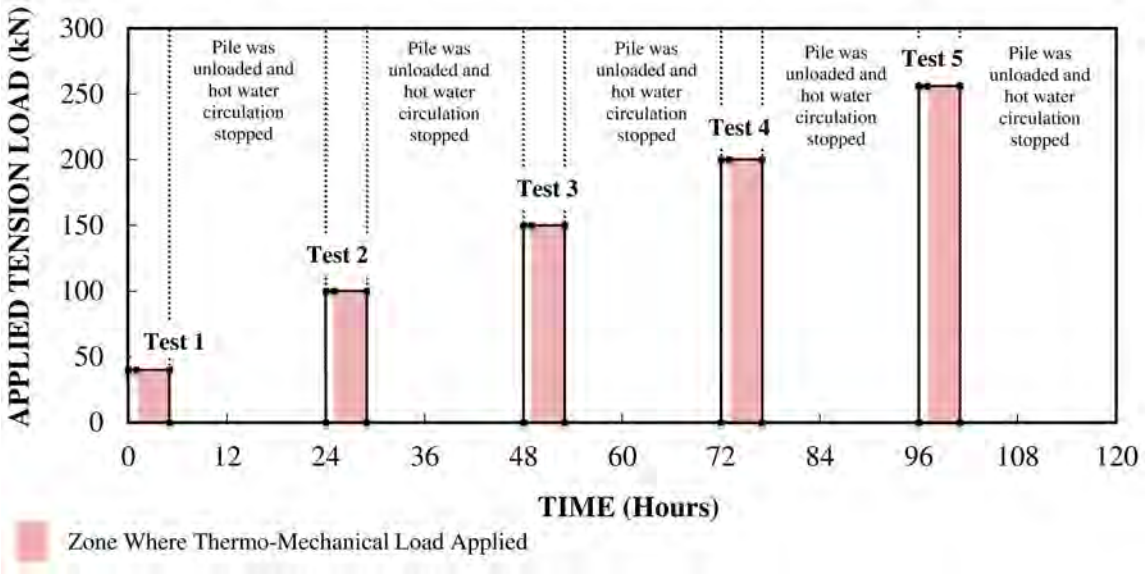

Figure 5-4 Full scale test schedule (Pile N7 – Round 1)

The loading setup showing the hydraulic jack and pump, water pump, power generator, water tank, readout boxes and data logger, and load cell is shown in Figure 5-5. Round 1 of the pile load tests were performed from the second to the sixth of August, 2013, starting with Test 1 and ending with Test 5, while Round 2 of the tests were performed from the 21st to 28th of October starting with N7-Test 3 and ending with N8-

Test 5. Each day, one load step was applied; by the end of the test, the pile was unloaded and the water pump was turned off.

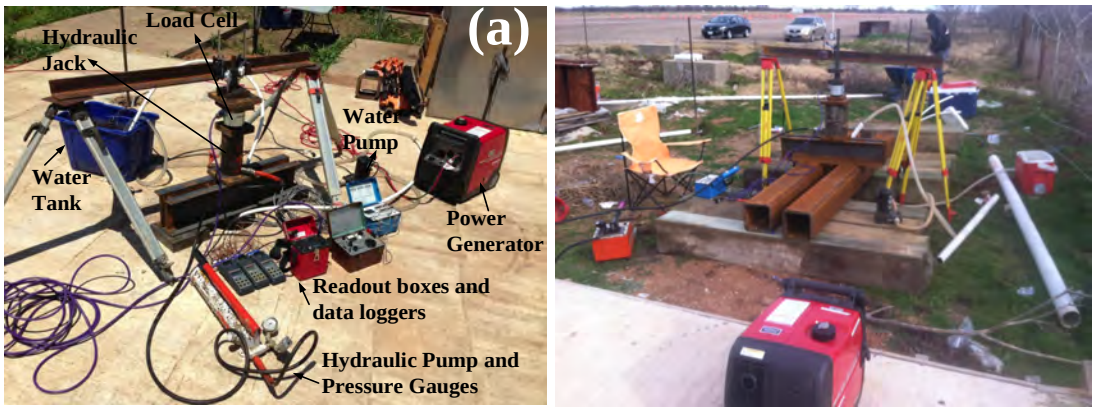

Figure 5-5 Test Setup a) piles N7 and N8, b) piles N9, N10, and N11

Piles N9 to N11 were tested to failure. N9 and N10 were similar in geometry with a 0.175 m. diameter and a 2.1 m. length. Pile N11 was 0.175 m. in diameter and 2.7 m. long. To evaluate the effect of temperature change on the ultimate capacity of energy piles, N9 was tested to failure under mechanical load only (without any temperature change), while N10 and N11 were subjected to cooling and heating loads prior to mechanically loading the pile to failure respectively. The load settlement curve was measured for each test and normalized for comparison purposes under mechanical and thermo-mechanical loads. Under mechanical loading, the tested pile was subjected to monotonic load steps until it reached failure, while under thermo-mechanical loads, the pile was heated or cooled for 4 hours until it reached a steady state and then

subjected to monotonic mechanical loading until failure. Pile N10 was cooled by circulating cold water, cooled using ice bags in a cooler to a temperature of 12 °C, while pile N11 was heated by circulated hot water heated in a water tank with a water heater to a temperature of 14 °C.

5.7 EXPERIMENTAL TEST RESULTS – PILE TEST UNDER SERVICE CONDITIONS – PILES N7 AND N8

In this section the main results obtained during the tests of piles N7 and N8 are presented for the different stages considered in the field experiments. First the variation of temperature in the pile and soil are presented alongside of the air temperature and relative humidity fluctuations during the tests. Then the movements of the pile during the loading tests are introduced. Finally the distribution of loads along the pile during the tests is presented.

5.7.1 Pile, soil, water, and air temperature

During each test, the pile, soil, circulating water, and ambient-air temperature was monitored using the instrumentation described in the previous section. The circulating water temperature (Figure 5-6) increased to an average of 44 ºC during N7-Round 1, 46 ºC during N7-Round 2, and 58 ºC during N8-Round 1 tests.

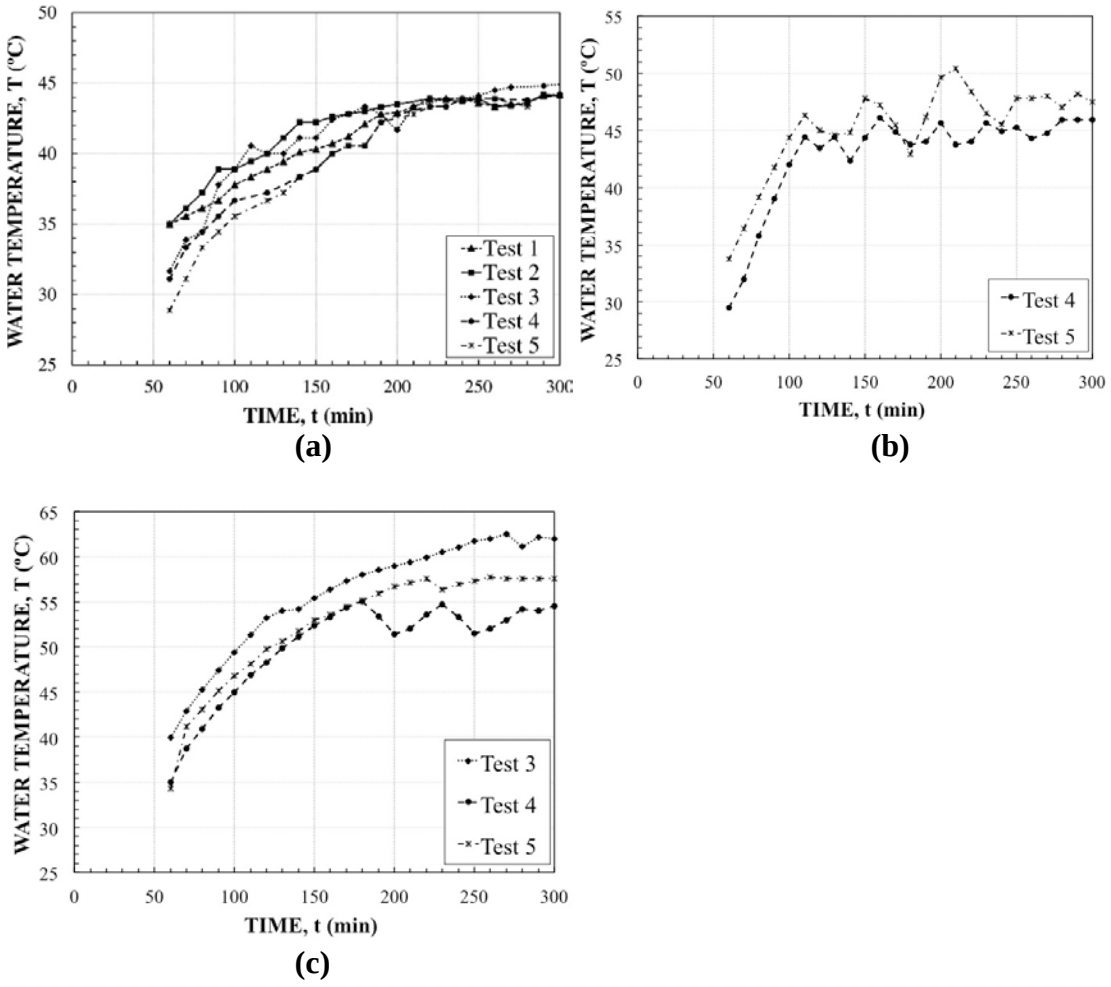

Figure 5-6 Circulating water temperature: a) N7-Round 1, b) N7-Round 2, c) N8-Round 1

During the five tests, the temperature gradient between the circulating water and the soil generated a heat flux from the pipes toward the concrete and the soil resulting in an increase in the pile and soil temperature. The initial soil and pile temperatures were not uniform because the pile was located in the shallow soil layer where the soil temperature is variable and highly affected by climatic conditions. As a result, the

temperature gradient between the circulating water and soil was not uniform, which caused a non-uniform increase in pile temperature. Figures 5-7, 5-8, and 5-9 show the pile and soil (BH) temperature for the different load steps at time t = 60, 120, 180, 240, and 300 min where time t = 60 min corresponds to the beginning of thermal load application and t = 300 min corresponds to the end of the test. The position BH corresponds to boreholes 1 and 2 (Figure 5-3, identified as BH1 and BH2). There was a very small increase in soil temperature at the borehole location because of the short duration of the test; therefore, the temperature reading in BH1 was used as a reference temperature to the temperature in the pile during the test. The air temperature and relative humidity during the period when the test was performed was recorded and is presented in Figure 5-10 and 5-11. The summary of temperature and RH is presented in Table 5-5.

Table 5-5 Summary of temperature and RH measurements

Pile – Round	Test ID	Pile ΔT (°C)	Air Temperature (°C)			Air RH (%)		
			T_{max}	T_{min}	T_{mean}	RH_{max}	RH_{min}	RH_{mean}
Pile N7 – Round 1	Test 1	9.31	39	24	30	96	22	63
	Test 2	9.40						
	Test 3	8.56						
	Test 4	7.16						
	Test 5	7.06						
Pile N7 – Round 2	Test 4	11.39	28	8	19	100	28	74
	Test 5	13.90						
Pile N8 – Round 1	Test 3	13.10	28	8	19	100	28	74
	Test 4	12.94						
	Test 5	15.00						

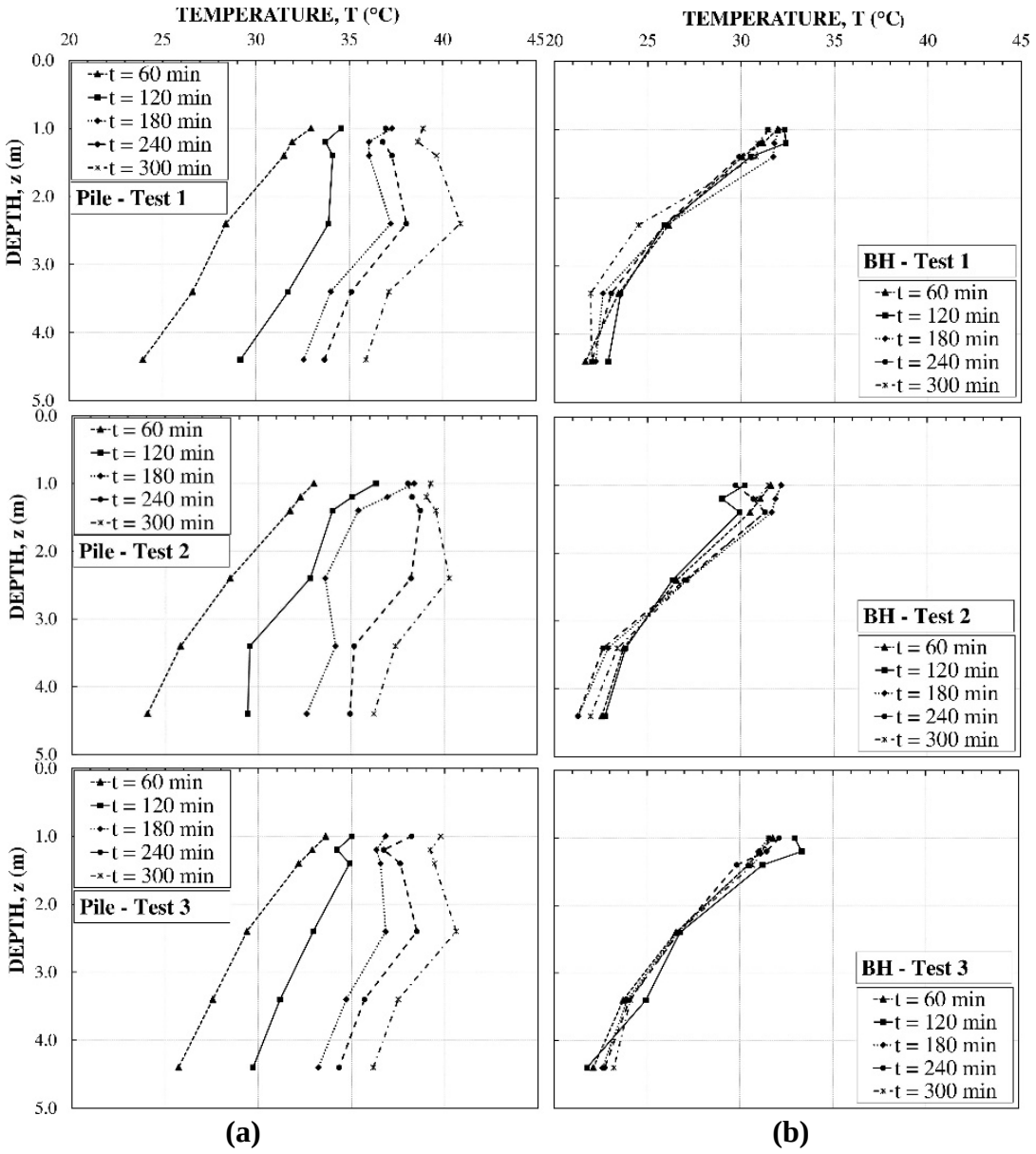

Figure 5-7 a) Pile and b) soil temperature during the test at different times and load steps – N7 – Round 1

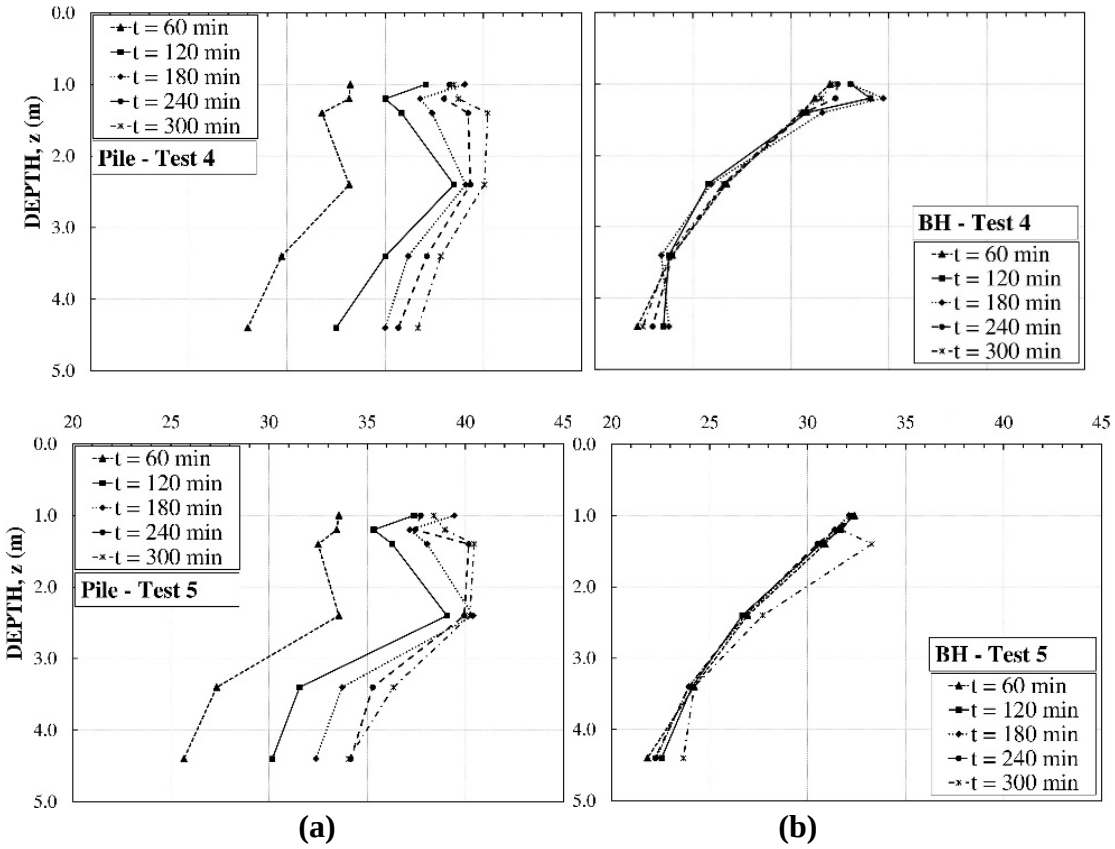

Figure 5-7 Continued

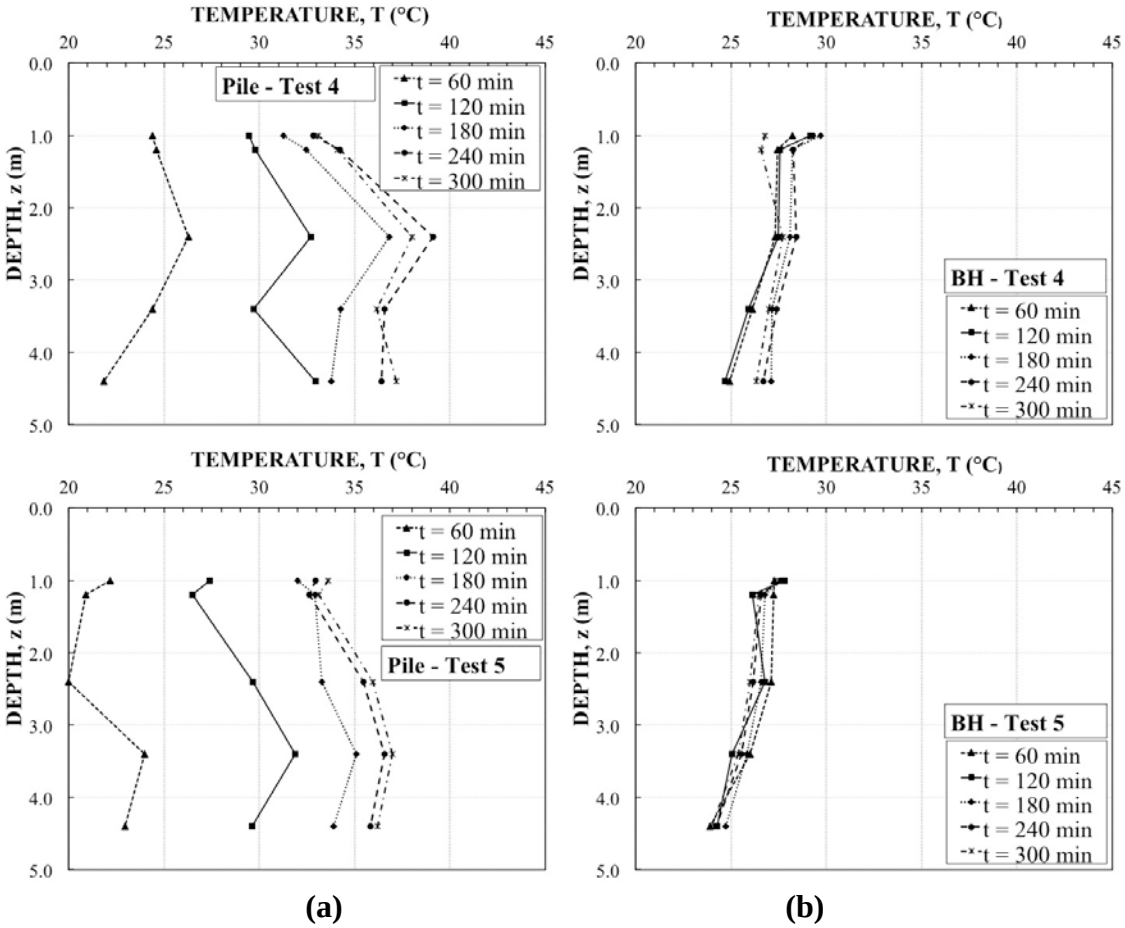

Figure 5-8 a) Pile and b) soil temperature during the test at different times and load steps – N7 – Round 2

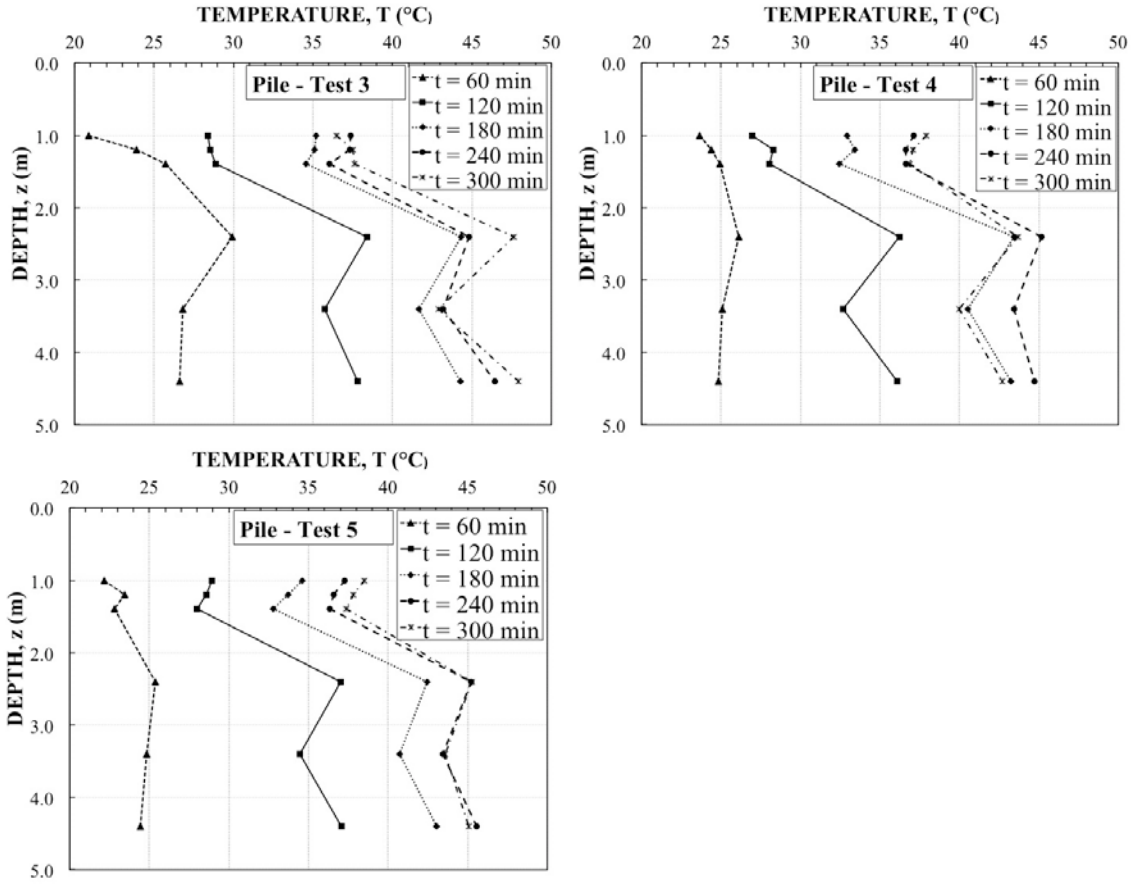

Figure 5-9 Pile temperature during the test at different times and load steps – N8 – Round 1

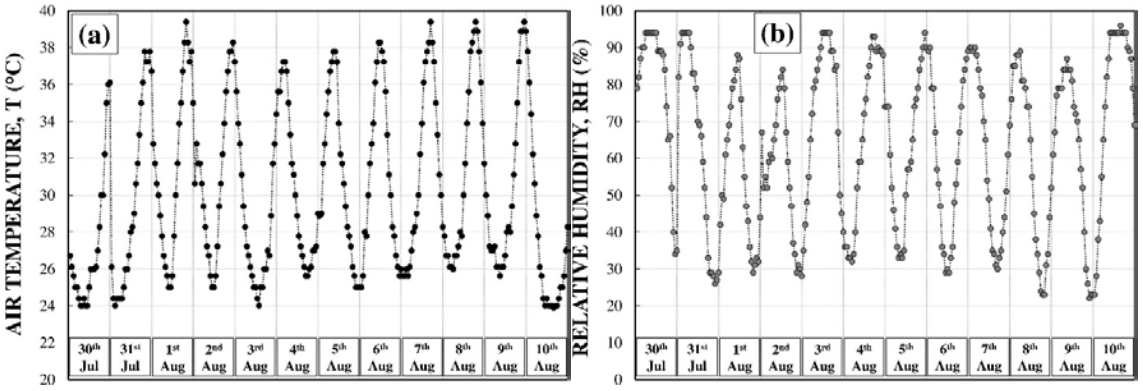

Figure 5-10 a) Air temperature and b) air relative humidity during round 1

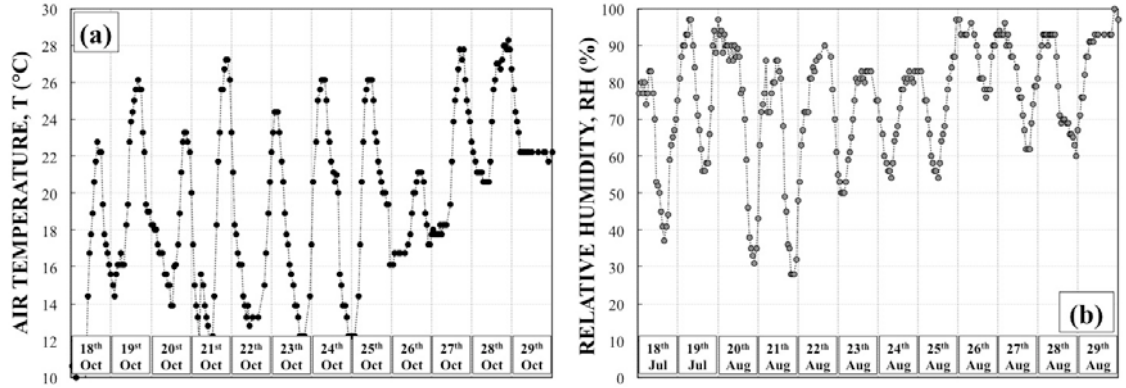

Figure 5-11 a) Air temperature and b) air relative humidity during round 2

5.7.2 Pile head movement

The load-displacement behavior of foundation piles directly impacts the serviceability and safety of the structure above it. To determine the amount of pile displacement associated with cyclic thermal loading of energy piles, dial gages were used during each of the five load steps (Figure 5-5). The load on the pile was kept constant during each test and the displacement versus time was measured. The load-displacement curves for

all the tests are shown in Figures 5-12, 5-13, and 5-14. The left side of those figures shows the pile displacement on a natural scale while the right side shows the pile displacement on a log-log scale for creep analysis. At the application of the tension load (t = 0 min), the pile exhibited a rapid increase in displacement for the first few minutes. This increase then slowed with time and became a nearly constant rate before applying the thermal load. After applying the thermal load (t=60 min), the displacement rate began to increase with the increasing temperature of the pile and the soil.

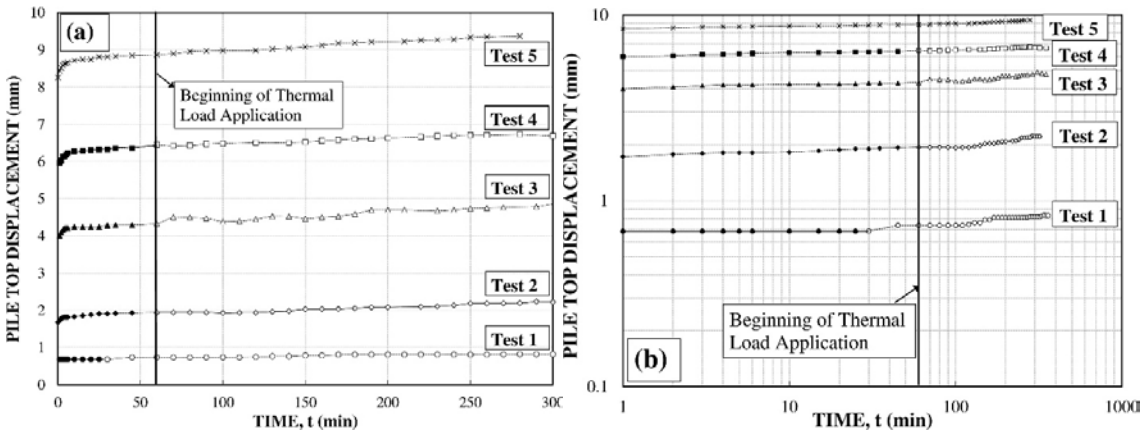

Figure 5-12 a) Pile head displacement on a natural; b) log-log scale – N7 – Round 1

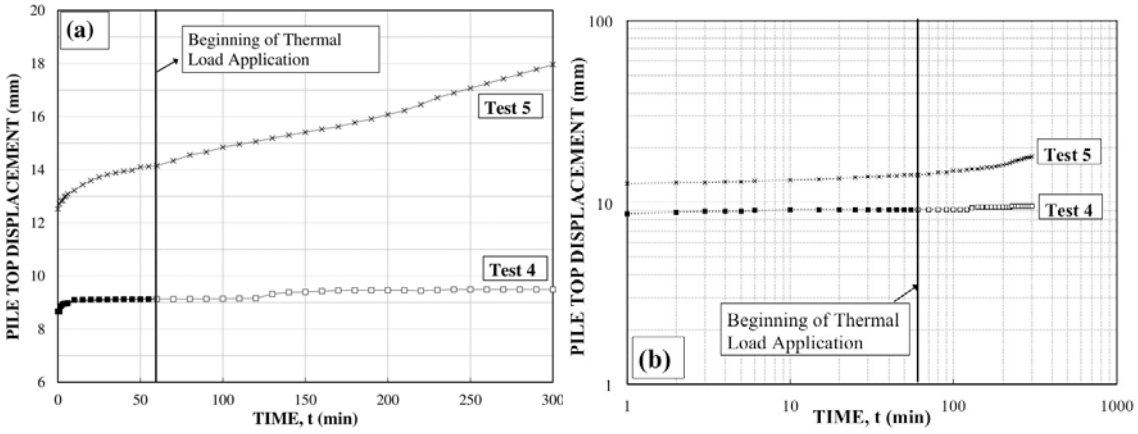

Figure 5-13 a) Pile head displacement on a natural; b) log-log scale – N7 – Round 2

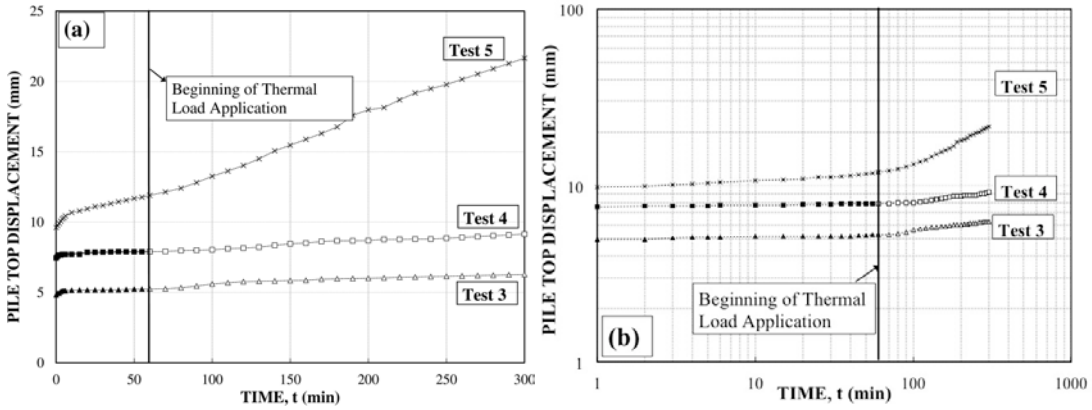

Figure 5-14 a) Pile head displacement on a natural; b) log-log scale – N8 – Round 1

5.7.3 Strain gauge readings and load distribution in the piles

The strain and temperature distribution changes during the test were monitored at different positions to learn about the pile deformation and the load distribution in the pile. It should be mentioned here that most of the strain gauges were not properly working during the tests; therefore, the most relevant data of the strain distribution is

presented (Figure 12). This data corresponds to the temperature and strain change in the pile at depths of 1.4 and 2.4 meters during Tests 4 and 5, where the applied tension was 200 and 256 kN, respectively. The thermo-mechanical data shown for the two tests corresponds to conditions similar to service conditions. In addition, the associated pile top displacement from these tests is presented on the same plot (Figure 5-15).

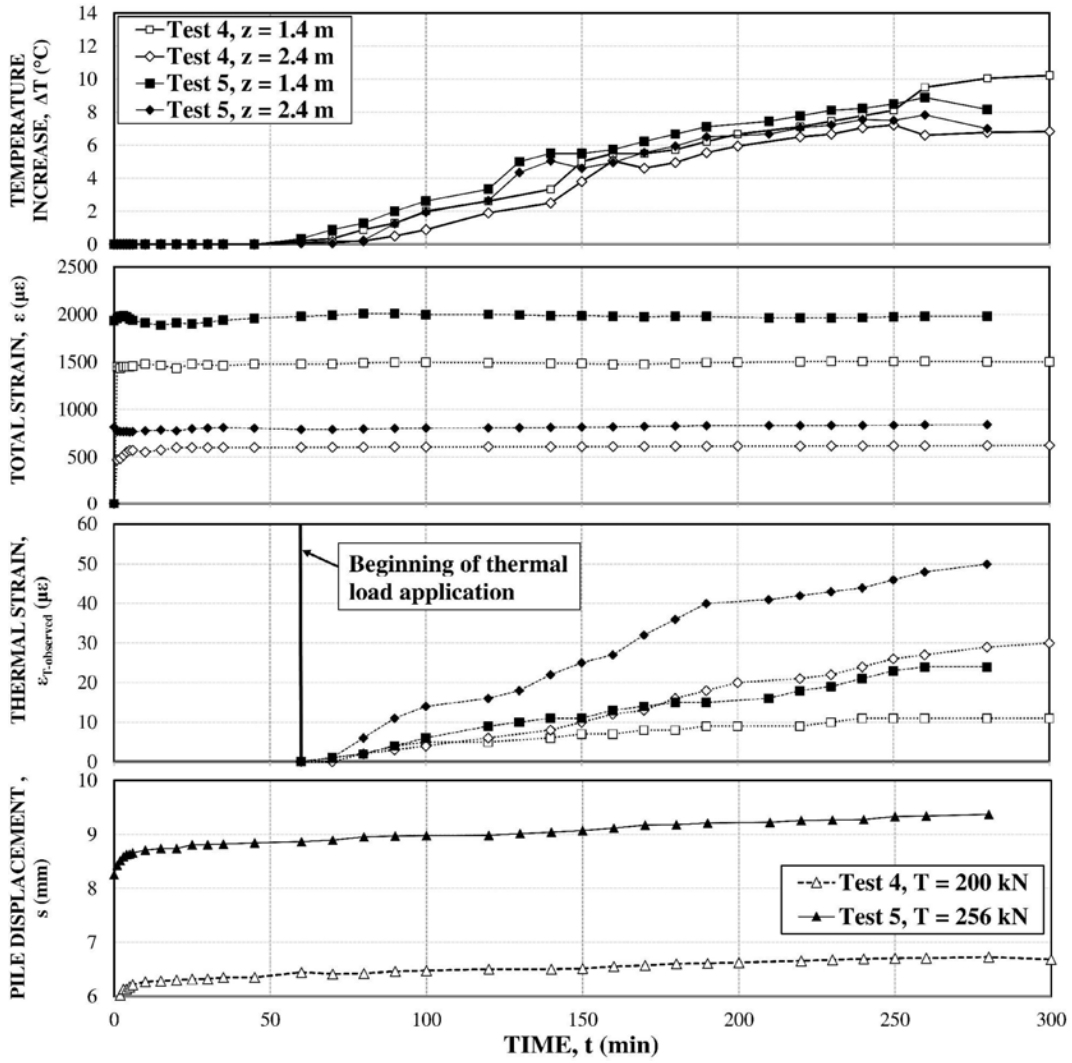

Figure 5-15 Measured temperature, strain, and pile top displacement

Based on the approach proposed by Broune-Webb et al. (2009), the expected load distribution in the pile resulting from the thermo-mechanical load is illustrated in Figure 5-16. Because of the tension load, the mechanical load P_M decreases linearly with depth with the maximum value located at the top of the pile and equal to the applied tension load, T. Because of the heating process, a compression force P_T resulting from the restrained strains develops along the pile with a maximum at the NP location, $P_{T,max}$ and with a value of $P_{Bearing}$ at the bottom of the pile. The thermo-mechanical load in the pile is the sum of the mechanical and thermal loads.

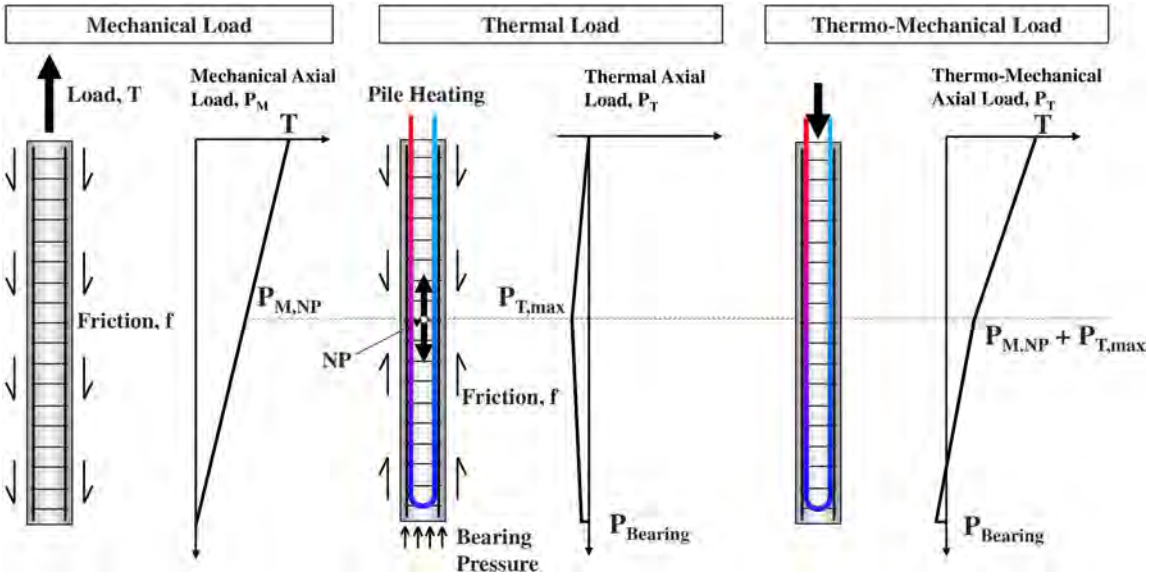

Figure 5-16 Load distribution in energy piles resulting from the mechanical, thermal, and thermo-mechanical loads

The load distribution (Figure 5-17) associated with the data presented in Figure 5-15 along the pile was calculated according to the method described in Section 5.2 of this dissertation, starting with the application of the load at t = 0 min (Mechanical Load only). On the same Figure, the load distribution during tests 4 and 5 at depths 1.4 and 2.4 meters resulting from the thermal load is plotted. The sum of the mechanical and thermal load is presented on the same figure (Thermo-Mechanical Load). The concrete tensile-strain capacity is 150 με or less (ACI 318, 2002). Because the stains in the concrete were all larger than 150 με (Figure 5-15), the concrete is assumed to be cracked and the steel bar is assumed to take all the force in the pile element. An inspection of Figure 5-17 indicates that the measured load distribution conforms to the approach described conceptually in Figure 5-16.

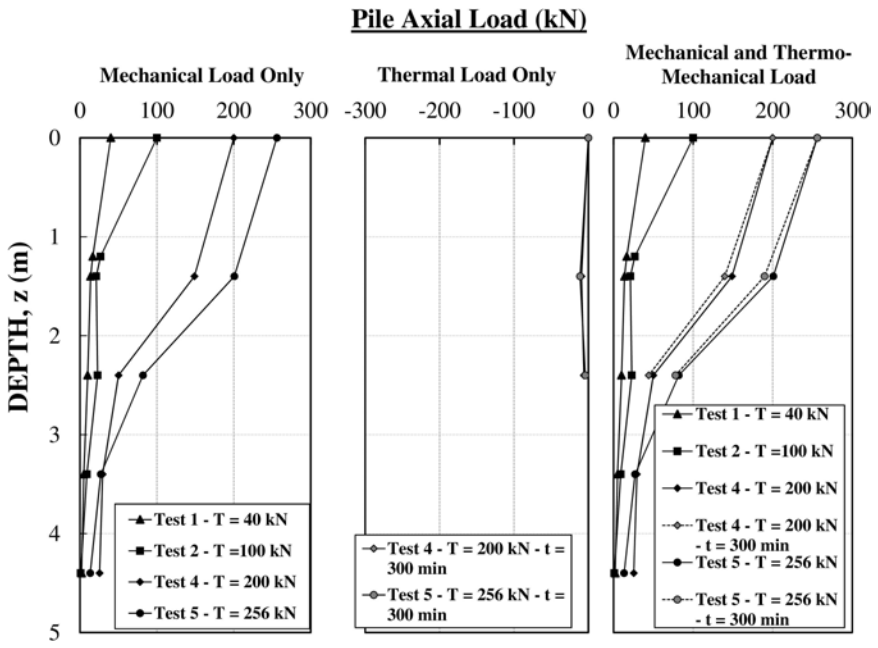

Figure 5-17 Measured load distribution in the pile – N7-Round 1

The yielding stress of the central reinforcing rebar was reached before reaching the ultimate tension capacity of the pile; therefore, the ultimate pile-soil friction f_u (kPa) could not be determined from the in-situ test. However, data from previous static pile load-test (Kubena and Briaud, 1989; Ballouz et al., 1991) at the site location were used to determine f_u. Kubena and Briaud (1989) back-calculated f_u and the results ranged from 113 to 143 kPa with an average of 132 kPa in the first layer where the energy pile was embedded. Ballouz et al. (1991) measured an overall average f_u along a 9.5 m long, 0.92 m diameter pile of 110 kPa, and the load distribution in the pile shows a f_u of 164 kPa in the first layer. Based on these measurements, the ultimate tension capacity of the tested energy pile was calculated as 460 kN.

5.8 EXPERIMENTAL TEST RESULTS – PILE TEST UNDER ULTIMATE STATE – PILES N9, N10, AND N11

In this section the main results obtained during the tests of piles N9 to N11 are presented for the different stages considered in the field experiments. Pile N10 was subjected to mechanical load only. Piles N10 and N11 were subjected to thermal load prior to the mechanical load by cooling down pile N10 by 12 °C and heating up pile N11 by 14 °C.

5.8.1 Pile top displacement and load-settlement curves

During the test on the piles, the load was kept constant during each step for 10 minutes and the displacement versus time was measured. The displacement-time behavior of the piles under mechanical load (N9) and thermo-mechanical load (N10 and N11) is plotted in Figure 5-18. The left side of this figure shows the pile head displacement vs. time for

the load steps on a natural scale while the right side of this figure shows the pile displacement on a log-log scale.

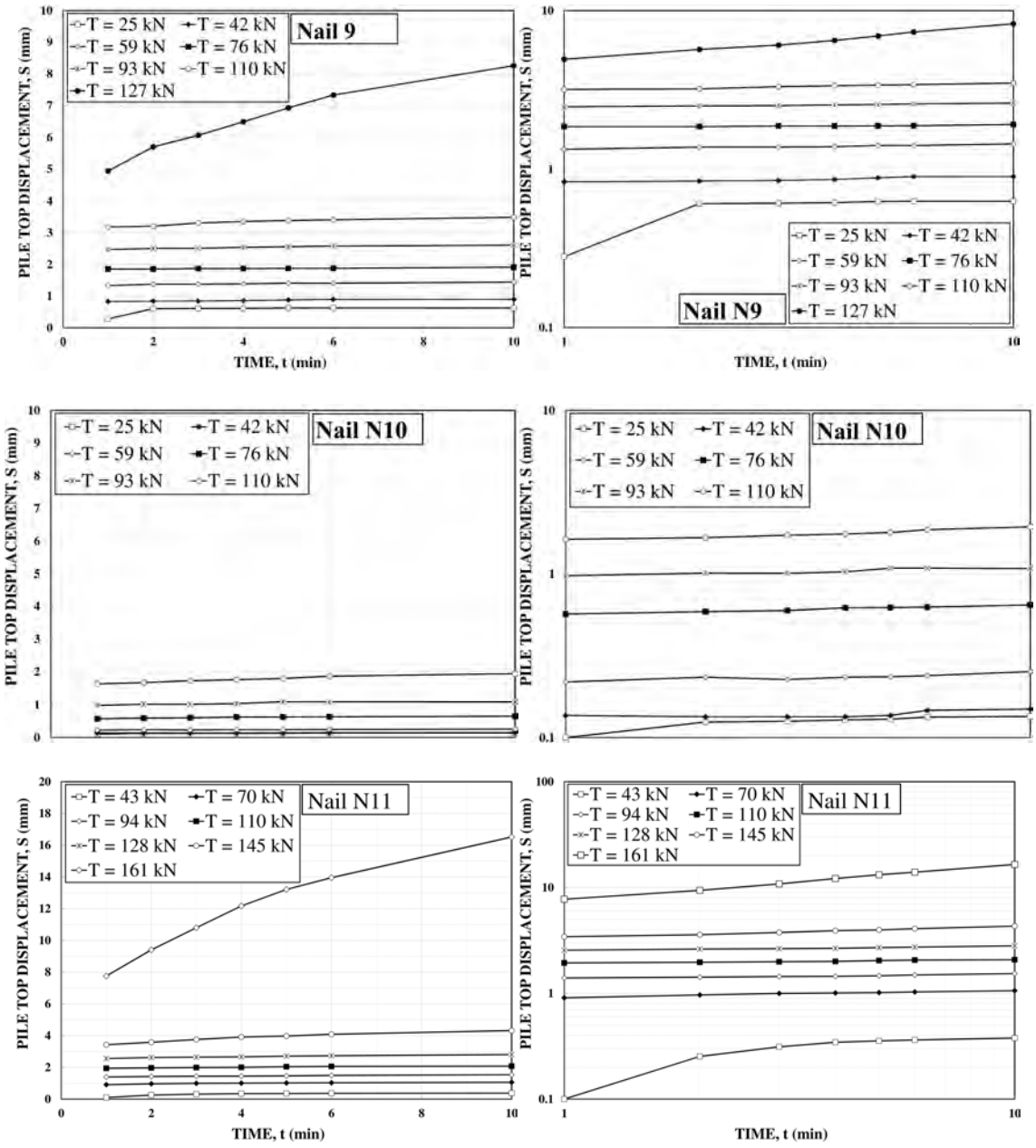

Figure 5-18 a) Pile head displacement on a natural; b) log-log scale – Piles N9, N10, and N11

The ultimate pile-soil friction was back calculated from the load test results on pile N9 that was subjected to mechanical load only and it was found that the ultimate friction f_u = 107 kPa. Because the ultimate capacity of pile N11 was only measured under thermo-mechanical load, the ultimate capacity of pile N11 under mechanical load can be evaluated from the back-calculated ultimate friction and it is equal to 167 kN. The measured ultimate capacity of N11 from thermo-mechanical load was measured and equal to 161 kN.

Figure 5-19 shows the normalized pile top displacement, S/B, where B is the pile diameter, versus the normalized tension load, T/T_{ult}, where T_{ult} is the ultimate capacity of the nail measured from the full-scale test.

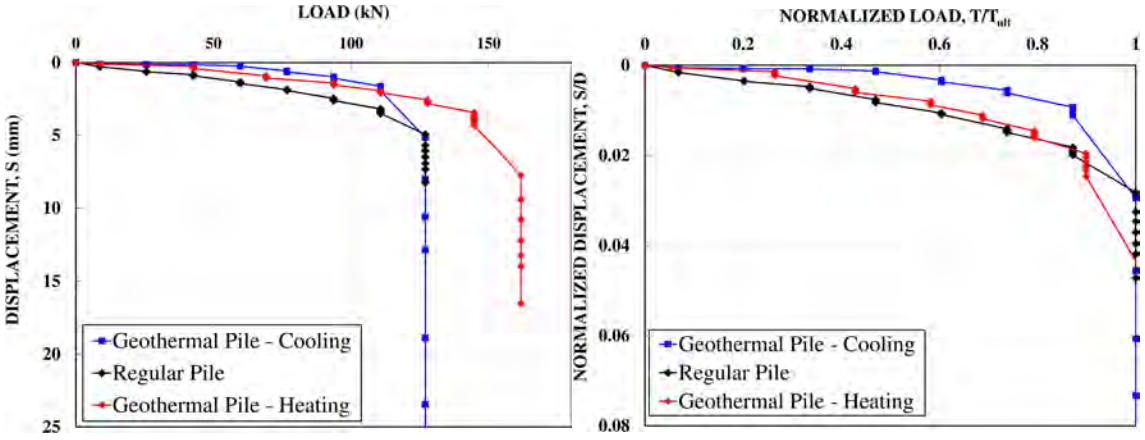

Figure 5-19 Energy pile load settlement curve

5.9 ANALYSES AND DISCUSSION OF THE RESULTS

The results and data presented section 5.7 and 5.8 were used to draw conclusions on the effect of temperature changes in the pile/soil on short-term and long-term service states and the ultimate state of energy piles.

5.9.1 Short-term impact – Load redistribution in the pile

At service conditions, the measurements showed that the load distribution in piles is affected when the pile is used as a ground heat exchanger for SGES. It is known that the friction angle is practically independent of temperature (e.g. Cekerevac and Laloui, 2004). The thermal expansion of the pile resulting from the increase in temperature resulted in a change in pile-soil friction. This change in the friction profile caused a change in the load distribution; a thermally induced tension load was generated in the pile. However, this change was insignificant when comparing the measured change in pile load to the ultimate tension capacity.

5.9.2 Long-term impact – Time dependent deformation

The viscous exponent *n* (Eq. 2.18) was evaluated for all of the tests from the displacement-time curve on the log-log scale before and after applying the thermal load (Figures 5-12, 5-13, and 5-14). The measured displacement-time data was used to back calculate *n* using Eq. 2.18 together with the data from t = 0 to 60 min for the mechanical load only, and from t = 60 to 300 min for the thermo-mechanical load. It was found that when the soil is subjected to thermal loading (in addition to mechanical loading), the creep exponent increases. It was also found that the temperature increase in the pile could cause a dramatic increase in the creep rate (Figure 5-20).

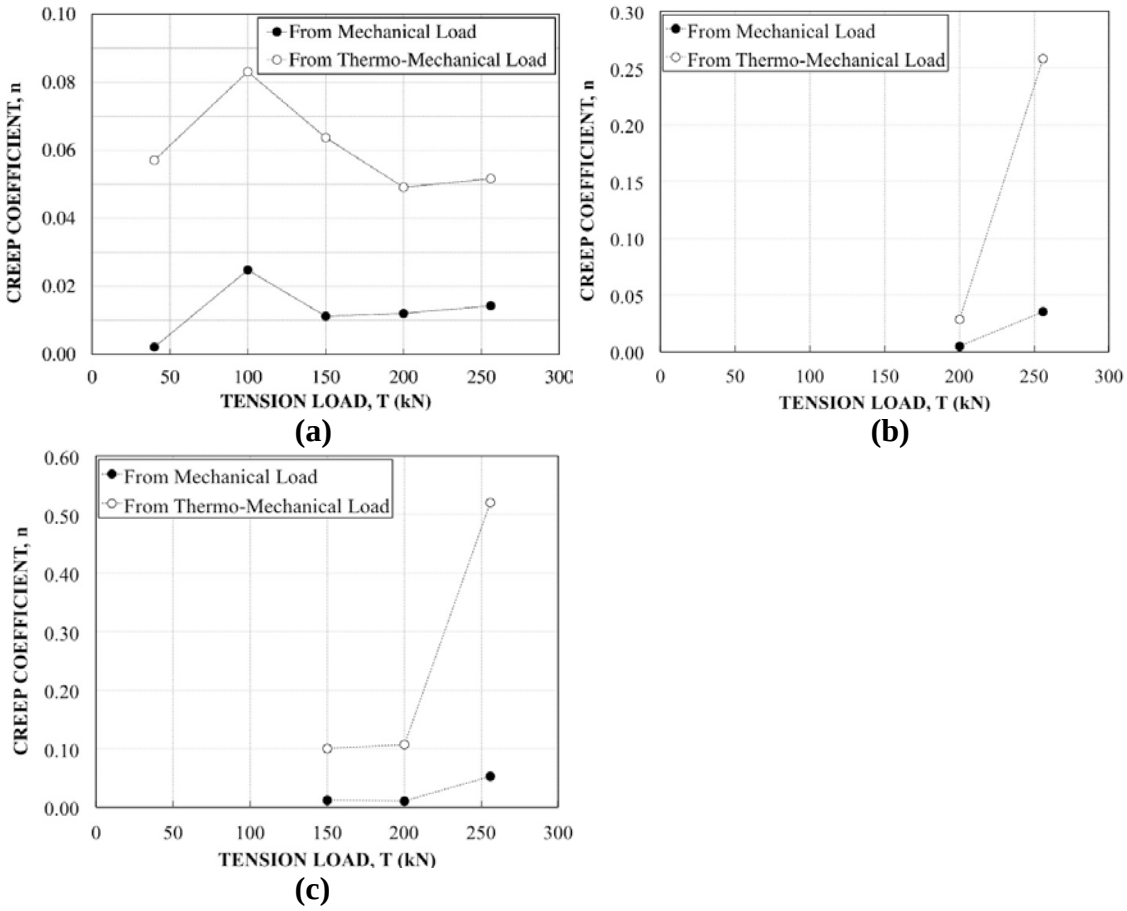

Figure 5-20 Creep exponent (n) vs. tension load: a) N7-Round 1; b) N7-Round 2 and c) N8-Round 1

The measured results from the load tests (N7-Round 1) were compared to the results reported by Mitchell et al. (1968) of viscous exponent ratio of thermo-mechanical load (n_2) to the mechanical load (n_1), n_2/n_1. This was done by plotting the strain vs. time measurement from Figure 2-9 in a log-log scale and comparing it to the displacement-time results from Test 3 (Figure 5-21). The viscous exponents of the two tests were different by a ratio of 10, which is not surprising as the clay tested by Mitchell and his

colleagues was much softer than the clay tested in this study. However, the ratio n_2/n_1 of the two tests was close. Note that the ratio of the viscous exponents in Figure 5-21b is for N7-Round 1-Test 3.

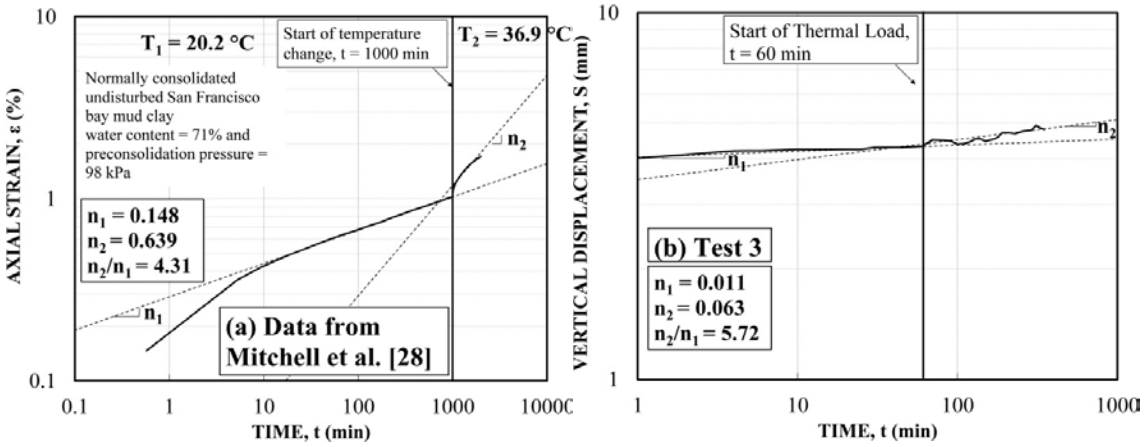

Figure 5-21 Comparison of creep exponents to data from the literature

The creep exponent ratio υ, defined as the ratio between the viscous exponent $n_{Thermo\text{-}Mechanical}$ under thermo-mechanical load to the exponent $n_{Mechanical}$ under mechanical load, was evaluated for all the performed tests on piles N7 and N8 as a function of the temperature increase (Table 5-7). It was found that an exponential model fits very well with measured data (Figure 5-22).

Table 5-6 Creep exponents results summary

Pile – Round	Test ID	$n_{Meachanical}$	$n_{Thermo-mechanical}$	Creep ratio υ	Temperature Increase, ΔT (°C)
Pile N7 – Round 1	Test 1	0.002	0.057	-	-
	Test 2	0.024	0.083	3.35	9.40
	Test 3	0.011	0.063	5.69	8.56
	Test 4	0.012	0.049	4.09	7.16
	Test 5	0.014	0.051	3.61	7.06
Pile N7 – Round 2	Test 4	0.0047	0.028	5.98	11.39
	Test 5	0.035	0.258	7.39	13.90
Pile N8 – Round 1	Test 3	0.011	0.100	8.42	13.10
	Test 4	0.010	0.106	9.92	12.94
	Test 5	0.053	0.520	9.97	15.00

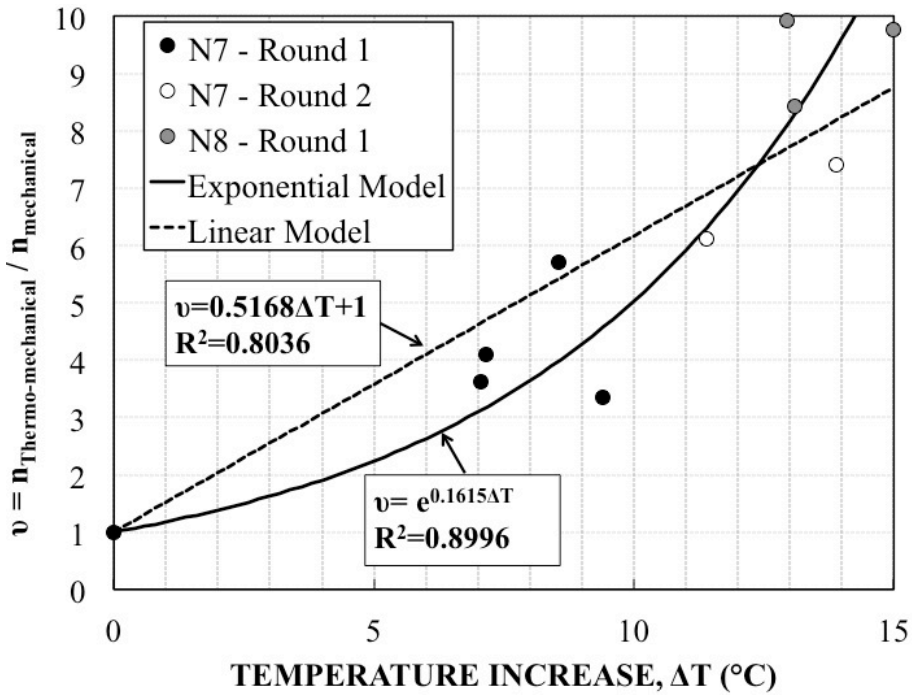

Figure 5-22 Creep exponent ratio vs. temperature increase

The creep exponent “n” when the geothermal pile is cooled down was evaluated from the in-situ tests on piles N9 and N10. The geothermal pile was cooled down by 12 °C from the initial temperature and the pile head displacement vs. time was measured for each of the applied load level during the in-situ tension load test. The exponent n vs. applied load is presented in Figure 5-23 for both geothermal and regular pile and it it was found that the creep exponent decreases by half in average. This decrease means that when the foundation pile is used as heat extractor, the time-dependent deformation process slows down and leads to less deformation over the life span of the building

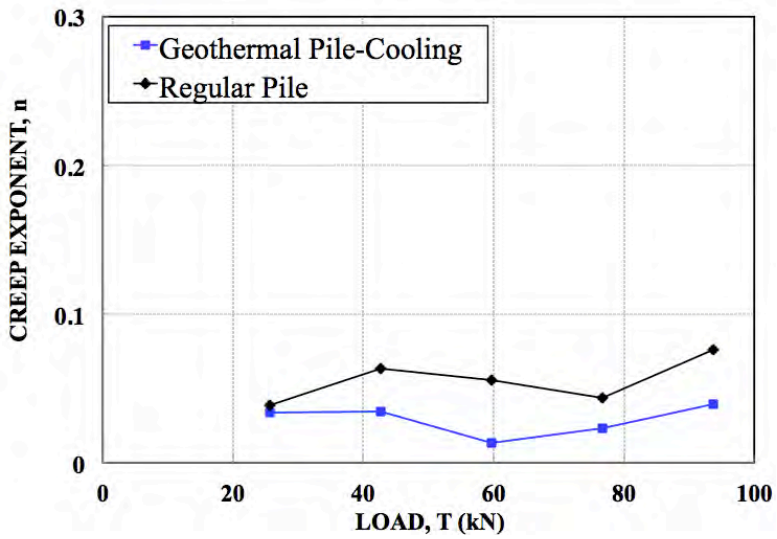

Figure 5-23 Creep rate of energy pile in cooling mode

The long-term performance of energy piles in terms of displacement (i.e. instantaneous plus creep) was evaluated based on the measurements of the viscous

exponent from the in-situ test. This analysis was done by extrapolating the load-settlement curve for N7-Round 1 measured at time t = 0 min using Eq. 2.18 and the measured viscous exponent. The extrapolation was performed for a structure life time of 50 years with and without the use of geothermal energy piles by using 'n' from the mechanical load and from the thermo-mechanical load results respectively. Figure 5-23 presents the measured load settlement curve at the time of load application (t = 0 min), at 60 min, and at the end of the thermo-mechanical load (t = 300 min). The extrapolated load-settlement curves are plotted on the same graph in Figure 5-23. The extrapolation showed that long-term displacement increases by a factor of approximately 2.7 because of the creep when piles are used for geothermal energy applications. However, this calculation was done assuming that the soil-pile will be subjected to heating during its lifetime. In reality, especially in cooling dominated climates, the pile heating process will only take place for 6 to 8 months of the year. During the rest of the year, the pile will be under cooling or idle mode and the creep rate will slow down because of the decrease in soil temperature. Therefore, the values predicted in this paper correspond to an extreme case. The actual values should be between the extrapolated curves with and without geothermal piles. It is also worth mentioning that this analysis considers the effect of the friction (i.e. vertical/side) resistance only.

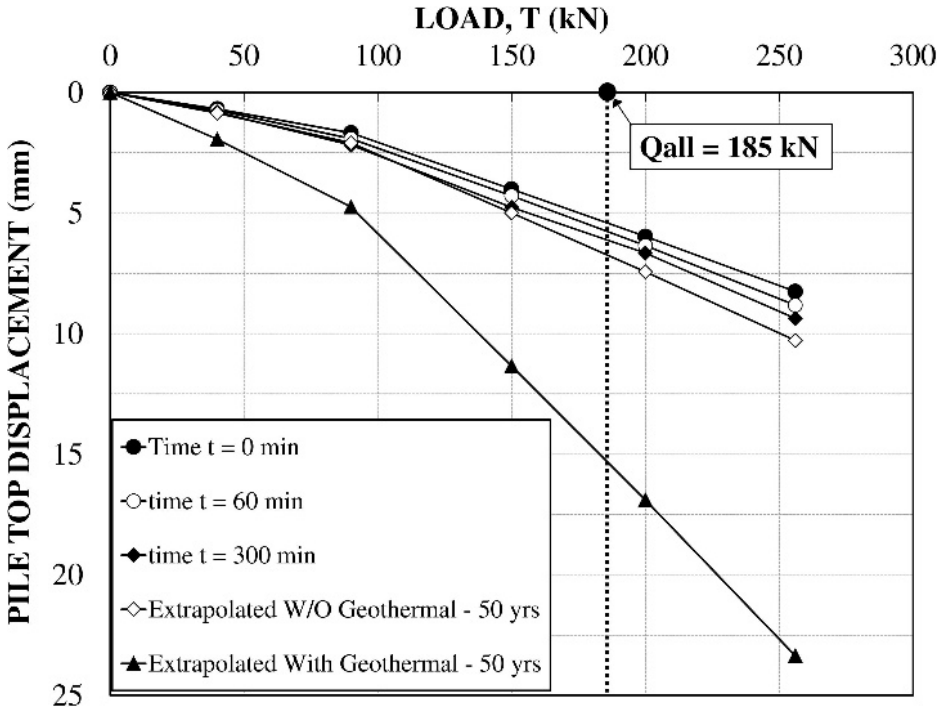

Figure 5-24 Measured and extrapolated load-settlement curve from results of N7-Round 1

5.9.3 Temperature impact on ultimate state of energy piles

The results presented in this section pertaining to the impact of a pile's temperature change on its ultimate capacity shows that use of foundation piles as ground heat exchangers do not adversely impact their ultimate capacity, but do affect their load-settlement behavior. This is contrarily to the results found by McCartney and Rosenberg (2911). However, the temperature change applied by McCartney and Rosenberg (2011) was much higher than the increase that would be experienced in service conditions. Based on the results presented in Figure 5-21, and for the soil conditions were the piles were tested, it can be concluded that the decrease in pile/soil temperature stiffen the soil

around the pile and causes an increase in pile stiffness, while the increase in pile/soil temperature does not impact the pile stiffness.

5.10 CONCLUSIONS

A thermo-mechanical tension load test on energy piles in high plasticity stiff clays was presented. The strain and temperature distribution, load-displacement behavior, and climatic conditions were monitored during the test. Based on the soil type, soil profile, soil properties, and the testing conditions, the following conclusion may be made:

1. The use of foundation piles for geothermal energy application induces thermal strains and stresses in the pile element because of the volume expansion/contraction of the pile and the soil-pile friction generated from this thermally induced volume change. However, the thermally induced pile load is practically insignificant (less than 1% per °C of temperature increase) compared to the ultimate values.
2. The increase in soil temperature caused an increase in the creep rate. Mathematically, this is represented by an increase of the viscous exponent *n* by a factor of 4.7. The measured results were compared to data from the literature and showed good consistency.
3. The time-dependent behavior of energy piles in high plasticity clays for cooling dominated climates is an important factor to consider. The increase in the soil viscous component results in an increase in long-term displacement.
4. The extrapolated load-displacement curve of an energy pile under the tested conditions for the extreme case considered (i.e. cooling mode only) shows that

the long-term displacement (50 years) for the energy pile is 2.35 times the displacement for the regular pile.

5. The design of energy piles in conditions similar to the ones presented in this paper should minimize the long-term displacement to within the tolerable limits by minimizing the initial settlement.
6. The ultimate capacity of foundation piles doesn't change when it is used as ground heat exchanger for SGES. But the stiffness of the pile increases when the pile is cooled and does not change when the pile is heated.
7. Further investigation on the time-dependent behavior of energy piles should be made through more load tests considering different soil types and in both heating and cooling conditions.

6 FULL SCALE TEST OF ENERGY PILES GROUP

6.1 INTRODUCTION

The aim of the full-scale test is to understand the thermodynamics of a full SGES and the heat transfer process from the room air, to the HCF, the GHE, and then to the soil. In addition, the full-scale test aims to provide experimental data to validate a calculation tool that simulates a full shallow geothermal energy system in cooling dominated climates. A group of three Auger Cast in Place (ACIPE) foundation piles of the newly constructed Liberal Arts Building at Texas A&M University campus were selected to work as GHE. The piles were fitted with one loop of HDPE pipes and connected to a GSHP. The piles were instrumented with thermistors along the center bar. In addition, three boreholes were drilled at different distances from the energy piles to monitor the heat flow in the ground because of the operation of the GSHP. The boreholes were instrumented with thermistors at the same levels as the thermistors in the energy piles. The GSHP was instrumented with two temperature and relative humidity sensors to monitor the inlet and outlet air temperature during operation. Each of the inlet and outlet legs of the pipes was instrumented with thermocouples to measure the inlet and outlet water temperature. The data measured from the full-scale test included the change in foundation pile temperature, the change in surrounding soil temperature, inlet and outlet HCF temperature (EWT and LWT respectively), inlet and outlet air temperature, and RH at the heat pump level during the operation of a geothermal heat pump. The calculation tool used was Hybrid Ground Coupled Heat Pump (HyGCHP), developed by the Energy

Center of Wisconsin at the University of Wisconsin – Madison College of Engineering's Solar Energy Lab (sponsored by ASHRAE and the US department of Energy) in 2011. HyGCHP is a simplified performance modeling tool for GSHP systems including several variations of hybrid systems. This tool uses the building heating and cooling loads, soil and GHE thermal properties, GSHP performance data, and GHE arrangement to predict the HCF temperature change, SGES performance, GSHP power consumption, and the change in the soil thermal mass temperature over the operational period of the system. This type of simulation is very important because it helps us to evaluate the long-term thermodynamic performance of the heating and cooling system and the yearly increase of the soil thermal mass temperature because of the highly unbalanced heating and cooling loads prevalent in cooling dominated climates. Unless property accounted for, this increase in soil temperature results in a decrease of heat pump performance and leads to an improperly designed system.

This section of the dissertation presents the test setup, site location, engineering and thermal properties at the site, instrumentation details, test results, calibration of the HyGCHP calculation tool, and conclusions from the full-scale SGES test. Even though only the HCF temperature was used to calibrate the calculation too, the other measured data is presented in this section for the understanding of the heat transfer mechanism and for any further numerical analysis.

6.2 TEST LOCATION AND SOIL ENGINEERING AND THERMAL PROPERTIES

The full-scale test was performed on energy piles that are part of the newly constructed Liberal Arts Building on the Texas A&M University campus in College Station, Texas. The building is located on Spencer Street on the eastern side of campus (Figure 6-1).

Figure 6-1 Liberal Arts Building location

The soil engineering properties under the liberal arts building were obtained from the soil report prepared for the project by STL Engineers and from five CPT test results reported in Section 3 of this dissertation for the thermal cone development (Figure 3-6). The soil stratigraphy and properties were also detailed in Section 3 and are repeated here in summary. The soil investigation concluded that the top 1.2 meters consists of fill low plasticity clay (CL). The second layer, which extends to a depth of 14 meters, was a high plasticity greenish gray to light brown, stiff to hard, clay layer (CH). This layer

becomes hard at a depth of 11.5 meters from the ground surface. The third layer consists of olive gray, stiff to hard, high plasticity clay (CH) that extends to the end of the borehole. The average undrained shear strength of the clay was approximately 90 kPa, and it became stiffer at a depth from 11 to 14 m., with average undrained shear strength of approximately 320 kPa. The average water content at the site was 28%. Soil thermal properties at the testing location were also reported in Section 3. The thermal properties were measured from soil samples extracted from two different locations at the site at different depths. The average thermal conductivity at site were measured as 0.61 W/m.K.

6.3 TEST LAYOUT AND SETUP DETAILS

The instrumented energy piles were 0.45 m in diameter and 17.8 m long. The piles were reinforced with 6 #6 steel rebar rods to a depth of 3.1 m and with a central #8 rebar rod that extended along the entire pile. The construction sequence of the energy piles is presented in Figure 6-2, which shows energy pile preparation at the site, the drilling process, pile cage lifting and insertion, and collection of pipes and instrumentation after finishing the pile cap. The HDPE pipes were coupled and connected to the GSHP and water pump using PVC pipe. The GSHP was used to extract/inject heat from/to the air-conditioned space while the water pump was used to circulate the HCF (only water was used in this experiment as HCF) that exchanges heat with the ground. The GSHP was located in the crawl space of the Liberal Arts building, which was thermally controlled by the building central air conditioning unit. The crawl space temperature was kept constant at 23 °C.

Figure 6-2 Energy piles construction

The three energy piles were fitted with one loop of 1” HDPE pipes. The HDPE pipes were attached to a center #8 steel rebar using spacers. The loop legs were spaced by 0.2 m center-to-center. The piles were instrumented using six thermistors each equally spaced vertically. The installed thermistors were model 3810 from Geokon and were installed at depth 0.6, 3.6, 6.6, 9.6, 12.6, and 15.6 m from the bottom of the pile cap (Figure 6-3). Note that the level of the instrumented pile top is 3.94 m. below the ground level. In addition, three boreholes (BH1, BH2, and BH3) were drilled, filled with bentonite, and instrumented with six thermistors each, equally spaced vertically, to measure the ground thermal response to the energy pile group operation. In addition to the piles and boreholes instrumentation, the geothermal heat pump was instrumented with two relative humidity (RH) and temperature sensors to measure the supplied and returned air. Air temperature and RH is useful to calculate the amount of heat exchanged with the thermally controlled space. Each inlet and outlet pipe connected to the piles was instrumented with a thermocouple, totaling six thermocouples type T from OMEGA to measure the temperature of the HCF. This information is useful to calculate the amount of heat exchanged between the energy pile and the soil. The general view of the test setup showing the piles, boreholes, GSHP, water tank, water pump, and instrumentation along the piles and wall is shown in Figure 6-3.

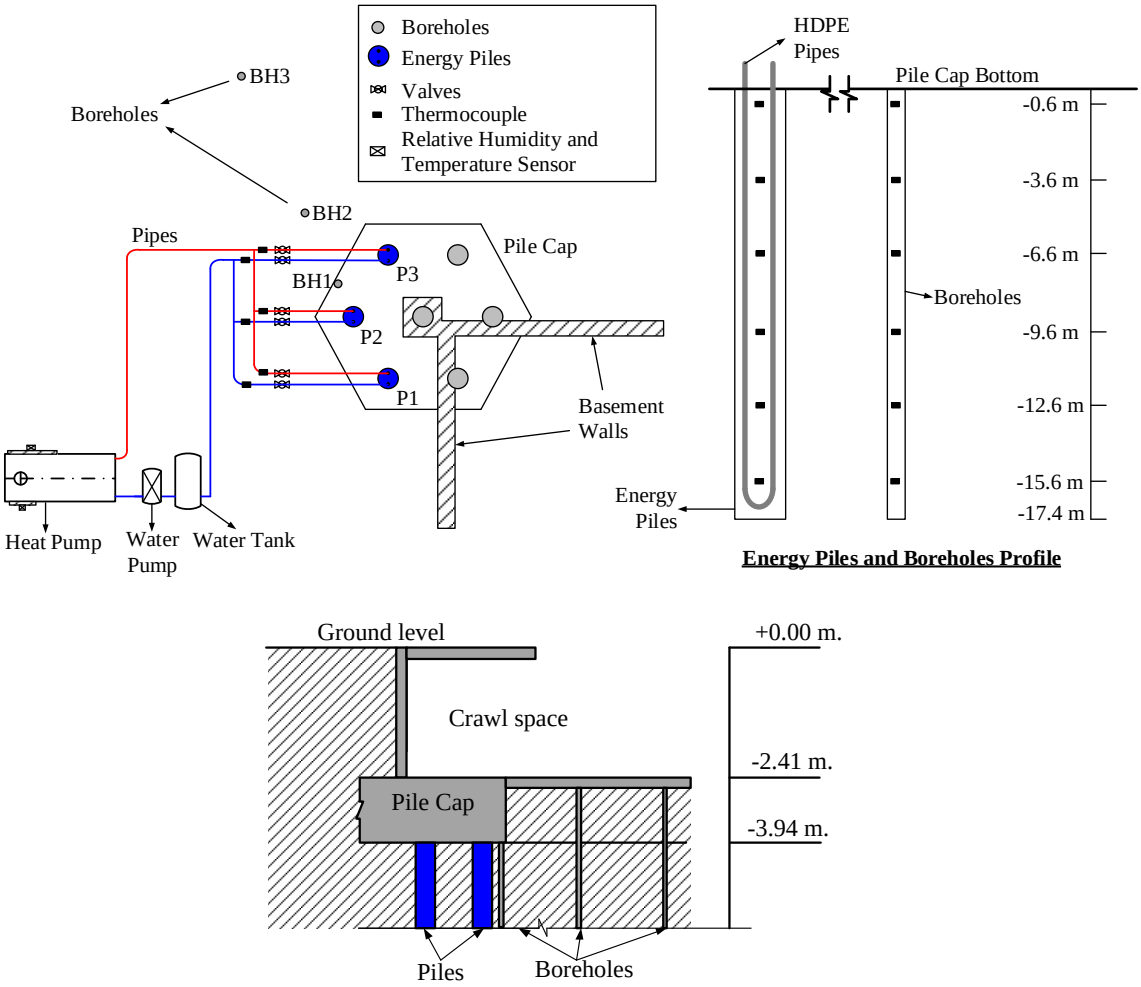

Figure 6-3 Full-scale test setup and details (Not to scale)

Figure 6-4 shows the top view of the energy piles and boreholes with as-built dimensions. In addition, Figure 6-4 shows the energy piles section from 0 to 3.1 m depth in section (a), and from 3.1 m to 17 .4 m depth in section (b). The summary of instrumentation is presented in Table 6-1.

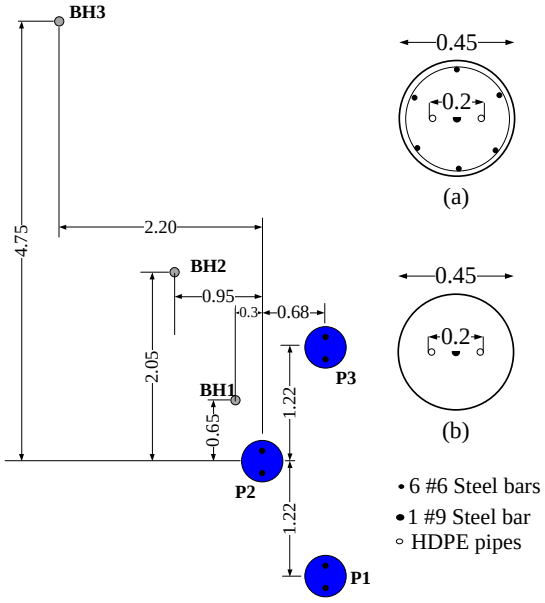

Figure 6-4 Energy piles top view

Table 6-1 Instrumentation summary

Instrument	Measurement	Number Used
Thermistors Model 3810 from Geokon	Temperature in the piles	18 (6/pile)
Thermistors Model 3810 from Geokon	Temperature in the boreholes	18 (6/pile)
Temperature and relative humidity model RHT10 from Extech	Temperature and relative humidity of the GSHP inlet and outlet air	2
Thermocouples type T from Omega	Temperature of the inlet and outlet HCF; temperature of each pile	6 (2/pile)

A preliminary test on the installed and instrumented system was performed and reported in Akrouch et al. (2013). The test was performed in heating mode for 24 hours where heat was extracted from the ground and injected into the thermally controlled

space. The variables listed in Table 6-1 were measured and the results demonstrated that the system and the instrumentation were properly working.

6.4 FULL SCALE TEST PLAN AND RESULTS

The full-scale test plan consisted of operating the geothermal heat pump in arbitrary intermittent cooling and heating modes. The selection of heating and cooling modes and time was arbitrary because the main objective of the full-scale test was to collect data for calibration purposes. The geothermal heat pump was set to operate in cooling mode for 80 hours, followed by heating mode for 65 hours, then another period of 39 hours on cooling mode followed by 33 hours of idle mode where no heating or cooling loads were applied. A short period (3 hours) of high heating mode was then applied followed by 72 hours of low cooling mode. After that time, the heat pump was turned to idle mode again. The operation sequence is visualized in Figure 6-5.

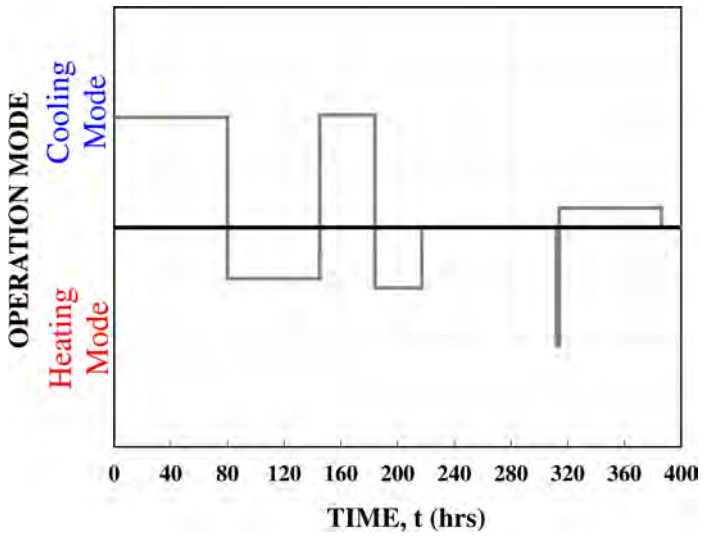

Figure 6-5 Geothermal heat pump operation during full-scale test

6.4.1 Pile, soil, water, and air temperature

During the operation of the heat pump, the inlet and outlet HCF temperature to each of the piles was measured, as presented in Figure 6-6. Note only a very small difference between the HCF temperatures in each of the piles, meaning that all the piles were thermally loaded in the same way. The average inlet and outlet temperature of the three piles was calculated and plotted on Figure 6-7. In cooling mode, the inlet water temperature is higher than the outlet water temperature because the heat is released from the HCF and injected into the ground. In heating mode the opposite is true; heat is extracted from the soil and gained by the HCF. Therefore, the outlet HCF temperature is higher than the inlet HCF temperature

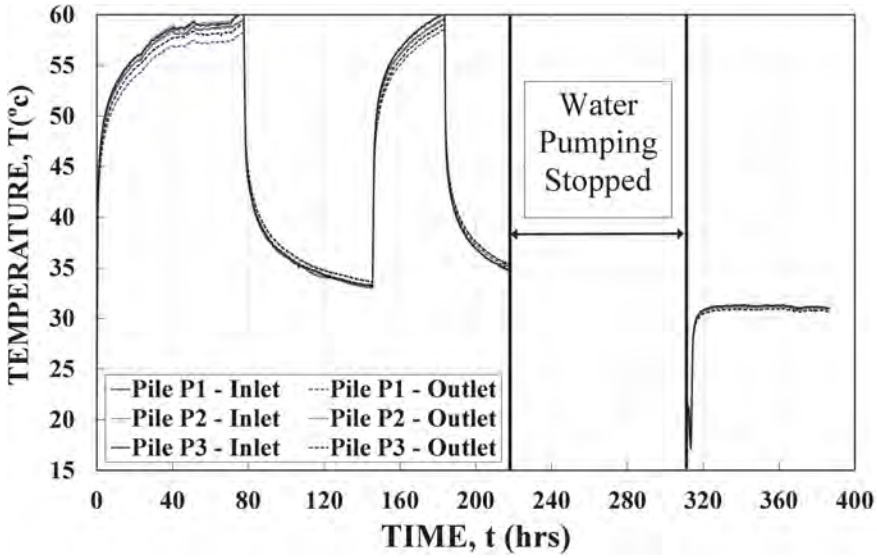

Figure 6-6 Energy piles inlet and outlet water temperature

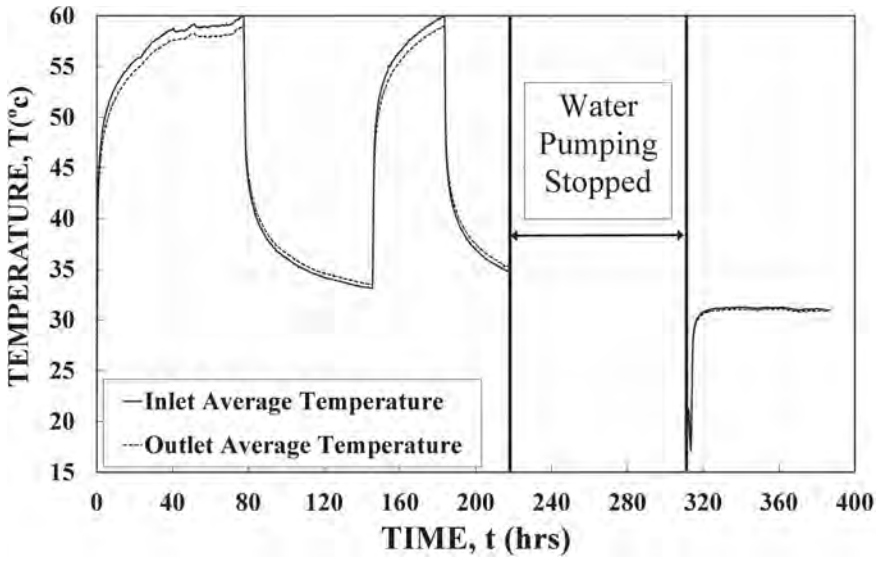

Figure 6-7 Average inlet and outlet water temperature

Based on the inlet and outlet water temperature, the heat injected/extracted can be calculated using Eq. 6.1 (Remund and Carda, 2009). In this equation, IWT is the inlet water temperature to the piles, OWT is the outlet water temperature from the pile, WF is the HCF flow. The small difference in temperature between inlet and outlet water temperature is plotted on Figure 6-8, along with total heat extracted from or injected into the ground Q (kW) (Eq. 6.1). A positive Q means that heat is injected into the soil, while a negative Q means that heat is extracted from the soil.

$$Q(kW)=\frac{500\times WF\,(GPM)\times(IWT\,(°F)-OWT\,(°F))}{3412} \tag{6.1}$$

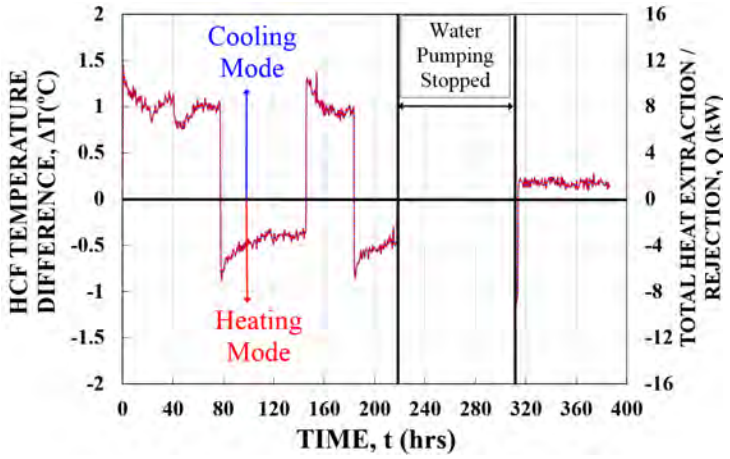

Figure 6-8 Inlet/outlet water temperature difference and total thermal pile load

For modeling purposes, using Finite Element Method for example, the heat exchange profile presented in Figure 6-8 can be simplified as presented in Figure 6-9. In the simplified diagram, heating and cooling loads are averaged over the period of application.

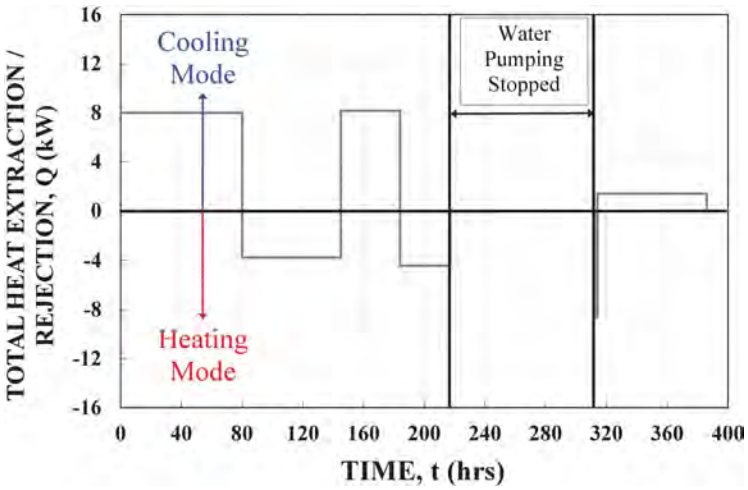

Figure 6-9 Simplified energy pile heating and cooling load profile

The soil/pile temperature changes in response to the operation of the GSHP operation. This change is monitored during the heating and cooling phases. Figure 6-10 shows the temperature change in piles P1, P2, and P3 at different depths and Figure 6-11 shows the change in temperature in BH1, BH2, and BH3 at the same depths as the piles. This temperature change is measured at the center of the piles and the boreholes. Note that two thermistors in each of BH1 and BH3 were not working properly. In addition, the measurements show a uniform temperature distribution in the pile while it is not in the boreholes. The author believe that some of the thermistors are not working properly because the thermistors are all located below the shallow soil layer and the temperature profile should be uniform. However, the author is presenting the data as measured from the site.

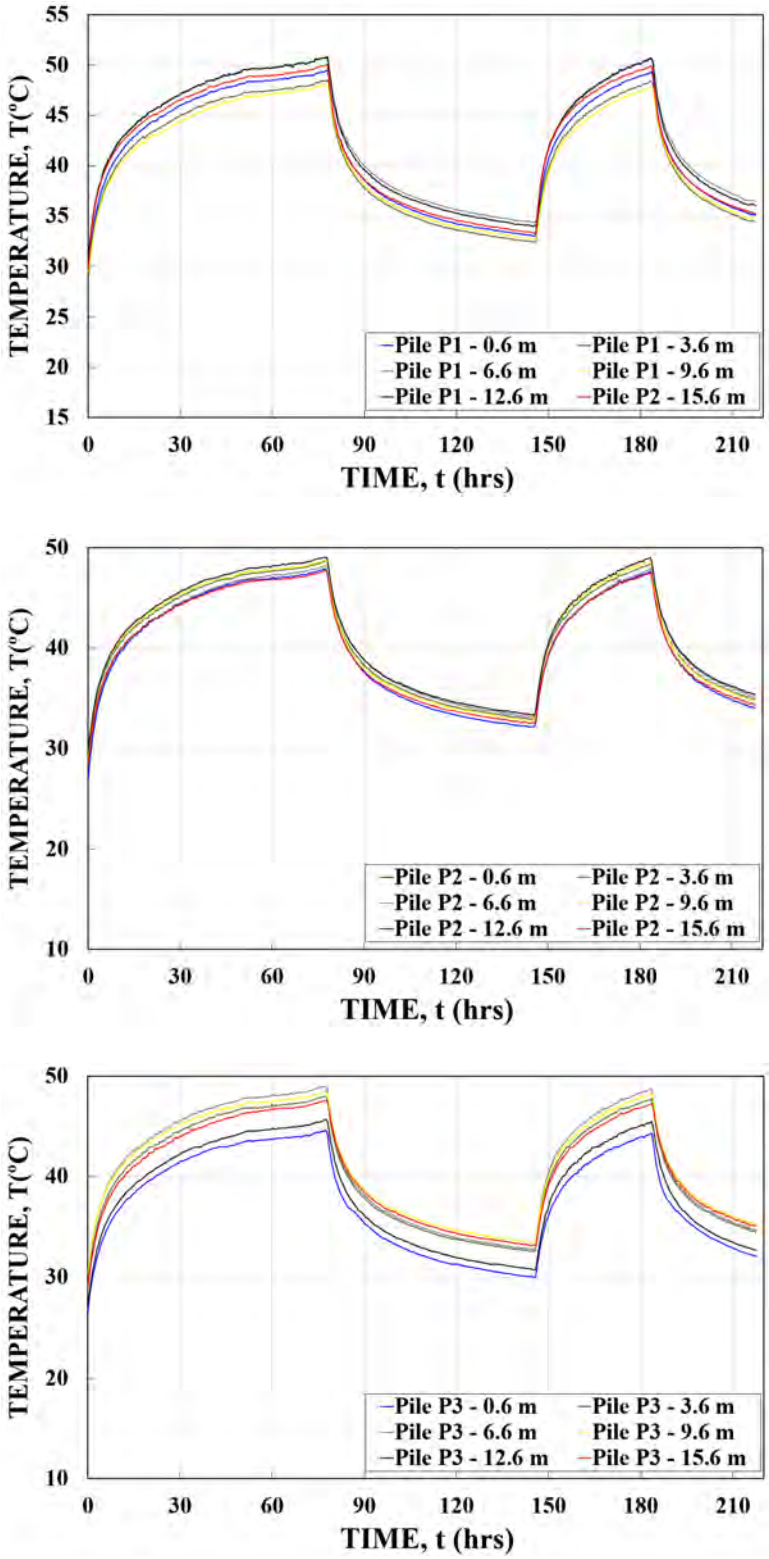

Figure 6-10 P1, P2, and P3 temperature change at different depths

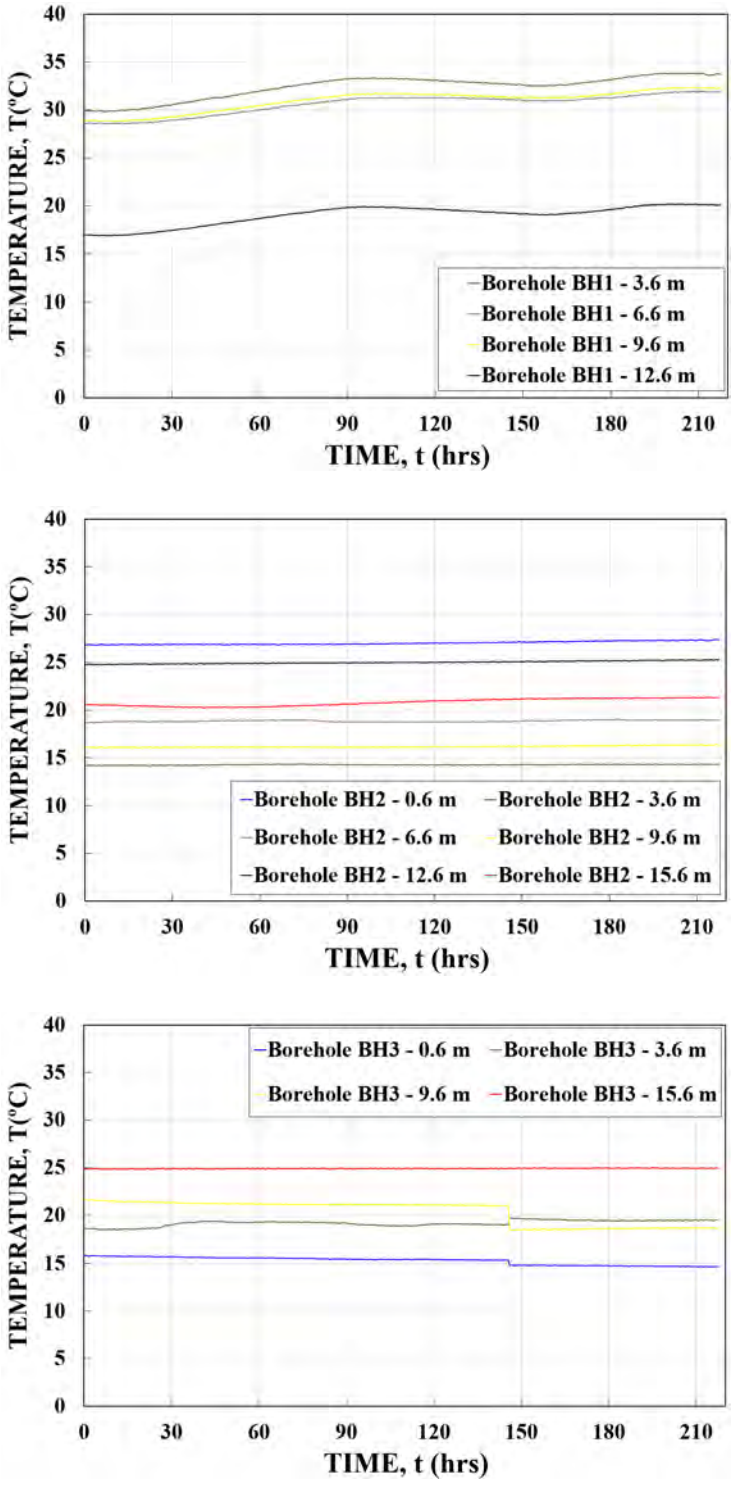

Figure 6-11 BH1, BH2, and BH3 temperature change at different depths

6.5 CALCULATION TOOL CALIBRATION

The measured heating and cooling loads, soil and pile thermal properties, and pile geometry and geometrical distribution were used as an input to the calculation tool HyGCHP. This calculation tool uses the Duct Storage (DST) model, originally created by Hellstrom (1989, 1991). This model decomposes the time-varying heat transfer profile into a series of individual step heat pulses and then superimposes the resulting ground thermal responses in time. The calculation tool was calibrated against the measured data by changing soil and pile thermal properties. The variable that HyGCHP calculates is the HCF temperature that leaves the GHE and enters to the pump and defined in practice as the entering water temperature, EWT. The comparison of measured and calculated HCF temperature is shown in Figure 6-12. Despite the larger offset of measured and calculated data at the beginning of the test, Figure 6-12 shows good consistency with measured results, which demonstrates the validity of using HyGCHP to analyze a full SGES at the Liberal Arts Building. Table 6-2 summarizes the parameters used for the calibration of HyGCHP. The input heating and cooling loads are as presented in Figure 6-8.

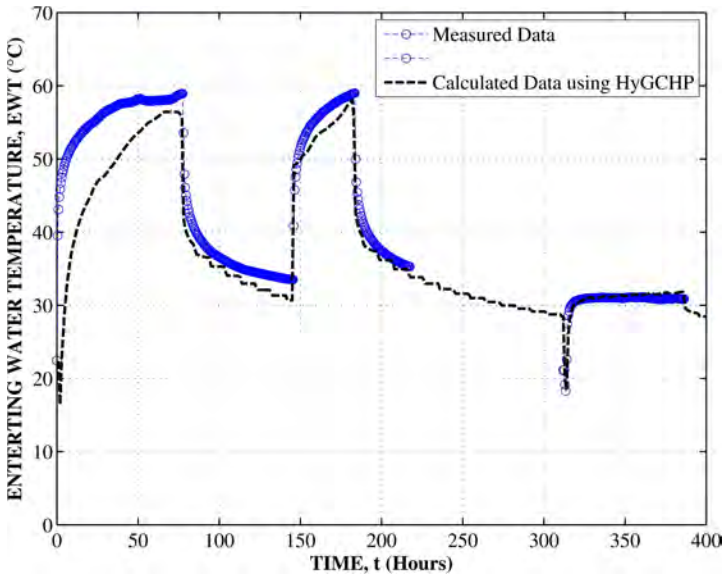

Figure 6-12 Comparison of measured and calculated HCF temperature

Table 6-2 Calibration parameters

Parameter	Value
Piles spacing (m)	1.46
Piles Diameter (m)	0.45
Pipes Spacing (m)	0.20
$\lambda_{Concrete}$ (W/m.K)	2.30
λ_{soil} (W/m.K)	1.87

6.6 CONCLUSIONS

This section of the dissertation presented a full-scale test on an energy pile group installed and instrumented at the Liberal Arts building at Texas A&M University. The results from the full-scale test were used to calibrate a calculation tool that will be

utilized in Section 7 of this dissertation to analyze a full SGES in the foundation system of the new Liberal Arts Building. The measured and calculated results provide good consistency, as shown in Section 6.5, which validates the use of the HyGCHP tool to perform the full building simulation. The measured data range presented in this section is higher than the range expected during the operation of a full SGES because of the significant under sizing of the full-scale test. However, the results are only used for the understanding of the full system behavior and data collection to calibrate HyGCHP. The measured data showed a quick pile thermal response and delayed soil pile thermal response. This behavior implies that thermal stresses and strains will develop very quickly in the pile because of the thermal load, while soil time-dependent behavior such as creep and thermal consolidation will depend on the heat propagation mechanism in the soil.

7 ECONOMIC STUDY OF SHALLOW GEOTHERMAL ENERGY SYSTEM USING FOUNDATION PILES

7.1 INTRODUCTION

This section of the dissertation presents an economic study of shallow geothermal energy systems using foundation piles as ground heat exchangers (GHE). The newly constructed Liberal Arts building provides the case study. The initial and operational cost of the SGES will be evaluated and compared to the initial and operation cost of a conventional HVAC system. The new building has been in operation since November 2012. Data of the total heating loads, total cooling loads, and corresponding electric power consumption of the system used for thermal control of the building was collected over a one year period of operation. The measured heating and cooling loads were used to analyze a full SGES using the existing foundation piles of the building, while the measured electric power consumption was used to evaluate the operational cost of the installed conventional system. Based on the initial and operational cost, a life cycle cost analysis was performed and the simple payback period of the system was calculated.

7.2 DESIGN PROCEDURE

In practice, the general steps for a typical design of a SGES (Figure 7-1) are:

1. Calculate the peak building heating and cooling loads.
2. Select a properly sized ground source heat pump (several pumps may be required depending on the size of the project) to deliver the peak heating and cooling loads.

3. Design the interior distribution system based on the maximum capacity of the heat pump.
4. Calculate the daily or hourly building heating and cooling loads throughout the year.
5. Calculate GHE thermal loads. In cooling mode, the GHE thermal load is the sum of the building thermal load and the heat resulting from the mechanical work of the system. In heating mode, the GHE thermal load is equal to the building thermal load minus the heat resulting from the mechanical work of the system.
6. Calculate the required number and length of ground heat exchangers to supply the building peak thermal loads.
7. Design the interior (mechanical room) and exterior (ground loops) piping systems and select a properly sized water pump.

However, in this particular project, the number and length of piles that were used as GHE was fixed, therefore, a modified design procedure was followed. This is one of the limitations of using foundation piles as GHE, where the number of foundation piles may not be enough to supply the required heating and cooling. For this reason, after calculating the peak heat and cooling loads, the amount of heating and cooling that these piles can supply was calculated, while keeping the circulating water temperature within tolerable limits.

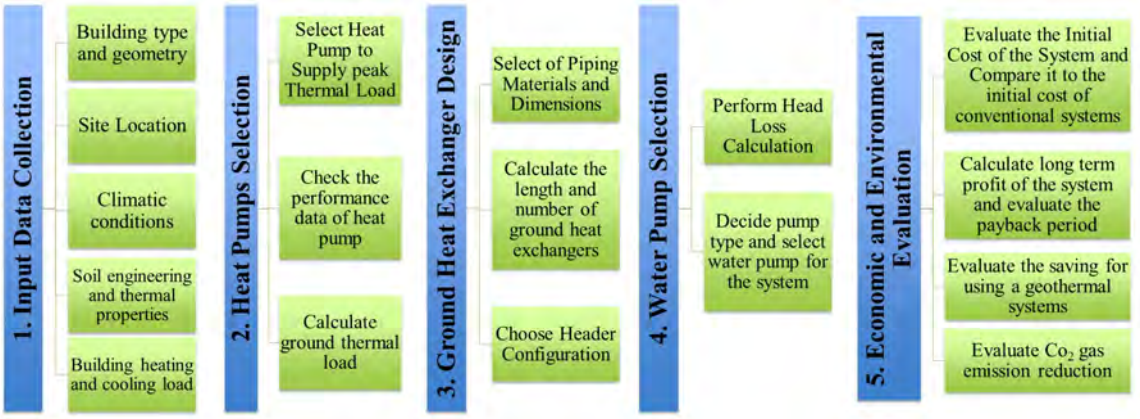

Figure 7-1 Steps for a typical design of shallow geothermal energy system

The parameters that affect the performance of GSHP are:

1. **Entering Water Temperature (EWT)**: Temperature of HCF that enters the heat pump coming from the GHE
2. **Entering Air Temperature (EAT):** Temperature of air entering the GSHP from the thermally controlled space
3. **Water Flow Rate (WF):** the flow rate of the heat carrying fluid. Typically, this value is 3gpm for every tons of heating and cooling.
4. **Air Flow Rate (AFR)**: the flow rate of air entering the GHSP from the thermally controlled space

The designer of the heating and cooling system selects these parameters as input parameters and the system is analyzed based on those data. In practice, the design of GHE should limit the EWT to the heat pumps to within tolerable limits set by the manufacture to insure a proper performance of the heat pump for different EWT values.

The performance of a GSHP can be measured using the following data. Note that the manufacturer of the heat pump provides these data.

1. **Heating Mode**
    a. **HC (Eq. 7.1):** Heating capacity of the heat pump. This is the maximum heating load that can be delivered to the thermally controlled space.
    b. **DMD:** Electric demands of the heat pump.
    c. **COP (Eq. 7.2):** Coefficient of performance of the heat pump, which is highly dependent on the EWT.
    d. **HE (Eq. 7.3):** Heat extracted from the ground
    e. **EAT:** Entering air temperature to the GSHP from the thermally controlled space
    f. **LAT:** Leaving air temperature from the GSHP into the thermally controlled space
    g. **HW:** Hot water generation capability
    h. **AFR:** Air flow rate in the GSHP measured in CFM (cubic feet per minute)
    i. **WF:** Water flow rate in the loops
2. **Cooling Mode**
    a. **TC**: Total cooling capacity of the heat pump. This is the maximum cooling load that can be delivered to the thermally controlled space.
    b. **SC (Eq. 7.5):** Sensible heating capacity
    c. **DMD:** Electric demand of the heat pump

d. **EER (Eq. 7.6):** Energy efficiency ratio of the heat pump, which is highly dependent of the EWT

e. **HR (Eq. 7.7):** Heat rejection into the ground

f. **HW:** Hot water generation capability

g. **AFR:** Air flow rate

h. **WF:** Water flow rate in the loops

$$\mathrm{HC(kW)}=\frac{1.08\times \mathrm{AFL(CFM)}\times\left(\mathrm{LAT}\left(^{\circ}\mathrm{F}\right)-\mathrm{EAT}\left(^{\circ}\mathrm{F}\right)\right)}{3412} \tag{7.1}$$

$$\mathrm{COP}=\frac{\mathrm{HC\ (kW)}}{\mathrm{DMD\ (kW)}} \tag{7.2}$$

$$\mathrm{HE(kW)}=\frac{500\times \mathrm{WF(GPM)}\times\left(\mathrm{EWT}\left(^{\circ}\mathrm{F}\right)-\mathrm{LWT}\left(^{\circ}\mathrm{F}\right)\right)}{3412} \tag{7.3}$$

$$\mathrm{HC\ (kW)=HE\ (kW)+DMD\ (kW)} \tag{7.4}$$

$$\mathrm{SC\ (kW)}=\frac{1.08\times \mathrm{AFL\ (CFM)}\times\left(\mathrm{EAT}\left(^{\circ}\mathrm{F}\right)-\mathrm{LAT}\left(^{\circ}\mathrm{F}\right)\right)}{3412} \tag{7.5}$$

$$\mathrm{EER}=\frac{\mathrm{TC(W)}}{\mathrm{DMD(W)}} \tag{7.6}$$

$$\mathrm{HR(kW)}=\frac{500\times \mathrm{WF(GPM)}\times\left(\mathrm{LWT}\left(^{\circ}\mathrm{F}\right)-\mathrm{EWT}\left(^{\circ}\mathrm{F}\right)\right)}{3412} \tag{7.7}$$

$$\mathrm{HR\ (kW)=TC\ (kW)+DMD\ (kW)} \tag{7.8}$$

The heat pump model that will be used in this project is Envision ND064 from Waterfurnace. Based on the data provided by the manufacturer catalog, the performance data of the selected model are presented in Figures 7-2 and 7-3 for cooling and heating

modes respectively, as a function of EWT. This figure shows the high dependency of the performance parameter on the entering water temperature. More data on this model and other models can be found in the company catalogues. The selected heat pump has a domestic hot water generation capacity of 10.55 kW that will be used when cooling mode is in operation to reduce the thermal loads on the ground and to benefit from free hot water.

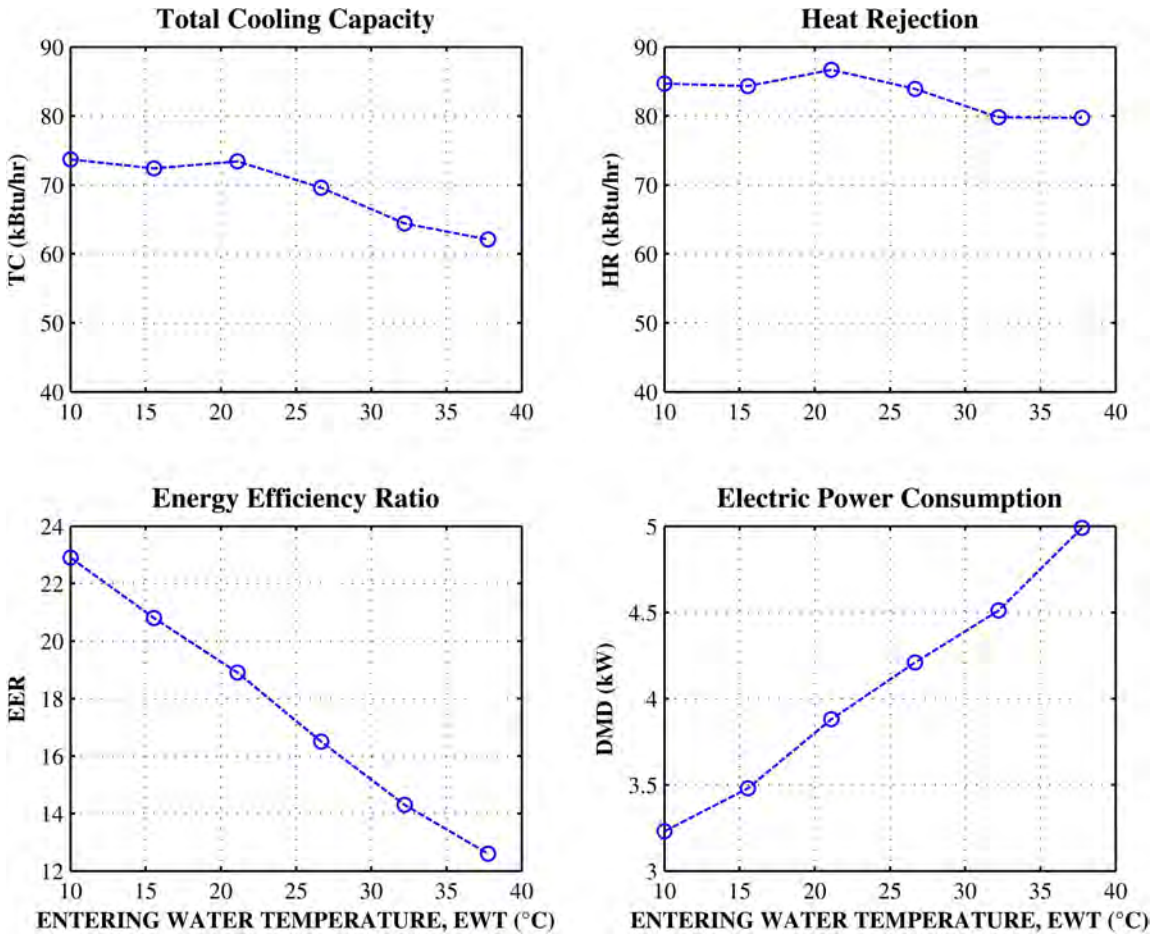

Figure 7-2 Envision ND064 heat pump performance data in cooling mode

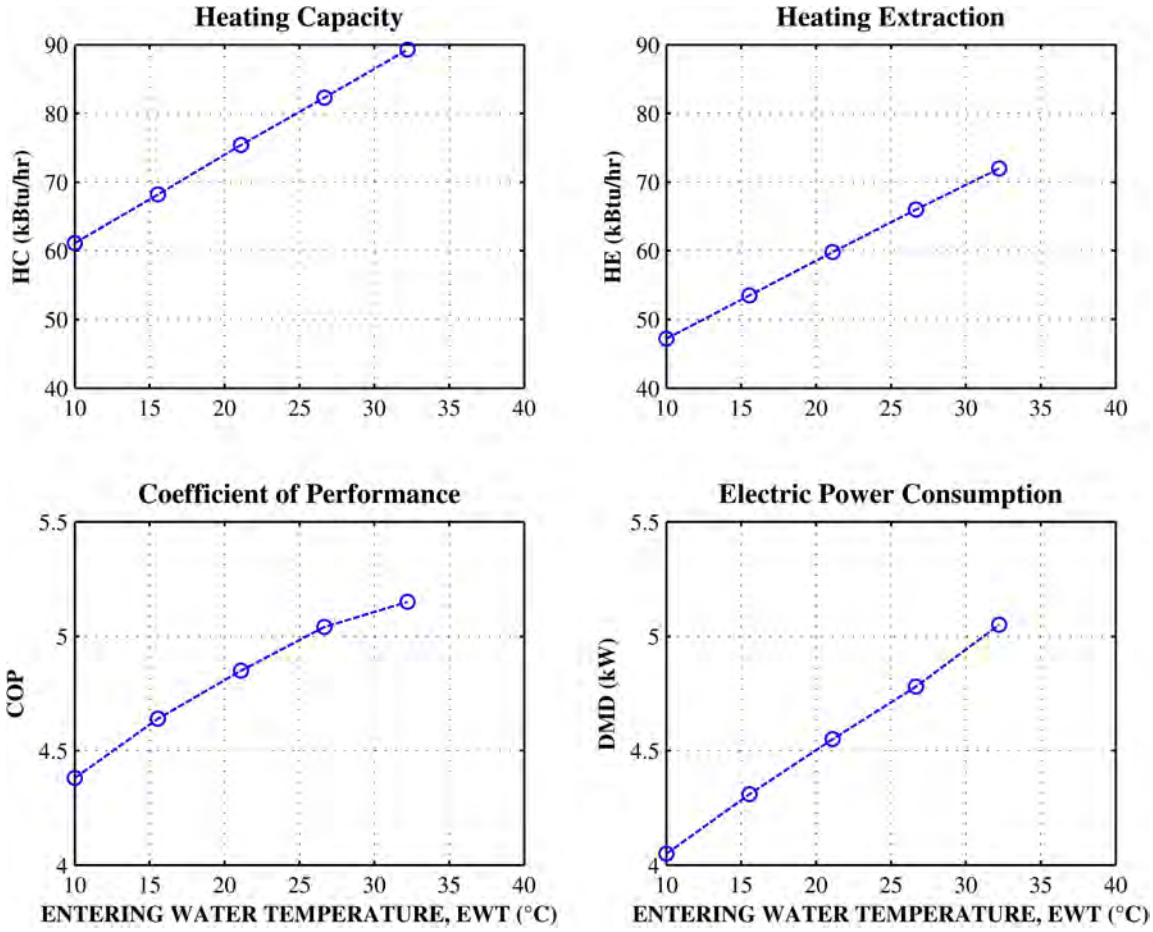

Figure 7-3 Envision ND064 performance data in heating mode

In cooling mode, the total capacity decreases with the increasing entering water temperature because the temperature difference between the heat pump refrigerant and the ground loop water temperature at the condenser level decreases. This results in an increase of electric demand with the increasing entering water temperature because the pump will have to work harder to reject heat into the ground. As a result, the energy efficiency ratio of the heat pump decreases with increasing entering water temperature. In heating mode, with the increasing entering water temperature, the heating capacity

increases because the temperature difference between the heat pump refrigerant and the ground loop water temperature increases at the evaporator level. This results in an increase of electric demand because part of the heat delivered to the building in heating mode comes from the heat generated by the mechanical work of the ground source heat pump. As a result, the coefficient of performance of the heat pump increases with the increasing entering water temperature.

The EWT is the most important parameter in the design of a SGES and it is set by the designer. During the lifetime of the structure, the EWT should remain within the tolerable limits to ensure a proper system performance. The EWT depends on the following parameters:

1. Total length of GHE: a Longer HCF path results in more heat exchanged between the HCF and the soil.
2. Soil and concrete/grout thermal properties: Higher soil/grout thermal conductivity results in better heat injection/extraction from the soil.
3. GHE diameter and the configuration of the HDPE pipes
4. Spacing between GHE: Larger distances between multiple GHE results in lesser thermal interaction between GHE.

For residential applications, the sizing equations of GHE proposed by Kavanaugh and Rafferty (1997) for heating and cooling modes respectively are presented in Eq. 7.9 and Eq. 7.10. These two equations show dependency of the EWT on the different parameters listed previously.

$$L_{Heating} = \frac{HC \times \left(\frac{COP-1}{COP} \right) \times \left(R_b + R_g \times F_H \right)}{TG - \frac{EWT_{min} + LWT_{min}}{2}} \quad (7.9)$$

$$L_{Cooling} = \frac{TC \times \left(\frac{EER + 3.4121}{EER} \right) \times \left(R_b + R_g \times F_C \right)}{\frac{EWT_{max} + LWT_{max}}{2} - TG} \quad (7.10)$$

Where:

L (m): Required total length

R_g (m^2.k/W): Ground thermal resistance that depends on soil thermal properties and distance between GHE (Bennet et al., 1987; Pahud et al., 1996; Paul (1996); Gu and O'Neal, 1998; Sharqawi et al., 2009; Lamarche et al., 2010;)

R_b (m^2.k/W): GHE thermal resistance that depends on GHE material thermal properties and HDPE pipes layout

TG (ºC): Ground initial temperature

FC: Time run fraction of the heat pump within the design month in cooling mode

FC: Time run fraction of the heat pump within the design month in cooling mode

As mentioned earlier, because of the total number and length of foundation piles that can be used as GHE is fixed, a modified design procedure is used and it shown in Figure 7-4.

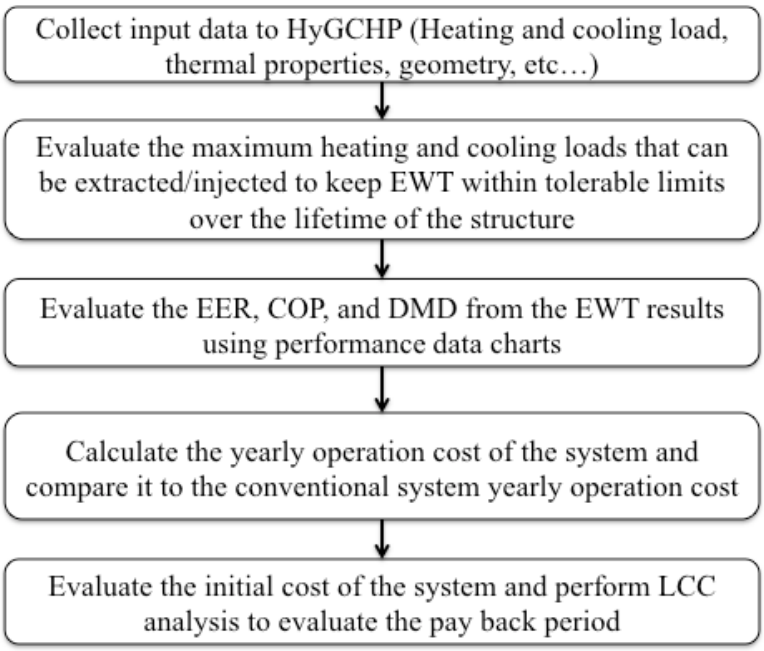

Figure 7-4 Modified design steps

7.3 INPUT DATA COLLECTION

7.3.1 Building type, geometry, foundation, and location

The construction of the Liberal Arts building started in March 2011 and was completed in November 2012 at a cost of 10 million US dollars. The building is located on Texas A&M University main campus in College Station, Texas. The building (Figure 7-5) is composed of five floors including the ground floor and one crawl space with an area of 447 m^2. The total area of the building is 11,575 m^2 with a foot print area of 2,885 m^2.

Figure 7-5 Liberal Arts Building at Texas A&M University

The building is resting on a total of 263 deep foundation piles of length 18 m. excluding the cut off length. The total combined length of the piles is 4,734 m. The piles are connected by pile caps that vary in thickness depending on column loading, and the pile caps are in turn connected by a thin concrete mat.

7.3.2 Weather conditions

The information and data presented in this part of the dissertation were obtained from www.weatherspark.com. The climate in College Station, Texas can be described as warm humid temperate climate with hot summers and no dry season. The temperature usually varies from 40 °F to 95 °F over the course of a year and rarely falls below 28°F or goes higher than 100 °F. The warm season lasts from May 28th to September 21st with an average daily high temperature above 88°F. The hottest day of the year is historically August 7th, with an average high of 95°F and low of 74°F. The coldest day of the year tends to be January 4th, with an average temperature of 40 °F. Figure 7-9 shows the trend of temperature change from January to December in College Station, with the thick red and blue lines representing the average daily high and low temperatures.

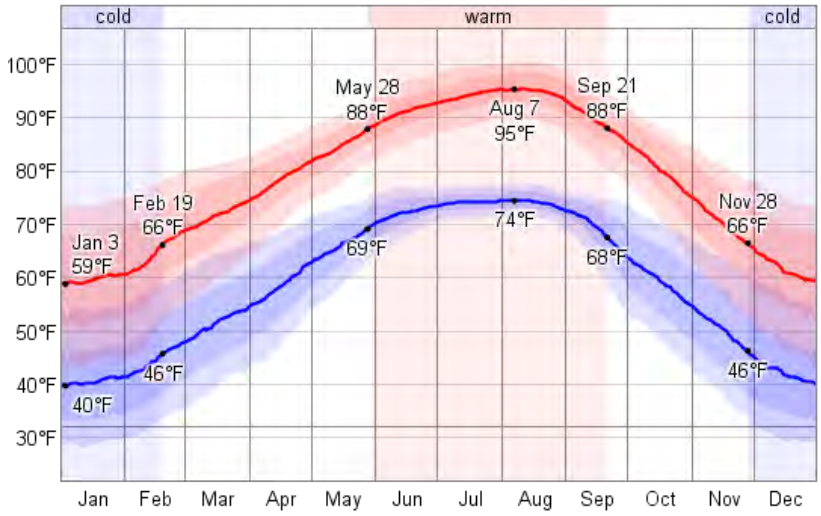

Figure 7-6 Temperature change over the course of a year in College Station

The relative humidity in College Station ranges from 42% (comfortable) to 94% (very humid) over the course of the year (Figure 7-10). Historically, the driest day of the year is around August 7th where relative humidity drops below 47% (very dry) for 75% of the time, while the most humid day of the year is around July 10th where the relative humidity exceeds 91% (very humid) for 75% of the time.

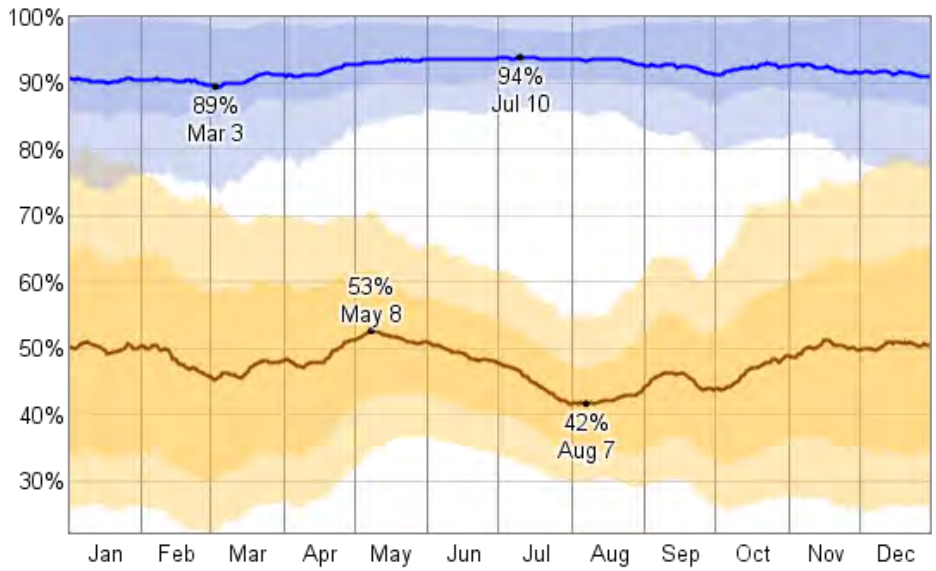

Figure 7-7 Average daily high (blue) and low (brown) relative humidity over the year course in College Station

7.3.3 Soil properties and temperature

Soil engineering and thermal properties were extensively discussed in Sections 3 and 6 of this dissertation. The average thermal properties measured from laboratory tests were 0.6 W/m.C for thermal conductivity, 1.9x10-7 m^2/s for thermal diffusivity, and 2.9

$MJ/m^3.C$ for volumetric heat capacity. However, the calibration of the HyGCHP calculation tool showed that a soil thermal conductivity of 1.87 W/m.K should be used.

The deep soil temperature was measured using the instrumented piles and boreholes presented in Section 6 of this dissertation. The method used in HyGCHP assumes a uniform soil temperature; therefore, the average pile temperature was used as the initial ground temperature and was set equal to 23 °C.

7.3.4 Liberal Arts building heating and cooling loads

The performance of the installed conventional heating and cooling system was monitored over a one year period starting December 13th, 2012 and ending December 12th 2013. The measured data includes the total heating and cooling loads supplied to the Liberal Arts Building and the corresponding electric power consumption. Data samples were taken every 15 minutes. The measured heating and cooling loads and corresponding electric power consumption from the one year cycle are presented in Figure 7-11. The total heating energy, cooling energy, and electric power used was 2,307,064 kBtu, 10,125,468 kBtu, and 817,951 kWh respectively.

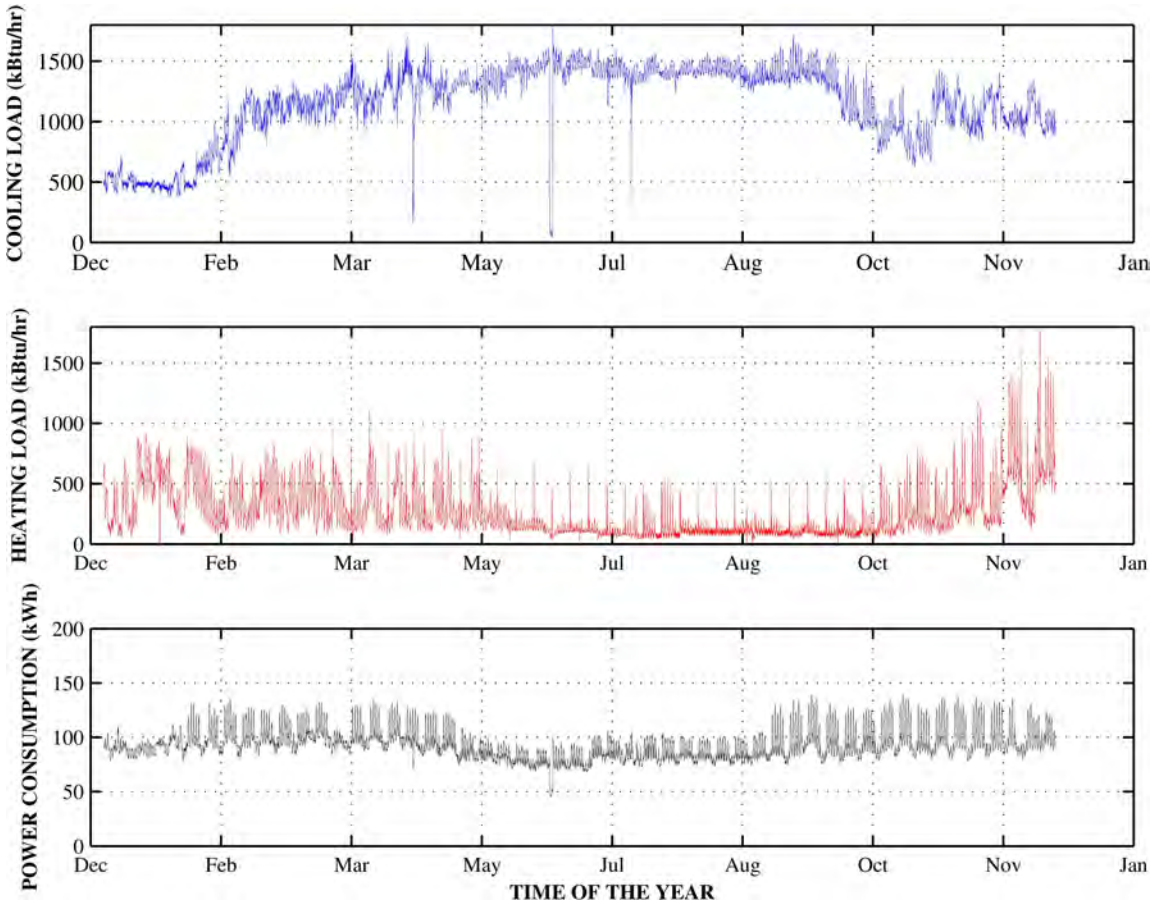

Figure 7-8 Liberal Arts Building measured heating and cooling loads and electric power consumption

7.4 SHALLOW GEOTHERMAL ENERGY SYSTEM ANALYSIS

7.4.1 Full system performance

As outlined in Figure 7-4, the system was analyzed in HyGCHP using the input data from Sections 7.2 and 7.3 to evaluate the EWT. From the EWT, the performance of the system could be evaluated using the performance data charts (Figures 7-2 and 7-3). Three water-to-air GSHP were used with domestic hot water generation capability to supply 13.34% of the total cooling load, 63.51 % of the total heating load, and 10.55 kW

for domestic hot water. The analysis was performed for a 30 years period. The EWT and the corresponding COP and EER are presented in Figure 7-12a, 7-12b, and 7-12c, respectively.

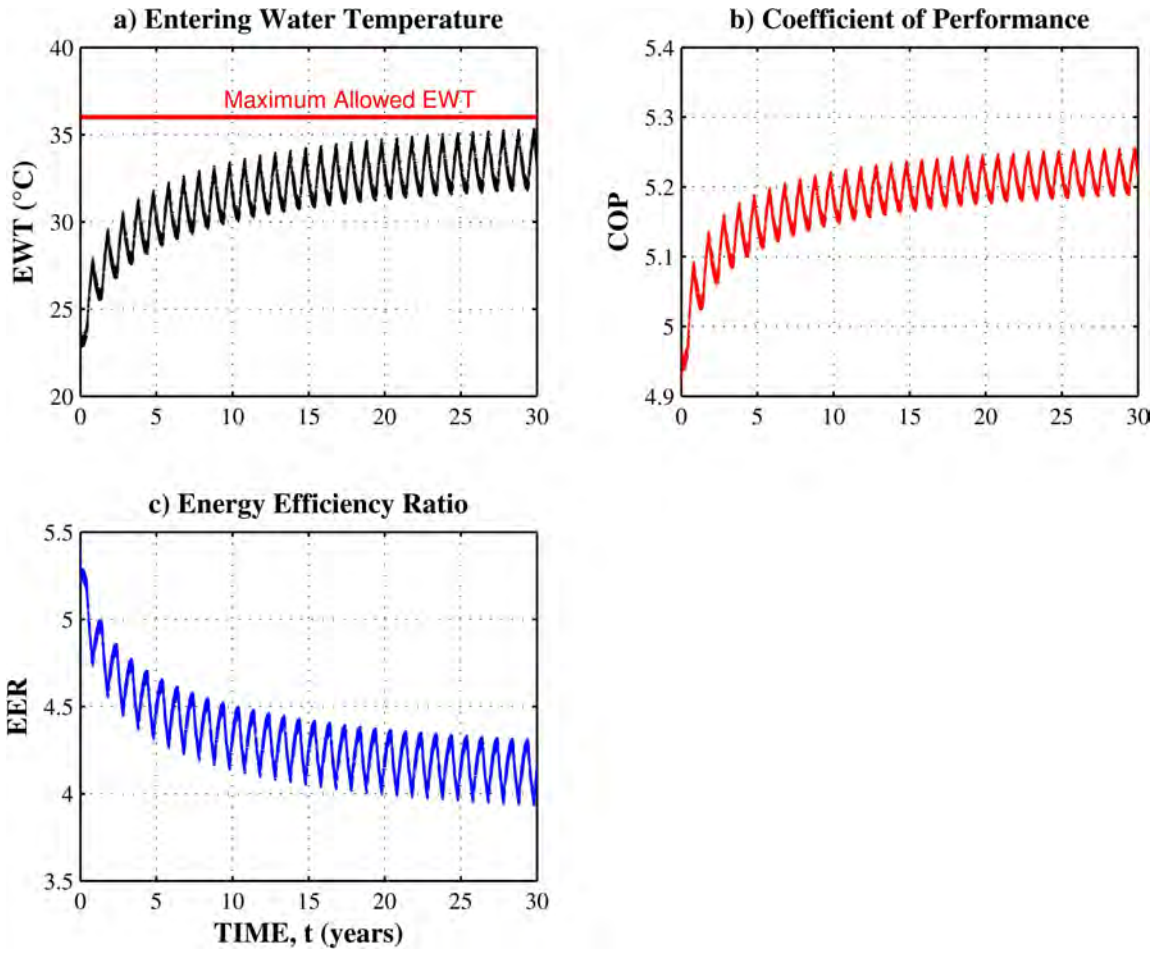

Figure 7-9 SGES System performance in a cooling dominated climate

The results in Figure 7-12 show that for a 30 years period of operation the EWT remains within tolerable limits. Also, because of the cooling dominant climate and the

unbalanced heating and cooling load, the EWT increases over time. The COP increases with time while the EER decreases. The increase in COP means that the efficiency of the system in heating increases with time because of the excessive stored heat in the ground during the cooling season. The decrease of EER implies that the efficiency of the system in cooling mode decreases with time because of the unbalanced heating and cooling load, which leads to excessive heat injection into the ground. The analysis also shows that the ground temperature is expected to increase by 0.28 °C every year.

7.4.2 Full system electric power consumption

The electric power consumption of the system was evaluated from the performance data charts and is presented in Figure 7-13. Figure 7-13a shows the measured hourly power consumption (DMD) of the conventional system used in the building and the calculated power consumption of the geothermal system analyzed here in this section. The geothermal system power consumption increases with time. This is resulting from the increasing EWT and the dependency of DMD on EWT as presented in Figures 7-2 and 7-3. The equivalent electric demand of the conventional system was evaluated based on the percentage of the heating and cooling loads that can be supplied by the geothermal system. Figure 7-13b shows the yearly power consumption of each system, which is equal to the sum of the daily power consumption. Figure 7-13c and 7-13d shows the hourly and yearly power consumption savings respectively, and it is equal to the difference between the conventional and geothermal system's power consumption. These plots show that the power consumption savings slightly decreases with time because of the increase in soil and pile temperature and the associated reduction in

efficiency. A power savings of 10.55 kW should be added to the total power saving resulting from the hot water generation capability.

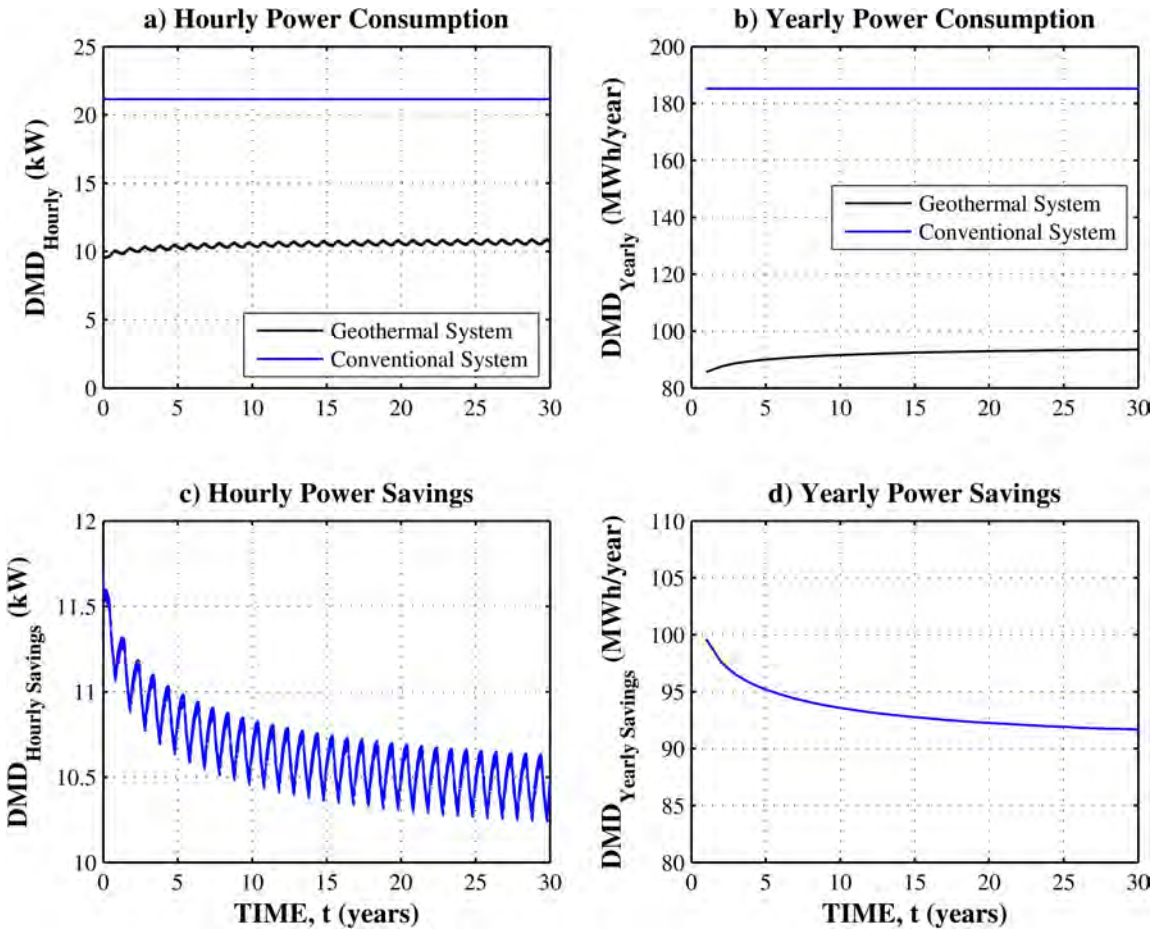

Figure 7-10 Conventional and Geothermal system power consumption and power savings in cooling dominated climates

The use of a SGES as part of the heating and cooling system at the Texas A&M Liberal Arts Building will reduce the electric power consumption by a total of 5,573 MWh over the course of 30 years. This reduction in electric power consumption will

result in a total reduction of 3932 metric tons of CO_2 gas emissions in 30 years. This reduction in CO_2 emissions is equivalent to one of the following environmental impacts being removed every year for 30 years:

1. 27 passenger vehicles from the road
2. 49.1 tons of waste sent to the landfill
3. 14,694 gallons of gasoline consumed
4. 18 homes' electricity use
5. 305 barrels of oil consumed

It is also equivalent to the positive benefit of Carbon sequestered by 107 acres of U.S. forests yearly for 30 years.

7.4.3 Full system economics

The full economic analysis considers the initial and operational cost. A preliminary feasibility study on the use of foundation piles as ground heat exchangers for the Liberal Arts Building was performed by Geothermal International. In summary, this preliminary study showed that using foundation piles as ground heat exchangers could save up to $36,280 in yearly operation costs and 210 tons of CO_2 emissions with an upfront cost of $583,070. Note that the upfront cost included the design, supervision, and heat pumps cost, which should be removed when comparing total costs of conventional and geothermal system because a conventional system will also include these costs. For simplification purposes, this analysis assumed that the design, supervision, and heat pump cost was the same for both systems.

This section of the dissertation presents a more detailed economic analysis. The present value of the operational cost was evaluated from the system power consumption presented in section 7.4.2. The present value of cumulative savings up to "n" year is the sum of yearly savings from year 1 to year "n."

The maintenance cost of the heating and cooling system should be also included in the LCC analysis because one of the advantages of the geothermal systems is that the service life of a commercial GSHP is approximately double the service life of commercial ASHP (Abramson et al., 2005; Akalin, M.T., 1978; ASHRAE, 2011). The service life of an ASHP is approximately 15 years while it's greater than 25 years for commercial GSHP. Therefore, during operation period, a building owner would need to replace the ASHP one time compared to zero times for GSHP during the service life of the heating and cooling system.

Figure 7-11 presents the present value yearly and cumulative yearly money savings from operation. The yearly savings decreases with time because of the decreased system efficiency with time. The detailed analysis shows that using a SGES as part of the heating and cooling system can save between $23,600 to $24,500 US$ on yearly operational costs, with a total present value cumulative savings of $715,000 after 30 years of operation. The assumed average price of electricity is 0.11 $/kWh.

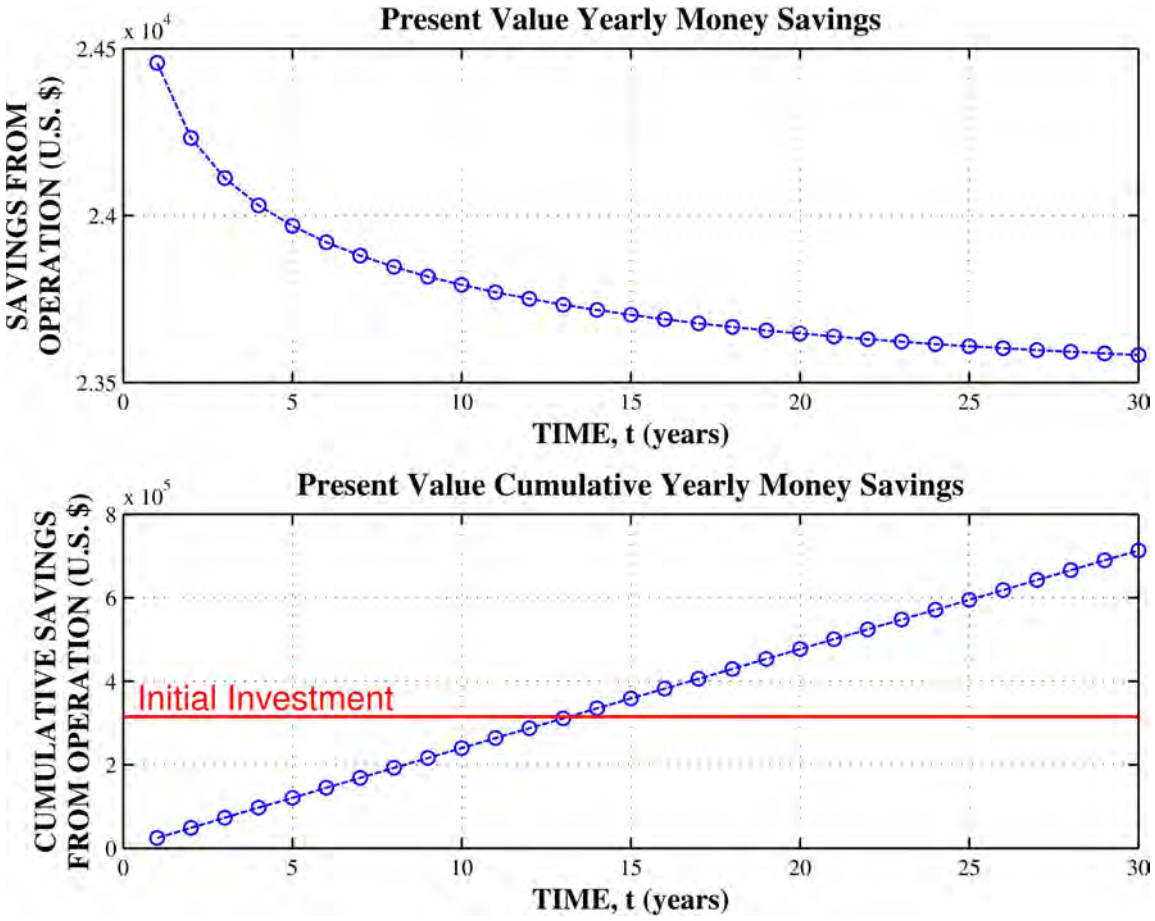

Figure 7-11 Yearly and cumulative yearly savings from system operation in cooling dominated climates

The initial cost of the system includes the different items listed in Table 7-1. Note that this table was prepared by Geothermal International as part of the preliminary feasibility study. The duct system sizing is out of the scope of this study because the same duct system will be used for conventional and geothermal heating and cooling systems; therefore, this part of the system will not impact the cost difference between the different heating and cooling systems.

Table 7-1 Initial Cost Items (From Geothermal International Feasibility Study)

Item	Description	Cost (US$)
Design and Supervision	Includes engineering costs, design drawings, site supervision, site co-ordination and mobilization time, site accommodation, and drilling feasibility study	123,100
Tube Installation and Headering	Includes ground loop pipe and connection materials, and labor for assembly of the header collection pipe work	158,570
Mechanical Room Pipe-Work	Includes the source circulation pump, all necessary connections and fittings for the circulation pumps and the heat pump main riser pipe work connecting to the external ground loop	106,940
Heat Pumps	Includes the heat pump and delivery to site	144,400
Electrical Installation	Includes final electrical wiring to heat pump, circulation pump and controls to wiring supplied by others to within 1 meter of the equipment	13,080
Testing and Commissioning	Includes ground loop testing and commissioning, unit testing and commissioning, controls testing and commissioning, operational guidance and instruction, and operation and maintenance manual	36,980
	Total Cost	**583,070**

Based on the information provided in Table 7-1, the initial investment, which is the difference in initial price between a conventional system and a geothermal system, is $315,570**.** The simple payback period can be evaluated from the intersection of initial investment cost line with the present value cumulative yearly savings curves shown on Figure 7-11. This simple payback period is 13 years for the Liberal Arts Building in cooling dominated climates. The total savings after 30 years of operation in present value is approximately $400,000.

7.5 ANALYSIS OF LIBERAL ARTS BUILDING IN HEATING DOMINATED CLIMATE

To assess the difference in performance and economy of SGES in heating and cooling dominated climates, the Liberal Arts Building was analyzed assuming conditions of a heating dominated climate. This was done by switching the heating and cooling loads as presented in Figure 7-12 and by setting the initial ground temperature to 10 °C, which is a typical value for soil temperature in Berlin, Germany. The original cooling load was considered as a heating load while and the original heating load was considered a cooling load. The electric power consumption and the performance data of the heat pump were assumed to be the same for both for heating and cooling dominated climates. The total heating energy, cooling energy, and electric power use was projected as 10,125,468 kBtu, 2,307,064 kBtu, and 817,951 kWh, respectively.

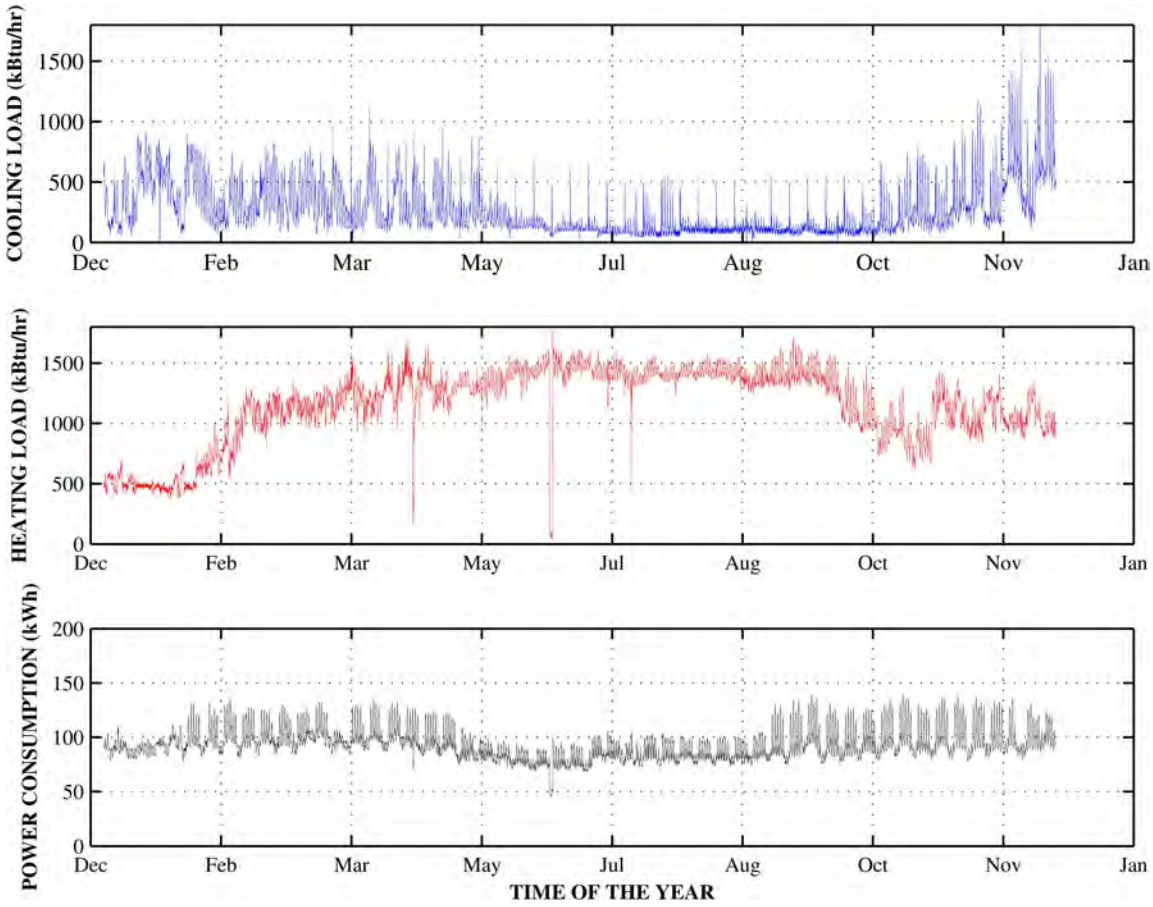

Figure 7-12 Liberal Arts Building measured heating and cooling loads, and electric power consumption in a simulated heating dominated climate

The SGES system was analyzed using the same calculation tool HyGCHP. In a heating dominated climate, the SGES can supply 78% of the total cooling load, 28 % of the total heating load, and 2.5 kW for domestic hot water. The EWT, COP, and EER were evaluated in the same manner as evaluated in section 7.4.1 of this dissertation (Figure 7-13). The results show that the EWT remains within tolerable limits. In addition, the results show that the COP decreases with time because of the decrease in soil temperature resulting from excessive heat extraction. This decrease in soil

temperature results in an increase of EER. When soil temperature decreases, the heat pump will have to work harder to extract the same amount of heat, which results in a lower COP. On the other hand, the soil temperature decrease creates more room for heat rejection, which results in an increase of EER in cooling mode.

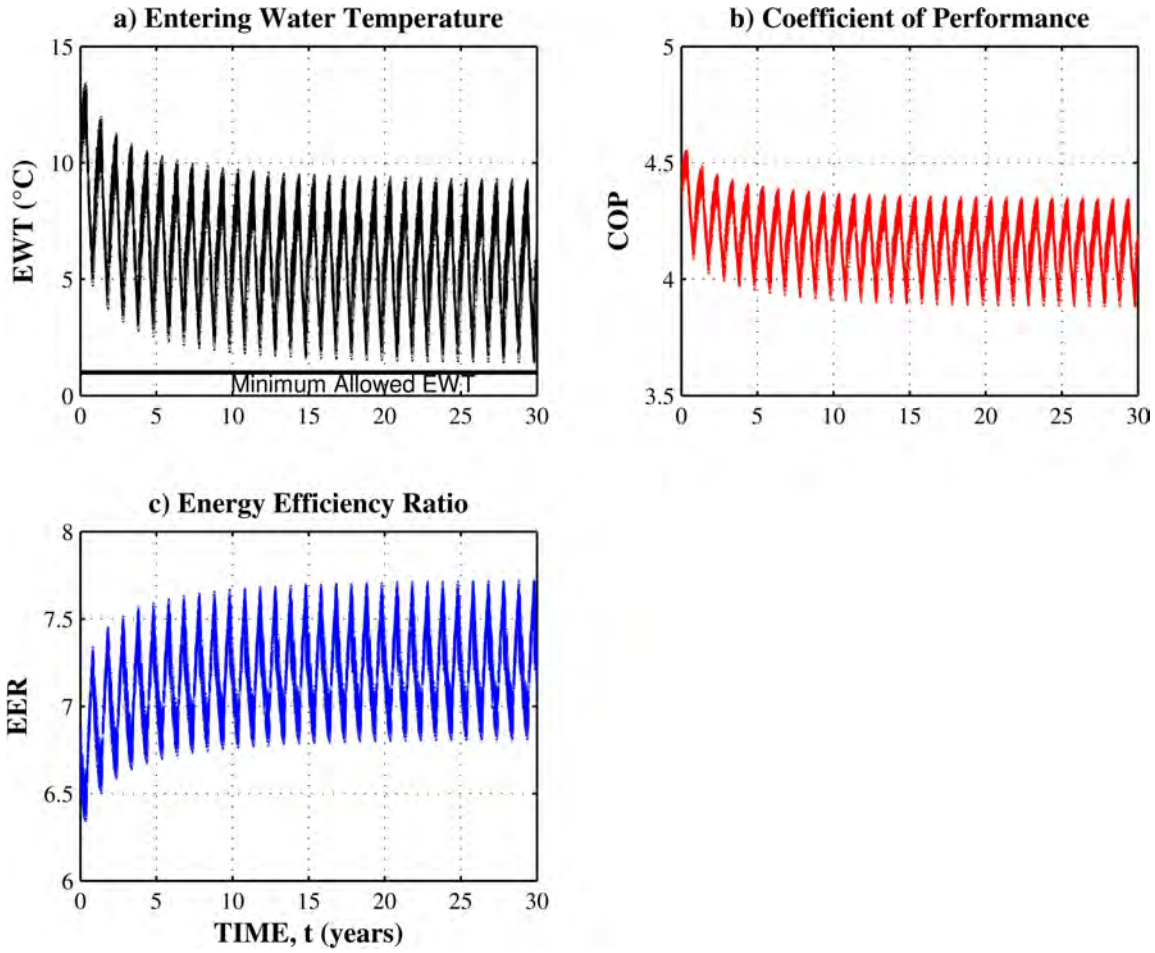

Figure 7-13 SGES System performance in heating dominated climate

The measured and calculated power consumption of the conventional and SGES systems in heating dominated climates was evaluated using in the same procedure described in Section 7.4.2. Figure 7-14 shows that using SGES as part of the heating and cooling system for buildings in a heating dominated climate can save 7,700 MWh of power consumption over 30 years of operation. This savings in power consumption will reduce the CO_2 gas emission by 5,460 metric tons which is equivalent to:

1. Removing 38 passenger vehicles from the road per year
2. 68.1 tons of waste sent to landfill yearly instead of recycling
3. 20,373 gallons of gasoline consumed yearly
4. 25 homes' electricity use for one year
5. 423 barrels of oil consumed per year
6. Carbon sequestered by 149 acres of U.S. forests in one year

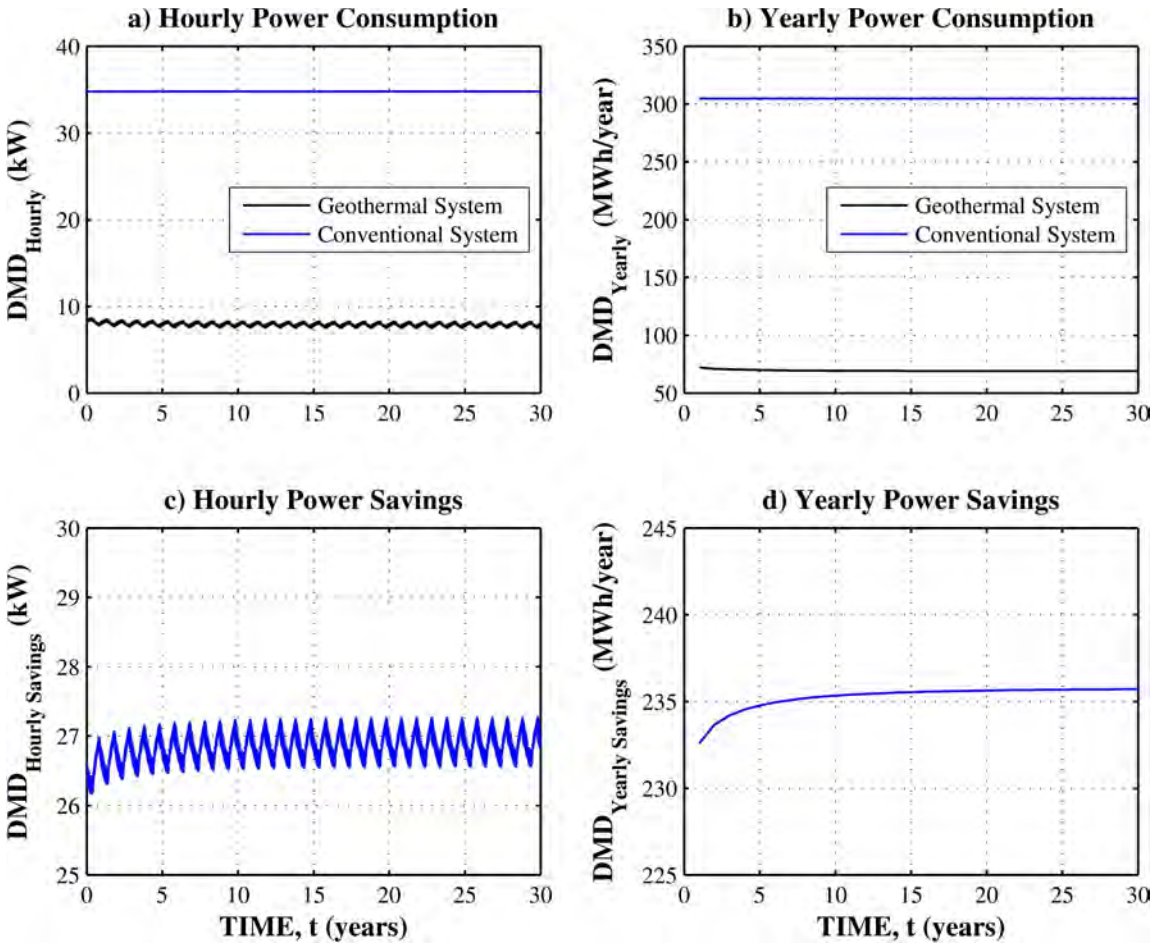

Figure 7-14 Conventional and Geothermal system power consumption and power savings in heating dominated climates

Figure 7-15 presents the present value yearly and cumulative yearly monetary savings from operation. The detailed analysis shows that using a SGES as part of the heating and cooling system can save approximately $31,100 on the yearly operational cost with a total present value cumulative savings of approximately $944,000 after 30 years of operation.

The simple pay back period can be evaluated from the intersection of initial investment cost line with the present value cumulative yearly savings curves shown on Figure 7-18. This simple pay back period is 10 years for the Liberal Arts Building in heating dominated climates, with a total present value savings of $629,000 after 30 years of operation.

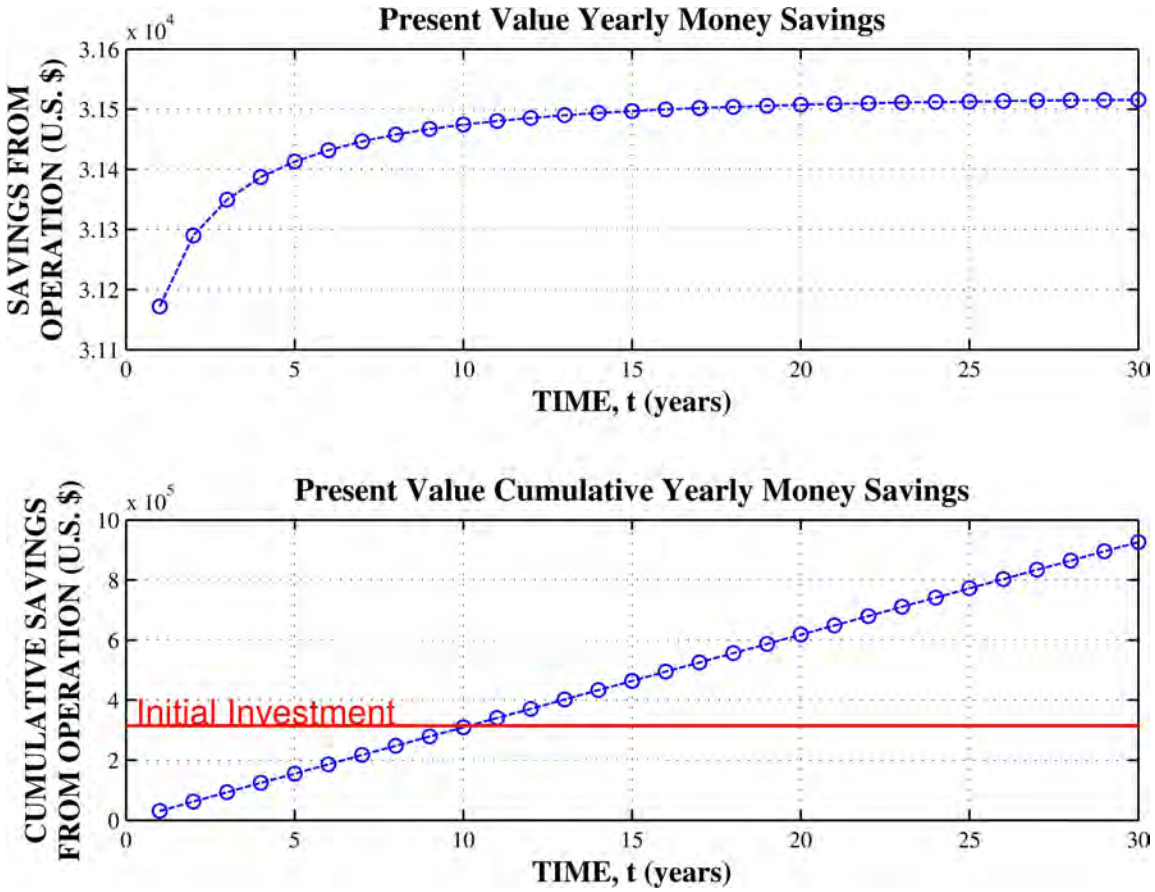

Figure 7-15 Yearly and cumulative yearly savings from system operation in heating dominated climates

7.6 CONCLUSION

This section of the dissertation answers the question posed in the problem statement of this dissertation and recalled here: “is the use of energy piles for SGES in hot and cooling dominated climates energy efficient and environmentally friendly?” In brief, the answer to this question is: yes.

This section of the dissertation presented an economic study on the use of SGES in cooling and heating dominated climates. The newly constructed Liberal Arts Building on Texas A&M University campus provided a case study. The analysis was based on measured total heating and cooling loads, HyGCHP calibration using full scale tests on three energy piles, and measured electric power consumption. The analysis of the SGES evaluated the performance of the system in heating and cooling mode as they pertain to electric power consumption and the yearly and cumulative monetary savings in present value. The results show that, for a building of the size of the Liberal Arts Buildings using the same number and length of foundation piles, the simple payback period of using SGES to provide part of the heating and cooling load is 13 years in cooling dominated climates and 10 years in heating dominated climates. The analysis did not include all the parameters for a life cycle cost, which can reduce the simple payback period if considered. The results show that SGES are more cost effective in heating dominated climates, but they are still cost effective in cooling dominated climates. This makes SGES an excellent choice for building owners or institutions who want to commit to bettering the environment while still profiting their bottom-line.

8 SUMMARY AND CONCLUSION

Are energy piles for heating and cooling purposes economical and environmentally friendly in cooling dominated climates? Yes they are! The work presented in this dissertation answered the question that was posed at the beginning of this research project and found that the use of energy piles as ground heat exchangers benefits in reducing the operation cost of the thermal control system and significantly save on CO^2 gas emission.

This dissertation presents the different aspects of energy piles in cooling dominated climates. The work presented in this dissertation will enable engineers to design shallow geothermal energy systems in cooling dominated climates while taking into account the different elements of the system and the interaction between them. The engineer will be able to evaluate the effect of soil saturation on thermodynamic efficiency of energy piles using a quick and easy method. Engineers will also understand the short- and long-term thermo-mechanical behavior of energy piles and take into account load redistribution in the pile and its time dependent behavior. Engineers, practitioners, and clients will understand the economic benefits of using shallow geothermal energy systems in cooling dominated climates.

The third section of the dissertation presents an in situ method called the Thermal Cone Test or TCT to evaluate soil thermal properties using the CPT cone. The proposed TCT relies on the friction naturally generated by the penetration of the cone point in the soil. The TCT was evaluated through laboratory tests, through 11 in-situ TCT tests, and

through numerical simulations. The proposed method enables the evaluation of soil effective thermal conductivity from in-situ measurement, while the evaluation of thermal diffusivity requires the evaluation of volumetric heat capacity from dry density and water content. The only parameter that needs to be measured from the TCT in the field is t_{50}. The proposed method was verified against data from 11 in-situ scale TCT tests. Future work may include an extensive experimental program to provide enough information to include other soil parameters to the proposed equations in this paper.

The fourth section of the dissertation presented a simple method to evaluate the heat exchange rate of energy piles in unsaturated soil conditions. The solution is based on the cylindrical heat source theory and gives the thermal efficiency function relating the ratio of the heat exchanged between an energy pile and the surrounding soil in unsaturated and saturated conditions. The ζ function depends on soil thermal properties, the degree of saturation, and the thermal resistance of the energy pile. The ζ function was first developed to work at a specific depth, and was verified by laboratory tests and numerical simulation results on pile sections simulating an energy pile slice at a certain depth. The measured data showed a good consistency with the analytical solution and also showed, for the given conditions during the test that the performance of energy piles could drop by 40% in sand and at very low saturation conditions. The analytical solution for ζ was then developed to account for the profile of the energy pile by introducing the matrix suction parameter in the degree of saturation equation, which includes the depth variable. The analytical solution for the ζ curve was compared to the results of the 2D numerical simulations of the energy pile in axisymmetric problem and

for various soil saturation profiles. The analytical solution showed relatively good consistency with the results from the numerical simulation. The difference between the two solutions may come from neglecting the propagation of heat in the vertical direction in the analytical solution. However, for preliminary sizing and design, and to avoid complicated numerical modeling of energy piles in partially saturated soils, the analytical solution can be useful.

The fifth section of the dissertation investigates the thermo-mechanical behavior of energy piles in cooling dominated climates. A series of mechanical and thermo-mechanical tension load tests on energy piles in high plasticity stiff clays was presented. The strain and temperature distribution, load-displacement behavior, and climatic conditions were monitored during the test. Based on the soil type, soil profile, soil properties, and the testing conditions, it was concluded that the use of foundation piles for geothermal energy application induces thermal strains and stresses in the pile element because of the volume expansion/contraction of the pile and the soil-pile friction generated from this thermally induced volume change. However, the thermally induced pile load is practically insignificant (less than 1% per °C of temperature increase) compared to the ultimate values. In addition, the increase in soil temperature caused an increase in the creep rate. Mathematically, this is represented by an increase of the viscous exponent n by a factor of 4.7. The measured results were compared to data from the literature and showed good consistency. Furthermore, the results showed that the long-term displacement (50 years) for the energy pile could increase by a factor of 2.35 times the displacement for the regular pile. Moreover, the results showed that that the

ultimate capacity of foundation piles doesn't change when it is used as ground heat exchanger for SGES. But the stiffness of the pile increases when the pile is cooled and does not change when the pile is heated.

The sixth section of the dissertation presented a full-scale test on an energy pile group installed and instrumented at the Liberal Arts building at Texas A&M University. The results from the full-scale test were used to calibrate a calculation tool that was utilized in Section 7 of this dissertation to analyze a full SGES in the foundation system of the new Liberal Arts Building. The measured and calculated results provide good consistency, as shown in Section 6.5, which validates the use of the HyGCHP tool to perform the full building simulation. The measured data showed a quick pile thermal response and delayed soil pile thermal response. This behavior implies that thermal stresses and strains will develop very quickly in the pile because of the thermal load, while soil time-dependent behavior such as creep and thermal consolidation will depend on the heat propagation mechanism in the soil.

The last section of the dissertation capped the study and answered the question posed in the problem statement of this dissertation and recalled here: "is the use of energy piles for SGES in hot and cooling dominated climates energy efficient and environmentally friendly?" In brief, the answer to this question is: yes. This section presented a detailed economic study on the use of SGES in cooling and heating dominated climates. The newly constructed Liberal Arts Building on Texas A&M University campus provided a case study. The analysis was based on measured total heating and cooling loads, HyGCHP calibration using full scale tests on three energy

piles, and measured electric power consumption. The analysis of the SGES evaluated the performance of the system in heating and cooling mode as they pertain to electric power consumption and the yearly and cumulative monetary savings in present value. The results show that, for a building the size of the Liberal Arts Buildings with the same number and length of foundation piles, the simple payback period of using SGES to provide part of the heating and cooling load is 13 years in cooling dominated climates and 10 years in heating dominated climates. The analysis did not include all the parameters for a life cycle cost, which can reduce the simple payback period if considered. The results show that SGES are more cost effective in heating dominated climates, but they are still cost effective in cooling dominated climates. This makes SGES an excellent choice for building owners or institutions that want to commit to bettering the environment while still profiting their bottom-line.

REFERENCES

Abramson, B., Herman, D., and Wong, L. (2005). "Interactive web-based owning and operating cost database (TRP-1237)." *ASHRAE Research Project, Final Report.*

ACI 318 (2002). *Building Code Requirements for Reinforced Concrete.* American Concrete Institute, Detroit, MI, USA.

Adam, D., and Markiewicz, R. (2009). "Energy from earth-coupled structures, foundations, tunnels and sewers." *Géotechnique,* vol. 59 (3), 229–36.

Akalin, M.T. 1978. "Equipment life and maintenance cost survey (RP-186)." *ASHRAE Research Project, Final Report.*

Akrouch, G., Sanchez, M., and Briaud, J.L. (2013). "Energy Piles for Heating and Cooling Purposes." *Proceedings of the 5th International Young Geotechnical Engineers' Conference*, vol. 2, p. 161 - 164, Paris, France.

Alonso, E., Vaunat, J., and Gens, A. (1999). "Modeling the mechanical behavior of expansive clays." *Engineering Geology,* vol. 54, 173–83.

Amatya, B., Soga, K., Bourne-Webb, P., Amis, T., and Laloui, L. (2012). "Thermo-mechanical behavior of energy piles." *Géotechnique,* vol. 62 (6), 503–519.

ASHRAE (2011). *Heating, ventilating, and air-conditioning applications.* ASHRAE, Atlanta, GA, USA.

ASTM (1993). "Standard test method for steady-state heat flux measurements and thermal transmission properties by means of the guarded-hot-plate apparatus." *C177-85*, West Conshohocken, PA, USA.

Ballouz M., Nasr, G., Briaud, J.L. (1991). "Dynamic and static testing of nine drilled shafts at Texas A&M University Geotechnical Research Sites." *Research Report to FHWA*, Civil Engineering, Texas A&M University, College Station, TX, USA.

Bennet, J., Claesson, J., and Hellstrom, G. (1987). "Multipole method to compute the conductive heat transfer to and between pipes in a composite cylinder." *Notes on Heat Transfer 3-1987*. Department of Building Physics, Lund Institute of Technology, Lund, Sweden.

Bourne-Webb, P., Amatya, B., Soga, K., Amis, T., Davidson, C., and Payne, P. (2009). "Energy pile test at Lambeth College, London: geotechnical and thermodynamic aspects of pile response to heat cycles." *Géotechnique,* vol. 59 (3), 237–248.

Brandl, H. (1998). "Energy piles and diaphragm walls for heat transfer from and into the ground." *Proceeding of the 3rd International Symposium on Deep Foundations on Bored and Auger Piles*, BAP III, Ghent, Belgium. p. 37–60.

Brandl, H. (2006). "Energy foundations and other thermo-active ground structures." *Géotechnique,* vol. 56 (2), 81–122.

Brandon, T.L., and Mitchell, J.K. (1989). "Factors influencing thermal resistivity of sands." *Journal of Geotechnical and Geoenviromental Engineering,* vol. 115 (12), 1683-1698.

Briaud, J.L. (1993). "National geotechnical experimentation sites at Texas A&M University: clay and sand Data collected until 1992." Department of Civil

Engineering, Texas A&M University, College Station, TX, USA. Report No. NGES-TAMU-001.

Briaud, J.L. (1997). "The national geotechnical experimentation sites at Texas A&M University: clay and sand." Department of Civil Engineering, Texas A&M University, College Station, TX, USA. Report No. NGES-TAMU-007.

Briaud, J.L., Powers, W.F., and Weatherby, D.E. (1998). "Should grouted anchors have short tendon bond length?" *Journal of Geotechnical and Geoenviromental Engineering,* vol. 124 (2).

Briaud J.L. (2013). *Geotechnical Engineering: Unsaturated and Saturated Soils.* John Wiley and Sons, New York, NY, USA. 1000 pp.

Briaud, J.L. (2013). "The pressuremeter test: expanding its use." *The 2013 Louis Menard Lecture, Proceeding of the 18th International Conference on Soil Mechanics and Geotechnical Engineering,* ENPC Press, Paris, France.

Brooks, R., and Corey, A. (1964). "Hydraulic properties of porous media." *Hydrology Paper No. 3,* Colorado State University, Fort Collins, CO, USA.

Bruner, R.F., Marcontell, M., and Briaud, J.L. (1994). "National geotechnical experimentation sites at Texas A&M University: clay and sand." Department of Civil Engineering, Texas A&M University, College Station, TX, USA. Report No NGES-TAMU-002.

Burghignoli, A., Desideri, A., and Miliziano, S. (2000). "A laboratory study on the thermomechanical behavior of clayey soils." *Canadian Geotechnical Journal,* vol. 37 (4), 764–780.

Campanella, R.G., and Mitchell, J.K. (1967). "Temperature effects on volume changes and pore pressures in soils." *Journal of the Soil Mechanics and Foundation Division*, vol. 94 (3).

Campbell, G.S. (1985). *Soil Physics with BASIC*. Elsevier, New York, NY, USA.

Carslaw, H. S., Jaeger, J. C. (1945). *Conduction of Heat in Solids.* Oxford University Press, UK.

Cekerevac, C., and Laloui, L. (2004). "Experimental study of thermal effects on the mechanical behavior of a clay." *International Journal for Numerical and Analytical Methods in Geomechanics,* vol. 28 (3), 209-228.

Choi, J.C., Lee, S.R., and Lee, D.S. (2011). "Numerical simulation of vertical ground heat exchangers: intermittent operation in unsaturated soil conditions." *Computers and Geotechnics,* vol. 38, 949-958.

Clayton, W.S. (1996). "Relative permeability-saturation-capillary head relationships for air sparing in soils." Ph.D. Dissertation, Colorado School of Mines, Golden, CO, USA.

Côté, J., and Konard, J.M. (2005). "A generalized thermal conductivity model for soils and construction materials." *Canadian Geotechnical Journal*, vol. 42, 443–458

Cui, Y.J., Le, T.T., Tang, A., Delage, P., and Li, X. (2009). "Investigating the time-dependent behavior of Boom clay under thermo-mechanical loading." *Géotechnique*, vol. 59 (4), 319–329.

David, B.L. (2008). *An Introduction to Thermogeology: Ground Source Heating and Cooling.* Wiley-Blackwell. New York, NY, USA. ISBN 978-1-4051-7061-1.

De Bruyn, D., and Thimus, J.F. (1996). "The influence of temperature on mechanical characteristics of Boom clay: the results of an initial laboratory program." *Engineering Geology*, vol. 41 (1-4), 117.

De Vries, D.A. (1952). "The thermal conductivity of soil." *Mededelingen van de Landbouwhogeschool to Wageningen* 52 (1), 1-73. Translated by Building Research Station (Library Communication No. 759), England.

De Vries, D.A (1963). "Thermal properties of soil." *Physics of Plant Environment* (ed. W.R. van Wijk) Amsterdam, North-Holland. 210-235.

Desmedt, J., Van Bael, J., Hoes, H., and Robeyn, N. (2010). "Experimental performance of borehole heat exchangers and grouting materials for ground source heat pumps." *International Journal of Energy Research,* vol. 36 (13), 1238–1246.

Energy Center of Wisconsin, (2011). *Hybrid Ground-Source Heat Pump Installations: Experiences, Improvements, and Tools.*

Eskilson, P. (1987). "Thermal analysis of heat extraction boreholes." Doctoral Thesis Department of Mathematical Physics, University of Lund, Lund, Sweden, 264 pp.

Farouki, O.T. (1986). "Thermal properties of soils." *Series on rock and soil mechanics.* vol. 11. Trans Tech Publ., Clausthal-Zellerfeld, Germany.

Forbes, J.D. (1849). "Account of some experiments on the temperature of the earth at different depths, and in different soils, near Edinburgh." Transactions of the Royal Society of Edinburgh, vol. 16, 189-236.

Fourier, J. B. (1822). *Théorie Analytique de la Chaleur*. A. Freeman. Translator. Dover Publications, New York. NY, USA.

Fredlund, D.G., and Xing, A. (1994). "Equations for the soil-water characteristic curve." *Canadian Geotechnical Journal,* vol. 31, 533-546.

Gao, J., Zhang, X., Liu, J., Li, K., and Yang, J. (2008). "Numerical and experimental assessment of thermal performance of vertical energy piles: An application." *Applied Energy, vol.* 85 (10), 901–910.

Gemant, A. (1952). "How to compute thermal soil conductivities." *Heating, Piping, and Air Conditioning,* vol. 24 (1), 122-123.

Gens, A., and Alonso, E.E. (1998). "Constitutive models for unsaturated soils: thermodynamic approach." *Proceeding of the 2nd International Conference on Unsaturated Soils,* Beijing, International Academic Publishers, vol. 1, 455-460.

Gu, Y., and O'Neal, D.L. (1998). "Development of an equivalent diameter expression for vertical U-tubes used in ground-coupled heat pumps." *ASHRAE Transactions* vol. 104, 347–355.

Hellström, G. (1989). "Duct ground heat storage model. Manual for computer code." University of Lund, Department of Mathematical Physics, Lund, Sweden.

Hellström, G. (1991). "Ground heat storage; thermal analysis of duct storage systems." Doctoral Thesis, Department of Mathematical Physics, University of Lund, Lund, Sweden, 310 pp.

Hellström, G., and Sanner, B. (1997). "EED - Earth Energy Designer, version 1.0, User's Manual." Prof. Knoblich & Partner GmbH, Virchowstrasse 4, D-35578 Wetzlar, Germany.

Hueckel, T., and Pellingrini, R. (1992). "Effective stress and water pressure in saturated clays during heating–cooling cycles." *Canadian Geotechnical Journal*, vol. 29, 1095–1102.

Ingersoll, L.R, Zobel, O.J., and Ingersoll, A.C. (1948). *Heat conduction with engineering and geological applications.* McGraw-Hill, New York, NY, USA. 278 p.

Ingersoll, L.R., Zobel, O.J., Ingersoll, A.C. (1954). *Heat conduction: with engineering, geological and other applications.* McGraw-Hill, New York, NY, USA.

Janbu, N., and Senneset, K. (1974). "Effective stress interpretation of in-situ penetration tests." *Proceedings of the European Symposium on Penetration Testing*, vol. 1, Stockholm, Sweden.

Jennings, S.P., Mathewson, C.C., Yancey, T.E., and Briaud, J. L. (1986). "National geotechnical experimentation sites at Texas A&M University: clay and sand, geology." Department of Civil Engineering, Texas A&M University, College Station, TX, USA. Report No. NGES-TAMU-005.

Johansen, O. (1975). "Thermal conductivity of soils." Ph.D. thesis. Trondheim, Norway (CRREL Draft Translation 637, 1977) ADA 044002.

Kalanhidou, A., Tang, A.M., Pereira, J.M., and Hassan, G. (2012). "Preliminary study on the mechanical behavior of heat exchanger pile in physical model." *Géotechnique*, vol. 62 (11), 1047-1051.

Kaunda, T., and Archenbach, P.R. (1965). "Earth temperature and thermal diffusivity at selected stations in the United States." *ASHRAE Transactions*, vol. 71, Part 1.

Kavanaugh, S.P. and Rafferty, K.D. (1997). *Ground-Source Heat Pumps: Design of Geothermal Systems for Commercial and Institutional Buildings*. ASHRAE, Atlanta, GA, USA

Kersten, M.S. (1949). "*Thermal properties of soils." Bulletin 28*. Minneapolis: Engineering Experiment Station, University of Minnesota, MN, USA.

Kenllwolf, C., Peron, H., and Laloui, L. (2011). "Geotechnical analysis of heat exchanger piles." *Journal of Geotechnical and Geoenviromental Engineering*, vol. 137 (10), 890-902.

Kubena, M.E., and Briaud, J.L. (1989). "Capacity of 2 drilled and grouted piles." Research Report 5887-2F to Minerals Management Service, Civil Engineering, Texas A&M University, College Station, TX, USA1989.

Laloui, L., Moreini, M., and Vulliet, L. (2003). "Comportement d'un pieu bi-fonction, fondation et échangeur de chaleur." *Canadian Geotechnical Journal*, vol. 40 (2), 388 – 402.

Laloui, L., Nuth, M., and Vulliet, L. (2006). "Experimental and numerical investigation of the behavior of a heat exchanger pile." *International Journal for Numerical and Analytical Methods in Geomechanics*, vol. 30 (8), 763 – 781.

Laloui, L. (2011). "In situ testing of a heat exchanger pile." *Proceeding of Geo-Frontiers Conference*, Dallas, TX, USA, 410-419.

Lamarche, L., Kajl, S., and Beauchamp, B. (2010). "A review of methods to evaluate borehole thermal resistances in geothermal heat-pump systems." *Geothermics*, vol. 39, 187-200.

Lu, N., and Likos, W.J. (2004). *Unsaturated Soil Mechanics*. John Wiley & Sons, Inc., Hoboken, NJ, USA. p. 584.

Lu, S., Ren, T., Gong, Y., and Horton, R. (2007). "An improved model for predicting thermal conductivity from water content at room temperature." *Soil Science Society of America*, vol. 71 (1), 8–14.

Lutenegger, A.J., and Lally, M.J. (2001). "In situ measurement of thermal conductivity in a soft clay." *International Conference on In-situ Measurement of Soil Properties and Case histories*, Bali, Indonisia.

Marcontell, M., and Briaud J.L. (1994). "National geotechnical experimentation sites at Texas A&M University: clay and sand data collected from January 1993 to July 1994." Department of Civil Engineering, Texas A&M University, College Station, TX, USA. Report No NGES-TAMU-003.

Mayne, P. (2007). "NCHRP synthesis 368, cone penetration test." NCHRP, Transportation Research Board, Washington D.C., USA.

McCartney, J.S., and Rosenberg, J.E. (2011). "Impact of heat exchange on the axial capacity of thermo-active foundations." *Proceedings Of Geofrontiers Conference*, Dallas, TX, USA.

McCartney, J.S., and Murphy, K.D. (2012). "Strain distributions in full-scale energy foundations." *DFI Journal*, vol. 6 (2), 28-36.

McCormac, C.J., and Brown, H.R. (2009). *Design of reinforced concrete*. John Wiley & Sons, New York, NY, USA.

Mitchell, J.L., and Campanella, R.G. (1964). "Creep studies on saturated clays. Symposium on laboratory shear testing of soils." ASTM-NRC, Ottawa, Canada, ASTM Special Tech. Publication no. 361.

Mitchell, J.K., Campanella, R.G., and Singh, A. (1968). "Soil creep as a rate process." *Journal of the Soil Mechanics and Foundation Division*, vol. 94 (1).

Mochlinkski, K. (1964). "Some industrial measurements of thermal properties of soil." *International Study Group on Soils.* Lectures at meeting in Cambridge, England, July 12- 26, o. 168-178.

Olgun, G.C., Martin, J.R., Abdul-Aziz, S.L., Iovino, P.L., Catalbas, F., Elks, C., Fox, C., and Gouvin, P. (2012). "Field testing of energy piles at Virginia Tech." *Proceedings of the 37th Annual Conference on Deep Foundations*, Houston, TX, USA.

Olivella, S., Gens, A., Carrera, J., and Alonso, E.E. (1996). "Numerical formulation for a simulator (CODE-BRIGHT) for the coupled analysis of saline media." *Engineering Computation*, vol. 13 (7), 87–112.

Ooka, R., Sekine, K., Mutsumi, Y., Yoshiro, and S. SuckHo, H. (2007). "Development of a ground source heat pump system with ground heat exchanger utilizing the cast-in place concrete pile foundations of a building." EcoStock, 8 pp.

Pahud, O., Hellström, G., and Mazzarella, L. (1996). "Heat storage in the ground. duct ground heat storage model for TRNSYS (TRNVDST)." User Manual for the October 1996 Version. Laboratoire des systèmes énergétiques, Département de Génie Civil, Ecole Polytechnique Fédérale de Lausanne (Lasen/DGC/EPFL), Lausanne, Switzerland.

Paul, N.D. (1996). "The effect of grout thermal conductivity on vertical geothermal heat exchanger design and performance." M.Sc. Thesis. South Dakota University, Vermillion, SD, USA.

Preene, M., and Powrie, W. (2009). "Ground energy systems: from analysis to geotechnical design." *Géotechnique,* vol. 59, 261–271.

Rees, S.W., Adjali, M.H., Zhou, Z., Davies, M., and Thomas H.R. (2000). "Ground heat transfer effect of the thermal performance of the earth contact structures." *Renewable and Sustainable Energy,* vol. 3, 213-265.

Remund, C. (1999). "Borehole thermal resistance: laboratory and field studies." *ASHRAE Transactions*, vol. 105 (1), 439 - 445.

Remund, C., and Carda, R. (2009). *IGSHPA residential and light commercial design and installation manual.* International Ground Source Heat Pump Association.

Romero, E. (1999). "Characterization and thermal-hydro-mechanical behaviour of unsaturated Boom clay: an experimental study." Ph.D. Thesis, Technical University of Catalonia, Spain.

Rosenberg, J.E., and McCartney, J. S. (2011). "Impact of heat exchange on side shear in thermo-active foundations." *Proceedings of Geofrontiers Conference*, Dallas, TX, USA, 488-498.

Sagia, Z., Stegou A., and Rakopoulos, C. (2012). "Borehole resistance and heat conduction around vertical ground heat exchangers." *The Open Chemical Engineering Journal*, vol. 6, 32-40.

Scott, R.F. (1969). "The freezing process and mechanics of frozen ground." CRREL Cold Regions Science and Engineering Monograph II-D1. AD 697136.

Sepaskhah, A.R., and Boersma, L. (1979). "Thermal conductivity of soils as a function of temperature and water content." *Soil Science Society of America Journal*, vol. 43, 439 – 444.

Shannon, W.L., and Wells, W.A. (1947). "Tests for thermal diffusivity of granular materials." *Proceedings of the American Society for Testing and Materials*, vol. 47, p. 1044-1055.

Sharqawi, M.H., Mokheimer, E.M., and Badr, H.M. (2009). "Effective pipe-to-borehole thermal resistance for vertical ground heat exchangers." *Geothermics*, vol. 38, 271– 277.

Simon, P., and Briaud, J.L. (1996). "National geotechnical experimentation sites at Texas A&M University: clay and sand, soil data in electronic form, 1995-1996." Department of Civil Engineering, Texas A&M University, College Station, TX, USA. Report No. NGES-TAMU-006.

Stewart, M., and McCartney, J. (2013). "Centrifuge modeling of soil-structure interaction in energy foundations." *Journal of Geotechnical and Geoenviromental Engineering*, vol. 10, 1061.

Tao, C., and Briaud, J.L. (1995). "National experimentation sites at Texas A&M University: clay and sand, soil data in electronic form, 1977-1955." Department of Civil Engineering, Texas A&M University, College Station, TX, USA. Report No. NGES-TAMU-004.

Tarnawski, V.R., and Gori, F. (2002). "Enhancement of the cubic cell soil thermal conductivity model." *International Journal of Energy Research*, vol. 26, 143 – 157.

Teh, C.I., and Houlsby, G.T. (1991). "An analytical study of the cone penetration test in clay." *Géotechnique*, vol. 41, 17-34.

Thomas, H.R., and Rees, S.W. (2009). "Measured and simulated heat transfer to foundation soils." *Géotechnique*, vol. 59 (4), 365–375.

Torstensson, B.A. (1975). "Pore pressure sounding instrument." *Proceedings of Specialty Conference on In-Situ Measurement of Soil Properties*, Raleigh, N.C, vol. 2, 48-54.

van der Held, E.F.F., and Van Drunen, F.G. (1949). "A method of measuring the thermal conductivity of liquids." *Physica*, vol. 15 (10), 865 – 881.

van Genuchten, M.T. (1980). "A closed-form equation for predicting the hydraulic conductivity of unsaturated soils." *Soil Science Society of America Journal*, vol. 44 (5), 892–898.

Van Rooyen, M., and Winterkon, H.F. (1957). "Structural and textural influences on thermal conductivity of soils." Highway Research Board Proceedings. 39:576 – 621.

Van Wijk, W.R. (Ed.) (1963). *Physics of Plant Environment.* Amsterdam, North Holland Publishing Company.

Vanapalli, S.K., Pufahl, D.E., and Fredlund D.G. (1999). "The influence of soil structure and stress history on the soil-water characteristic of a compacted till." *Géotechnique*, vol. 49 (2), 143-159.

Wissa, A.E.Z., Martin, R.T., and Garlanger, J. E. (1975). "The piezometer probe." *Proceedings of Specialty Conference on In Situ Measurement of Soil Properties*, Raleigh, N.C., vol. 1, 536 – 545.

Wood, C.J., Liu, H., and Riffat, S.B. (2009). "Use of energy piles in a residential building, and effects on ground temperature and heat pump efficiency." *Géotechnique*, vol. 59 (3), 287–290.

Xia, C., Suna, M., Zhanga, G., Xiaoa, S., and Zoua, Y. (2012). "Experimental study on geothermal heat exchangers buried in diaphragm walls." *Energy and Buildings* vol. 52, 50–55.

Zeng, H., Diao, N., and Fang, Z., (2002). "A finite line-source model for boreholes in geothermal heat exchangers." *Heat Transfer Asian Research*, vol. 31, 558–567.